DOE/PC/92104--T9

92PC92104-TPR-10

ADVANCED THERMALLY STABLE JET FUELS

Technical Progress Report
October 1994 - December 1994

H.H. Schobert, S. Eser, C. Song, P.G. Hatcher, A. Boehman, M.M. Coleman

Contributions from:

R. Arumugam, J.M. Bortiatynski, R. Byrne, C. Chan, K. Gergova, E. Kazakova, W.-C. Lai, J. Li, D. E. McKinney, M. Reddy, P. Sanghani, A.D. Schmitz, P. Vijay, E. Yoon, and J. Yu

February 1995

Prepared for U.S. Department of Energy
under
Contract No. DE-FG22-92PC92104

OBJECTIVES

The Penn State Program in advanced thermally stable coal-based jet fuels has five objectives: 1) development of mechanisms of degradation and solids formation; 2) quantitative measurement of growth of sub-micrometer and micrometer-sized particles suspended in fuels during thermal stressing; 3) characterization of carbonaceous deposits by various instrumental and microscopic methods; 4) elucidation of the role of additives in retarding the formation of carbonaceous solids; and 5) assessment of the potential of production of high yields of cycloalkanes and hydroaromatics by direct liquefaction of coal.

SUMMARY

A literature review was completed on approaches to quantitative description of the degradation chemistry of fuels. The computational fluid dynamics and chemistry model predicts general trends in deposition rates. However, to bring its predictions to a quantitative level and to complete the picture of the deposition process, a detailed description of chemical reactions in the system is necessary. Detailed kinetic modeling of pure single hydrocarbon systems provides reasonable agreement with experiments, but for multicomponent mixtures the reaction mechanisms appear to be extremely complicated and involve many uncertain parameters. Structure-oriented lumping and probability density function methods allow avoidance of extreme complexity in detailed modeling by using systematic reaction-reaction descriptions and statistical sampling from a large set of compounds.

Decalin produced no solid deposit even with eight hours' stressing at 450°C; decalin seems an ideal candidate for a future jet fuel. *trans*-Decalin is much more stable than *cis*-decalin; their stabilities are close to those of methylcyclohexane and *n*-butylcyclohexane, respectively. Conformational isomerization is the dominant reaction for *cis*- and *trans*-decalin at 450°C.

After six hours of heating of 1-phenylhexane, only 35% remained. In contrast, the degradation of 1-phenyl-1-^{13}C-hexane in the presence of a thermally stable coal-derived jet fuel, JP-8C, was drastically different. At the end of six hours, 96.5% of 1-phenyl-1-^{13}C-hexane remained unreacted in the mixture. This difference indicates that the reaction kinetics for the two different systems are not the same and therefore the mechanism for the thermal degradation of neat 1-phenylhexane versus that in the JP-8C are not equivalent. It appears that as radicals are formed by the degradation of 1-phenylhexane in the jet fuel mixture, they are quickly quenched by hydrogen-donor molecules in the fuel itself. In the neat compound, there are no hydrogen-donor molecules available to retard the thermal breakdown of the 1-phenylhexane.

Critical temperature calculations using six different methods showed that while most of the methods can give satisfactory critical temperature predictions for the petroleum-derived jet fuels, they are less reliable for the coal-derived fuels because of the differences in the composition of these fuels. A new correlation was developed on the basis of the boiling points and specific gravities of the compounds found in the coal-derived jet fuels. The new correlation gives satisfactory critical temperature predictions for the coal-derived jet fuel samples.

A recently renovated Chemical Data Systems bench-scale reaction system has been used to begin developing data on surface effects on deposit formation in a flow reactor system. This reactor is essentially a constant-surface-temperature type of reactor.

An uncertainty analysis for growth and deposition of particles during heating of coal-derived jet fuels has been started. Uncertainty analysis for species concentration is ongoing. The uncertainty associated with thermal and concentration gradients within the microautoclave reactor still needs to be addressed.

The surface chemistry of PX-21 activated carbon was investigated for thermal stressing of Jet A-1 and *n*-dodecane. The nature and activity of the activated carbon surface during thermal stressing is an important parameter in deposit formation. The surface oxygen concentration can be reduced by outgassing at 900°C in nitrogen. The activity of PX-21 in preventing carbon deposition increases considerably with the pretreatment. The outgassed carbon showed lower catalytic activity in promoting hydrogen-transfer reactions and converting decalin to naphthalene. Surface complexes on the carbon surface apparently act as active sites for hydrogen-transfer reactions.

Screening of potentially superior jet fuel stability additives was continued. Reactions of a variety of compounds have been continued using both Jet A-1 and *n*-dodecane. The properties of a good additive are: 1) thermal stability of the additive itself at temperatures above 400°C; 2) hydrogen atoms in the additive molecule that can be transferred or abstracted by hydrocarbon radicals (the greater the number of hydrogen atoms available for abstraction, the better); and 3) resonance stabilization of the radicals generated from hydrogen atom abstraction from the additive.

Work was started on novel approached to low-severity liquefaction and co-processing using water and dispersed catalysts. This work will provide valuable mechanistic information concerning the chemical influence of the water/dispersed catalyst systems on coal depolymerization reactions and will contribute to the development of novel low-severity catalytic coal liquefaction processes.

Hydrogenation experiments with naphthalene show that *cis*-decalin is rapidly formed and isomerizes to *trans*-decalin. A unique catalyst, platinum on HY zeolite, produces *cis*-decalin with high selectivity and does not promote the isomerization.

Work was also begun on the development of mesoporous molecular sieve catalysts for coal liquids upgrading to jet fuels. This work will involve synthesis of mesoporous molecular sieves,

characterization of these materials, and their catalytic evaluation for the conversion of polycyclic aromatic model compounds and then coal-derived oils.

Two new reactor systems are currently in the design stages for performing studies in coal liquefaction. The design and assembly of a 300 mL batch autoclave reactor system is currently being done. A conceptual process scheme has been developed for a continuous flow mini-pilot plant reactor system for liquefaction and upgrading of the coal-derived liquids.

Task 1. Investigation of the Quantitative Degradation Chemistry of Fuels

1. Literature Review on Thermal Stability of Jet Fuels (Contributed by Elena Kazakova)

Introduction

The stability of an aviation fuel is a major consideration in the design of aircraft fuel systems. In the formative years of gas turbine development, it was thought that the engine could run on most liquid fuels. Then it was found that much better performance would be obtained if fuel properties were restricted. The current hydrocarbon-based jet fuels are supposed to comply with quite a few requirements on physical and chemical properties. The list of these characteristics contains vapor pressure, distillation range, freeze point, viscosity, electrical conductivity, and, among others, stability.

In fact, stability is a convenient quantity for specifying the tendency of a jet fuel to change the characteristics affecting the efficiency of its performance. These changes may occur due to conditions of either storage or usage. The most important changes affecting a fuel performance are those involving formation of insoluble materials that can deposit in fuel lines, on heat transfer surfaces, and on injection nozzles.

In the case when solid deposition is formed due to fuel storage we are dealing with *storage stability*. The second type of instability related to fuel changes at elevated temperatures in aircraft fuel systems is known as *thermal stability*. Sometimes the term *thermal stability* is used for thermal decomposition processes in the absence of both dissolved or input oxygen. The *thermal oxidative stability* is considered when oxidation is involved; whenever the pyrolysis takes place, it is referred to by the general term *thermal stability*. Although thermal stability is already one of the most important characteristics for current jet fuels, its significance will increase in the future. The reason for this is that the operating temperature of aircraft fuel is expected to rise due to the elevated environmental temperature of high-performance jet engines. The present limits for fuel stability regimes are 436 K for JP–4, JP–5, JP–8, and 561 K for JP–7 fuel.[1] Therefore, a good theoretical base is needed to handle the deposition problems and develop more thermally stable fuels.

Although the problem has been studied for more than 35 years, there are many more questions than answers. There are three main reasons for the absence of a clear physical picture of fouling.

First, the formation of insoluble materials is a complex process including several steps. The chemical part comprises the decomposition of the components initially present in the bulk fluid and on the hot surfaces of aircraft fuel systems, two very different

processes in terms of interpretation. The composition of a jet fuel varies from sample to sample; also it changes during the thermal degradation or oxidative reactions. A detailed kinetic mechanism for just one hydrocarbon might include hundreds of steps; the chemistry of real fuel is expected to be much more complicated. Precursors of solid deposits formed in the bulk must be transported to surfaces by either diffusion or turbulent flows. That is the physical part of the problem. The formation of solid residua on heated metal surfaces is a catalytic process of known initial and unknown intermediate species that is complicated enough to represent a separate problem. The relative importance and interaction of various processes, different by nature, complicate the understanding and prediction of the deposition paths.

The second reason is the global character of empirical data. Current experiments provide information on thickness of deposits, their thermal resistivity, rates of deposition, dissolved oxygen consumption, and methane production.[2-5] However, almost no data on chemical composition of these deposits exist. Detailed knowledge of the contents would help to identify the chemical reactions that contribute to the overall deposition rate.

The third factor complicating the development of a fundamental pattern of fouling in jet aircraft systems is the empirical nature of derived correlations involving many adjustable parameters having no physical meaning.

Numerical modeling is an alternative method for fouling process analysis. A realistic model can help to identify the major factors governing the complex process and predict the system behavior under different conditions. At this point a comprehensive model of real jet fuel decomposition in aircraft engine systems cannot be developed since many of the physical and chemical processes involved are not well understood. An additional difficulty is caused by limitations on computer speed. Therefore, two general ways to approach the problem exist: the accurate description of fluid dynamics with simplified chemistry, and detailed chemical kinetic simulations neglecting flow conditions.

A Computational Fluid Dynamics and Chemistry Model of Jet Fuel Thermal Stability

Computational fluid dynamics and chemistry (CFDC) models have been developed as computational tools for combustor design. They are also used for simulation of carbon deposition processes.

The idea had its origins in theoretical analysis of surface thermal fouling by Kern and Seaton.[6] Since then many empirical models have been applied to design of aircraft fuel systems. A typical example of such models is a recent work of Epstein.[7] Fouling processes are divided into six different classes that are described by several empirical constants. The disadvantage of such approach is the non-chemical treatment of the fouling.

The CFDC model [1,8] is the incorporation of the existing fluid dynamics codes solving the system of conservation equations of mass, momentum, and energy with an averaged Reynolds number and the thermal decomposition model in the simplest form.

The short description should be started at the point of the initial one-step CFDC model [1] produced as a modification of the existing combustion code (block-implicit multigrid method) for two-dimensional, Reynolds averaged Navier-Stokes, mass, and energy equations in gas flows. The modification consists of supplementing of the ideal gas law and gas flow characteristics with fluid properties of viscosity, thermal conductivity, specific heat, and density. It is worthwhile to point out that these properties are very sensitive to variations in composition.

Among the processes leading to the carbon deposition on surfaces, heat transfer from the wall to the bulk is responsible for the formation of initial deposit precursors. Thermally initiated decomposition reactions proceed to create radical species, forming insoluble precursors. The latter can be decomposed, or foul surfaces by convective mass flow or diffusion transport.

These processes can be described by the following general transport equation

$$\nabla(\mathbf{G}C_i) = \nabla(\Gamma_c \nabla C_i) + S_f - S_d \qquad (1)$$

Here **G** is mass flux field for convection flow from bulk liquid to walls, C_i is the concentration of species i, Γ_c represents the effective diffusion coefficient for turbulent and molecular diffusion, and S_f, S_d are the overall rates of the species formation and destruction respectively.

The formation rate for a deposit precursor in the bulk fluid is written as

$$S_f = A_f \exp(\frac{-E_f}{RT_{bulk}})[\mathrm{Fu}]_b^{a_f}[\mathrm{O_2}]_b^{b_f} \qquad (2)$$

where A_f, E_f, and T_b are pre-exponential factor, activation energy, and bulk temperature respectively. $[\mathrm{Fu}]_b$ and $[\mathrm{O_2}]_b$ are bulk liquid concentrations of fuel and dissolved oxygen. Values a_f and b_f are assumed to be 1. The A_f and E_f must be determined experimentally.

The destruction of deposit precursors is generally two processes: chemical decomposition in the bulk liquid and transport of bulk–formed precursors to the wall surface followed by deposition. The rate of the former is represented by the equation

$$S_{cd} = A_{cd} \exp\left(\frac{-E_{cd}}{RT_{bulk}}\right)[\mathrm{Pre}]_b \qquad (3)$$

where $[\mathrm{Pre}]_b$ is bulk precursor concentration. The second process is described as

$$S_{wd} = K[\mathrm{Pre}]_w^n \qquad (4)$$

where $[\mathrm{Pre}]_w^n$ is the concentration of deposit precursors at the wall and K is the parameter that can be interpreted as a deposition coefficient. The order of the reaction n is assumed to be 1.

In order to solve the equation (1) for deposit precursors, the boundary condition is imposed

$$D_{[\mathrm{Pre}]}\left(\frac{\partial[\mathrm{Pre}]}{\partial r}\right)_{wall} = -K[\mathrm{Pre}]_w \qquad (5)$$

where $D_{[\mathrm{Pre}]}$ is the diffusion coefficient of deposit precursors.

Deposits are also formed due to heterogeneous reactions at the wall/fuel interface described by equation (1) for oxygen and the additional boundary condition

$$D_{\mathrm{O}_2}\left(\frac{\partial[\mathrm{O}_2]}{\partial r}\right)_{wall} = -A_w \exp\left(\frac{-E_w}{RT_{wall}}\right)[\mathrm{Fu}]_w^{a_w}[\mathrm{O}_2]_w^{b_w} \qquad (6)$$

where $[\mathrm{Fu}]_w$, $[\mathrm{O}_2]_w$ are fuel, oxygen concentrations at walls, respectively; A_w, E_w are experimentally determined Arrhenius parameters for a particular fuel; and the value 1 is used for reaction orders a_w and b_w.

Obviously, the considered model involves many unknown parameters. These parameters can be obtained from experiments with isolated mechanisms as were performed in the Marteney test program [9] for JP-5 jet fuel. It was found that the average rate of carbon deposition in long, thin, electrically heated tubes (constant heat flux boundary

condition) is correlated with the initial wall temperature. The obtained dependence is presented in the Figure 1.[9] The character of the dependence reveals behavior typical for two competitive reaction channels with activation energies of 10 *kcal/mol* for low temperatures below 533 K and 40 *kcal/mol* for higher temperatures. Activation energies of the magnitude 10 *kcal/mol* are characteristic for heterogeneous processes. This points to the predominance of deposit formation reactions at wall/fluid interface in the low-temperature regime. At higher temperatures, closer to the pyrolysis region, bulk fluid dissociation of products may play an important role. The activation energy for the latter is approximately 40 *kcal/mol*.

Prior to calibration several model parameters were fixed. The value of K in the equation (5) was set to a large number, 10^{20}, *i.e.*, practically all precursors reaching the wall surface deposit on it. A baseline value of 50 wppm was used for the inlet oxygen concentration of air saturated JP-5 fuel. The activation energies were stated as above.

The calibration of the model requires determination of additional parameters: the pre–exponential factors A_W, A_f, and A_{cd} in the equations (2), (3), and (6) respectively; and activation energies E_f and E_{cd} in equations (2) and (3). In the low–temperature region (T_{wall}< 533 K) the wall reaction dominates and the model can be calibrated by adjusting only A_W. At higher temperatures where the deposition rate results mostly from the bulk reaction the wall reaction rate is considered to be negligible. The experimental data [9] were well fitted by lines corresponding to activation energies of 8–10 *kcal/mol* and 40 *kcal/mol* in low–temperature and high–temperature regions, respectively (Figure 2a).[8] For the turbulent data below 533 K, the activation energy was fixed at 8 *kcal/mol* and the pre–exponential factor was varied to fit the data. The best match for A_W is given by the value of $4.0\times10^{1} cm^{3} mol^{-1} s^{-1}$. The parameters for the autooxidative reaction (2) were adjusted to fit high-temperature turbulent flow data as well as dissolved oxygen concentrations.[8] The values $A_f = 1.0\times10^{13} cm^{3} mol^{-1} s^{-1}$ and $E_f = 30 kcal/mol$ result in good agreement with the experiments. Additional laminar flow data were used to adjust kinetic parameters of precursor decomposition reaction (3). The obtained values of the pre–exponential factor and activation energy were $3.0\times10^{15} s^{-1}$ and $35 kcal/mol$, respectively. The comparison of the adjusted CFDC model results and experimental data of TeVelde and Glickstein (taken from the paper of Chin and Lefebvre [2]) is shown in the Figure 2b. The model qualitatively reproduces the characteristic shape of the experimental curve.

This comparison indicates the ability of the model to predict general tends in fuel decomposition rates. However, further refinement of this approach is critical for quantitative analysis.

Although the physical part of the model seems to be close to the real processes, the treatment of chemical reactions is oversimplified.

Kinetic Studies of Jet Fuel Stability

Aircraft jet fuels are derived from a relatively high-boiling range distillation of crude oil often referred to as the kerosene fraction. These fuels are composed mostly of the hydrocarbons (up to 98%), primarily of aliphatic and naphthenic molecules, with aromatic hydrocarbon concentration 20–25%, and olefin content up to 5%. [10] The complex mixture is expected to exhibit very complicated chemistry.

The simplified description of a thermal cracking mechanism for a model hydrocarbon is suggested below. The kinetic scheme is constructed according to a free-radical chain mechanism, originally proposed by Rice [11] and refined later by Kossiakoff and Rice.[12] Let P_N; $P_1,...,P_{N-1}$; $Q_1,...,Q_M$; $R_1,...,R_N$ be the initial substrate, classes of reactive hydrocarbons, inert products, and free radicals, respectively. The following sequence of reactions can be used to describe thermal cracking of P_N.

chain initiation

$$P_N \xrightarrow{k_1(m)} R_m + R_i, \qquad (m = 1,...N;\ i = f_1(m))$$

chain propagation

$$R_n + P_m \xleftarrow{k_2(n,m),k_2(m,n)} R_m + P_n \qquad (n = 1,...N;\ m = 1,...N)$$

$$R_n \xleftarrow{k_3(n,m),k_3(m,n)} R_m \qquad (n = 1,...N;\ m = 1,...N)$$

$$R_n \xrightarrow{k_4(n,m)} R_m + Q_j \qquad (n = 1,...N;\ m = 1,...N;\ j = f_2(n,m))$$

chain termination

$$R_m + R_n \xrightarrow{k_5(n,m)} P_{n+m} \qquad (n = 1,...N;\ m = 1,...N)$$

The additional assumption is made that $k_3(n,m) \neq 0$ only if R_n, R_m are isomers, and $k_3(i,i) = 0$ for all i. Similarly $k_4(n,m) \neq 0$ only when R_n is a higher radical than R_m.

If the reactions take place in a closed system of constant volume and temperature, the concentrations p_n, r_n of P_n, R_n satisfy the equations

$$\dot{p}_n = -\left(\sum_{m=1}^{N} k_2(m,n) r_m\right) p_n + \left(\sum_{m=1}^{N} k_2(n,m)\right) r_n - y_n + z_n \qquad (7)$$

$$\dot{r}_n = \left(\sum_{m=1}^{N} k_2(m,n) r_m\right) p_n - \left(\sum_{m=1}^{N} k_2(n,m) p_m\right) r_n - k_3(n) r_n + \sum_{m=1}^{N} k_3(n,m) r_m -$$

$$-k_4(n) r_n + \sum_{m=1}^{N} k_4(n,m) r_m + y'_n + z'_n \qquad (8)$$

this means the overall rates are equal to ordinary chemical rates, where y_n, z_n and y'_n, z'_n are the contributions of the initiation and termination reactions in equations (7) and (8) respectively, V is the volume of the system,

$$k_3(n) = \sum_{m=1}^{N} k_3(n,m); \; k_4(n) = \sum_{m=1}^{N} k_4(n,m)$$

and the dot represents differentiation with respect to time.

For constant pressure the chain rates can be written as follows

$$\dot{p}_n^{P=const} = \dot{p}_n^{V=const} - \frac{p_n}{V}\dot{V}$$

$$\dot{r}_n^{P=const} = \dot{r}_n^{V=const} - \frac{r_n}{V}\dot{V}$$

The coefficients $k_j(n,m)$ (j=1,4) are some functions of temperature and pressure, the term V is the volume of the system. The temperature dependence of rate coefficients is usually described by an Arrhenius relation. Different types of reactions reveal various pressure dependencies. For monomolecular processes it is a linear function at low-pressure conditions and a constant at high pressure. If all parameters describing the set of chemical reactions are known, the solution of the system of differential equations like (7), (8) can be obtained numerically using standard ODE integrators.[13]

The first approach is to treat a jet fuel as a single chemical compound.[11,12]

Zabarnick [14] modeled the autoxidative processes in jet fuels in the presence (or absence) of an antioxidant AH, handling the bulk fuel as a single compound RH, which has chemical properties of a straight-chain alkane. The proposed kinetic mechanism is

presented in Table 1. Unfortunately, the time scale in his work is so small that the results cannot be compared with the existing experimental data. It is difficult to compare the predictions of the model even with the experimental results of the same authors.[15] The experiments consider air stressed systems while the model describes autoxidation. However, the mechanism predicts the general tends in system behavior.

In Figure 3 [14] the oxygen decay rate is presented as a function of antioxidant concentration. The dependence displays characteristic U–form. This type of behavior, where large concentrations of antioxidant actually decrease the oxidative stability, has been experimentally observed in fuel systems.[16]

This approach does not give insight into the nature of jet fuel stability because of its oversimplification. Much more information can be obtained from detailed kinetic modeling of pure hydrocarbons those are paraffin and aromatic compounds.

The pioneering works of Rice and Kossiakoff [11,12] proposed the free-radical mechanism for the thermal cracking of paraffins that may be used to predict the product distribution. The theory in its various extensions has been developed primarily from studies on paraffins up to about C_6. It had been found to fit semi–quantitatively longer paraffins.[17] A better agreement can be obtained when the assumption of isomerization [18] expands the simple chain cracking theory.

The critical point in construction of a chemical reaction mechanism is the knowledge of rate coefficients and thermodynamic data. The major reactions of small hydrocarbon combustion and pyrolysis were extensively studied during recent years and there are comprehensive data bases available.[19-26] The rate parameters for unknown reactions can also be estimated using modern theoretical methods such as Benson's rules.[27] Unfortunately, all the above hold true only for elementary chemical reactions. For higher hydrocarbons detailed mechanisms become too complicated.

The formation of solid deposits suggests that cycloalkanes and aromatics must be included in any attempt at modeling the chemical reactions since the gas-phase formation of carbonaceous materials is presently related to growth of polycyclic aromatic hydrocarbons (PAH).

There appear to be three possible pathways to rapid molecular weight growth: (1) cycloaddition reactions between alkenes and dienes (Diels-Alder) [28]; (2) ion-molecular reactions with their very large rate constants [29]; and (3) radical addition to unsaturated hydrocarbons. A major difficulty with the first pathway is that the equilibrium constants for this type of reactions suggest that at the high temperatures where growth is observed the cyclic species would tend to dissociate to the linear smaller fragments. A major difficulty with an ionic mechanism is that it appears unlikely that the concentration of ions in a

pyrolytic process (this type might still be sufficient for oxidation reactions) could be sufficiently high to have any impact. Therefore, the attention has focused upon radical addition.

Acetylene plays the leading role in gas-phase PAH formation from small hydrocarbons [30-32]. The most important path for two-ring aromatic production goes through acetylene, Figure 4a.[33] The reaction of benzene and phenyl radical [30] might be significant important for PAH formation in high benzene concentrations (Figure 4b).

For higher straight chain hydrocarbons the picture is not even that clear. There are few detailed works on decomposition of ethylene, propane, and butane.[34-37] Although reasonable agreement for C_1-C_4 species production has been achieved by the group of Dagaut [34,35], no calculation has been performed for aromatic products. The model of Mallinson [36] is also limited to the formation of alkanes and alkenes.

Very few kinetic calculations for long straight-chain hydrocarbons have been made.[38-40] The authors also limited their models to major alkane and alkene production.

Savage and Klein [41,42] proposed the method of cross kinetics for binary mixtures of alkylcyclohexanes and alkylbenzenes. The model is restrained by the formation of two–membered ring structures and does not describe the polycyclic aromatic hydrocarbons (PAH) which are of main importance for solid deposits.

There are some qualitative attempts to propose mechanisms for PAH formation from long-chain alkanes under relatively low temperature conditions.[28,43] In contrast to premixed flames where PAH and soot grow by the addition of acetylene, aromatic species appear to be primarily responsible for the growth of PAH and solid deposits in pyrolytic processes.[44] Nohara and Sakai offered the well-known Diels-Alder type of reactions between butadiene/allyl radical and an alkene for the first ring formation and ring growth (Figure 5a). Song and coworkers [43] also suggested the ring-closure reaction through the cyclization of 5-hexenyl radical (Figure 5b). This type of reaction is considered responsible for the formation of five-membered ring compounds and, to a lesser extent, of six-membered cyclic species. Unfortunately no modeling can be performed through the above assumptions due to non-elemental character of the processes and uncertain kinetic data. According the information on identified products and intermediates in stressed *n*-tetradecane, *n*-dodecane, and jet fuels, the possible mechanisms for the formation of PAH have been also suggested by Song and coworkers (Figure 5c).[45]

Aromatic compounds are abundant species in jet fuels. It was logical to investigate their decomposition behavior and simulate it. Benzene combustion has been modeled by Zhang and McKinnon [46] to the point of naphthalene formation but the detailed molecular weight-growth chemistry was not included in the mechanism. Nevertheless, it is the most

complete kinetic scheme for benzene thermal transformations. The mechanism is a extension of the work of Emdee, Brezinsky, and Glassman [47] on benzene-toluene combustion coupled with the submodel of benzene destruction by Howard and Vaughn.[48] Bittner and Howard [49] reported a detailed pre-particle study on benzene preservation and destruction that went up to PAH formation. They found that a proper mixture of monocyclic aromatic species, *e.g.*, benzene, phenyl radical, toluene, and benzyl radical, and non-aromatics such as acetylene, ethylene, and vinylacetylene results in rapid production of higher molecular weight PAH. This interesting result suggests that acetylene and polyacetylenic species are essential to the formation of PAH in aromatic combustion. The mechanism for growth of fused-ring aromatic structures through acetylenic compound addition is slightly different from that proposed later by Frenklach [33] but also includes the acetylene addition-hydrogenation-dehydrogenation sequence of reactions. The possible radical addition schemes for PAH formation in benzene flames are given in Figure 6.

A very interesting recent work on PAH formation was published by Mukherjee, Sarofim and Longwell.[50] The subject of the paper is not kinetic modeling but a topological attempt to explain the achieved results. They proposed the importance of molecular weight growth channels involving direct polymerization of aromatics under conditions of high–temperature pyrolysis of polyaromatics. The authors pointed out that their results can be explained by steric and statistical factors. In other words, the composition of product mixture depends on the abundance of particular reaction sites rather than change in enthalpy.

The knowledge of PAH concentration profiles enables the prediction of the soot mass by using models for nucleation, coagulation and surface growth.[31, 51, 52]

The subject of non-traditional approaches to the simulation of chemical processes during thermal degradation of hydrocarbons will be discussed next.

Non-Traditional Simulation of Chemical Processes

Molecular Level Lumped Modeling. An interesting attempt was made by Liguras and Allen [53] for the purpose of coupling the advantages of both detailed molecular modeling and lumping simulation. The authors used a ten-class model to describe the heavy hydrocarbon mixture, but instead of taking uniform kinetic parameters for all compounds in a class, they included the dependence of the rate constants on carbon numbers of reactants, and probability that a reactant will form a product with definite number of carbon atoms when it undergoes a certain reaction. It was assumed that the cracking reaction rate constant

depends on the square of the carbon number according to the results of Voge and Good [17], while for disproportionation, polymerization, and addition reactions, it was assumed that the rate decreases as the carbon number increases, i.e., reversed first-order dependence. The binomial, gamma, and uniform functions were used to describe product distribution. The model yields concentration profiles along with mean carbon number distribution in compound classes (Figure 7). Unfortunately, the results of the work are not comparable with current experimental data but it still looks quite promising.

Structure Oriented Lumping. Another interesting work was that of Quann and Jaffe [54] and concerns structure-oriented lumping (SOL). SOL represents an individual hydrocarbon molecule as a vector function of the structure. The hydrocarbon mixture is represented as a set of such vectors with the appropriate distribution function. The approach makes it possible to construct reaction networks of the mixtures, using the existing group contribution methods for the estimation of molecular thermodynamic properties, and provides the base for molecular modeling of hydrocarbon mixture reactions.

The core of the theory is the description of a complex molecule as a system of structural subsystems such as a six-carbon aromatic ring, an alkyl group, different heteroatoms and many others. Some of these subsystems exist as separate molecules (Figure 8a), others can be found only as a part of more complex structures (Figure 8b).

Structure-oriented lumping provides a convenient tool for treating chemical reactions as transformations of the reactant structural increments to the product structural increments. Specific transformations of the structural coordinates that describe chemistry are specified as *reaction classes* (A6 saturation, A4 saturation, N4 ring opening and so on) and are determined by *reaction rules.* A reaction rule is a specification of a class of reactions that different molecules may undergo. A reaction rule has two components: a *reactant selection rule* to determine if a molecule has the proper structural elements to participate in the reaction and a *product generation rule* to obtain the product structure vector. Naphthalene and its hydrogenation in vector notation are shown in Figure 8c. The SOL allows creation of the reaction pool for multicomponent systems by using matrix-vector rate equation

$$\mathbf{y}' = \mathbf{K}\mathbf{y}$$

The matrix **K** of rate coefficients should be determined for each case specifically. Although the SOL method helps to construct **K** in the sense of equal-not equal to zero, it

does not produce values of rate constants. In fact, the purpose of the described method is not to resolve the system of rate equations, but automatically generate a kinetic model.

Kinetic Simulation in Graph Theory Notation. Another very elegant work belongs to Broadbelt, Stark, and Klein.[55] This work was aimed at development of a computer generator of kinetic mechanisms. As a whole, the problem can be represented as the scheme in Figure 9.[56] The authors specifically concentrated on the reaction mechanism part.

The central part of the method is using 2D representation for any 3D molecular structure and applying the graph theory algorithms to chemical reactions.

It is interesting to mention that the notations used in chemistry today (letters enclosed in circles to represent atoms and connectivity lines to represent bonds) are already graph theory applications. The implementation of graph theory concepts and algorithms requires efficient representation and encoding of the graphs. Several approaches currently exist.[56] Broadbelt and coworkers [55] are using the bond and electron (BE) matrix that provides description of not only the environment of an atom but also of its formal electronic state. The diagonal element, *ii*, of a BE matrix gives the number of nonbonded valence electrons of atom *i*; and off–diagonal entries, *ij*, provide the connectivity and bond order of atoms *i* and *j*. The obtained matrix is symmetrical, with zero diagonal for non–radical species and non–zero one for radicals. A reduced BE submatrix describing only atoms that take part in a certain chemical reaction is sufficient for reactant–product representation. Therefore, the mathematical transformation

$$\mathbf{R}+\mathbf{B}=\mathbf{E}$$

where **R** is the reaction matrix, **B** the reactant submatrix or 'minimal representation,' and **E** is a product submatrix composed of the same atoms with changed connectivity represents a chemical reaction. All reactions are considered to be elementary. The incorporation of **E** back in the primary BE matrix gives the overall matrix of products. When the reactive atoms come from different molecules (bimolecular reactions) the $i\times i$ matrix of a reactant 1 and the $j\times j$ matrix of a reactant 2 are merged into a single $(i+j)\times(i+j)$ matrix from which the minimal representation is obtained. The H-abstraction from methane is shown in the Figure 10 to illustrate the briefly described approach.

The logic of the algorithm for the generation of reaction mechanisms and rate constants is shown in Figure 11. The reaction mechanism part is a matter of programming technique and the kinetic rate part remains unclear.

The authors used the structure/reactivity parameter approach that consists of categorizing the elementary reactions in terms of reactivity families, the reactivity of each sterically similar family being described by a single Arrhenius factor and different activation energy or a reactivity index RI_i

$$\log k_i = a + bRI_i$$

The reactivity index might be a function of the heat of reaction, the heat of formation of one reactant, electron affinity, electron density, or other molecular properties. The semi–empirical relationship of activation energy E and the heat of reaction $\Delta H_{reaction}$ for exothermic reactions attributed to Polanyi [55] can serve as a simple example of such dependence

$$E = E_0 + \alpha(\Delta H_{reaction})$$

where for H-abstraction the slope is 0.25 and the intercept 11.5, for β-scission of simple alkyl radicals E_0 is equal 15.8 and α - 0.58 (in kcal/mole).

The molecular properties needed for the estimation of RI_i can be obtained by using a semi–empirical quantum chemistry software package.[57] The original graph structure represented by the BE matrix was optimized to obtain the realistic 3D structure and corresponding molecular properties.

Statistical Sampling (Monte Carlo) Methods. The approach alternative to lumping used for the description of complex reaction systems is statistical sampling accomplished by Monte Carlo methods.

There are no direct applications of Monte Carlo methods to the decomposition of jet fuels or pure hydrocarbons available in the literature but a few works are devoted to Monte Carlo simulations of complex reaction systems such as heavy oils or polymers.[58-60] The first work describes asphaltene (heavy hydrocarbon) stock in terms of probability density functions, *pdf's*. Each asphaltene molecule is characterized by a degree of polymerization, a number of aromatic rings, a number of naphthenic rings, a degree of substitution, and a chain length for each aliphatic substituent. This information about an asphaltene molecule is expressed in terms of pdf's that gives the probability that the attribute should take on the value of the abscissa or less (Figure 12).[60]

The pdf's of each of these varieties are derived experimentally. The Monte Carlo method was used to construct a pool of 10,000 different molecules that represent the generic asphaltene feedstock. After the reactant array was simulated, a structure/reactivity

relationship allowed determination of the sequence of rate constants for each reactive site of each component in the stock. The reactions of each stock molecule proceeded event-by-event until the final simulation time was reached. Then a new molecule was taken from the stock array and reacted stochastically until all 10,000 molecules had undergone the process. The predicted global coke yield (the yield of solid products) from reaction at 720 K conforms to the laboratory experiments [59], Figure 13.

The methods discussed in this section suggest efficient systematic description of complex reacting mixture composition and possible reactions between components of the mixture. The dynamics of the system can be resolved by using lumping or statistical sampling (Monte Carlo) methods.

Concluding Remarks

The thermal stability of high hydrocarbon mixtures, in particular jet fuels, was discussed in terms of different models for solid materials formation. The computational fluid dynamics and chemistry model (CFDC) predicts general tends in deposition rates. However, to bring its predictions to the quantitative level and to complete the picture of the fouling process, the detailed description of chemical reactions in the system is necessary. Detailed kinetic modeling of pure single hydrocarbon systems provides reasonable agreement with experiments but for multicomponent mixtures reaction mechanisms appear to be extremely complicated and involve many uncertain parameters. Structure–oriented lumping and pdf methods allow avoidance of extreme complexity in detailed modeling by using systematic reactant–reaction description and statistical sampling from a large set of compounds.

References

1. Roquemore, W.M., Pearce, J.A., Harrison III, W.E., Krazinski, J.L. & Vanka, S.P. Fouling in Jet Fuels: a New Approach,*Prepr. - Amer. Chem. Soc., Div. Petr. Chem.* , **34**, 841 (1989).

2. Chin, J.S., Lefebvre, A.H. & Sun, F.T.-Y. Temperature Effects on Fuel Thermal Stability,*J. Eng. Gas Turb. Power* , **114**, 353 (1992).

3. Chin, J.S. & Lefebvre, A.H. Influence of Flow Conditions on Deposits From Heated Hydrocarbon Fuels,*J. Eng. Gas Turb. Power* , **115**, 433 (1993).

4. Heneghan, S.P., Martel, C.R., Williams, T.F. & Ballal, D.R. Studies of Jet Fuel Thermal Stability in a Flowing System, *J. Eng. Gas Turb. Power* , **115**, 480 (1993).

5. Klavetter, E.A., Martin, S.J. & Wessendorf. Monitoring Jet Fuel Thermal Stability Using a Quarts Crystal Microbalance,*Energ. Fuel* , **7**, 582 (1993).

6. Kern, D.Q. & Seaton, R.E. A Theoretical analysis of Thermal Surface Fouling,*Brit. Chem. Eng.*, **4**, 258 (1959).

7. Epstein, N. in *Heat Exchanger Sourcebook* (eds. Palen, J.W.) 677 (Hemisphere Publishing Company, Washington, DC, 1986).

8. Krazinski, J.L., Vanka, S.P., Pearce, J.A. & Roquemore, W.M. Computational Fluid Dynamics and Chemistry Model for Jet Fuel Thermal Stability,*J. Eng. Gas Turbines & Power* , **114**, 104 (1992).

9. Marteney, P.J. & Spadaccini, L.J. Thermal Decomposition of Aircraft Fuel,*J. of Engineering for Gas Turbines and Power* , **108**, 648 (1986).

10. Coordinating Research Council I.*Handbook of Aviation Fuel Properties* (Society of Automotive Engineers, Inc., Atlanta, GA, 1983).

11. Rice, F.O. *J. Amer. Chem. Soc.* ,**55**, 3035 (1933).

12. Kossiakoff, A. & Rice, F.O. Thermal Decomposition of Hydrocarbons, Resonance Stabilization and Isomerization of Free Radicals,*J. Amer. Chem. Soc.* ,**65**, 590 (1943).

13. Hindmarsh, A.C. in *Scientific Computing* (eds. Stephen, R.S.) 55-64 (IMACS, Amsterdam, 1983).

14. Zabarnick, S. Chemical Kinetic Modeling of Jet Fuel Autooxidation and Antioxidant Chemistry,*Ind. Eng. Chem. Res.* ,**32**, 1012 (1993).

15. Heneghan, S.P. & Zabarnick, S. Oxidation of Jet Fuels and the Formation of Deposits,*Fuel* ,**73**, 35 (1994).

16. Mayo, F.R. & Lan, B.Y. Gum and Deposit formation from Jet Turbine Diesel Fuels at 130 C,*Ind. Eng. Chem. Prod. Res. Dev.* ,**25**, 333 (1986).

17. Voge, H.H. & Good, G.M. Thermal Cracking of Higher Paraffins,*J. Amer. Chem. Soc.* ,**71**, 593 (1949).

18. Doue, F. & Guiochon, G. The Mechanism of Pyrolysis of Some Normal and Branched C6 to C9 Alkanes. Composition of Their Pyrolysis Products,*J. Phys. Chem..*, **73**, 804 (1969).

19. Tsang, W. Rate Constants for Decomposition and Formation of Simple Alkanes Over Extended Temperature and Pressure Ranges,*Comb. Flame* ,**78**, 71 (1989).

20. Tsang, W. Chemical Kinetic Data Base for Combustion Chemistry. Part 4. sobutane,*J. Phys. Chem. Ref. Data* ,**19**, 1 (1990).

21. Tsang, W. Chemical Kinetic Data Base for Hydrocarbon Pyrolysis,*Ind. Eng. Chem. Res.*,**31**, 3 (1992).

22. Alberty, R.A. & Gehrig, C.A. Standard Chemical Thermodinamic Properties of Alkane Isomer Groups,*J. Phys. Chem. Ref. Data* ,**13**, 1173 (1984).

23. Alberty, R.A. Standard Chemical Thermodynamic Properties of Alkylbenzene Isomer Groups,*J. Phys. Chem. Ref. Data* ,**14**, 177 (1985).

24. Alberty, R.A. & Reif, A.K. Standard Chemical Thermodynamic Properties of Polycyclic Aromatic Hydrocarbons and Their Isomer Groups I. Benzene Series,*J. Phys. Chem. Ref. Data* ,**17**, 241 (1988).

25. Allara, D.L. & Shaw, R. A Compilation of Kinetic Parameters for the Thermal Degradation of *n*-Alkane Molecules,*J. Phys. Chem. Ref. Data* ,**9**, 523 (1980).

26. Baulch, D.L., *et al.* Summary Table of Evaluated Kinetic Data for Combustion Modeling: Supplement 1.,*Comb. Flame* 59 (1994).

27. Benson, S.W. *Thermochemical Kinetics* (John Wiley & Sons, New York, 1976).

28. Nohara, D. & Sakai, T. Kinetic Study of Model Reactions in the Gas Phase at the Early Stage of Coke Formation,*Ind. Eng. Chem. Res..*, **31**, 14 (1992).

29. Calcote, H.F. Mechanism of Soot Formation in Flames-a Critical Review,*Combust. Flame* , **42**, 215 (1981).

30. Frenklach, M., Clary, D.W., Gardiner, W.C. & Stein, S. *Effect of Fuel Structure on Pathways to Soot* 1-1067-1076 (The Combustion Institute, 1986).

31. Colket, M.B. & Hall, R.J. *Mechanistic Models of Soot Formation* (United Technologies Research Center,1992).

32. Kern, R.D., Singh, H.J. & Wu, C.H. Thermal Decomposition of 1,2 Butadien,*Int. J. Chem. Kinet.* ,**20**, 731 (1988).

33. Frenklach, M., Clary, D.W., Gardiner, W.C. & Stein, S.E. *Detailed Modeling of Soot Formation in Shock-Tube Pyrolysis of Acetylene* 1-887 (The Combustion Institute, 1984).

34. Dagaut, P., Boettner, J.-C. & Cathonnet, M. Ethylene Pyrolysis and Oxidation: A Kinetic Modeling Study,*Int. J. Chem. Kinet.* ,**22**, 641 (1990).

35. Dagaut, P., Cathonnet, M. & Boettner, J.-C. Kinetic Modeling of Propane Oxidation and Pyrolysis,*Int. J. Chem. Kinet.* ,**24**, 813 (1992).

36. Mallinson, R.G., Westbrook, C.K. & Burnham, A.K. Detailed Chemical Kinetics Study of the Role of Pressure in Butane Pyrolysis,*Ind. Eng. Chem. Res.* ,**31**, 37 1992).

37. Edelson, D. & Allara, D.L. A Computational Analysis of the Alkane Pyrolysis Mechanism: Sensitivity Analysis of individual Reaction Steps,*Int. J. Chem. Kinetics* **12**, 605 (1980).

38. Billaud, F., Elyahyaoui, K. & Baronnet, F. Mechanistic Modeling of the Pyrolysis of *n*-Hexane,*J. Anal. Appl. Pyrolysis* ,**19**, 29 (1991).

39. Domine`, F. Kinetics af Hexane Pyrolysis at Very High Pressures. 2. Computer Modeling,*Energ. Fuels* ,**4**, 2 (1990).

40. Domine`, F. Kinetics of Hexane Pyrolysis at Very High Pressures-3. Application to Geochemical Modeling.,*Org. Geochem.* ,**18**, 41 (1992).

41. Savage, P.E. & Klein, M.T. Kinetics of Coupled Reactions: Lumping Pentabenzene Pyrolysis into Three Parallel Chains,*Chem. Eng. Sci..*,**44**, 985 (1989).

42. Savage, P.E. Pyrolysis of A Binary Mixtures of Hydrocarbons: Reaction Modeling,*Chem. Eng. Sci.* ,**45**, 859 (1990).

43. Song, C., Lai, W.-C. & Schobert, H.H. Condensed-Phase Pyrolysis of *n*-Tetradecane at Elevated Pressure for Long Duration. Product Distribution and Reaction Mechanisms,*I&EC Research* , **33**, 534 (1994).

44. Wornat, M.J., Sarofim, A.F. & Longwell, J.P.*Pyrolysis-Induced Changes in the Ring Number Composition of Polycyclic Aromatic Compounds from a High Volatile Bituminous Coal* 1-135 (1988).

45. Song, C., Peng, P., Jiang, H. & Schobert, H.H. On the Mechanisms of PAH and Solid Formation during Thermal Degradation of Jet Fuels, *j Prepr. - Amer. Chem. Soc., Div. Petr.Chem..*, **37**, 484 (1992).

46. Zhang, H.Y. & McKinnon, J.T.*Elementary Reaction Modeling of High-Temperature Benzene Production* 1-in press(The Combustion Institute, 1994).

47. Emdee, J.L., Brezinsky, K. & Glassman, I. A Kinetic Model for the Oxidation of Toluene near 1200K,*J. Phys. Chem.* ,**96**, 2151 (1992).

48. Vaughn, C.B., Howard, J.B. & Longwell, J.P. Benzene Destruction in Fuel-Rich Jet-Stirred Reactor Combustion,*Comb. Flame* , **87**, 278 (1991).

49. Bittner, J.D. & Howard, J.B.*Composition Profiles and Reaction Mechanisms in a Near-Sooting Premixed Benzene/Oxygen/Argon Flame* 1-1105 (The Combustion Institute, 1981).

50. Mukherjee, J., Sarofim, A.F. & Longwell, J.P. Polycyclic Aromatic Hydrocarbons from the High Temperature Pyrolysis of Pyrene,*Combustion and Flame* , **96**, 191 (1994).

51. Frenklach, M. & Wang, H.*Soot modeling* 1-1559 (The Combustion Institute, 1991).

52. Mauss, F., Schäfer, T. & Bockhorn, H. (The Combustion Institute, in press).

53. Liguras, D.K. & Allen, D.T. Comparison of Lumped and Molecular Modeling of Hydropyrolysis,*Ind. Eng. Chem. Res..*, **31**, 45 (1992).

54. Quann, R.J. & Jaffe, S.B. Structure-Oriented Lumping Describing the Chemistry of Complex Hydrocarbon Mixtures,*Ind. Eng. Chem. Res..*, **31**, 2483 (1992).

55. Broadbelt, L.J., Stark, S.M. & Klein, M.T. Computer Generated Pyrolysis Modeling: On-the Fly Generation of Species, Reactions, and Rates,*Ind. Eng. Chem. Res..*, **33**, 790 (1994).

56. Trinajstic, N.*Chemical Graph Theory* (CRC Press, Boca Raton, 1992).

57. Stewart, J.J.P.*Quantum Chemistry Exchange Program (Indiana University, Bloomington, Indiana, 1983), No. 455.* .

58. Neurock, M., Libanati, C., Nigam, A. & Klein, M.T. Monte Carlo Simulation of Complex Reaction Systems: Molecular Structure and Reactivity in Modeling Heavy Oils,*Chemical Engineering Science* , **45**, 2083 (1990).

59. Libanati, C., *et al.* Mechanistic Modelling of Polymer Pyrolysis Using Monte Carlo Methods,*Molec. Simulation* , **11**, 187 (1993).

60. Sapre, A.V. & Krambeck, F.J.*Chemical Reactions in Complex Mixtures: the Mobil Workshop* (Van Nostrand Reinhold, New York, 1991).

2. Pyrolytic and Catalytic Reactions of Potential Endothermic Fuels: cis- and trans-Decalin. (Contributed by Wei-Chuan Lai, Cindy Chan, and Chunshan Song)

Introduction

We have previously shown that *trans*-decalin (*trans*-DHN) has the desirable ability of inhibiting the solid deposit formation from jet fuels and their components (Song et al., 1994a). For example, adding 50 vol% *trans*-DHN to a JP-8P fuel, *n*-C_{14}, and *n*-butylbenzene thermally stressed at 450 °C for 4 h significantly reduced the deposit formation from 3.1 to 0.1 wt%, from 3.0 to 0.1 wt%, and from 5.6 to 0.0 wt%, respectively. It was also shown in literature that decalin (DHN) may be one of the potential endothermic jet fuels that can serve as the primary heat sink to cool the hot surfaces and system components (Donath and Hess, 1960; Lander and Nixon, 1987; Taylor and Rubey, 1987). In order to obtain a better understanding of potential endothermic fuels such as saturated cyclic hydrocarbons, in this report we present the experimental results of *cis*- and *trans*-DHN pyrolysis at 450 °C for 0.5-8 h under initial (cold) N_2 pressure of 0.79 MPa. The pyrolysis results show that *trans*-DHN is much more stable than *cis*-decalin (cis-DHN). Thus, in this report we also present some exploratory studies on the catalytic isomerization of *cis*-DHN to *trans*-DHN.

Experimental

The chemicals (*cis*-DHN, *trans*-DHN, and DHN, an almost equimolar mixture of *cis*- and *trans*-DHN) were obtained from Aldrich Chemical Company and were used as received. Their purities (>99%) were analyzed in our laboratory using gas chromatography (GC) and gas chromatography-mass spectrometry (GC-MS). Pyrolytic experiments were performed using 5-mL sample in 28-mL vertical type stainless steel tubing bomb reactors at 450 °C for a heating period of 0.5-8 h under an initial pressure of 0.79 MPa UHP-N_2.

The catalysts used in the catalytic isomerization reactions include: a hydrogen Y zeolite (HY), a metal ion-exchanged Y zeolite (LaHY), a hydrogen mordenite (HM38), and three metal ion-exchanged mordenites (PtM38, PdM38, and PtM21). The details of the preparation and properties of the catalysts are described elsewhere (Song et al., 1994b; Schmitz et al., 1994). Catalytic isomerization reactions were carried out in 28-mL horizontal type stainless steel tubing bomb reactors, which were charged with 1 g of *cis*-DHN or DHN (7.23 mmol) and 0.2 g of catalyst, at 200–275 °C for 0.15-8 h under an initial pressure of 0.79 MPa UHP N_2 or H_2. The uniformity of concentration and temperature inside the reactor was obtained by agitating the reactor vertically at 240 cycles/min.

The gaseous products were quantitatively analyzed using a Perkin-Elmer Autosystem GC equipped with two detectors, a thermal conductivity detector (TCD) and a flame ionization detector (FID). The liquid products were analyzed on an HP 5890II GC coupled with an HP 5971A Mass Selective Detector (MSD) and quantified by a Perkin-Elmer GC 8500 equipped with an FID. More analytical details may be found in previous reports.

Results and Discussion

1. Pyrolytic reactions. Table 2 shows the products distribution from pyrolysis of *cis*-DHN, *trans*-DHN, and DHN. There are several features of the product distribution patterns. First, there was no solid deposit formed from these reactants even after an 8-h thermal stressing at 450 °C. This demonstrates that DHN has a much higher thermal stability than a JP-8C fuel (2.6 wt% solid deposit after 8 h at 450 °C) or a JP-8P fuel (8.9 wt% solid deposit after 8 h at 450 °C).

Second, *trans*-DHN is much more stable than *cis*-DHN. The average first-order rate constants over the stressing range studied are 0.31 ± 0.04 h^{-1} for *cis*-DHN and 0.06 ± 0.02 h^{-1} for *trans*-DHN, respectively. The first-order rate constants for *cis*-DHN and *trans*-DHN are close to that of *n*-butylcyclohexane and methylcyclohexane, respectively. Substantially (≈3–4 times) higher gas yields were produced from *cis*-DHN than from *trans*-DHN as shown in Table 2. The major gas components are CH_4, C_2H_6, and C_3H_8. These results imply that there existed higher degree of ring-opening reactions and subsequent dealkylation for *cis*-DHN. In short, the steric isomers of cycloalkanes react at different rates, and in general, *trans*-isomers are more stable than their *cis*-counterparts. Some of the examples include DHN as well as 1,2-, 1,3-, and 1,4-dimethylcyclohexanes. In terms of high temperature applications of jet fuels for high-Mach aircraft, it implies that *trans*-isomers might be the more desirable compounds for the advanced jet fuels because, generally speaking, most of their product compounds are more stable and have lower tendency to form solid deposits.

Third, isomerization is the dominant reaction under the conditions employed (450 °C). For pyrolysis of *cis*-DHN at 450 °C, the dominant products are two types of isomers: *trans*-DHN (from conformational isomerization) with about 55% selectivity (defined as the ratio of molar yield of the product to the conversion) and C_4-cyclohexene or cyclohexylbutene (ring-opening isomerization) with about 10% selectivity. Other major products include: 1) C_0–C_2-benzene, alkanes/alkenes (dealkylation and dehydrogenation products subsequent to ring-opening reactions); 2) tetralin and naphthalene (dehydrogenation products); 3) alkyldecalins. In addition, the very low yields of three- or

four-ring aromatics should also be noted. As can be seen from Table 2, isomerization products are also the major ones for the pyrolysis of *trans*-DHN at 450 °C. However, the conformational isomerization of *trans*- to *cis*-DHN (30% selectivity) is not as dominant as that of *cis*- to *trans*-DHN (55% selectivity). On the other hand, the yields of C_4-cyclohexene and cyclohexylbutene from *trans*-DHN are higher (20% selectivity) than those from *cis*-DHN (10% selectivity). Besides, tetralin (from dehydrogenation) also becomes a significant product, for example, with about 22% selectivity after 1-h treatment.

It was believed that the three major product groups (isomerization, dehydrogenation, and decomposition products) share the same initiation pathway. Roberts and Madison (1959) studied the di-*tert*-butyl peroxide-initiated isomerization of *cis*-DHN at 195 °C and suggested that the initiation proceeds through H-abstraction by a free radical from the weakest bonds in *cis*-DHN, i.e., those on the 9- or 10-position, to form a 9-decahydronaphthyl radical. It was suggested that the thermal isomerization at 450 °C proceeds through the same initiation mechanism. The 9-decahydronaphthyl radical then undergoes one of the following three competitive reactions. The first is H-transfer to produce either *trans*- or *cis*-DHN; the second is β-scission to start the ring-opening isomerization and cracking; the third is H-abstraction to form dehydrogenation products such as tetralin and naphthalene. The first reaction (conformational isomerization) is the dominant one below 450 °C. This is significantly different from that in literature for high-temperature (≥ 700°C) pyrolysis of *cis*-DHN, where the dominant primary process yielded light cracking products (Bredael and Rietvelde, 1979).

2. Catalytic reactions. Table 3 shows the products distribution from catalyzed isomerization of *cis*-DHN using 1-g commercial DHN (an almost equimolar mixture of *cis*- and *trans*-isomers) as staring reactant at 200 or 250 °C for 2 h with 0.79 MPa of UHP H_2 or N_2. Pt- and Pd-loaded mordenites, i.e., PtM38, PtM21, and PdM38, are very effective catalysts under H_2 atmosphere for the conformational isomerization of *cis*-DHN to *trans*-DHN even at low temperature, 200 °C. The conversion selectivity towards *trans*-DHN reaches 100%; in other words, there are no side-products accompanying the isomerization. The experimental final product composition of 92.7% *trans*-DHN and 7.3% *cis*-DHN at 200 °C as shown in Table 3 is very close to the calculated equilibrium composition (95.35% *trans*-DHN, 4.65% *cis*-DHN), which is shown in Table 4. Pt- and Pd-loaded mordenites are effective catalysts under H_2 atmosphere; however, they are less effective under N_2 atmosphere (see Table 3). PtM38 is a better catalyst than PdM38 at 200 °C under N_2 atmosphere in terms of conversion and *trans*-DHN selectivity although they are almost equally effective under H_2. For the other three catalysts studied, HY, LaHY, and HM38, they are much less effective than Pt- and Pd-loaded mordenites, and do not react at all at

200 °C. It is also interesting to note that although the effectiveness of Pt- and Pd-loaded mordenites depends on the gas environment (H_2 or N_2), H_2 has no impact on the performance of LaHY. The data in Table 3 seem to show that the hydrogen Y zeolite (HY) performs about as well as the metal ion-exchanged Y zeolite (LaHY), and HM38 is the least effective one among the catalysts studied.

We further investigated the performance of HY and LaHY intending to get the kinetic data. These isomerization reactions were carried out using 1 g of *cis*-DHN instead of DHN mixture, and 0.2 g of catalyst, at 235-275 °C for 0.15-8 h under an initial pressure of 0.79 MPa UHP N_2. The results are shown in Table 5, where the rate constants, k (h^{-1}), based on first-order rate law were also calculated. The rate constant (k) is correlated by the Arrhenius law as shown in Eq. (1)

$$k = A\, e^{-E_a / RT} \qquad (1)$$

where A (h^{-1}) is the frequency (or preexponential) factor, E_a is the apparent activation energy (cal/mol), and R is the gas constant (cal mol^{-1} K^{-1}). Figure 14 presents the Arrhenius plots for the catalyzed isomerization of *cis*-DHN using catalysts HY and LaHY. The E_a and A values are as follows:

for HY $\quad E_a = 51.8$ kcal/mol $\quad$ and $\quad A = 3.84 \times 10^{21}$ h^{-1}

for LaHY $\quad E_a = 57.3$ kcal/mol $\quad$ and $\quad A = 4.76 \times 10^{23}$ h^{-1}

There are a few features that may be pointed out from examining Table 5. First, the more complete data in Table 5 seem to indicate that HY performs slightly better than LaHY in terms of criteria such as activity and selectivity. This observation is somewhat different from what we said earlier that they perform equally well judging from the data in Table 3. Second, selectivity towards *trans*-DHN seems to decrease with increasing temperature. This is not unexpected since the isomerization from *cis*-DHN to *trans*-DHN is exothermic, 95 J/g or 41 Btu/lb (our calculation based on data in Reid et al., 1987). Third, the product (*trans*-DHN) selectivity decreases with increasing conversion level under isothermal condition.

Summary

The results of pyrolysis at 450 °C and catalytic reactions at lower temperatures (200-275 °C) are summarized as follows. There was no solid deposit formed from decalin even after 8 h at 450 °C; decalin may be a candidate compound for future jet fuel. *trans*-

DHN is much more stable than *cis*-DHN, and their stability is close to that of methylcyclohexane and *n*-butylcyclohexane, respectively. Conformational isomerization is the dominant reaction for *cis*- and *trans*-DHN at 450 °C.

PtM38, PtM21, and PdM38 are very effective catalysts under H_2 atmosphere for the conformational isomerization of *cis*-DHN to *trans*-DHN at 200 °C; however, they are less effective under N_2 atmosphere. HY, LaHY, and HM38 are much less effective than Pt- and Pd-loaded mordenites, and their performance was not affected by H_2. HY performs slightly better than LaHY in terms of activity and selectivity, and HM38 is the least effective one among the catalysts studied. Selectivity towards *trans*-DHN seems to decrease with increasing temperature, and decreases with increasing conversion level under isothermal condition.

References

1. Bredael, P.; Rietvelde, D. Pyrolysis of Hydronaphthalenes. 2. Pyrolysis of *cis*-decalin. *Fuel* **1979**, *58*, 215-218.

2. Donath, E. E.; Hess, M. Thermally Stable Hydrocarbon Fuels. *Chemical Engineering Progress*. **April 1960**, *56(4)*, 68-71.

3. Lander, H. R.; Nixon, A. C. Endothermic Fuels for High Mach Vehicles. *Prepr. Pap.-Am. Chem. Soc., Div. Petro. Chem.* **1987**, *32* (2), 504-511.

4. Reid, R. C.; Prausnitz, J. M.; Poling, B. E. *The Properties of Gases & Liquids*. Fourth Edition. **1987**, McGraw-Hill Book Company: New York, N.Y.

5. Roberts, R. M.; Madison, J. J. Free-Radical-Initiated *cis-trans* Isomerization of Decahydronaphthalene. *J. Am. Chem. Soc.* **1959**, *81*, 5839-5839.

6. Schmitz, A. D.; Bowers, G.; Song, C. Shape-Selective Naphthalene Hydrogenation for Production of Thermally Stable Jet Fuels. In *Advanced Thermally Stable Jet Fuels*. Technical Progress Report (July 1994 - September 1994), Schobert, H. H.; Eser, S.; Song, C.; Hatcher, P. G.; Boehman, A.; Coleman, M. M., Eds., The Pennsylvania State University, October **1994**, pp37-42.

7. Song, C.; Lai, W.-C.; Schobert, H. H. Hydrogen-Transferring Pyrolysis of Long-Chain Alkanes and Thermal Stability Improvement of Jet Fuels by Hydrogen Donors. *Ind. Eng. Chem. Res.* **1994a**, *33*, 548-557.

8. Song, C.; Moffatt, K. Zeolite-Catalyzed Ring-Shift Isomerization of *Sym*-Octahydrophenanthrene and Conformational Isomerization of *cis*-Decahydronaphthalene. *Microporous Materials* **1994b**, *2*, 459-466.

9. Taylor, P. H.; Rubey, W. A. Gas-Phase Thermal Degradation Behavior of Future Jet Fuels. *Prepr. Pap.-Am. Chem. Soc., Div. Petro. Chem.* **1987**, *32* (2), 521-525.

3. Use of Site Specific ^{13}C-Labeling to Examine the Thermal Stressing of 1-Phenylhexane: A Case Study for the Determination of Reaction Kinetics in Complex Fuel Mixtures Versus Model Compound Studies (Contributed by Daniel E. McKinney, Jacqueline M. Bortiatynski and Patrick G. Hatcher)

Introduction:

Many past and present investigators have determined reaction kinetics and chemical mechanisms for the thermal breakdown of individual hydrocarbons by model compound studies (Song et al., 1994 and references therein; Schobert et al., 1994 and references there in). These studies are adequate in understanding the chemical reactions of those materials in there most elementary forms, and are useful for interpreting general reactions that occur upon thermal alterations. They are an appropriate first step in comprehending complex radical reactions which occur upon the pyrolysis of hydrocarbons. However, do model compound stressing or degradation experiments mimic the reaction kinetics and mechanisms of the same model compound in complex organic matrices? Recently, Burnham et al. (1995) have shown that the reaction kinetics for the thermal decomposition of hexadecane neat versus that in a crude oil varied by nearly 60%. They also demonstrated that product formations from the pyrolysis of hexadecane were different.

Are there techniques available for tracing the reaction pathways of individual compounds tin complex organic matrices? Liquid fuels and the materials derived from them have been analyzed considerably by ^{13}C NMR in recent years due to improved instrumentation and analytical techniques. However, only a few studies have taken advantage of ^{13}C-labeling techniques in order to monitor individual compounds in a complex organic matrix (McKinney et al., 1993; Schobert et al, 1994; Burnham et al., 1995). Burnham et al. have developed a new isotopic method involving a double-^{13}C label detected by gas chromatography-mass spectrometry, whereas McKinney et al. used primarily ^{13}C NMR techniques to follow the decomposition of labeled benzyl alcohol and bibenzyl. A major problem with developing methodologies that utilize labeled compound tracer studies is the cost involved with obtaining ^{13}C-labeled compounds at specific sites in the molecules. Many compounds cost as much as $5000 for only 0.5g of labeled material. Therefore, these methods can become very costly when applied to fossil fuel systems.

In this study, we have developed a synthetic strategy from relatively inexpensive starting materials to incorporate isotopic ^{13}C-labels at specific sites in target molecules. In addition, we demonstrate the applicability of ^{13}C NMR labeling in combination with standard ^{13}C NMR experiments to examine thermally induced changes in a complex fossil fuel system, jet fuel. Finally, we determine whether reaction kinetics and mechanisms of

model compound studies are applicable for the same compounds in complex organic matrices.

Experimental

1. Reagents and Fuels. Reagent grade chemicals were purchased from Aldrich and isotopically enriched $K^{13}CN$ was purchased from Isotech Inc. The jet fuel sample used in this work was coal derived JP-8C produced by hydrotreating of tar liquids produced from the Great Plains Gasification plant and supplied by the Air Force Wright Laboratory/Aero Propulsion and Power Directorate[Song et al. 1993; Furlong et al., 1989].

The synthesis of 1-phenyl-1-^{13}C-hexane was accomplished in a three step synthetic pathway shown in Scheme 1.

Scheme 1: Synthetic scheme for the production of 1-phenyl-1-^{13}C-hexane
Step 1:

$$K^{13}CN + CH_3CH_2CH_2CH_2CH_2Br \xrightarrow{\text{catalyst}} CH_3CH_2CH_2CH_2CH_2{}^{13}CN$$

Step 2:

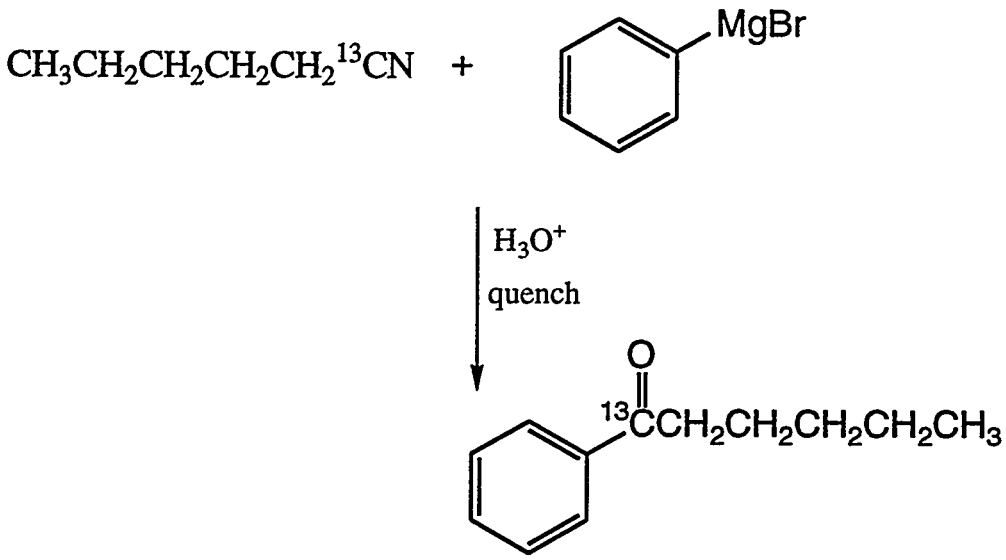

Step 3:

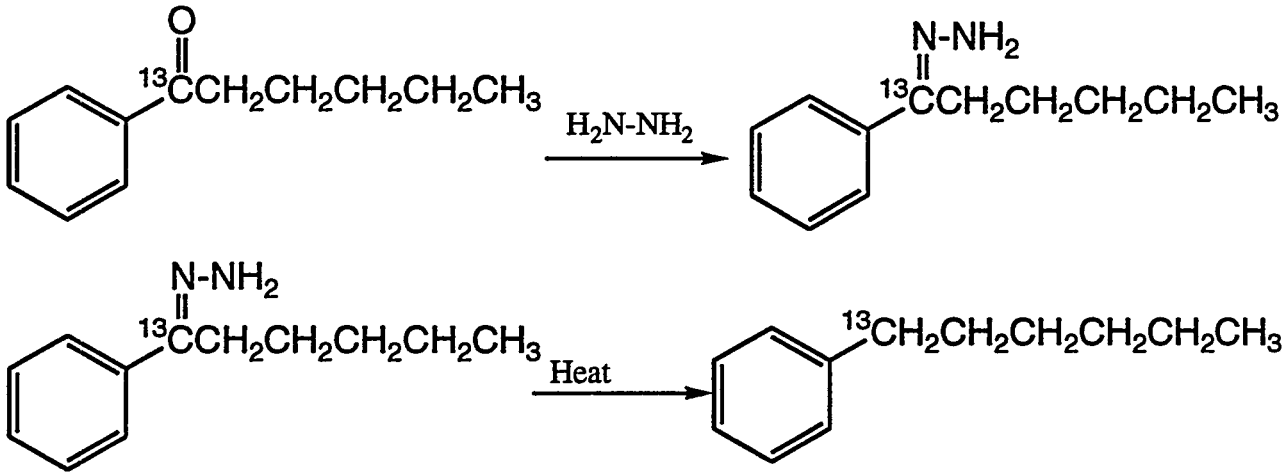

1-^{13}C-Hexanenitrile. 1-^{13}C-Hexanenitrile was synthesized using published procedures by Stark (1971). To a round bottomed flask equipped with a stir bar and reflux condenser, 2.5 g K^{13}CN was mixed in 5 mL of H_2O. After dissolving the K^{13}CN, 1.8 mL of 1-bromopentane was added to the cyanide solution and refluxed for a few minutes. The mixture was cooled to below 50°C and approximately 0.1 g of hexadecyltributylphosphonium bromide was added. The mixture was heated rapidly to 100-105°C and refluxed at this temperature for 2 hr's. Upon cooling the reaction mixture, the product was worked up in the usual way by extracting with ether, drying over $MgSO_4$, followed by vacuum evaporation. Liquid chromatography on silica gel was used to purify the product.

α-^{13}C-Caprophenone. α-^{13}C-Caprophenone was synthesized using modifications to published procedures by Hauser et al. (1948) To a two-necked, round bottomed flask equipped with a stir bar, dropping funnel, and reflux condenser, 2.42 mL of 3 M phenylmagnesium bromide plus 5.60 mL of dry ether were mixed and stirred vigorously under N_2. To this solution, an ethereal solution of 0.800 mL of 1-^{13}C-hexanenitrile was added dropwise over approximately 15 min., and the reaction mixture was refluxed for 9 hrs. The reaction mixture was cooled and quenched with approximately 6 mL of dilute HCl acid and reheated for 1 hr. The ketone was extracted with ether, washed with brine and dried over $MgSO_4$. The solvent was removed and the liquid chromatography on silica gel was used to purify the ketone.

1-phenyl-1-^{13}C-hexane. 1-Phenyl-1-^{13}C-hexane was synthesized by reducing the above ketone using the Huang-Minlon modification of the Wolf-Kishner reduction (Huang-Minlon, 1946, 1949). In a three-necked, round bottomed flask equipped with a stirring

bar, thermometer, reflux condenser, and take-off adapter, 0.85 mL of α-^{13}C-caprophenone, 0.61 g KOH, 4.6 mL of triethylene glycol and 0.46 mL of 85% hydrazine hydrate were refluxed for 2 hrs. The aqueous layer was then removed using a take-off distillation piece until the temperature of the liquid rose to approximately 240°C. The remaining mixture was subsequently heated for an additional 3 hrs. Upon cooling the mixture, the reaction mixture and aqueous distillate were combined and extracted with ether, washed with brine, and dried over $MgSO_4$. The solvent was removed in vacuo and the product purified using liquid chromatography on silica gel.

Analytical Procedure. Pyrolysis experiments for neat 1-phenylhexane were performed in 25 mL tubing bomb reactors at 400°C for heating periods of 1, 2, 4, and 6 hrs under an initial inert pressure of 6.9 MPa UHP-N_2 (cold). The details of the tubing bomb reactors were described elsewhere (Song et al., 1993, 1994). The reactors were loaded with 10 mL of sample each and purged repetitively with 6.9 MPa UHP-N_2 (3 times) to remove oxygen/air in the reactor or dissolved in the sample. After reaction of the sample was complete, the reactor was removed from the fluidized sand bath and quenched in a cool water bath. Only the liquid product was collected upon opening of the bomb and analyzed by gas chromatography.

Pyrolysis experiments for 1-phenyl-1-^{13}C-hexane in JP-8C were carried out in similar fashion to the above analytical procedure with the following exceptions: a 15 mL stainless steel tubing bomb was used in place of the 25 mL reactor in order to conserve the labeled material. The reactor was charged with 5 mL of JP-8C and 0.05 mL of 1-phenyl-1-^{13}C-hexane (1% by volume).

Instrumentation. Quantitative gas chromatography was carried out on each sample using a Hewlett-Packard 5890 II Gas Chromatograph with flame ionization detection. The column used was a 30 m, 0.25 i.d., 0.25μm film thickness, fused silica capillary column (J&W DB-5). The internal standard used for these experiments was 1-phenyloctane. Briefly, samples were prepared by mixing, in a 25 mL volumetric flask, approximately 3-4 μL of thermally stressed 1-phenylhexane, 3.00 μL of internal standard, and 25 mL of hexane. Approximately 1μL of the diluted sample was injected onto a split/splitless injector operating in the splitless mode and the column temperature was programmed from 40–240°C at a heating rate of 8°C/min after a 5-min. isothermal period. Each sample was run three times and the average of these runs used for kinetic parameters.

The ^{13}C NMR spectra were obtained on a 360 MHz AMX Bruker Instrument with a 5 mm broad band inverse probe tuned to 90.55 MHz. Samples were prepared by placing in a 5 mm NMR tube 0.10mL of 23% tetramethylsilane in deuterated chloroform followed by 0.5mL of the reacted JP-8C laced with 1% 1-phenyl-1-^{13}C-hexane. An inverse-gated

pulse sequence with a pulse width of 45° and a pulse delay of 80 seconds was used to ensure quantitative data. The spectra were referenced and integrated relative to tetramethylsilane. The raw data were Fourier transformed with 1 Hz line broadening and the spectra were integrated using the UXNMR software supplied by Bruker.

Results and Discussion

A series of ^{13}C NMR spectra were obtained for thermally stressed neat 1-phenylhexane. Figure 15 contains the ^{13}C NMR spectra of neat 1-phenylhexane prior to and after 6 hours of thermal stressing at 400° C. The spectra have been expanded to highlight the changes in chemical composition that occur to the aliphatic hexyl side chain which exhibits carbon resonances in the chemical shift region from 60 ppm to –10 ppm. The experimental parameters for the thermal stressing experiments were chosen based on previous model studies with butylbenzene (Schobert et al., 1994). The spectrum of the neat 1-phenylhexane prior to stressing is characterized by six sharp signals from approximately 40 ppm to 10 ppm. The spectrum of the 1-phenylhexane after six hours of stressing contains a number of additional signals which are characteristic of chemical changes that occur as a result of thermal decomposition. The amount of 1-phenylhexane remaining after 1hr., 2 hr., 4 hr., and 6 hr. of thermal stressing was quantified by capillary gas chromatography analysis and the results are found in Table 6. After six hours of stressing only 35 % of the 1-phenylhexane remains thus confirming the presence of thermal decomposition products in the ^{13}C NMR spectra.

The next series of experiments were carried out to determine whether or not the decomposition observed for neat 1-phenylhexane is representative of the thermal stressing of this model compound in the presence of complex reaction matrix such as a jet fuel. In an effort to follow the reaction of one component in a complex reaction mixture, the 1-phenylhexane was ^{13}C labeled at the alpha carbon of the aliphatic side chain. This position was chosen based on its propensity to participate in bond cleavage reactions leaving behind a highly stable benzyl radical. The ^{13}C label found in 1-phenyl-1-^{13}C-hexane enhances the ^{13}C NMR signal observed from this carbon thus providing a means of tracking the fate of the target molecule in the reaction mixture. Evidence of this enhancement is shown in Figure 16 in which the dominant feature of the ^{13}C NMR spectrum of 1-phenyl-1-^{13}C-hexane in the presence of JP-8C is the signal obtained for the ^{13}C labeled alpha carbon of the hexane side chain. This signal is well above the level of the natural abundance ^{13}C signals which appear at approximately 100 times less intense than that of the ^{13}C labeled carbon. When the 1-phenyl-1-^{13}C-hexane is thermally stressed in the presence of the JP-8C, the ^{13}C NMR spectrum obtained after 6 hours of heating is vertually the same as that

obtained for the starting material. The results are again quantified in Table 6 and clearly demonstrate that only 3.4 % of the 1-phenyl-1-^{13}C-hexane underwent any chemical transformation. Figure 17 is a graph of the percent 1-phenylhexane versus the amount of thermal stressing time in minutes. When the results of the thermal stressing experiments are compared to those of the model studies with neat 1-phenylhexane, it is obvious that a completely different reaction rates and possibly reactions themselves are occurring in the presence of JP-8C.

Conclusions

Site specific isotopic ^{13}C-labeling of organic compounds in complex organic matrices provides an invaluable analytical tool in the examination of reaction kinetics and mechanisms of those compounds. A complex mixture like jet fuel constrains the use of conventional analytical methods for the examination of the thermal degradation of individual hydrocarbons in the mix. We were successful in following the degradation of 1-phenyl-1-^{13}C-hexane mixed with JP-8C at a concentration level of only 1%. Therefore, it is possible to examine labeled compounds in the mix at relatively normal concentration levels with respect to other compounds.

From the model compound studies at 400°C, it was obvious that increased thermal stressing times reduced the amount of 1-phenylhexane. After 6 hours of heating, only 35% of the model compound remained. In contrast, the degradation of 1-phenyl-1-^{13}C-hexane in the presence of a thermally stable coal derived jet fuel, JP-8C, was drastically different. At the end of 6 hours in the mix, 96.5% of 1-phenyl-1-^{13}C-hexane remained unreacted. This obvious difference in the concentration of the model compound at various thermal stressing times indicates that the reaction kinetics for the two different systems are not the same and therefore the mechanism for the thermal degradation of 1-phenylhexane neat versus in JP-8C are not equivalent. It appears that, in the jet fuel mixture, as radicals are formed in the degradation of 1-phenylhexane, they are quickly quenched by H-donor molecules in the jet fuel itself. Whereas in the neat solution, there are no H-donor molecules available to retard the thermal breakdown of 1-phenylhexane. Song et al. (1993, 1994) has shown that H-donor molecules similar in structure to those found in JP-8C suppress the thermal degradation of *n*-C_{14} and provide stability to the coal derived fuel versus petroleum derived fuels.

This study demonstrates how site-specific labeling facilitates the interpretation and quantification of target components in complex ^{13}C NMR spectra. The thermal degradation data obtained in this study corroborate that of similar studies (Burnham et al., 1995) which

also indicate that model compound studies should be used as a first step in the understanding of reaction kinetics of thermal degradation in complex mixtures. The model compound studies provide preliminary data that can be used to predict which components in the mixture are likely to participate in reactions of interest. The compounds chosen for further study should then be examined using the site-specific isotopic labels that allow the reaction products to be analyzed directly thus providing an accurate description of the thermal degradation that occurs in this complex fuel mixture.

References:

1. Burnham, A.K.; Gregg, H.R.; Braun, R.L. *Energy Fuels* in press.

2. Hauser, C.R.; Humphlett, W.J.; Weiss, M.J. *J. Am. Chem. Soc.* **1948**, 70, 426.

3. Huang-Minlon *J. Am. Chem. Soc.* **1946**, 68, 2487.

4. Huang-Minlon *J. Am. Chem. Soc.* **1949**, 71, 3301.

5. McKinney, D.E.; Bortiatynski, J.M.; Hatcher, P.G. *Energy Fuels* **1993**, 7, 578.

6. Schobert, H.H.; Eser, S.; Song, C.; Hatcher, P.G.; Walsh, P.M.; Coleman, M.M. *Advanced Thermally Stable Jet Fuels* Technical Progress Report, 92PC92104-TPR-6, January, 1994.

7. Schobert, H.H.; Eser, S.; Song, C.; Hatcher, P.G.; Walsh, P.M.; Coleman, M.M. *Advanced Thermally Stable Jet Fuels* Technical Progress Report, 92PC92104-TPR-9, July, 1994.

8. Song, C.; Eser, S.; Schobert, H.H.; Hatcher, P.G. *Energy Fuels* **1993**, 7, 234.

9. Song, S.; Lai, W.C.; Schobert, H.H. *Ind. Eng. Chem. Res.* **1994**, 33, 534.

10. Song, S.; Lai, W.C.; Schobert, H.H. *Ind. Eng. Chem. Res.* **1994**, 33, 548.

11. Starks, C.M. *J. Am. Chem. Soc.* **1971**, 93, 195.

4. Estimation of Critical Temperatures of Jet Fuels (Contributed by Jian Yu and Semih Eser)

Introduction

In previous work the critical temperatures of nine jet fuels, including six petroleum-derived jet fuels and three coal-derived jet fuels, were measured using a sealed tube method (Hicks and Young, 1975; Mogollon et al., 1982) and the critical temperatures and pressures of the fuels were estimated using the methods recommended in API Technical Data Book (1987). It was found that the measured results are satisfactory and exhibit good reproducibility. It was also found that while the API method (API Technical Data Book, 1987) can give satisfactory predictions of the critical temperatures of the petroleum-derived jet fuels, the same method fails to give acceptable results for the coal-derived jet fuels (Schobert et al., 1993).

In this work, five other methods, developed by Cavett (1962), Kesler and Lee (1976), Riazi and Daubert (1980), Brule et al. (1982), and Twu (1984), were used to estimate the critical temperatures of the jet fuels. The API method (API Technical Data Book, 1987) was also presented for comparison. The measured and estimated critical temperatures were compared and the suitability of the estimation methods was discussed. In view of the shortcomings of these methods in estimating the critical temperatures of the coal-derived fuels, a new correlation was developed in the form of the Roess equation (API Technical Data Book, 1987) using the properties of the compounds found in the coal-derived jet fuels.

Critical Temperature Calculations

The critical temperatures (T_c) of the jet fuels were estimated by the method described in the API Technical Data Book (1987) and five other correlation methods, developed by Cavett (1962), Kesler and Lee (1976), Riazi and Daubert (1980), Brule et al. (1982), and Twu (1984). All the methods selected require only specific gravity and boiling point data as input.

API Method (API Technical Data Book, 1987). The API Technical Data Book (1987) recommends the Roess equation for T_c estimation:

$$T_c = 186.16 + 1.6667\Delta - 0.7127 \times 10^{-3}\Delta^2 \quad (1)$$

$$\Delta = SG(VABP + 100.0)$$

(2)

where T_c is in degrees Fahrenheit, SG is specific gravity, 60 °F/60 °F, and VABP is the volumetric average boiling point in degrees Fahrenheit which is the average of the ASTM D86 distillation temperatures at 10, 30, 50, 70, and 90 volume percent distilled points. The ASTM D86 distillation temperatures were obtained from ASTM D2887, simulated distillation (SD) by gas chromatography, using the method described in API Technical Data Book (1987). Cavett Correlation (1962).

$$T_c = 768.07121 + 1.7133693T_b - 0.10834003 \times 10^{-2}T_b^2 - 0.89212579 \times 10^{-2}API \times T_b + 0.38890584 \times 10^{-6}T_b^3 + 0.53094920 \times 10^{-5}API \times T_b^2 + 0.32711600 \times 10^{-7}API^2 \times T_b^2$$

(3)

where T_c is in °R, T_b is the boiling point in °F, and API = 141.5 / SG - 131.5.

Kesler and Lee Correlation (1976).

$$T_c = 341.7 + 811SG + (0.4244 + 0.1174SG)T_b + (0.4669 - 3.2623SG) \times 10^5 / T_b$$

(4)

where T_c and T_b are in °R.

Riazi and Daubert Correlation (1980).

$$T_c = 24.2787T_b^{0.58848}SG^{0.3596}$$

(5)

where T_c and T_b are in °R.

Brule Correlation (Brule et al., 1982).

$$T_c = 429.138 + 0.886861T_b - 4.596433 \times 10^{-4}T_b^2 - 2.410089 \times 10^{-3}API \times T_b + 1.630489 \times 10^{-7}T_b^3 - 9.323778 \times 10^{-7}API \times T_b^2 - 1.430628 \times 10^{-8}API^2 \times T_b^2$$

(6)

where T_c is in K and T_b is in °F.

Twu Correlation (1984).

$$T_c = T_c^\circ[(1 + 2f_T) / (1 - 2f_T)]^2$$

(7)

$$f_T = \Delta SG_T[-0.362456 / T_b^{1/2} + (0.0398285 - 0.948125 / T_b^{1/2})\Delta SG_T]$$

(8)

$$\Delta SG_T = \exp[5(SG^\circ - SG)] - 1$$

(9)

$$SG^\circ = 0.843593 - 0.128624\alpha - 3.36159\alpha^3 - 13749.5\alpha^{12}$$

(10)

$$\alpha = 1 - T_b / T_c^\circ$$

(11)

$$T_c^\circ = T_b / (0.533272 + 0.191017 \times 10^{-3}T_b + 0.779681 \times 10^{-7}T_b^2 - 0.284376 \times 10^{-10}T_b^3 + 0.959468 \times 10^{28} / T_b^{13})$$

(12)

where T_c and T_b are in °R.

Most of the correlations presented above were developed for petroleum fractions. The Brule correlation (Brule et al., 1982), which was modified from the Cavett correlation (Cavett, 1962), was developed for nonpolar coal fluids. The Twu correlation (Twu, 1984) was developed for both petroleum fractions and coal-tar fluids.

The properties of the jet fuels necessary for determining their critical temperatures can be found in the previous report (Schobert et al., 1993).

Results and Discussion

Table 7 shows the deviations of the estimated critical temperatures, calculated by the methods discussed above, from the measured values for the nine fuels. From Table 7 one can see that the Roess (API Technical Data Book, 1987), Brule (Brule et al., 1982), and Twu (1984) correlations give satisfactory T_c predictions for the petroleum-derived jet fuels. The Riazi and Daubert (1980) and Cavett (1962) correlations predict T_c moderately well and the Kesler and Lee (1976) correlation gives less satisfactory T_c prediction for the petroleum-derived jet fuels. All the methods fail to predict T_c satisfactorily for the coal-derived jet fuels (the last three fuels in Table 7). The larger deviations of the estimated critical temperatures from the measured values for the coal-derived fuels result from the different composition of these fuels. The methods used in the calculations were developed either for petroleum fractions which are composed mainly of paraffinic compounds or for coal fluids which consist mainly of aromatic compounds. Since coal-derived jet fuels are dominated by cycloalkanes (Lai et al., 1992), the methods presented above may not be

applicable to these fuels. This can be further illustrated by Table 8 which shows the deviations of the estimated temperatures, calculated by the methods presented above, from the literature values for the selected hydrocarbons. From Table 8 it can be seen that while all the methods predict T_c quite well for the paraffins and aromatics, they all fail to predict T_c satisfactorily for the cycloalkanes. It is clear that a new correlation needs to be developed for the coal-derived jet fuels.

Since the coal-derived jet fuels are composed mainly of monocyclic and bicyclic alkanes and some hydroaromatic compounds (Lai et al., 1992), a new correlation must be developed on the basis of the properties of these compounds. Table 9 shows the selected model compounds and related properties, namely specific gravity, boiling point and critical temperature, used to develop the correlation for the coal-derived fuels. All the data were obtained from API Technical Data Book (1987). The functional form of the Roess equation (API Technical Data Book, 1987) was used to regress the T_c data in Table 9. Using the method of least squares, the following correlation was obtained with a correlation coefficient of 0.99695:

$$T_c = 138.98 + 2.1132\Delta - 1.4085 \times 10^{-3}\Delta^2 \quad (13)$$

The definition for Δ is given in eq 2. For all twenty-five compounds in Table 3, eq 13 gave an average absolute deviation of 0.86% and a maximum deviation of 2.75%, indicating a good fit of the data. Figure 18 shows a comparison of seven T_c estimation methods. It can be seen that the new correlation gives satisfactory predictions of the critical temperatures of the coal-derived fuel samples.

Conclusions

The critical temperature calculations using six different methods showed that while most of the methods can give satisfactory critical temperature predictions for the petroleum-derived jet fuels, they are less reliable for the coal-derived jet fuels because of the differences in the composition of these fuels.

On the basis of the boiling points and specific gravities of the compounds found in the coal-derived jet fuels, a new correlation was developed. The new correlation gives satisfactory critical temperature predictions for the coal-derived jet fuel samples.

References

1. API *Technical Data Book-Petroleum Refining*, 4th ed.; American Petroleum Institute: Washington, DC, 1987.

2. Brule, M. R.; Lin, C. T.; Lee, L. L.; Starling K. E. Multiparameter Corresponding-States Correlation of Coal-Fluid Thermodynamic Properties. *AIChE J.* **1982**, *28*, 616.

3. Cavett, R. H. Physical Data for Distillation Calculations: Vapor-Liquid Equilibria. Paper Presented to Session on Computer Applications, 27th Midyear Meeting of the API Div. Ref. **1962**, *42*(III), 351.

4. Hicks, C. P.; Young, C. L. The Gas-Liquid Critical Properties of Binary Mixtures. *Chem. Rev.* **1975**, *75*, 119.

5. Kesler, M. G.; Lee, B. I. Improve Prediction of Enthalpy of Fractions. *Hydrocarbon Process.* **1976**, *3*, 153.

6. Lai, W.-C.; Song, C.; Schobert, H. H.; Arumugam, R. Pyrolytic Degradation of Coal- and Petroleum-Derived Jet Fuels and Middle Distillates. *Prepr.--Am. Chem. Soc., Div. Fuel Chem.* **1992**, *37*, 1671.

7. Mogollon, E.; Kay, W. B.; Teja, A. S. Modified Sealed-Tube Method for the Determination of Critical Temperature. *Ind. Eng. Chem. Fundam.* **1982**, *21*, 173.

8. Riazi, M. R.; Daubert, T. E. Simplify Property Predictions. *Hydrocarbon Process.* **1980**, *59*, 115.

9. Schobert, H. H.; Eser, S.; Song, C.; Hatcher, P. G.; Walsh, P. M.; Coleman, M. M. *Advanced Thermally Stable Jet Fuels*. Technical Progress Report (July 1993 - September 1993), December **1993**, The Pennsylvania State University.

10. Twu, C. H. An Internally Consistent Correlation for Predicting the Critical Properties and Molecular Weights of Petroleum and Coal-Tar Liquids. *Fluid Phase Equil.* **1984**, *16*, 137.

5. Surface Effects on Deposit Formation in a Flow Reactor System (Contributed by Jun Li and Semih Eser)

Introduction

Mechanistic studies of jet fuel thermal stability using a flow reactor system are at least equally desirable as by static reactor systems. There are generally two kinds of flow reactors [1]: constant-heat-flux, resistant-heated long tube flow reactor [2], and constant-surface-temperature, jacket-heated short tube flow reactor [3]. The constant-surface-temperature type flow reactor generally has a better temperature control over the reactor and the fuel.

In this subsection, we will report some of the results regarding metal surface effects on deposit formation from thermal stressing of jet fuel (JP-8P) in our renovated flow reactor, which, in essence, is a constant-surface-temperature type reactor.

Experimental

The flow reactor used in this study is a renovated Chemical Data Systems (CDS) CDS Model 803 Bench Scale Reaction System. As shown in Figure 19, reactant fuel is pumped (using a Waters M600A HPLC pump, not shown) into the system, mixed with inert gas (ultra-high purity N_2), and then preheated to a maximum of 300 °C in the valve oven. The preheated mixture of fuel and inert gas is directed by an eight-port valve either to pass or by-pass an external reactor and gas/liquid separator. The stainless steel reactor can be jacket-heated up to 700 °C, and has an "isothermal" volume of about 5 mL (1/4" x 6" heated, total volume is measured at about 8 mL). Reaction products (or by-passed mixture) then pass through a back pressure regulator, which can hold the system pressure up to 1500 psi, and are collected in two sample loops (1 mL and 50 μL) for subsequent on-line GC analysis. This reactor system has one capillary column with FID detector and one small molecule column and one molecular sieve column with TCD detector, thereby is capable of analyzing a full range of gaseous compounds encountered in the thermal reactions of jet fuels or their model compounds. The gas-phase products are condensed through a copper coil tubing condenser (not shown). The condensed liquid is recovered, and the remaining gaseous products are finally vented to a hood.

Reactant fuel used in the experiments was petroleum derived JP-8P. It was pumped into the system at a flow rate of F_{fuel} 2 mL/min. The system pressure was maintained at 500 psi during the reactions. To study the effects of metal surface on both bulk phase pyrolysis chemistry and on deposit formation, we inserted metal coupons of nickel, copper, and stainless steel (1–10 cm long) into the reactor as we had done in tubing bomb reactor

experiments, and then monitored the compositional change of the vapor phase by on-line GC and characterized the morphology of deposit on the metal surface by SEM. Before heating, the reactor was purged with UHP N_2. While heating the reactor, fuel was pumped into the system and by-pass the reactor. Reaction started when the preheated fuel/N_2 mixture was switched to pass the reactor. The space time (or mean residence time) of the reactant in the reactor can be calculated from mass balance as follows:

$$\tau = \frac{V\ (ml)}{\upsilon\ (ml/sec)} \qquad \text{while}$$

$$\upsilon = \frac{(n_{N_2} + n_{fuel})\ (mol/sec)}{\rho\ (mol/ml)} = \frac{\frac{F_{N_2}}{22400} + \frac{F_{fuel} d_{fuel}}{M_{tfuel}}}{\frac{P_{rxt}}{RT_{rxt}}}$$

where F_{N2} and F_{fuel} are the flow rate of N_2 and the fuel, P_{rxt} and T_{rxt} are the pressure and temperature of the reaction, R is the gas constant, d_{fuel} and Mt_{fuel} are the density and the molecular weight of the jet fuel. The density of JP-8P fuel is reported as 0.79 g/mL [4]. The molecular weight of this jet fuel is estimated by the method of [5] to be 155 g/mol, almost the same as of undecane (C_{11}). After a certain reaction time, the mixture was switched back off the reactor. Fuel intake was shut off. The reactor was purged again with N_2 for at least 30 minutes. Metal coupons were then taken out, rinsed with hexane, and weighed to find the deposit weight due to the reaction.

Results and Discussion

Gas Phase Analysis. A set of JP-8P thermal reactions are run at temperatures from 450–625°C without the insertion of metal coupons as the baseline test. As shown in Figure 20a, JP-8P fuel is composed mainly of C_8–C_{16} normal alkanes. Up to 500°C, there is little thermal cracking of the original fuel. However, at about 525°C, we can see the low end products (C_5–C_7 normal alkanes) starting to show up. By 550°C, the build-up of *n*-pentane (retention time t_r = 2.10 min.) and *n*-hexane (t_r = 2.37 min.) has really become obvious. As temperature continues to increase, low end alkanes become the major components in the cracked products (Figure 20b). Also from Figure 20, we can see that higher alkanes diminish earlier. At 550 °C, most of the C_{12} and higher alkanes have been converted to lower compounds. And it takes temperature as high as 625°C to convert the primary and/or secondary C_9–C_{11} alkanes to smaller compounds such as pentane and hexane. It is noticed that the opposite process of cracking, polymerization, which should be part of the reaction

mechanisms to form carbonaceous deposit in static tubing bomb experiments, does not occur under these circumstances.

With the experience from the baseline test, nickel coupons of 1, 3, 5, 7, and 9 cm long and 0.5 cm wide are inserted into the reactor to collect deposit. The reaction takes place at 600°C for 5 and 10 hours. Figure 21a shows the gas chromatogram of samples collected at the reaction times of 100 min. (jpni6002), 195 min. (jpni6003), and 295 min. (jpni6004). Similarly, Figure 21b shows the gas chromatogram of samples collected during a different run at reaction times of 35 min. (jpni5991), 370 min. (jpni5993), and 570 min. (jpni599 5). The reaction products as well as their distribution are shown not to change with the existence of the nickel coupons. Neither do they change with the reaction time. However, a more detailed quantitative analysis of the products distribution may give more convincing proof.

Since not much deposit is formed on nickel surface after 10 hours of reaction, the temperature is raised to 625 °C to study the copper and stainless steel surface. Figure 22 shows the chromatogram of samples collected at reaction times of 5 min. (jpcu6251), 90 min. (jpcu6252), 190 min. (jpcu6253), and 270 min. (jpcu6254) while copper coupons of 1, 3, 5, 7, and 9 cm long and 0.5 cm wide are inserted in the reactor. As expected, the conversion of higher end hydrocarbons to smaller compounds increases compared to the above nickel tests. However, the cracking products as well as their distribution do not seem to change with the reaction time. Similar results are found from Figure 23, which shows the chromatogram of samples collected at reaction times of 10 min. (jpst6251) and 100 min. (jpst6252) with stainless steel coupons of 1, 3, 5, 7, and 9 cm long and 0.5 cm wide inserted in the reactor.

The conversion of large molecules and products distribution with or without metal coupons involved are more clearly shown in Figures 24a and 24b. From Figure 24a, we can see that much more large molecules are converted to small compounds such as pentane or hexane as temperature increased from 600°C with nickel surface to 625°C with copper and stainless steel surfaces. The conversion is lower without any metal coupons than with copper or stainless steel coupons at the same temperature, and is also lower than with nickel coupons at a lower temperature. This is not definitely proved because the mean residence time in the neat jet fuel runs is shorter. The time is about 2, 7, 9, and 9 seconds for neat, with nickel, copper, and stainless steel coupons, respectively. From Figure 24b, we can see that while the conversion increases with the presence of metal coupons, the distribution of the products does not seem to change. This indicates that the current metal coupon surface does not significantly alter the bulk cracking chemistry, due most likely to the small area of the metal exposed to the reactants.

Deposit Morphology. As mentioned above, less than 1 μg deposit formed on any of the nickel coupons after 5 or even 10 hours of thermal reaction. Nevertheless, the nickel coupons are discolored (blackened and purpled). Under an SEM, we can see that there are a few deposit particles scattered on the coupon surface (Figure 25a and b). These particles do not have a preference to the surface sites, be they rough (Figure 25a) or polished (Figure 25b), grains or their boundaries. After a separate 10 hour test run, aggregates of deposit can be seen on the nickel surface (Figure 26a), the aggregates most likely result from gas-phase, chain-like carbon black (Figure 26b). On two of the nickel coupons, the aggregates are observed to grow to cover some extended areas (Figure 27a). forming a thick deposit layer taking the shape of the substrate surface (Figure 27b). These micrographs suggest that the nickel surface has little effect on the incipient deposition on the surface under the conditions studied.

Things are different with copper coupons. Heavy deposition is observed on the coupon surface after 5 hour test at 625°C. 37 μg of deposit, for example, is formed on a 5 x 90 mm copper coupons. The metal coupons become brittle after the reaction. Under the SEM, colonies of deposit aggregates are observed on the copper surface (Figure 28). The aggregates are formed of entangled whisk carbon. (Figures 29a and 29b). It can also be seen that the copper surface is first covered by a thin layer of arrow-head carbon deposit (Figure 30a and b), similar to those reported by Albright [6]. Under these conditions, the copper surface is seen to be more active than the nickel surface at a lower temperature.

With stainless steel (304) coupons present in the reactor, more deposit is formed (the reactor was even clogged after 3 hours of reaction). The deposit is spherical (Figure 31a and b) and is aggregated in chains to form particulate mound. This deposit is most likely formed in the gas phase.

References

1. H. H. Schobert, S. Eser, C. Song, P.G. Hatcher, P.M. Walsh, and M.M. Coleman,*Advanced Thermally Stable Jet Fuels*, Technical Progress Report, 92PC92104-TPR-3, 15-40, 1993.

2. P. J. Marteney and L. J. Spadaccini, *J. Eng. Gas Turbines & Power*, **108**, 648-653, 1986

3. J. S. Chin, A. H. Lefebvre, and F. T. Y. Sun, *J. Eng. Gas Turbines & Power*, **114**, 353-358, 1992.

4. H. H. Schobert, S. Eser, C. Song, P.G. Hatcher, P.M. Walsh, and M.M. Coleman, *Advanced Thermally Stable Jet Fuels*, Technical Progress Report, 92PC92104-TPR-5, 10-18, December, 1993.

5. Technical Data Book - Petroleum Refining, 4th ed., American Petroleum Institute, Division of Refining, Washington, DC, **2-15**, 1987.

6. L.F. Albright and T.C. Tsai, in Pyrolysis: Theory and Industrial Practice, L.F. Albright, B. L. Crynes and W.H.Corcoran, Editors. Academic Press, New York, 233-254, 1983

Task 2. Investigation of Incipient Deposition

Uncertainty Analysis on Growth and Deposition of Particles During Heating of Coal-Derived Aviation Gas Turbine Fuels (Contributed by Prashant C. Sanghani and Andre Boehman)

In the previous report we described the uncertainty analysis for measurements of the kinetics of deposit and particle formation [1]. We are presenting further analysis on describing uncertainty in our data. Deposit formation occurs through liquid phase, vapor phase or direct reaction at the wall i.e. reactive species from the gas phase reacts directly with wall solids and becomes part of deposit layer. The amount of solid formed varies from 5 mg to 500 mg. Identifying the important mechanisms which contribute significantly towards deposit formation is part of development of the kinetic model.

We need to associate the solid formed to the respective mechanism and then associate that with a change in fuel composition, time, heating rate, presence of oxygen and evolution and growth of particles in our model. This model then can be incorporated in to computational fluid dynamics codes for air craft systems. We have mentioned earlier that the accuracy of the model depends on the uncertainties associated with the measurement of relevant variables such as weight change, species concentration, particle size, temperature, pressure and the overall reproducibility of the tubing bomb.

Particle size measurement was found to be a strong function of the refractive index when particles absorb light and/or are very small (<0.1μm). Size measurement is also sensitive to the concentration of particles. When a particle absorbs light and it is larger than 0.5 μm the size distribution is not sensitive to refractive index (R.I.), if both real and imaginary components of the refractive index are used in the measurement. A particle size we observed range from 0.8 μm to 4.5 μm. This size is much larger than 0.1 μm. Therefore in our measurement system a decent "ball park" figure for refracive index will serve the purpose.

Measurement of particle size is found to be dependent on particle concentration also. The sensitivity of particle size to particle concentration depends on particle size. Larger particles (>20μm) were indicated to be smaller in size as the percentage of laser light passing through the solution of suspended particles drops to 70%. When the solution is further concentrated so that only 35% of laser light passes through the solution, the measured median particle size of 20μm size particle drops to 8μm. Since the particle size that we encounter falls in the range of 0.8μm to 5μm, measured particle size will not be sensitive to concentration. Figures 32 and 33. show measured particle size for 100nm and

900nm particles at various concentration. In the case of 900 nm particles the size drops from a value of 880nm to 850 nm when the percentage laser light passing reduces from 94% to 36%. In the case of 100nm particles, the size measured by laser changes from 103nm to 84nm when the percentage laser light transmitted changes from 98% to 50%. Thus as long as we are in the concentration range that allows greater than 60% laser light to pass, the sample the data should be fairly accurate.

Another important point that we need to address is using the correct diluent to measure particle size. Hexane is found to precipitate significant amounts of soluble gums during the measurement process. Also the elapsed time between opening the reactor and making the measurement, affects the measured particle size.

Deposit formation is measured by the weight change of the tubing bomb on a weighing balance. During this process the tubing bomb goes through a variety of changes. The accuracy of the balance was found to be ±0.3 mg and it does not change with an increase in weight, i.e. accuracy, remains the same whether we measure 10 g or 170 g. During the early stages of deposit growth, deposited material may weigh as little as 15 mg or less. Compared to the uncertainty interval of ±0.3 mg, a deposit weight of 15 mg is substantial with a relative uncertainty of just 2%. However this is not the case. The tubing bomb needs thread lubrication and it is inserted into a sand bath and then quenched in water. Very often it is difficult to open the reactor (especially after long reaction times) without applying force or a gentle tapping with a hammer. During this process it is very likely that we will alter the weight of reactor significantly. To address this problem, several dummy tubing bomb reactions were carried out with lubricant on the thread and no sample in the reactor. Standard deviation (2σ) of the weight change process was determined to be ±3.5 mg, which represents 95% confidence interval for the weight change measurements. An error of ±3.5 mg for weight change of 100 mg is only ±3.5%. Error bars for the deposit measurement on the vertical wall of the tubing bomb are shown in Figure 34. Relatively high error was found for 16 hour reaction, which was due to difficulty in opening the reactor without losing some deposited material.

Uncertainty analysis for species concentration is ongoing. As mentioned earlier, there are at least ninety species that have been identified. And the species that will lead to solid formation and particle growth will be in low concentration. Though tetradecane was deliberately added as the reactive species and the formation of deposits was found to be proportional to tetradecane concentration, a more refined model requires more careful identification of the minute quantity of species that plays a significant role in solid deposition on the wall and particle formation in the bulk.

In addition, the reactor used to study degradation behaviour was considered as an ideal batch reactor with no mass transfer effects. However about 20% of the total volume of reactor is not immersed in the sand bath, consequently this portion of the reactor will be cold compared to the portion which is in the sand bath. This will cause thermal and concentration gradients within the reactor. Uncertainty associated with this effect needs to be addressed. Once all the associated uncertainties have been identified and quantified, we can determine the overall uncertainty in the data and its effect on our kinetic model using Moffat's [2] method. This analysis is underway and it will be included in our future work.

References

1. Schobert H. H. et al, Advanced Thermally Stable Jetfuel, Technical Progress Report, July 1994 - September 1994, 92PC92104-TPR-9.

2. Moffat R. J., *Experimental Thermal and Fluid Science*, 1, pp 3-17, 1988.

Task 3. Characterization of Solid Gums, Sediments, and Carbonaceous Deposits

Studies of Surface Chemistry of PX-21 Activated Carbon during Thermal Degradation of Jet A-1 Fuel and n-Dodecane. (contributed by Katia Gergova, Rathnamala Arumugam, and Semih Eser)

Introduction

In our previous studies we showed that the presence of high surface area activated carbon PX-21 together with hydrogen donor decalin prevented solid deposition on reactor walls and reduced the extent of decomposition of *n*-dodecane and jet fuel even after 5h at 450°C [1]. Adding decalin as H donor additionally reduced the extent of decomposition of jet fuel and *n*-dodecane in the presence of the carbon only. The activated carbon appears to promote H transfer reactions during thermal treatment [2]. We have suggested that the active sites of PX-21 carbon act to stabilize the pyrolysis products, enhance the H-transfer reactions and promote some cracking reactions.

The thermogravimetric studies of PX-21 stressed with *n*-dodecane or Jet A-1 fuel mixed with decalin showed that some compounds are adsorbed into the pore structure of the carbon. The desorption of these compounds during heating in N_2 up to 1000°C took place in 2–3 steps most likely due to the presence of different types of active sites or porosity.

Chemisorption of oxygen on carbon surface as well as the manufacturing process leads to generation of oxygen surface groups [3,4]. The surface groups are most often present as carboxyl, phenol, hydroxyl, carbonyl, and quinone groups. Less common on carbon surfaces are ether, peroxide, and ester groups, as well as lactones, anhydrides, and cyclic peroxides [5-7].

A distinct catalytic effect of activated carbon was observed in different reactions [8,9]. Although the nature of the carbon surface and the presence of carbon-oxygen surface structures play dominant roles in some reactions, the surface area and accessibility of the active sites are important factors in other reactions. Goughlin [10] suggested that the catalytic carbon properties could also be related to the electronic structure of the materials.

However, many of solid carbon properties, including their catalytic activities are found to be related to the presence of surface complexes. Perhaps the most important surface property of carbons as related to the surface complexes is their acid/base character. The changes on carbon surfaces occur over a range of temperature with the exact properties

depending on the carbon and the pretreatment conditions. In this study we investigate the influence of outgassing PX-21 activated carbon at 900°C for 2h in N_2 on the degradation chemistry of jet fuel and model compound *n*-dodecane at 425°C as compared to the activity of untreated PX-21.

Experimental

Thermal stressing experiments were carried out on 10 mL dodecane and petroleum derived Jet A-1 fuel mixed with 5% decalin and 50 mg PX-21. In some of the experiments PX-21 was added after outgassing at 900°C for 2h in N_2 in stainless steel vertical reactor placed in tube furnace. The experiments were carried out in microautoclave reactors pressurized with N_2 to 100 psi. The *n*-dodecane and *cis/trans* -decalin used as a model compounds were purchased from Aldrich.

Gas chromatography (GC) of liquid products was conducted using Perkin-Elmer 8500 GC with a DB-17 fussed silica capillary column. Relative percentages of the components were calculated. Compounds in the liquid products were identified by capillary gas chromatography/mass spectrometry (GC/MS) using a Hewlett-Packard 5890 II GC coupled with HP 5971 A mass selective detector.

The thermogravimetric analyses of PX-21 carbon before and after stressing experiments were carried out on a Mettler-TA 4000 System. PX-21 activated carbon before and after outgassing as well as before and after thermal stressing was characterized by N_2 adsorption at 77K using a Quantachrome automated adsorption apparatus Autosorb 1- Model ASIT, and the BET surface areas were calculated [11]. The microstructure of the PX-21 carbon after interaction with jet fuel and model compounds at 425°C, for 5h was examined using a polarized-light microscope (Nixon-Microphot-FXA) and a scanning electron microscope (SEM) ISI ABT, model SX-40A. Samples for optical microscopy were mounted in an epoxy resin and polished using alumina.

Results and Discussion

Analysis of the liquid products after thermal stressing of *n*-dodecane and A-1 jet fuel mixed with 5% decalin and 50 mg PX-21. Two series of thermal stressing experiments were carried out simultaneously on 10 mL *n*-dodecane and commercial jet A-1 fuel mixed with 5% decalin at 425°C. In the first series, the thermal stressing experiments were carried out at 425°C for different periods of time in the presence of 50 mg of original PX-21 and in the second series, 50 mg outgassed carbon at 900°C in N_2 was added to the mixture of dodecane or jet fuel with decalin. Jet fuel samples with 5% decalin as well as *n*-

dodecane mixed with 5% decalin without PX-21 were also thermally stressed under the same experimental conditions.

Some of the results obtained after stressing of *n*-dodecane+decalin+50 mg PX-21 at 425°C for different period of times are listed in Table 10. The presence of original PX-21 and outgassed PX-21 leads to suppressing of solid deposition on the metal reactor walls even after 5h at 425°C. The comparison of the color of the stressed liquids shows that the liquids obtained after thermal stressing of dodecane+decalin are always darker then the liquids obtained after stressing of dodecane+decalin+PX-21. There is a considerable change in the color of liquid obtained after thermal stressing without carbon at 425°C for 5h, from colorless liquid to light brown. These results indicate that addition of 5% decalin is not enough to suppress the thermal degradation of dodecane under the stressing conditions used. The color of the liquid obtained after stressing of dodecane+decalin+ outgassed PX-21 is lighter then the color of the liquid obtained after stressing of dodecane+decalin with original PX-21. Further, the outgassed PX-21 appears to be more active than the untreated carbon, as noted by the color after stressing at 425°C for 5h. In addition, the reactor pressure at the end of the experiments is lower, the liquid yield is higher and the increase of the weight of solid is lower for the PX-21 treated initially in N_2 at 900°C. All these data show the active role of PX-21 surface and its interactions with the model compounds during thermal stressing. In order to get a better idea on the activity of outgassed PX-21 carbon during thermal stressing of dodecane+decalin we plotted area percent of alkanes identified in the liquids obtained after stressing at 425°C for 0.5h (Figure 35). The concentration of dodecane is 5% higher for the liquid obtained after stressing with outgassed PX-21 carbon than with the untreated PX-21 carbon. On the other hand, the concentration of C_7-C_{11} alkanes produced as a result of decomposition of *n*-dodecane at this temperature have significantly lower concentrations in the liquid obtained after stressing of dodecane+decalin+outgassed PX-21. The increase in surface activity of outgassed samples can be attributed to increasing number of active sites which were not available before outgassing the carbon.

Figure 36 shows the variation of area percentage of decalin and naphthalene in the liquids obtained after thermal stressing of dodecane+decalin+PX-21 at 425°C for 0.5h. In our previous work[1] we reported that activated carbon addition appears to promote H-transfer reactions during thermal stressing and enhances the conversion of decalin into naphthalene. Figure 36 compares the activity of original PX-21 carbon and outgassed carbon as a catalyst for enhancing H transfer reactions. The concentration of naphthalene is lower in the liquid obtained after thermal stressing of dodecane+decalin+outgassed PX-21 carbon and the concentration of *cis*- and *trans*-decalin is noticeably higher, respectively.

Evidently, the conversion of tetralin into naphthalene which is negligible in the absence of carbon, proceeded more rapidly in the presence of PX-21. Furthermore, the original carbons showed higher activity than the outgassed carbons in promoting H transfer reactions. The difference can be attributed to the capacity of the carbon surface to abstract more hydrogen and redonate to stabilize the free radicals in the liquids. Original PX-21 carbon contained probably appreciable amounts of chemisorbed oxygen functional groups which were removed during outgassing. In this case, the surface oxygen complexes present on the original PX-21 carbon may be the active sites for hydrogen transfer.

Figure 37 compares the concentration of naphthalene in the liquids obtained after stressing of dodecane+decalin alone, mixed with 50 mg original PX-21, and with 50 mg outgassed PX-21 at different stressing times (0.5, 1, 3, and 5 h) at 425°C. One can see from Figure 37 that the area percentage of naphthalene does not increase linearly with the increase of thermal stressing time from 0.5 to 5h. However, there is a significant rise of the amount naphthalene identified in all liquids obtained after 0.5 h stressing. The concentration of naphthalene in the liquids obtained after stressing with outgassed PX-21 carbon is lower for all thermal stressing times used compared to the naphthalene concentration in the liquid obtained with untreated PX-21. However, the naphthalene concentration of the liquids stressed with both outgassed and original PX-21 carbon is higher than the concentration of naphthalene in the liquid obtained after thermal stressing of dodecane+decalin alone. These data suggest that part of the naphthalene comes from the pyrolytic degradation that takes place during thermal stressing. The active sites of PX-21 carbon could also promote some cracking reactions during thermal stressing resulting in higher concentration of alkanes and naphthalene. Venkateswaran et al[12] also found that carbon film deposited on the surface of quartz vessel acts both as catalyst by promoting some reactions, or as inhibitor by suppressing other reactions.

Figure 38 shows the area percentage of dodecane in the liquids obtained from thermal stressing of dodecane+ decalin without carbon, dodecane+decalin+ 50 mg original PX-21 and dodecane+decalin+50 mg outgassed PX-21 at 425°C for different time of thermal stressing. For the evaluation of the effectiveness of activated carbon in reducing the extent of decomposition of dodecane, the most important parameter will be the concentration of dodecane after thermal stressing. The amount of dodecane left after different stressing times decrease in the order: concentration of dodecane in the liquid obtained after stressing of dodecane+decalin+outgassed PX-21, followed by the concentration of dodecane in the liquid obtained after stressing of dodecane+ decalin+ original PX-21, and the lowest is the concentration of dodecane in the liquids obtained after stressing of dodecane+decalin alone. It should be noted that the concentration of dodecane

in the liquids obtained after stressing of dodecane+decalin alone and with original PX-21 does not differ substantially (maximum 3%). However, the preservation of dodecane during thermal stressing with 50 mg outgassed PX-21 is high and varies from 45 to 63% for different stressing times. One can see that the differences between the dodecane concentration in the liquids obtained after stressing of dodecane+decalin and PX-21 before and after outgassing became larger with increasing thermal stressing time from 0.5 to 5h. For instance, while for 0.5h the difference in the dodecane concentration between both liquids is 5%, for 5h thermal stressing time this difference is already 18% in favor of the liquid obtained after thermal stressing with outgassed PX-21. These data suggest that initially some of the active sites of PX-21 carbon were blocked by chemisorption of oxygen and other molecules such as hydrogen, nitrogen, sulfur, etc. The fact that the activity of the carbon diminished clearly indicated that the active sites were responsible, to a large extent, for suppressing the decomposition of dodecane during thermal stressing.

Table 11 shows the weight percentage of compounds identified in the liquids obtained after stressing of dodecane+5% decalin+50 mg PX-21 at 425°C for different stressing times. There is a large number of compounds which are not listed in Table 11 because their concentration is negligible. It appears that the pretreatment of PX-21 in N_2 at further inhibits cracking reactions and formation of smaller alkanes, cycloalkanes and naphthalenes. It is interesting that the area percentage of n-hexane coeluted with 1-hexene in the liquid obtained after stressing of dodecane+decalin+original PX-21 for 5h is much higher (22.5%) compared to that obtained with outgassed PX-21 under the same stressing conditions (5.24%). Most probably hexane is the primary product of cracking of dodecane initiated by activated carbon. The concentration of dodecane in the liquid obtained after 5h of thermal stressing of dodecane+decalin+ original PX-21 carbon is considerably lower than the amount of dodecane in the liquid obtained after thermal stressing with outgassed PX-21 at the same conditions. There is a strong possibility that the carbonaceous solid is deposited on the surface of original PX-21 carbon because of the long stressing period. These deposit can contribute to the initiation of cracking reactions and decomposition of dodecane. The surface oxygen complexes as well as the active sites formed on carbonaceous overlayers can promote cracking reactions as well as stabilize the free radicals.

Figure 5 shows the area percent of C_5-C_{12} alkanes, *cis*- and *trans*-decalin, and naphthalene in the liquids obtained after thermal stressing of A-1 jet fuel +5% decalin+50 mg PX-21 at 425°C for 5h. The short-chain alkanes, which appear as a result of cracking reactions, have the lowest concentrations in the liquid obtained after stressing of A-1+decalin+ outgassed PX-21, followed by the liquid obtained after thermal stressing with

original PX-21 and the liquid obtained after stressing of dodecane+decalin without carbon. On the other hand, the long-chain alkanes (C_{10}-C_{12}), which are present in the original jet fuel, follow the opposite trends, i.e. the outgassed PX-21 appears to preserve the long-chain alkanes present in the jet fuel. The decalin concentration is higher for the liquids obtained after stressing in the presence of outgassed carbon and the concentration of naphthalene is respectively lower compared to the amount of decalin and naphthalene in the liquid obtained after thermal stressing with original PX-21. This is most likely due to the diminished activity of outgassed carbon as a catalyst for hydrogen transfer because of preliminary removal of oxygen complexes as discussed above.

Characterization of PX-21 before and after thermal stressing with dodecane+5% decalin. Table 12 shows the BET N_2 surface area of original and outgassed PX-21 carbon and the BET surface area of the same carbons after thermal stressing with dodecane+decalin at 425°C for 5h. One can see that outgassed PX-21 before thermal stressing has slightly lower surface area than original PX-21 carbon. The decrease after outgassing is not significant, especially considering the very high surface area of both original and outgassed PX-21 carbons. The activity of PX-21 carbon does not depend only on the surface area because the outgassed carbon, which although showed a slightly lower BET surface area, was more efficient in suppressing the solid deposition and reducing the extent of decomposition of dodecane.

Table 12 also shows that there is a dramatic decrease in the surface area of PX-21 carbon after stressing with dodecane+decalin. This substantial decrease of the surface area can be associated with carbonaceous deposit on the surface of activated carbon and/or blocking of the smaller micropores by deposit. However, there should be some open porosity left after thermal stressing of original PX-21 with dodecane+decalin because the surface area of stressed PX-21 is 180 m^2/g. The outgassed carbon has rather high surface area after thermal stressing compared to the surface area of original PX-21 carbon. As we mentioned above the outgassed carbon have higher specific activity for reducing degradation of dodecane and preventing carbon deposition than the original PX-21. Most likely the outgassed carbon prevents completely the solid deposition while the original PX-21 carbon helps for reducing carbonaceous formation and deposited on the carbon surface instead on the surface of reactor walls. There is also a possibility that the carbonaceous solid deposits on the outgassed and original carbon surfaces are different type and the deposit on the outgassed carbon surface have some active species which stabilize the free radicals during thermal stressing.

We study original and outgassed PX-21 carbon as well as the carbons after stressing with dodecane and decalin at 425°C for 5h by thermogravimetric analysis and optical and scanning electron microscopy in order to determine the reason for the higher activity of the outgassed carbon. Figure 40 shows the thermogravimetric analysis of original PX-21(a) and PX-21 outgassed in N_2 at 900°C(b). During heating up to 1000°C in N_2 the total weight loss of outgassed carbon is only 16%, while the total weight loss of original PX-21 is 36%. These substantial difference of 20% in observed mass loss is an indication of presence of various functional groups on the surface of original PX-21 carbon.

In order to get some information on the amount of liquid adsorbed during thermal stressing, the thermogravimetric analysis of the original and outgassed carbons after thermal stressing was carried out in a nitrogen flow during heating up to 1000°C. Figure 41 shows the thermograms obtained. The original sample (Figure 41a) shows a sharp drop in the weight up to 200°C and continuous loss of weight there after up to 1000°C. The comparison between the weight loss of the original PX-21 and the PX-21 after thermal stressing with dodecane+decalin at 425°C for 5h indicates that the carbon adsorbed only very small amount liquid because the weight loss before and after stressing is almost the same (Figure 40a and Figure 41a). The only difference observed is that there is a sharp drop up to 200°C in the thermogram of the original sample after stressing with dodecane. The weight loss at this temperature can be considered as water desorption and desorption of some gasses initially chemisorb on the activated carbon surface. The weight loss of unstressed sample at low temperatures is smaller and is due mostly to desorption of water. After 200°C there is continuous weight loss in both stressed and unstressed samples. These results suggest that the increase of the weight of original carbon PX-21 after thermal stressing (Table 10) is due mostly to carbon deposition.

The data show different results for the outgassed PX-21 carbon. There is 10% difference in the weight loss between the unstressed sample and the sample thermally stressed at 425°C with dodecane+decalin. The 10% difference (Figure 40b and 41b) evidently results from the liquid adsorbed during thermal stressing. After the initial weight loss up to 100°C, which is attributed to the water weight loss (Figure 41b) there is a slight increase of the weight between 150 and 250°C of outgassed sample followed by continuous weight loss up to 1000°C. The increase in the weight of sample during heating in N_2 at 150–250°C can be explained by the capacity of the carbon surface to accumulate functional groups most probably with the "active" hydrogen present on the carbon surface or because of some unsaturated sites left after stressing with dodecane. In these low temperatures physical adsorption also becomes important. However, even after extensive adsorption the

weight loss of thermally stressed outgassed PX-21 carbon is 7% lower than the weight loss of thermally stressed original PX-21 carbon (Figure 41a and b). Evidently, the weight that the outgassed PX-21 gained due to the adsorption of liquid during thermal stressing is smaller than the weight that original carbon gained because of carbon deposition. These data suggest that the outgassed carbon present during thermal stressing of dodecane+ decalin not only suppress the carbon deposition on the reactor walls but also prevents the formation of carbon deposition during thermal stressing at 425°C.

We studied the structure of original and outgassed PX-21 carbon after stressing with dodecane and decalin at 425°C for 5h by optical and scanning electron microscopy. Figure 42 shows the polarized-light micrographs of original PX-21 (a and b) and outgassed PX-21 (c) after thermal stressing with dodecane+decalin. Polished surfaces of PX-21 show anisotropic structure which is unusual for activated carbons. One can clearly see that no carbonaceous solid is deposited on the surface of outgassed activated carbon (Figure 42c). Figure 42a and b shows that some carbonaceous solids are deposited on the external surface of the carbon particles with no visible deposit formation in the pore structure. Figure 42a suggests formation of liquid-phase solid deposit, while the micrograph in position b appeared to be thin flake of gas-phase deposit.

Figures 43-45 show different magnification scanning electron micrographs of original and outgassed PX-21 carbon stressed with dodecane and decalin at 425°C for 5h. These micrographs confirm our assumption that outgassed carbon prevents formation of solid deposition during thermal stressing with dodecane+decalin at 425°C. All micrographs show considerable carbon deposition on the surface of original activated carbon after thermal stressing (Figures 43-45a). This deposit appears to be mainly in the form of distinct particles which most probably blocked the considerable part of original activated carbon porosity. On the other hand, the outgassed PX-21 (Figures 43-45b) does not show visible solid deposition but the carbon surface is round and smooth and no pores can be observed. These results are confirmed by the surface area of stressed PX-21 carbons (Table 12). The N_2 BET surface area of both PX-21 carbon decreases considerably after thermal stressing. However, the surface area of the original PX-21 shows that the large part of its porosity is blocked due to carbon deposition (surface area 180 m^2/g). The N_2 surface area of outgassed PX-21 after thermal stressing is considerably higher (440 m^2/g) than the surface area of stressed original PX-21. Evidently, some of the pores of outgassed carbon do not adsorb much during thermal stressing, most probably due to their shape or because of their inaccessibility inside the carbon material, which results in higher surface area.

Conclusions

The nature and activity of activated carbon surface during thermal stressing is one of the most important parameters. The surface oxygen concentration can be reduced by outgassing of PX-21 at high temperature (900°C) in N_2. The activity of PX-21 carbon in preventing carbon deposition increases considerably with the pretreatment of activated carbon in N_2 at 900°C. The outgassed carbon showed lower catalytic activity in promoting H transfer reactions and converting decalin into naphthalene. Apparently, surface complexes on the carbon surface act as active sites for H transfer reactions.

The original PX-21 carbon contains appreciable amounts of chemisorbed oxygen, which was removed during outgassing, rendering the active sites available for the free radicals. Probably, faster termination of free radical chains reduced the degradation of model compounds and jet fuel stressed with 5% decalin.

The optical and scanning electron microscopy, of stressed carbons showed that outgassed PX-21 not only suppressed the carbon deposition on the reactor walls but also significantly reduced the formation of carbonaceous solids. The carbonaceous solid in the form of discrete particles deposited on the surface of original PX-21. The increase of solid weight of original PX-21 after stressing with dodecane or jet fuel and decalin is due to solid deposition, while the increase of solid weight of outgassed PX-21 is mostly due to adsorption of selective compounds during thermal stressing. The thermogravimetric analysis and the surface area measurements of original and outgassed PX-21 before and after thermal stressing with dodecane+decalin are in good agreement with the results obtained from optical and scanning electron microscopy.

In conclusion, the activity of activated carbon is not only dependent on its surface area but also on the nature of the carbon surface.

References

1. H. H. Schobert, S. Eser, C. Song, P. G. Hatcher, A. Boehman, M. M. Coleman, Advanced Thermally Stressed Jet Fuels, Technical Progress Report, 92PC92/04-TPR-9, July-September 1994.

2. K. Gergova, S. Eser, R. Arumugam, H. H. Schobert, Effect of High Surface Area Activated Carbon on the Thermal Stability of Jet Fuel, 5th National Conference on Stability and Handling of Liquid Fuels, Rotterdam, The Netherlands, October 3-7, 94.

3. B. R. Puri, In Chemistry and Physics of Carbon (Edited by P.L. Walker, Jr.), Vol 6, p. 191, Marcel Dekker, New York 1970.

4. K. Kinoshita, Carbon, Electrochemical and Physicochemical Properties, p.86, John Wiley and Sons, New York 1988.

5. J. Zawadzki, Carbon 16, 981, 1978.

6. C. Jshizaki and J. Marti, Carbon 19, 409, 1981.

7. H. P. Boehm and H. Knozinger, In catalysis Science and Technology, (Edited by J. K. Anderson and M. Bondart), vol. 4, p.39, Springer Verlag, Berlin 1983.

8. G. Szymanski and G. Rychlicki, Carbon 29, 489, 1991.

9. A. Guerrero-Ruiz and J. Rodriguez-Ramos, Carbon 32, 23, 1994.

10. R. W. Coughlin, Reprint 71, Proc. 4th. Intern. Conf. on Catalysis, Moscow 1968.

11. S. J. Gregg and K. S. W. Sing, Adsorption, Surface Area, and Porosity, Academic Press, London 1982, p. 285.

12. R. Venkateswaran, M. H. Back, and G. Scacchi, Carbon 32, 5, 911.

Task 4. Coal-based Fuel Stabilization Studies

Exploratory screening and development of potential jet fuel thermal stabilizers over 400°C (Contributed by Emily M. Yoon and Michael M. Coleman)

Introduction and Objectives

Thermal stability, defined as the resistance to formation of undesirable carbonaceous solids in the fuel system, is of great concern for future jet fuels. The operating temperature of aircraft fuel is expected to increase significantly in the future due to the high temperature environment of high performance engines and higher heat loads from cooling aircraft system components. Exposure to the high temperatures may result in the thermal degradation of the fuel and formation of solid deposits on critical engine parts. With the development of high-Mach craft, thermal stability of fuels would be more crucial. The fuel in supersonic aircraft may reach temperatures of 538°C (1000°F), or higher.[1]

The techniques or processes to attain a suitable thermal stability will depend upon economics, logistics, and safety. Hydrogenation and additive treatment are considered because they could be accomplished at a refinery. However, hydrogenation is costly and hydrogen may be in short supply in the future as the refining industry reduces reforming for gasoline production, in response to environmental concerns.[2] Additive treatment can be inexpensive, but the understanding on additive functions at high temperature will be required before this option is seriously considered. The objective of this study is to screen and develop a superior potential jet fuel stabilizer.

Preliminary Results of Research Performed to Date

I. Exploratory Screening of Potential Jet Fuel Stabilizers: Thermal stabilizers and well-estalished antioxidants used to protect polymers and rubbers against degradation were screened initially. Three classes of antioxidants were selected. The first class was hydrogen-donating antioxidants, such as hindered phenols and secondary aromatic amines, which inhibit oxidation by trapping free radicals. The second class was preventive antioxidants that consist of organosulfur compounds that act as peroxide decomposers. Finally, the third class of antioxidants was organotin stabilizers and aryl derivatives of tin utilized for the prevention of color formation during high temperature processing of the polymers. Table 13 lists the antioxidants screened.

Thermal stressing was performed on 10 mL samples (Jet fuel + antioxidants) at 425°C in 25 mL type 316 stainless steel microreactors under 100 psi of either air or UHP-

grade N_2. The concentration of antioxidants was varied from 0.3 to 5.0 volume%. The microreactor containing the sample was purged with UHP-grade N_2 five times at 1000 psi to minimize the presence of dissolved oxygen and finally pressurized with either 100 psi of air or N_2. It was then placed in a preheated sand bath at 425 °C for 3 hours, followed by quenching into cold water and depressurization to remove head-space gases.

Using color as a primary indicator of the degree of the degradation, it was found that none of the compounds listed in Table 13 had any significant advantageous effect on the rate of degradation of Jet A-1 fuel, and some antioxidants even promoted the rate of degradation. This may be due to the fact that most of these antioxidants were designed to function at much lower temperatures. Since conventional antioxidants failed at 425 °C, the classic hydrogenation agents employed in coal liquefaction [3] and oil products [4] were tested in next step.

The physical appearance of the neat Jet A-1 fuel after thermal stressing at 425 °C for 6 hours under 100 psi of air was compared with and without 5 volume% of the compounds, tetralin () or 1,2,3,4-tetrahydroquinoli (). These classic liquefaction reagents inhibited the degradation of Jet A-1 fuel. Similarly, the compound (benzyl alcohol) studied by Selvaraj [5] was found to have a potential as a thermal stabilizer, retarding the degradation of Jet A-1. Judging by the degree of transparency and intensity of the color, tetralin and 1,2,3,4-tetrahydroquinoline showed similar effects to that of benzyl alcohol. Since jet fuels are intricate chemical mixtures of hydrocarbons that become even more complex following thermal stressing at elevated temperatures, dodecane (a significant component of Jet A-1 fuel) was chosen as a model compound to quantitatively evaluate different potential thermal stabilizers.

II. Preliminary Studies of Potential Jet Fuel Stabilizers using Dodecane as a Model Compound: The following additives were compared by adding 5 vol% of; tetralin(**I**), 9,10-dihydrophenanthrene(**II**), 1,2,3,4-tetrahydroquinoline(**III**) and benzyl alcohol(**IV**) to dodecane (Dod). The chemical structures of these additives are shown below. A similar experimental procedure of thermal stressing to that described in section I, except the sand bath temperature was increased to 450 °C in order to shorten the reaction time, was performed. Quantification of the liquid products was performed by using a Hewlett Packard GC with a FID detector.

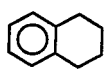

I

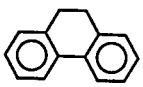

II

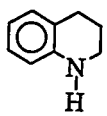

III

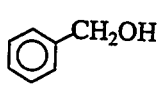

IV

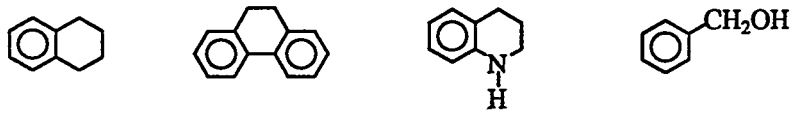

I II III IV

Figure 46 represents the effects of the additives on the mol% dodecane conversion after thermally stressing for the period of 10, 20, 30, 40 min at 450°C. In the absence of additives, the conversion of dodecane is approximately 43% after 40 min at 450°C. Based on a constant of the 5 vol% additive, 1,2,3,4-tetrahydroquinoline(**III**) inhibited dodecane decomposition the most. For example, after 40 min, 43 mol% of neat dodecane decomposed whereas only 10 mol% of dodecane decomposed in the presence of compound **III**. In order to understand the hydrogen donor mechanism and compare the free radical scavenging capabilities of the additives, studies based on molar equivalents instead of volume were performed in next step. Some additional hydrogen donor additives were also screened.

III. Quantitative Studies of Potential Jet Fuel Stabilizers based on Molar Equivalents and using Dodecane as a Model Compound: For comparison purposes, five volume% of benzyl alcohol was chosen as a standard concentration. In terms of molar equivalents this is approximately 10 mol%. Accordingly, 10 mol% (equivalent to about 5 to 6 volume% for most additives) of each additive was added to dodecane. The additives considered were tetralin(**I**), 9,10-dihydro-phenanthrene(**II**), 1,2,3,4-tetrahydroquinoline(**III**), benzyl alcohol(**IV**), benzaldehyde dimethyl acetal(**V**), phthalan(**VI**), and 1,2,3,4-tetrahydro-1-naphthol(**VII**) as shown below.

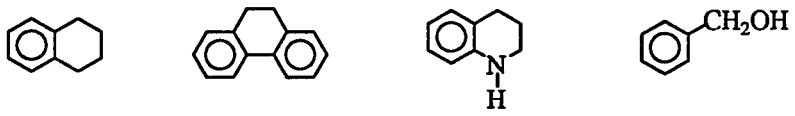

I II III IV

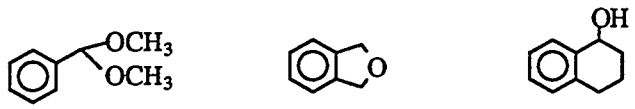

V VI VII

Thermal stressing was performed in the same manner as described in section II with initial N_2 pressure of 100psi. The liquid products were quantitatively analyzed using GC. A

Hewlett Packard GC with mass detector was used for the qualitative analysis of reaction products.

Figures 47, 48, and 49 show the effect of the additives on the degradation of dodecane after thermally stressing for periods of 10 to 45 min at 450 °C. In the absence of additives, the amount of dodecane remaining after 10, 20, 30, 40 min is 96, 73, 65, 56 mol%, respectively. Except for compound **V** (benzaldehyde dimethylacetal) which is not included in figures, the presence of the additives significantly reduces the amount of dodecane conversion. Compound **V** was totally ineffective as a radical scavenger, most probably due to the cleavage of the side group at 450 °C.

Figures 47 and 48 illustrate that compounds **II** (9,10-dihydrophenanthrene) and **III** (1,2,3,4-tetrahydroquinoline) are superior to the other additives. For example, after 45 min of reaction, about 92 mol% of the original dodecane remains in the presence of compounds **II** and **III**. Compounds **I** (tetralin), **IV** (benzyl alcohol), and **VII** (1,2,3,4-tetrahydro-1-naphthol) significantly retard degradation and are intermediate as thermal stabilizers, i.e., about 70 mol% dodecane is left after 45 min of reaction. Compound **VI**(phthalan) is not a good radical scavenger although it did inhibit the dodecane decomposition somewhat. Although compound **VII** was anticipated to be a superior thermal stabilizer compared to benzyl alcohol, because of the additional hydrogen atoms, the decomposition rate is similar to that of benzyl alcohol. This may be explained by the relatively rapid decomposition of compound **VII** to naphthalene as indicated in scheme I.

Scheme I

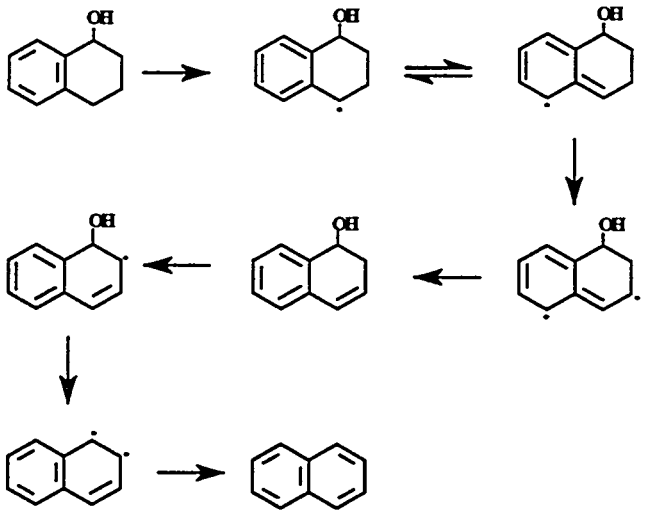

In essence, although compound **VII** gives up four protons in forming naphthalene, the conversion is too rapid and none of the additive **VII** exists in the mixture after 25 min stressing at 450°C as determined by GC/MS. Similarly, but for reasons not fully elucidated, compound **VI** in dodecane is decomposed after 35 min of reaction.

The superior performance of the compound **II** and **III** is due to the fact that they have excellent thermal stability at 450 °C in conjunction with an increase in resonance stabilization of the radical scavenger relative to benzyl alcohol. Since the compounds **II** (9,10-dihydrophenanthrene) and **III** (1,2,3,4-tetrahydroquinoline) inhibit the rate of dodecane decomposition better than benzyl alcohol (**IV**), further investigation was performed to attempt understand the mechanistic nature of stabilization by evaluating the effects of a number of new hydrogen donor additives.

IV. Additional Studies of Potential Jet Fuel Stabilizers: The results presented in the last two sections suggested the testing of further possible compounds that might be good thermal stabilizers for jet fuels and might also help to elucidate the main factors required for superior thermal stability. The additives evaluated were 3-pyridylcarbinol (**1**), 4-pyridylcarbinol (**2**), 2-hydroxybenzyl alcohol (**3**), 2-chlorobenzyl alcohol (**5**), 4-chlorobenzyl alcohol (**6**), anthrone (**7**), 1-naphthalenemethanol (**8**), 9-anthracenemethanol (**9**), 9-hydroxyfluorene (**10**), indene (**11**) as shown below, together with 1,2,3,4-tetrahydroquinoline (**4**), 9,10-dihydrophenanthrene (**12**), and benzyl alcohol (**13**).

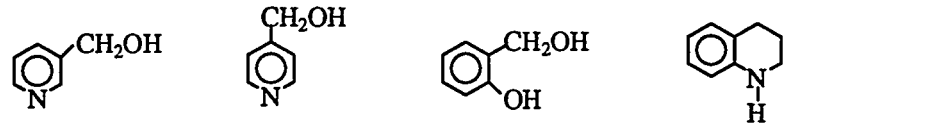

1 **2** **3** **4**

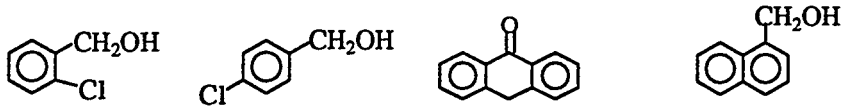

5 **6** **7** **8**

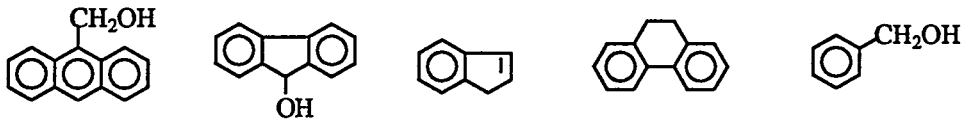

9 **10** **11** **12** **13**

Ten mol% of each additive was added based on dodecane. Due to solubility problems of some of these compounds, thermal stressing was performed at 425°C for 6 hours. The liquid products were analyzed by using a Perkin-Elmer GC with a FID detector. The side products were analyzed by using GC/MS.

Both electron-donating (**1,2,3,4**) and electron-withdrawing (**5,6**) substituents on or in the aromatic ring, as well as additional aromatic rings in succession (**7,8,9,10,11,12**), were studied in order to probe their effects on radical stability. This in turn would help to further understand the properties necessary for an efficient additive.

Shown in Figure 50 are the results from the 6 h thermal stressing of dodecane at 425°C in the presence of additives **1-6,8,10-12.** Compounds **7** (anthrone) and **9** (9-anthracene methanol) were insoluble in dodecane even after stressing at 425°C for 6 h, and resulted in the formation of various solids. The molar yields of dodecane when stressed with compounds **5** (2-chlorobenzyl alcohol) and **6** (4-chlorobenzyl alcohol) were 30% and 27% respectively. The inability of these compounds to act as efficient radical scavengers was evidenced by the formation of benzene, toluene, chlorobenzene, and chloromethylbenzene, the products of additive degradation. This appears to suggest that the presence of electron-withdrawing substituents on the aromatic ring facilitates and accelerates side group cleavage.

When compound **10** (9-hydroxyfluorene) was stressed with dodecane the molar yield of dodecane increased somewhat, although not substantially. The byproducts from this reaction were fluorene, from loss of OH, and fluorenone, the product of oxidation. The stressing of dodecane with compound **3** (2-hydroxybenzyl alcohol) resulted in a molar yield of 35% with the byproducts being benzyl alcohol, benzene and toluene. Up to this point it was discovered that any side groups on additives will undergo thermal cleavage at 425°C, which in turn results in degradation of the additive and thus decreases stabilization of dodecane.

The presence of electron-donating groups within the additives **1** (3-pyridyl carbinol) and **2** (4-pyridyl carbinol) resulted in a relative increase in the molar yields of dodecane. However, the byproducts pyridine, methylpyridine and pyridine carboxaldehyde again suggest an acceleration in side group cleavage when compared to that of benzyl alcohol, **13.**

The effect of an increase in radical resonance energy (and thus radical stability) was evaluated with compounds **4, 8, 11,** and **12.** Compounds **8** (1-naphthalenemethanol) and **11** (indene) had a relative increase in the molar yields of dodecane, but compound **8**

produced naphthalene and methylnaphthalene while compound **11** produced unidentified reaction products, again the result of additive decomposition.

Compound **12** (9,10-dihydrophenanthrene) produced a similar molar yield of dodecane compared to benzyl alcohol after stressing at 425°C. The only byproduct formed from this reaction was phenanthrene. However, a major drawback to compound **12** is that after stressing at 425°C for 6 h only 20% of the additive remains. In contrast, stressing with benzyl alcohol under the same conditions, 48% of the additive remains. Accordingly, there appears to be a definitive correlation between "additive efficiency" and the overall thermal stability of the additive. Further evidence for this conclusion was determined with compound **4** (1,2,3,4-tetrahydroquinoline).

The molar yield of dodecane when stressed under standard conditions with compound **4** was 93%. This is a dramatic improvement over benzyl alcohol (75%). Furthermore, the amount of additive **4** remaining after thermal stressing at 425°C for 6h was 78%, a marked increase relative to that of benzyl alcohol (48%). The major byproduct from the stressing of additive **4** was quinoline. A plausible mechanism for this transformation is shown in scheme II. At 425°C, initial abstraction of the N-H hydrogen by a dodecane radical leads to intermediate **A**. This radical can then be resonance stabilized by delocalization through the aromatic ring. Subsequent abstraction of a second hydrogen atom leads to a diradical intermediate, **B**, which again enjoys resonance stabilization.

Scheme II

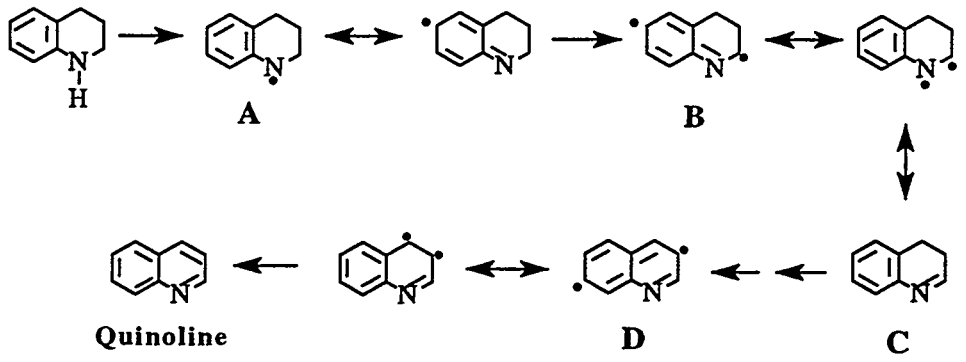

This then leads to dihydroquinoline, **C**. Abstraction of an additional two hydrogen atoms leads to a second diradical species, **D**, which again benefits from resonance stabilization. The diradical **D** presumably then rapidly aromatizes to quinoline. Hence, there are two main reasons for the dramatic efficiency of tetrahydroquinoline, **4**, relative to benzyl alcohol. First, compound **4** exhibits superior thermal stability at 425°C that infers an

increased lifetime of the additive. Second, compound **4** has four hydrogen atoms available for abstraction instead of the two available with benzyl alcohol.

From this study we have developed a set of parameters to predict the effectiveness of organic additives that can be used to thermally stabilize hydrocarbon fuels and prevent the formation of carbonaceous solids. The properties of a good additive are summarized as follows:

1. The additives must be thermally stable at temperatures above 400°C. In other words, it must not possess any side groups that could undergo cleavage and therefore promote degradation.
2. The additive must have hydrogen atoms that can be transferred or abstracted by hydrocarbon radicals. The greater the number of hydrogen atoms available for abstraction the better.
3. The radicals generated from hydrogen atom abstraction should be stabilized by resonance.

Plan for future research

Figure 51 shows the details of the past and the future research work. Based on the preliminary results, we understand that the additive itself has to be thermally stable at 425 °C. Also, the increase in resonance stabilization of the radical scavenger plays an important role. The side group on the additive has a negative effect because of its cleavage at high temperatures. Since 1,2,3,4-tetrahydroquinoline is found to be superior to benzyl alcohol, future work lies to determine the effects of the mixture of benzyl alcohol and 1,2,3,4-tetrahydroquinoline in dodecane. Also, future study will focus on improving the effectiveness of 1,2,3,4-tetrahydroquinoline, possibly through the addition of ethanol, which was shown to increase the lifetime of benzyl alcohol at 425°C.[6] Furthermore, the optimization of the additives will be studied.

References

1. Moler, J.L.; Steward, E.M.; *Prepr.Pap.Am.Chem.Soc., Div.Petrol.Chem.*, 1989, 34(4), 837-840.

2. Hazlett, R.N. Thermal Oxidation Stability of Aviation Turbine Fuels; ASTM Monograph 1, ASTM: Philadelphia, 1991.

3. Gerhartz, W., Yamamoto, Y.S., Campbell, F.T., Eds.; Ullmann's Encyclopedia of Industrial Chemistry, 5th ed.; VCH Publishers: New York, 1985; Vol. A7, 197.

4. Kubo, J. *Fuel Process. Technol.*, 1991, 27, 263.

5. Coleman, M.M.; Selvaraj, L.; Sobkowiak, M.; Yoon, E.; *Energy & Fuel*, 1992, 6(5), 535.

6. Selvaraj, L.; Stallman, J.B.; Sobkowiak, M.; Coleman, M.M; *Advanced Thermally Stable Jet Fuels*, Technical Progress Report, 92PC92104-TPR-8, July 1994.

Task 5. Exploratory Studies on the Direct Conversion of Coal to High-Quality Jet Fuels.

1. Novel Approaches to Low-Severity Coal Liquefaction and Coal/Resid Co-processing using Water and Dispersed Catalysts. (Contribution by Russell Byrne and Chunshan Song).

Introduction

The cost of coal-derived syncrudes by conventional processes ($30–35 per barrel) is not competitive with current petroleum price. Significant cost reduction of syncrudes could be achieved through the development of a more efficient liquefaction process. New approaches or further improvements of existing technologies are required.

Conventional opinion holds that water is detrimental to catalyst activity during catalytic coal hydroliquefaction [1-3]. Contrary to conventional wisdom, however, recent work in this laboratory [4-7] has demonstrated a remarkable synergistic enhancement in the conversion of Wyodak subbituminous coal through the co-use of a dispersed Mo catalyst and water under 'low-severity' conditions (325–375°C for 30 mins). This effective temperature range is much lower than those employed in current liquefaction technologies (400–470°C).

An example of this observed synergistic enhancement in conversion of Wyodak Subbituminous coal through co-use of dispersed Mo catalyst and water is illustrated in Figure 52 for reactions performed at 350°C for 30 mins in the absence of any organic solvent. The catalyst precursor employed was the water soluble inorganic salt ammonium terathiomolybdate (ATTM) at a loading of 1 wt% Mo to dmmf coal, catalyst impregnation was achieved by incipient wetness. The water/dmmf coal weight ratio employed was 0.46. As can be seen from the data represented in Figure 52, relative to the non-catalytic run of the dried coal, the addition of water alone improved coal conversion from 14.5 to 22.5 wt% (dmmf). The use of ATTM alone increased conversion from 14.5 to 29.8 wt%. When a small amount of water was added to the catalytic reaction at 350°C, however, coal conversion increased dramatically to 66.5 wt%. This represents a 359% increase from the non-catalytic run without water, and a 123% increase from the catalytic run without water.

Significantly, in stark contrast, our preliminary work has also revealed that at higher reaction temperatures (400–450°C) water addition has a detrimental impact on catalyst activity and coal conversion, as illustrated in Figure 53. The influence of reaction temperature on overall conversion for the Wyodak coal/ATTM/water system is also

depicted in Figure 54. Figure 54 clearly displays a volcano-shaped change in conversion with increasing reaction temperature, indicating a maximum conversion for Wyodak coal of almost 80 wt% at 375°C.

These interesting findings have provided the impetus behind an ongoing project which is designed to be a fundamental and exploratory study of the promotional effects of water on catalytic coal hydroliquefaction and their co-processing with residual materials. The overall goal being to develop an efficient low-severity liquefaction process resulting in high conversion of coal into solvent-soluble materials amenable to subsequent facile upgrading to produce thermally stable jet fuels.

Overview of Research Approach

The primary objectives of this research are 1) to clarify the origin of the promotional effects of water on low-severity catalytic coal liquefaction using dispersed catalysts, and 2) to explore the potential of H_2O-promoted catalytic reactions for application in coal liquefaction and co-processing of coal with petroleum resids.

The research will comprise of two complementary technical approaches: 1) conducting model compound studies on the effects of water on bond cleavage and cross-linking reactions of various coal-related structures containing etheric C–O, methylenic C–C linkages, and other O-containing functionalities such as phenolic OH and carbonyl C=O groups in the presence of dispersed Mo catalyst; and 2) performing catalytic liquefaction of coals and their co-processing with petroleum resid under low- and high-severity conditions.

The first technical approach involving the study of the catalytic hydrothermal reactions of a series of model compounds is intended to yield fundamental information regarding the physical/chemical role of water on the thermal reaction pathways of various coal structures in the presence of dispersed catalyst, and molecular hydrogen. These reactions should lead to a more secure understanding of key structural transformations occurring within coal in the presence of water and dispersed catalyst.

The second major technical approach is to perform a comprehensive series of coal liquefaction and co-processing experiments with the intent of identifying relevant catalyst/coal reaction systems and process conditions for optimum catalyst-water synergistic effects for promoting low severity coal conversion. The distinction between the liquefaction and co-processing experiments lies in the use of a petroleum residuum as a process solvent in the latter runs. The inherent advantages of co-processing include the simultaneous coal conversion and upgrading of heavy petroleum resids, a reduction in the need for solvent recycle, and an increase in 'petroleum-like' character of resulting

transportation fuels. There are also additional chemical benefits, such as synergistic effects in hydrogen transfer and the adsorption of metal species in the resids by coal, which reduces deactivation of supported catalysts in down-stream processing.

The following reaction variables will be examined: 1) choice of dispersed catalyst including both water soluble and an oil soluble precursor; 2) effect of catalyst loading level; 3) influence of coal rank; 4) effect of reaction temperature in the range of 325–425°C; 5) effects of reaction vehicles including pure solvents and process solvents—in particular, the use of a petroleum residuum as process solvent will be investigated to determine whether there are any strong promotional effects between water and dispersed catalyst under co-processing conditions; and 6) effect of H_2 partial pressure.

The culmination of these approaches will provide valuable mechanistic information concerning the chemical influence of water/dispersed catalyst systems on coal depolymerization reactions, and may contribute to the development of novel low-severity catalytic coal liquefaction processes.

References:

1. Bockrath, B.C.; Finseth, D.H.; Illig, E.G. *Fuel Process. Technol.* **1986**, 12, 175.
2. Ruether, J.A.; Mima, J.A.; Kornosky, R.M.; Ha, B.C. *Energy & Fuels.* **1987**, 1, 198.
3. Kamiya, Y.; Nobusawa, T.; Futamura, S. *Fuel Process. Technol.* **1988**, 18, 1.
4. Song, C.; Saini, A.K. *Energy & Fuels*, **1995**, 8(6), in press.
5. Song, C.; Schobert, H.H.; Saini, A.K. *Am. Chem. Soc. Div. Fuel Chem. Prepr.* **1993**, 38, 1031.
6. Song, C.; Schobert, H.H.; Saini, A.K. *Energy & Fuels.* **1994**, 8, 301.
7. Song, C.; Saini, A.K. *Am. Chem. Soc. Div. Fuel Chem. Prepr.* **1994**, 39, 1103.

2. Shape-Selective Naphthalene Hydrogenation for Production of Thermally Stable Jet Fuels. (Contributed by Andrew D. Schmitz and Chunshan Song)

Introduction

In our first report on the hydrogenation of naphthalene (Nap), we discussed our initial screening tests of platinum- or palladium-loaded zeolite catalysts. Several key observations were made: 1) catalysts based on dealuminated mordenite (HM38) gave the highest *trans*-decalin (t-DeHN) selectivity, 2) palladium catalysts afford higher t-DeHN selectivity than platinum catalysts, 3) metal crystallite sizes are highly dependent on the zeolite—palladium generally had higher dispersion than platinum on the same zeolite, 4) there is a loose correlation between decreasing particle size and increasing t-DeHN selectivity, and 5) there are striking differences in activity and selectivity between original and repeat catalyst tests which were thought to be linked to catalyst moisture content.

Reproducibility of the catalyst test results is very important. This report addresses several fundamental studies aimed at furthering our understanding of parameters that affect reproducibility as well as initial selectivity of some catalysts. One important variable is the catalyst's moisture content. Moisture contents were determined by thermal gravimetric analysis (TGA). The performance of two catalysts were compared after the following catalyst treatments: storage in a desiccator for an extended period, freshly calcined, and freshly calcined with added water.

In some cases, hydrogen-pressurized reactors were stored overnight to test for leaks evidenced by pressure loss. We speculated that naphthalene could react in the hydrogen-pressurized reactors, even at room temperature. In order to test this theory, two loaded reactors were allowed to stand at room temperature for 12 h before the contents were removed and analyzed. Additional fundamental studies were done to probe the kinetics and the thermodynamics of *cis*- to *trans*-decalin isomerization.

Previously, we reported naphthalene conversions at approximately 100% in all catalyst tests by A. Schmitz [1]. This was true even in 15 min tests of Pt/HM38 and Pd/HM38. It is of interest here to examine the conversion and product distribution in still shorter runs. HM38-supported samples prepared by G. Bowers were in short supply, so new samples were prepared for these tests. HY-supported catalysts were also examined in short runs because their product distributions are so interesting: Pt/HY produces a high concentration of c-DeHN, while Pd/HY is more selective for t-DeHN.

Experimental

Preparation of 6% Pt/HM38(AS). The incipient wetness pore volume of HM38 was determined by impregnation with water, 0.88 mL/g. Accordingly, 5.72 g of HM38 should require 5.0 mL impregnation solution. For 6% loading of platinum, 0.85 g $H_2PtCl_6 \cdot xH_2O$ (Aldrich, 99.995% Pt on metal basis, 38.7% Pt in the salt) was weighed into a test tube and 5.0 mL water was added. Even after allowing the mixture to stand overnight, and then warming, the salt was not completely dissolved. Three drops conc. hydrochloric acid were added, then 0.5 mL water, neither increased solubility. Since the residual solid could not be dissolved, the supernatant was decanted by pipette onto the support so as to achieve incipient wetness, 5.3 mL. The mixture was allowed to stand overnight to assure even penetration of the support. Subsequently, water was removed on a rotary-evaporator in temperature stages from 40–80 °C. The solid was dried overnight in vacuo at 100 °C, then calcined 4 h at 450 °C in air. Since not all of the metal salt was dissolved and transferred, the metal loading on the support will be somewhat less than 6%. Initials are added to the catalyst name to denote this catalyst as having been prepared by A. Schmitz, rather that the Pt/HM38 catalyst prepared earlier by G. Bowers.

It is important that sufficient impregnation solution be added to reach the *viscous fluid state*: suspension of the support powder in a very slight excess of impregnation solution. Prior to this point, the wetted support behaves as a clay, and wetting of the support is uneven. At the point when enough impregnation solution has been added, the solid no longer clumps together as a clay, but flows slowly as a very viscous liquid. It is not possible to insure even wetting of the support unless the *viscous fluid state* is reached.

Preparation of 6% Pd/HM38(AS). Dissolved 0.5509 g PdCl2 (Aldrich, 99.999% Pd on metal basis, 59.8% Pd in the salt) in 5.3 mL 2.3 M hydrochloric acid. Complete dissolution required letting the mixture stand overnight. To 5.17 g HM38 was added 4.8 mL of the impregnation solution to reach the *viscous fluid state*. Drying and calcination procedures were the same as described for Pt/HM38(AS). From formulation, the palladium loading is ca. 5.9% based on the dry zeolite mass. Again, the *AS* initials denote that this catalyst was prepared by A. Schmitz, rather than the Pd/HM38 catalyst prepared earlier by G. Bowers.

Thermogravimetric Analysis (TGA). TGA runs were done on a Mettler TG50 thermobalance using 200 mL/min air flow. The temperature was ramped from 30 to 800 °C at 10 °/min. Sample weight losses were corrected for weight loss of the empty sample crucible under the same run conditions.

Reactor Tests and Product Analyses. The methods used here are identical to those reported earlier. Reactions were run in horizontal tubing-bomb reactors charged with 0.4 g catalyst, 1.0 g (7.8 mmol) Nap, 4.0 g *n*-tridecane reaction solvent, and 0.35 g *n*-nonane internal standard. For the room temperature runs, Pt/HM17 and Pd/HM17 were loaded in two separate reactors in the usual manner. The reactors were pressurized with hydrogen and allowed to stand at ambient (25 °C) for 12 h.

Results and Discussion

Equilibrium Decalin Isomer Distribution. The data in Table 14 were collected to determine the maximum attainable trans/cis-DeHN ratio. Pd/HM38 afforded the highest t-DeHN selectivity in our earlier tests but was in short supply. Therefore, catalyst Pd/HM21 was chosen for these experiments since it showed the second highest t-DeHN selectivity of all the catalysts previously tested. As shown in Table 14, an approximately constant trans/cis-DeHN ratio of 13.6 is obtained within 6 h reaction time. The equilibrium *trans/cis*-DeHN ratio calculated by W-C. Lai is 20.5 at 200 °C. However, 13.6 may be the practical limit. Some decalin may reside in the portion of the reactor that extends above the sand level in the fluidized sand bath, the cold zone, and may not react. According to calculations, if even 5% of the decalin doesn't react to form an equilibrium amount of t-DeHN, the equilibrium ratio falls to 13.0 .

Product Distribution as a Function of Reaction Time. We had already seen with catalysts prepared by G. Bowers in 1 h, 200 °C runs that Pt/HY produces a high concentration of c-DeHN, while Pd/HY is more selective for t-DeHN [1]. Thus it is possible to choose the decalin isomer that is formed by the proper choice of catalyst. We wanted to find out if even higher c-DeHN selectivity could be obtained with Pt/HY in short runs; Pd/HY runs were done for comparison. These data are shown in Tables 15 and 16, respectively. In all cases, the Nap conversion is approximately 100%. Some tetralin (TeHN) is formed over Pt/HY. It should be pointed out that the shortest reaction time used, 6 min, is the approximate time required for the interior of the reactor to heat-up to the reaction temperature of 200 °C.

The trend for Pd/HY is similar to that observed for HM38-supported catalysts; that is, initial selectivity for t-DeHN is moderately low, but increases with time as c-DeHN is isomerized to t-DeHN. However for Pt/HY, the initial selectivity for t-DeHN is very low and remains approximately unchanged with time (*trans/cis*-DeHN = 0.25). For some reason, Pt/HY does not promote the thermodynamically favored isomerization. The earlier test of Pt/HY gave *trans/cis*-DeHN of 0.18 (run 166). This value is 28% lower, so the difference is probably not simply due to experimental error. For run 166, the pressurized

reactor was allowed to stand at ambient for 3.5 h before it was placed in the sand bath for the reaction. Also, three reactors were placed in the sand bath simultaneously. However for runs 184-187, the time between pressurization and the start of the runs was only 5–20 min, and only one or two reactors were in the sand bath at any given time. It is now known that Nap does react at room temperature to form mostly TeHN (vide infra). But it is not clear if, or how, this would effect the decalin isomer distribution. Having multiple reactors in the sand bath simultaneously may jeopardize temperature uniformity, possibly causing cool spots. Since the isomerization of c-DeHN becomes more favorable as the temperature is raised, cool spots would result in lower *trans/cis*-DeHN ratios.

The newly prepared metal-loaded HM38(AS) catalysts were also tested over a progression of reaction times. These data are compared with earlier data from catalysts prepared by G. Bowers in Tables 17 and 18. Both AS- catalysts give complete Nap conversion, with little or no TeHN, even in very short runs. However, the differences in t-DeHN concentrations afforded by A. Schmitz and G. Bowers catalysts are amazing. In only 1 h reaction time, both Pt/HM38(AS) and Pd/HM38(AS) give a decalin isomer distribution approaching the practical equilibrium of 13.6 (see Table 1). Data for AS catalysts are also compared graphically in Figure 55. Pd/HM38(AS) has higher initial selectivity for t-DeHN, but both catalysts give essentially the same isomer distribution within 1 h reaction time. We have already seen with the various G. Bowers catalysts that higher metal dispersions generally give higher *trans/cis*-DeHN ratios. It is suspected that the metal dispersions are very high for the AS-catalysts. XRD line broadening and/or TEM measurements will be made for confirmation.

Kinetics of Decalin Isomerization Over Metal-Loaded HM38 Catalysts. The following is a reaction scheme for Nap hydrogenation, where N = naphthalene, C = *cis*-decalin, and T = *trans*-decalin. Since TeHN is an intermediate and is not observed at significant levels in the more recent work, it is not included.

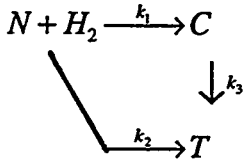

The rate equations for each of the species in the scheme is given below.

$$-\frac{dN}{dt} = (k_1 + k_2)N \qquad (1)$$

$$\frac{dC}{dt} = k_1 N - k_3 C \qquad (2)$$

$$\frac{dT}{dt} = k_2 N + k_3 C \qquad (3)$$

The hydrogenation is assumed to be pseudo first-order in naphthalene which is considered a valid approximation. Equation (1) is then a simple first-order expression that can be integrated to give

$$N = N_o \exp[-(k_1 + k_2)t] \qquad (4)$$

Substitution of N from (4) into (2) gives (5) which is a standard differential equation with integral form shown in (6).

$$\frac{dC}{dt} = N_o k_1 \exp[-(k_1 + k_2)t] - k_3 C \qquad (5)$$

$$C = N_o \frac{k_1 + k_2}{k_1 + k_2 - k_3}\left\{\exp(-k_3 t) - \exp[-(k_1 + k_2)t]\right\}$$

$$= N_o K\left\{\exp(-k_3 t) - \exp[-(k_1 + k_2)t]\right\} \qquad (6)$$

Naphthalene is very rapidly hydrogenated to a mixture of decalins, highly enriched in *cis*; *cis*-decalin is then isomerized to *trans*-decalin in the much slower second-step of this consecutive reaction series. Therefore, the relative magnitudes of the rate constants can be summarized as $k_1 >> k_3 \geq k_2$.

Considering (6) again, since $(k_1 + k_2 \sim k_1) >> k_3$, the exponential term is dominated by $\exp(-k_3 t)$. Therefore, following rapid hydrogenation of naphthalene to predominantly *cis*-decalin, the concentration of *cis*-decalin should decrease exponentially with time as shown by the first-order expression in (7).

$$C = N_o K \exp(-k_3 t) \qquad (7)$$

In the range of 15–60 min, the G. Bowers Pt/HM38 and Pd/HM38 show a linear decrease in log *cis*-decalin concentration vs. time (see Figure 56). Values for k_3, the rate constants for cis- to trans-decalin isomerization, determined from linear least-squares regression, are given here: for Pt/HM38, 0.78/h or 15.3 mmol/g-cat.h; and for Pd/HM38, 0.84/h or 16.3 mmol/g-cat.h. All of the rate constants could be determined if $k_1 + k_2$ could be measured from naphthalene concentration vs. time data. However, reaction

conditions would have to be changed to slow the reaction to make theses measurement; e.g., decrease the catalyst mass charged into the reactor. Regardless, it is seen that not only does palladium have a higher initial selectivity for t-DeHN, it also isomerizes c-DeHN more rapidly than platinum on HM38 support.

An expression for *trans*-decalin concentration can be obtained from the mass balance

$$T = N_o - N - C \qquad (8)$$

$$T = N_o\{1 - \exp[-(k_1 + k_2)t] - K\exp(-k_3 t)\}$$
$$\approx N_o - K\exp(-k_3 t) \qquad (9)$$

From (9), the *trans*-decalin concentration is equivalent to the initial naphthalene concentration minus the *cis*-decalin concentration, which is reasonable given that the rate of direct hydrogenation of naphthalene to *trans*-decalin is comparatively very slow.

First-order plots for Pt/HM38(AS) and Pd/HM38(AS) are shown in Figure 57. The reaction over AS catalysts is equilibrium limited, even after very short reaction times. The first-order plots are therefore not linear and can't be used for calculation of rate constants.

It is interesting to note that in the case of Pt/HY catalyst, the value of k_3 is approximately zero since c-DeHN is not isomerized by this catalyst. The relative magnitudes of k_1 and k_2 can be estimated from the trans/cis-DeHN ratio obtained over this catalyst at 200 °C, 0.25. Hydrogen addition to the same face of Nap to produce c-DeHN occurs four-times faster than hydrogenation on opposite faces to produce t-DeHN. Trans-addition requires multiple adsorption events with sequentiial addition of hydrogen to opposite faces of Nap.

Room Temperature Reactions. In some cases, hydrogen-pressurized reactors were stored overnight to test for leaks evidenced by pressure loss. Two reactors were loaded with catalyst, one with Pt/HM17 and the other Pd/HM17, and allowed to stand at room temperature for 12 h. The contents were then removed and analyzed. Naphthalene reacts in the hydrogen-pressurized reactors, even at room temperature, to produce mainly TeHN as shown in Table 19. Although we were surprised to learn that Nap reacts so readily at room temperature, it is not surprising that only small amounts of DeHN are formed. The rate of Nap hydrogenation to TeHN is ca. 21 times faster than that for TeHN hydrogenation. It has also been shown that palladium supported on strongly acidic supports is electron deficient. Electron rich species such as Nap may adsorb very strongly which slows the hydrogenation reaction. This may explain why Nap conversion is much higher over Pt/HM17.

Influence of Catalyst Moisture Content. Differences in reactivity and selectivity between initial and subsequent tests of catalysts prepared by G. Bowers have always been puzzling to us. Room temperature activity provides a possible explanation for differences in activity, but does not seem to explain the enhanced t-DeHN selectivity observed for some re-tests of stored G. Bowers catalysts. Another curiosity is the increase in t-DeHN selectivity brought about by re-calcining stored samples. As a first step to investigate these problems, the moisture content of two stored and re-calcined samples were determined by TGA (see Table 20). Calcination removes approximately 5% moisture. Interestingly, Pd/HM21 retains a higher moisture content than Pt/HM21. This may be due to the preparation methods. $PdCl_2$ is not soluble in water so dilute hydrochloric acid is used as an impregnation solvent; whereas, water is the impregnation solvent for $H_2PtCl_6 \cdot xH_2O$. Hydrochloric acid at concentrations as low as 1 M leaches a significant amount of aluminum from the framework of mordenite. During the impregnation of $PdCl_2$, the aluminum salts are not washed from the surface of the zeolite, rather they remain as strong acid sites. These new surface acid sites will provide additional sites for water adsorption, and possibly, increased acid-catalysis activity. The surface aluminum may act in synergy with palladium or may be sufficiently mobile to interact with other adsorbed species during the reaction.

Tables 21 and 22 compare the performance of the metal-loaded HM21 catalysts with the various treatments. For Pt/HM21, neither re-calcination nor added water changes the amount of TeHN produced or the Nap conversion to coincide with G. Bowers data. For both Pd/HM21 and Pt/HM21, calcination increases the trans/cis-DeHN ratio; whereas, added water brings the trans/cis-DeHN ratio into the range coinciding with G. Bowers data but does not effect conversion or TeHN yield.

Conclusions

We were somewhat surprised to learn that a significant portion of the Nap can react when the pressurized reactors are allowed to stand at ambient temperature. Room temperature reaction of Nap may explain some discrepancies in data for repeated catalyst test. We also learned that Pt/HM17 has higher activity than Pd/HM17 at 25 °C. At 200 °C with the chosen reactor loading, it is not possible to rank catalyst activity due to complete conversion of Nap, even in very short runs. During the next phase of this work, we will reduce the metal loading on the zeolite to 2% and decrease the catalyst charge in the reactor to 0.1 g. This should allow us to compare catalyst activities at 200 °C and evaluate sulfur tolerance.

Catalyst moisture content effects the decalin product distribution. Freshly calcined catalysts give the best t-DeHN selectivity. Addition of water to a reactor with freshly calcined catalyst does not result in a measurable change in activity, but does seem to poison c-DeHN isomerization active sites.

The newly prepared catalysts, Pt/HM38(AS) and Pd/HM38(AS) have very high activity. With both of these catalysts, a near equilibrium trans/cis-DeHN ratio is obtained within 1 h reaction time. It is thought that the careful impregnation procedures used for these catalysts led to higher metal dispersions than were achieved in earlier preparations by G. Bowers. Physical characterization studies will be used to confirm this.

It is generally observed in the Nap hydrogenation experiments that c-DeHN is rapidly formed and isomerizes to t-DeHN. However, we have succeeded in identifying a unique catalyst, Pt/HY. It produces c-DeHN with high selectivity and does not promote the isomerization.

References

1. Schmitz, A.D.; Bowers, G.; Song, C. *Advanced Thermally Stable Jet Fuels*, Technical Progress Report, 92PC92104-TPR-9, p 37.

2 Lai, W.-C.; Fuel Science Program, The Pennsylvania State University, University Park, PA, personal communication, 12/94.

3. Design of a Batch Mode and a Continuous Mode Three-Phase Reactor Systems for the Liquefaction of Coal and Upgrading of Coal Liquids (Contributed by P. Vijay and Chunshan Song)

INTRODUCTION

Experiments in Tubing Bomb Microautoclave Reactor. Extensive research studies on various aspects of the liquefaction of coal in the presence of a solvent and dispersed catalyst were conducted earlier [1]. Researchers have studied and documented the effect of temperature programmed liquefaction (TPL) of coal in the presence of a dispersed catalyst and solvent [1]. Results pertaining to the strong synergistic effects between water and dispersed molybdenum catalyst for promoting low-severity liquefaction of coal at lower temperatures have been published elsewhere [2]. All these experiments were successfully conducted in a 25 ml tubing bomb microautoclave reactor.

Significance of a Continuous Flow Reactor System for the Liquefaction of Coal and the Upgrading of Coal Liquids. In order to simulate conditions prevalent in an industrial-type reaction atmosphere, it is necessary to conduct coal liquefaction experiments and the upgrading of coal liquids in a continuous reactor system. Besides, in a continuous flow reactor system the catalyst moves with the products rather than staying in the reactor for extended periods, thus prolonging the life of the catalyst, and enhancing once-through reactor productivity.

The reactor system can be operated in a continuous fashion (feed in and product out) for a substantially longer time, leading to an increase in the quantity of the product obtained. If the coal liquefaction products stay in the reactor for a prolonged period of time, retrograde reaction occurs that converts desirable small product molecules into less desirable larger macromolecules, by the recombination of two small product molecules or by addition of these product molecules back onto the coal [3]. Since the coal liquefaction products that are formed are continuously removed from the flow reactor system, there would be an alleviation in the effect of retrograde reactions thereby increasing the yield and quality of coal-derived liquids.

Topics Presented in this Report. Two reactor systems are currently in the design stages for performing studies in the liquefaction of coal process. In order to translate and better understand the results obtained from the 25 mL tubing bomb microautoclave reactor and to apply them to a larger scale reactor system, the design and assembly of a 300 mL

batch autoclave reactor system is currently being done and will be discussed later in this report.

Description of the coal liquefaction and the upgrading of the coal liquids facilities, at the Advanced Coal Liquefaction Facility in Wilsonville, Alabama, the Hydrocarbon Research Institute, Inc. Unit at Lawrenceville, New Jersey, and the bench-scale unit for the coal liquefaction process at the Pittsburgh Energy Technology Center (PETC), Pittsburgh, will also be presented in this report.

A conceptual process scheme for the continuous flow mini-pilot plant reactor system for the liquefaction of coal and upgrading of the coal-derived liquids has been proposed. This reactor system incorporates the novel reaction schemes that were developed here earlier in the tubing bomb microautoclave reactor, which includes the temperature programmed liquefaction of coal and addition of water at relatively lower temperatures, to improve the quality and quantity of the products. Detailed description of this process scheme will be presented later in this report.

BATCH REACTOR SYSTEM FOR COAL LIQUEFACTION PROCESS

A schematic of the 300 mL batch autoclave reactor system that was recently designed and assembled is shown in Figure 58. The reactor manufactured by Autoclave Engineers, Inc. is provided with a heating jacket capable of elevating the reactor temperature to 400 °C. The internals of the autoclave reactor which is equipped with a Magnedrive, includes a dispersimax turbine to continuously agitate the reactor feed, a baffle to prevent vortex that would develop inside the reactor at high agitation speeds, a cooling coil to rapidly cool the reactor charge at the completion of the reaction, a thermowell to measure and control the reactor temperature, and a gas inlet tube (which extends all the way to the tip of the impeller) that is equipped with a frit to prevent any solids (< 20 μm) from accidentally entering the gas line. The Magnedrive is also provided with a cooling jacket to maintain it at a lower temperature due to its proximity to the high temperature of the reactor.

The feed gas line to the reactor includes a feed gas cylinder, a forward pressure regulator, a check valve that is designed to open at 90 psi, a flow control valve to feed the gas at a controlled rate to the reactor filled with coal-catalyst-solvent slurry, and an on-off valve that is to be maintained in the off position once the reactor reaches the desired pressure.

The gas outlet line is equipped with a pressure indicator to continuously monitor the reactor pressure, and an on-off valve that is to be maintained at the off position during the pressurization of the reactor and during the reaction process itself and in the on position during the depressurization of the reactor. The outlet line to vent is also provided with a

liquid collection bomb in case of any accidental carry over of the liquid, and a gas sampling outlet valve. The autoclave reactor system will be enclosed by steel walls (3/16 inch thick) to provide safety to the operator.

The system is batch with respect to all the reactant and product species (gas, coal, catalyst, and solvent) involved in the coal liquefaction process.

Experiments will be performed with a feed gas of either H_2 or syngas, a mixture of H_2 and CO (H_2/CO = 25/75). The subbituminous coal will be slurried along with a molybdenum catalyst precursor, e.g., ammonium tetrathiomolybdate (ATTM), Molyvan L, or molybdenum naphthenate and a solvent such as the hydrogen donor tetralin or a non-donor 1-methylnapthalene. Along with the effect of coal, catalyst, and solvent loading, the effect of water addition on the product composition will also be studied using the 300 mL stirred autoclave reactor. The operating temperature will be in the range of 350–400 °C. The temperature programmed liquefaction of coal will also be conducted. The initial pressure will be 1000 psi (cold).

BRIEF OVERVIEW OF EXISTING COAL LIQUEFACTION AND COAL LIQUIDS UPGRADING UNITS

The numerous advantages associated with a continuous flow coal liquefaction and the upgrading of coal liquids processes have been discussed earlier. It was decided to study three of the well documented liquefaction processes before embarking on the design and assembly of our novel mini-pilot plant reactor system for coal liquefaction and coal liquids upgrading. The process systems we studied included the ones at the Advanced Coal Liquefaction Facility in Wilsonville, Alabama, the Hydrocarbon Research Institute, Inc. Unit at Lawrenceville, New Jersey, and the bench-scale unit for the coal liquefaction process at the Pittsburgh Energy Technology Center (PETC), Pittsburgh. A brief description of these process systems is presented here.

Advanced Coal Liquefaction Facility at Wilsonville, Alabama. The liquefaction facility at Wilsonville initially operated with two ebullated reactors in series, with supported catalysts in both the reactors [4]. Please refer to Figure 59 for the schematic flow diagram of the Wilsonville facility. There are several well documented disadvantages of using supported catalysts instead of dispersed catalysts in the 1st reactor [4]:

§ Relatively lower coal conversion due to poorer coal/catalyst contact, lesser percentage of available surface sites and surface area, higher amount of retrograde reactions, and relatively slower hydrogen transfer rate, in supported catalysts processes compared to the dispersed catalyst processes.

§ First stage catalyst deactivation is relatively severe in supported catalysts processes due to uniform coke deposits and a calcium shell on the surface. Stable activity could not be maintained thus severely affecting the reactor productivity.

Hence it was decided in Wilsonville to conduct a few experiments using dispersed catalysts in the first reactor and supported catalysts in the second reactor. Dispersed catalysts are desirable because the majority of atoms are coordinately unsaturated and have a large percentage of surface sites that are readily accessible for chemisorption and catalysis, due to which a lesser amount of catalyst can be used. The dispersed catalysts can control retrogressive reactions and avoid char formation, better than the supported catalysts. Ideally the dispersed catalyst is active at preconversion conditions to limit the amount of retrogressive reactions that occur in the initial stages of the coal liquefaction.

The use of fine-particle size unsupported catalysts in direct coal liquefaction can result in improved economics due to enhanced yields of desired products and decreases reaction severity. Since this observation was confirmed by our own independent researchers [1], it was decided to study this coal liquefaction process using dispersed catalysts in 1st stage reactor and supported catalysts in 2nd stage reactor. Since the general process system of Wilsonville facility and the HRI, Inc. Unit are similar, this process is described in greater detail after discussing the operating conditions of the HRI, Inc. Unit.

Operating Conditions of the Wilsonville Coal Liquefaction Plant (Run 262 E, 263 IJ) - Closed Coupled - Integrated Two Stage Liquefaction (CC-ITSL) Process

Coal: -	Black Thunder subbituminous variety - < 200 mesh size (25 30 wt. % in solvent) *Solvent-to-coal ratio* : 2.33 *Feed Rate*: 300 - 350 lb/h (110 lb MF coal/h/cu.ft. cat. in 2nd stage)
1st Stage Catalyst:	Iron oxide (1 - 3 wt. % coal) and Molybdenum (dispersed) mixed with dimethyl disufide (DMDS) - 100 ppm by coal - < 200 mesh size
2nd Stage Catalyst: unconverted coal,	Criterion 324 - 1/16" Cylindrical Extrudates of Nickel-Molybdenum - supported (exposed to ash, and a preasphaltene-rich environment)
Solvent: distillation vacuum flash bottoms (vacuum flash bottoms)	Recycle process solvent - Mixture of HVGO (From of solvent recovered from flash units), containing CI, and hydrotreated resid from ROSE-SR unit.

Composition: 40 - 45 wt. % resid, 20 wt. % C. I. (Cresol Insolubles), 35 - 40 wt. % HVGO (Heavy Vac. Gas Oil)

Interstage Separator: Separation of vapor (including water present in high moisture, low-rank coals) and slurry, Increases partial pressure of H_2 in 2nd stage, Decreases production of light hydrocarbon gases (C_1 - C_3) from further cracking

Remainder of 1st stage product sent to 2nd stage without depressurizing or deashing.

ROSE - SR Critical Solvent Deashing Unit:

Proprietary extraction process - solid-liquid separation

1st Stage Conditions: 840 °F, 2650 psi (4400 - 5100 scfh of H_2)

2nd Stage Conditions: 810 °F, 2475 psi

Product:		
	Boiling end point	715 - 780 °F
	Maximum Distillate Production	190 lb/h
	High H_2 content	10.1 - 12.2 wt. %
	Low Heteroatoms	0.02 - 0.06 wt.% S
		0.1 - 0.9 wt. % N
		0 - 3.9 wt. % O

Overall H_2 Consumption: 5.7 wt. %

Coal Conversion: 92 %

The hybrid catalyst system with a combination of dispersed catalyst in the first reactor and supported catalyst in the second reactor, improved the distillate production by 30–60 %, and increased coal & resid conversions, compared to using the dispersed and supported catalysts separately.

The U.S. DOE and participants have been developing and scaling-up direct coal liquefaction technologies at the 3–5 ton/day Wilsonville Advanced Coal Liquefaction Research & Development Center for about 20 years until its closure in early 1992. A contract was then awarded to Hydrocarbon Research Inc. in October of 1992 to conduct demonstrations of Direct Coal Liquefaction in a 3 ton/day Proof of Concept facility located at the Hydrocarbon Research Development Center in Lawrenceville, N. J.

Hydrocarbon Research Institute (HRI) Inc. Unit, NJ. The reactor configuration in the HRI unit was similar to that in Wilsonville. Please refer to Figure 60 for a schematic of the process. Very few runs were made in the Wilsonville facility with dispersed catalyst in the 1st reactor and supported catalyst in the 2nd reactor. Hence HRI, Inc. decided to conduct a few more runs with this reactor configuration. Experiments were performed using both, pure H_2 feed and syngas (H_2 + CO) feed to the 1st reactor, and pure H_2 feed to

the 2nd reactor [5]. The purpose of the CO is to improve the economics by simplifying or totally eliminating a separate water-gas shift step and perhaps help remove oxygen in the product slate.

Operating Conditions of the HRI Inc. Unit (Run CMSL-03, Conditions 1-3)

Coal:	Black Thunder Mine (43 lb MAF coal/h/cu ft of cat. per stage) - < 200 mesh size
Catalyst: DMDS	*1st Stage* - Molybdenum as AHM (1500 ppm of Mo) + - < 200 mesh size
(Supported)	*2nd Stage* - Shell 317 1/32" Extrudates of Ni/Mo
Solvent:	Recycle process Solvent liquid from Run 227-76 containing 38.27 wt. % of resid.
Gas:	H_2, Syngas (H_2 + CO) for 1st stage (2500 psi) H_2 for 2nd stage
Operating Conditions:	1st stage - 730 - 750 °F 2nd stage - 800 °F Solvent to coal ratio - 1.1, 1.2 H_2 Conversion (%) - 7.8 for H_2 feed to 1st stage - 7.1 - 7.7 for syngas feed to 1st stage Coal Conversion (%) - 89.5 for H_2 feed to 1st stage - 92.5 for syngas feed to 2nd stage

A higher distillate yield, coal, and residuum conversion was obtained when syngas was used in the 1st stage instead of H_2. A high proportion of "Coal Oxygens" are being removed as carbon oxides, mostly in the form of carbon dioxide when an interstage separator is used.

In a few of the experimental runs an on-line hydrotreater was in service to further remove heteroatoms from the separator and atmospheric still overhead products. It is the "Optional" arrangement shown in Figure 60.

Operating Conditions of Bench Run CMSL-01:

Coal:	Black Thunder Mine (70 lb MAF coal/h/cu ft of cat. per stage) - < 200 mesh size
Catalyst:	*1st Stage* - ATTM (300 ppm of Mo) + FeOOH (6150 ppm of Fe)
(Supported)	*2nd Stage* - Shell 317 1/32" Extrudates of Ni/Mo

Hydrotreater - Criterion 411 Ni/Mo (Supported)

Solvent: Recycle process Solvent liquid from Run 227-76 containing 38.27 wt. % of resid.

Gas: H_2

Operating Conditions: 1st stage - 825 °F
2nd stage - 775 °F
Hydrotreater - 660 °F
H_2 Conversion (%) - 8.7
Coal Conversion (%) - 93

The coal conversions were the highest values obtained for this type of coal. The light distillates (IBF - 650 °F) contained ten times less nitrogen and 17W% more hydrogen than that of the 2 ebullated-bed reactors in series configuration.

Other studies in the HRI Inc. unit includes [6]:

- Fixed Bed Finishing Reactor: A fixed-bed hydrocracker was installed as a finishing reactor (second or third stage) after the ebullated bed reactors.
- Three Stage CSTR System: Addition of a third ebullated bed reactor in series (plug flow simulation) along with 2 ebullated bed reactors.
- Lowering the solvent/coal ratio to 0.9 in 2 ebullated bed reactors in series

General Description of the Process Flow in the Wilsonville Facility and in the HRI Inc. Unit - 1st stage dispersed catalyst, 2nd stage supported catalyst. Coal, dispersed catalysts, and recycle solvent are added to the slurry feed mix tank which is maintained at 300 °F and ambient pressure. This slurry mixture is well agitated in the tank to keep the solid particles in suspension. This slurry is then fed to the preheater by a slurry pump. Prior to entering the preheater, feed gas containing either pure H_2 or syngas is contacted with the slurry feed. This mixture of slurry and gas exits the preheater at a temperature of 250–300 °C and flows into the 1st stage backmixed reactor. The gas and slurry exiting the 1st stage reactor flows into the interstage separator.

The interstage separator serves to remove all the gases, "coal oxygens", water, and some of the light distillates from the first stage products. This helps to prevent water from reacting in the second stage of the reaction system and also aids in increasing the partial pressure of hydrogen. The gas from the interstage separator flows through the condenser where the condensables (H_2O, NH_3, H_2S) are removed. The noncondensables flow through a back pressure controller, into a compressor, and recycled back to the inlet gas stream of the 1st stage reactor.

The slurry from the interstage separator containing ash, unconverted coal, and the dispersed catalyst, flows into the 2nd stage ebullated bed reactor. Prior to entering the 2nd

stage reactor, the slurry feed is contacted with pure H_2 gas feed. The gas and slurry products from the 2nd stage reactor flows into a vapor-slurry separator. The vapor from this separator flows through a condenser into a cold separator where the distillate is condensed. The vapor exiting this separator flows through a back pressure controller, into a compressor, and is recycled back to the inlet feed gas stream to the 2nd stage reactor.

The slurry from the separator flows into a continuous atmospheric still, where the overheads provide the distillate liquid. In the Wilsonville facility, the slurry is sent to the Critical Solvent Deashing unit which is a series of mixers and settlers to separate the solvent from the rest of the ash and other insolubles. In the HRI unit, the slurry is sent to a filtering unit. The liquid from this slurry is recycled back to the slurry feed mix tank. The unconverted coal, ash, catalyst, and other insolubles are removed as filter cake.

Pittsburgh Energy Technology Center (PETC) Coal Liquefaction Unit. In PETC, coal liquefaction research studies are being conducted in a computer-controlled bench-scale continuous unit. A schematic of the unit is shown in Figure 61. The experiments are being conducted in a 1-liter autoclave reactor [7].

Typical Operating Conditions of the PETC Unit

Feed: (<	Coal:	- Bituminous - Illinois No. 6 (Burning Star No. 2) 200 mesh)
	Gas:	- Hydrogen
	Reaction Solvent:	- Second Stage Heavy Distillate from Wilsonville Advanced Coal Liquefaction Unit
	Catalytic Precursor:	- Coal Impregnated with Iron (FeOOH) Catalyst, Dispersed Molybdenum Catalyst as Ammonium tetrathiomolybdate
aqueous (ATTM)		

Operating Conditions:	Temperature:	435 °C
	Pressure:	2500 psig of H_2 (3% H_2S for Experiments with Iron)
	Flow Rate of H_2:	4 scfh
	Slurry Feed Rate:	240 g/h
	Solvent to Coal Ratio:	2/1, 1/1
	Residence Time:	1 hr. in Reactor (20 minutes in the Intermediate Activation Stage Experiments with Iron - 275
for °C)		

Brief Description of the PETC Coal Liquefaction Process. A mixture of coal (30 wt. %)-catalyst-solvent slurry is prepared and stored in a slurry feed mix tank. This slurry is then fed to the preheater by a slurry pump. Prior to the preheater, a mixture of H_2 and H_2S (in case of iron catalysts) or plain H_2 in case of molybdenum catalysts is fed into the coal slurry feed line. This mixture of gas and slurry from the preheater at a temperature of 200 °C, flows into an intermediate activation reactor and then to the coal liquefaction reactor (whenever iron catalyst is used), or to the coal liquefaction reactor directly whenever molybdenum catalytic precursors are used.

After the desired residence time, the contents of the reactor exit through an overflow line extending from the bottom of the reactor and flows into a H. P. product recovery vessel (V/L separator) where the gas escapes from the top and flows through a condenser. Prior to entering the condenser, water is added through a high pressure water pump to condense H_2S and NH_3. The light oils and other condensables are collected in the H.P light oil recovery vessel from where the coal liquid flows into the L.P recovery vessel. The vapors from this vessel flows through a condenser, into a flash gas meter, and vented to atmosphere. The vapors exiting the H.P. light oil recovery vessel flows through a back pressure controller, into a tail gas meter, and to vent.

The heavy slurry products from the H.P. product recovery vessel flows into the L.P recovery vessel. The vapors from this vessel is connected to the vapors exiting the other L.P recovery vessel. The slurry from this L.P. recovery vessel is filtered to separate the coal liquids from the unconverted coal, the dispersed catalysts, ash, and other insolubles. The coal liquids from both the L.P recovery vessels are collected and analyzed.

CONCEPTUAL DESIGN OF CONTINUOUS MODE REACTOR SCHEMES FOR LIQUEFACTION OF COAL AND UPGRADING OF COAL LIQUIDS

Mini-Pilot Plant for Coal Liquefaction. Based on the existing coal liquefaction units and our own laboratory research efforts in microautoclave reactor systems, the design of a continuous flow reactor system for the liquefaction of coal and upgrading of coal liquids is presently underway. A conceptual process flow diagram (PFD) of a continuous mode reactor scheme for the liquefaction of coal is presented in Figure 62. It should be

mentioned that this PFD is tentative and is being modified as deemed necessary to satisfy our requirements.

In our process, two technologies have been coupled in an attempt to improve the economics over existing coal liquefaction processes. The technologies incorporated are temperature programmed liquefaction (TPL) of coal and addition of water to the coal liquefaction process. Microautoclave studies done prior to, and in support of the bench scale unit operation will help to provide some basic information in guiding the selection of operating conditions for the continuous unit. The key parameters of the continuous unit that would be benefited by the microautoclave runs include, temperatures of the 1st stage reactor and 2nd stage reactor, pressure of the feed gas in the reactor system, residence time of the coal-catalyst-solvent slurry in the reactor system, the quantity of water that is to be added to the liquefaction runs, the size of coal particles, the size of catalyst particles, the type of solvent, and the concentration of coal and catalyst in solvent.

Significant Features of the Continuous Flow Reactor Scheme. The significant features of this proposed novel reactor scheme for the coal liquefaction process can be summarized as follows:

§ Use of dispersed catalysts in the coal-solvent slurry.
§ Temperature-programmed liquefaction (TPL) of coal in a multistage (2 stages) reactor scheme.
§ Option of adding water to the coal-catalyst-solvent slurry to the 1st stage reactor.
§ Incorporation of an interstage separator between the two stages of the reactor to primarily remove water, when fed to the 1st stage reactor.
§ A feed gas blending (syngas - H_2 + CO) and compression (H_2 or syngas) system to provide the capability of feeding syngas or pure H_2 to the 1st stage reactor at elevated pressures.
§ Continuous sampling and G.C. analysis of gas and liquid from the slurry lines at several vantage points to periodically monitor the progress of the reaction.

Details of the Proposed Novel Multistage Continuous Flow Reactor and its Peripheral Units for the Coal Liquefaction Process

Slurry Feed Mix Tank—Feed slurry to the reactors consisting of coal (subbituminous/bituminous), dispersed catalyst (MoS_2 catalyst from soluble precursors—ATTM, Molyvan, Molybdenum naphthenate), and recycle or pure solvent (or petroleum resids) will be thoroughly mixed in this 5 gallon feed mix tank equipped with an agitator, to maintain this slurry in suspension. The temperature and the pressure of this vessel are expected to be maintained at 100 °C and 75 psi respectively.

Slurry Pump—The slurry from the feed mix tank will be fed to the reactors through a preheater by the slurry pump. This pump will be capable of handling high concentration of solids loading in slurry (35 %) and pressures as high as 4000 psi.

Prior to entering the preheater, the slurry will be contacted by pure feed gas (H_2 or $H_2 + CO$) and recycle gas (H_2, C_1 - C_4) exiting the 1st stage reactor.

Feed Gas Blending ($H_2 + CO$) and Compression (H_2 and $H_2 + CO$) System —The maximum pressure of the pure feed gas from the manufacturer's gas cylinders is 2500 psi. Since we will require a steady flow of either pure gas (H_2) or syngas ($H_2 + CO$) at pressures around 2500 psi., it was necessary to design a feed gas blending and compression system.

In case of H_2 gas as the feed, the gas will flow from the pure gas cylinder, through a flow control valve which is maintained at a desired back pressure, and into a pneumatic compressor, where it is compressed to the desired high pressure and stored in a compressed gas storage tank for pure H_2 feed. The pneumatic compressor will be capable of compressing the inlet feed gas to pressures as high as 5000 psi, depending on the inlet pressure and the desired exit flow rate to the compressed gas storage tank. The maximum pressures used for the liquefaction, however, will be below 3000 psi.

In case of a mixture of gases (syngas - $H_2 + CO$) as the feed, it is necessary to feed the pure gases from the manufacturer's pure gas cylinders at relatively low pressures (150 psi) to a feed gas blender. This blender consists of mass flow meters and control valves that will monitor and control the percentage of individual components in the gas mixture and deliver an outlet gas according to the desired proportions. The blended gas then flows through a back pressure regulator and into the pneumatic compressor, where it is compressed to the desired high pressure and stored in a compressed gas storage tank for the mixture feed. Sampling lines are provided for monitoring the feed syngas composition with the aid of G.C. analysis.

The outlet lines from both the compressed gases storage tanks are also provided with a common vent line (since only one of the gas cylinders will be in use at a time) to depressurize the system at the completion of the experimental runs. The outlet from these compressed storage tanks serves as the feed inlet line to the reactor system. The feed gas inlet to the slurry line before the preheater is equipped with a forward pressure regulator, a check valve, and a mass flow controller. The slurry line is also contacted with the recycle gas (H_2, C_1 - C_4) from the outlet of the 1st stage reactor. Thus the inlet to the preheater is a combination of three process flows—slurry, feed gas, and recycle gas.

Preheater—Gas and Slurry —The gas and slurry that enters the 300 mL agitated autoclave vessel which serves as a preheater, will be maintained at a temperature of 200–

300 °C. The preheated gas and slurry then flows into the 1st stage reactor. G.C. analysis of the feed gas to the reactor will be performed with the sampling loop provided.

1st Stage Coal Liquefaction Reactor—The 1st stage reactor is a 1-liter autoclave vessel equipped with a dispersimax turbine type impeller, which will be maintained at a temperature of 350–375 °C. The gas and slurry entering from the preheater will undergo primary reactions in this reactor.

Provision is made for continuous injection of water into the reactor vessel. Water from the feed reservoir will be fed to the reactor with the aid of a water pump. This water will then react with the gas and slurry to form primary products which includes the product vapors and the coal-derived liquid which remains in the slurry.

The unreacted and product gas then flows through the gas outlet provided, into the condenser where small quantities of H_2O, H_2S, and NH_3 are removed as liquid. The noncondensables (H_2, C_1 - C_4) flows through a back pressure controller which maintains the entire lines between itself and the slurry pump at the desired operating pressure of the 1st stage reactor (approx. 2600 psi.). This gas line is also provided with a pressure gauge and a sampling line for G.C. analysis. This product gas from the 1st stage reactor is partially vented to atmosphere and the rest of the gas is sent through a mass flow controller to be contacted with the slurry and fresh feed gas line as inlet to the preheater. The composition of the liquid in the reactor will be monitored with the sampling loop for G.C. analysis. The gas and slurry (along with the product liquids) then flows into the interstage separator.

Interstage Separator.—This interstage separator is a 1-liter vessel equipped with a turbine type impeller, whose main function is to ensure the complete separation of any amount of water remaining in the system. The product vapors exiting this separator flows through a condenser to remove any condensables remaining in the system like H_2O, H_2S, and NH_3. The noncondensables (H_2, C_1 - C_4) then flows through a back pressure controller which maintains the line between itself and the exit of the 1st stage reactor at a lower pressure (approx. 150 psi. less) than the reactor, to flash out the condensables from the system.

A part of this vapor is vented to atmosphere and the rest of the vapor flows through a pressure regulator, a pressure gauge, and a mass flow controller which regulates its feed to be contacted with the slurry stream for the 2nd stage reactor inlet. The gas and slurry exiting this interstage separator which is devoid of any condensables at the existing operating condition is contacted with a fresh feed gas from the compressed cylinders, and the recycle gas stream consisting of H_2 and C_1 - C_4 vapors exiting the 2nd stage reactor.

Provision is made for analysis of gas from this interstage separator which is one of the feed lines to the 2nd stage, and the liquid inside the separator, to be analyzed by G.C.

2nd Stage Coal Liquefaction Reactor—The process stream consisting of gas and slurry from the exit of interstage separator, fresh feed gas, and recycle gas streams from the exit of interstage separator and the exit of the 2nd stage reactor is the feed to the 2nd stage reactor. The feed gas to the 2nd stage reactor will be analyzed by G.C. through a sampling line.

The 2nd stage reactor is a 1-liter autoclave equipped with a turbine type impeller, which will be maintained at 400–425 °C. The gas and slurry entering this reactor undergo secondary reactions to form more coal liquids. The gas and slurry containing the desired product coal-derived liquids flows into a vapor-liquid separator. A sampling line for G.C. analysis of the liquid exiting the 2nd stage reactor will be installed.

Vapor-Liquid Separator.—The gas and slurry products exiting the 2nd stage coal liquefaction reactor flows into the vapor-liquid separator, which is a 1-liter autoclave vessel equipped with a turbine type impeller. The gas exiting this separator is cooled by a condenser. The condensables fill the liquid collection bomb, which is a 1-liter vessel. Provision is made for G.C. analysis of the liquid collected in this bomb. The noncondensables flow through a back pressure controller which maintains the line between itself and the exit of the interstage separator at a lower pressure (approx. 150 psi.) than the separator.

A part of the gas exiting this back pressure controller is vented to atmosphere. The rest of the gas is recycled to the inlet of the 2nd stage reactor, through a pressure indicator and a mass flow controller. The liquid stream from this V/L separator will be analyzed by a G.C. The slurry exiting the vapor-liquid separator will be sent through a Bureau of Mines (BOM) valve which will be capable of handling the throttling of a high temperature and high pressure, process stream. The process stream (gas and slurry) then flows into an atmospheric flash tank.

Atmospheric Flash Tank—The gas and slurry flowing from the V/L separator and through the BOM valve, enters the atmospheric flash tank which is a 1-liter agitated vessel equipped with a turbine type impeller. The gas exiting this vessel is vented to atmosphere. Periodic G.C. analysis of this exiting gas will be performed. The slurry exiting this atmospheric flash tank flows into a solid-liquid separator.

Solid-Liquid Separator—The slurry entering this separator is separated into solids and liquid. The solids containing insolubles, unreacted coal, resids, and catalysts are removed. The product liquid containing the coal liquids is separated from the solvent using methods

described elsewhere [1]. This coal liquid is sent to the upgrading section of the mini-pilot plant.

Mini-Pilot Plant for Coal Liquids Upgrading Process

The schematic of the preliminary conceptual process flow diagram of the coal liquids upgrading mini-pilot plant is shown in Figure 63.

Details of the Proposed Continuous Flow Reactor and its Peripheral Units for the Coal Liquids Upgrading Process

Feed Mix Tank—The feed to the reactor consisting of coal liquids from the liquefaction section of the mini-pilot plant will be mixed and stored in this 5 gallon feed mix tank equipped with an agitator. The temperature and the pressure of this vessel is expected to be maintained at 100 °C and 75 psi respectively.

Feed Pump—The liquid mixture from the feed mix tank will be fed to the reactors through a preheater by the feed pump. This pump will be capable of handling pressures as high as 4000 psi. The maximum operating pressure of the system will be below 3000 psi.

Prior to entering the preheater, the liquid feed will be contacted by pure feed gas (H_2) from the compressed gas cylinder (flowing through a forward pressure regulator, check valve, and a mass flow controller) and recycle gas containing mainly unreacted H_2 exiting the vapor-liquid separator.

Preheater—Gas and Liquid Feed—The gas and liquid feed that enters the 300 mL agitated autoclave vessel which serves as a preheater, will be maintained at a temperature of 200–250 °C. The preheated gas and liquid mixture then flows into the coal liquids upgrading reactor. G.C. analysis of the feed gas to the reactor will be performed with the sampling loop provided.

Coal Liquids Upgrading Reactor—This reactor is a 1-liter autoclave vessel equipped with a Robinson-Mahoney Spinning Catalyst Basket, which will be maintained at a temperature of 370–425 °C.

The catalysts to be tested in the spinning catalyst basket which will assist in catalyzing the upgrading reactions, will include conventional supported catalysts, and catalysts prepared in the laboratory, such as mesoporous alumino-silicate molecular sieves.

After the feed gas and the liquid feed has reacted with each other in the presence of the catalyst, they exit the reactor and flow into the vapor-liquid separator. Provision is made for the periodic analysis of the liquid exiting the reactor to monitor the progress of the reaction.

Vapor-Liquid Separator—The gas and liquid exiting the reactor flows into the vapor-liquid separator, which is a 1-liter autoclave vessel equipped with a turbine type impeller.

The unreacted and product gas then flows through the gas outlet provided, into the condenser where small quantities of condensables are removed. The noncondensables containing mainly unreacted H_2, flows through a back pressure controller which maintains the entire lines between itself and the feed pump at the desired operating pressure of the reactor (approx. 2600 psi.). This gas line is also provided with a pressure gauge and a sampling line for G.C. analysis. This product gas from the reactor is partially vented to atmosphere and the rest of the gas is sent through a mass flow controller, to be contacted with the liquid feed and fresh feed gas line as inlet to the preheater.

The liquids and a portion of the gas exiting this vapor-liquid separator flows into the atmospheric flash tank. The composition of the liquid exiting the separator will be monitored with the sampling loop for G.C. analysis.

Atmospheric Flash Tank—The gas and liquid flowing from the V/L separator, enters the atmospheric flash tank which is a 1-liter agitated vessel equipped with a turbine type impeller. The gas exiting this vessel is vented to atmosphere. Periodic G.C. analysis of this product gas and the liquid collected in the vessel will be performed to monitor the progress of the reaction. The liquid stays in the vessel.

The entire continuous mini-pilot plant system involving both the coal liquefaction reactors unit and the coal liquids upgrading reactor unit will be controlled with a computerized digital control system.

FUTURE PLANS

The design and assembly of the batch coal liquefaction reactor unit is nearing completion. Experiments will be conducted in this reactor system, according to the plan outlined in detail in the earlier section on the design of this reactor system. The conceptual design for the continuous mode, fully computerized, mini-pilot plant for liquefaction of coal and the upgrading of coal liquids, will be completed and finalized. Quotations for several of the required equipments have already been received from competitive vendors. Accordingly, orders will be placed with the corresponding vendors and the assembly of this mini-pilot plant system is expected to commence soon.

REFERENCES

1. Song, C., Parfitt, D. S., and Schobert, H. H.; *Energy & Fuels*, Vol. 8, No. 2, 313-319, 1994.

2. Song, C. and Saini, A. K.; *Preprints of Papers presented at the 208th ACS National Meeting*, Washington, D.C., August 20-25, 1994, 1103-1107.

3. Provine, W. D., Porro, N. D., LaMarca, C., Klein, M. T., Foley, H. C., Bischoff, K. B., Scouten C. G., Cronauer, D. C., and Tait, A. M.; *Ind. Eng. Chem. Res.*, Vol. 31, No. 4, 1170-1176, 1992.

4. Lee, J. M., Vimalchand, P., Cantrell, C. E., and Davies, O. L.; *Proceedings of the Liquefaction Contractors' Review Conference*, September 22-24, 1992, Pittsburgh Energy Technology Center, U.S. Department of Energy, pp 35-96.

5. Lee, L. K., Comolli, A. G., Pradhan, V. R., and Stalzer, R. H.; *Proceedings of the Coal Liquefaction and Gas Conversion Contractors Review Conference*, September 27-29, 1993, Pittsburgh Energy Technology Center, U.S. Department of Energy, pp 547-559.

6. Pradhan, V. R., Comolli, A. G., Johanson, E. S., Lee, L. K., Stalzer, R. H., *Proceedings of the Coal Liquefaction and Gas Conversion Contractors Review Conference*, September 27-29, 1993, Pittsburgh Energy Technology Center, U.S. Department of Energy, pp 425-454.

7. Cugini, A. V., Krastman, D., Hickey, R. F., and Lett, R. G.; *Proceedings of the Liquefaction Contractors' Review Conference*, September 22-24, 1992, Pittsburgh Energy Technology Center, U.S. Department of Energy, pp 203-209.

4. Exploratory Studies on Coal Liquids Upgrading using Mesoporous Molecular Sieve Catalysts (Contributed by Madhusudan Reddy Kondam and Chunshan Song)

Introduction:

Upgrading coal liquids to produce useful products like jet fuels involves catalytic hydroprocessing to achieve molecular weight reduction, hydrogenation and the removal of heteroatoms. The hydroprocessing is usually done over supported catalysts. Commercial hydroprocessing catalysts consist of a combination of metals (Co, Ni, W and Mo) distributed over a porous, high surface area (150-300 m^2/g) supports of γ–alumina or silica stabilized γ–alumina. The principal reactions which occur during catalytic hydroprocessing are hydrogenation, hydrocracking, heteroatom removal and reactions which lead to the deposition of metals and carbonaceous materials on the catalyst. The latter are the major causes of catalyst deactivation.

The conventional hydroprocessing catalysts were designed for refining distillate feeds and they have been successfully used in petroleum hydroprocessing for several decades. However, these catalysts are unable to contend with the stringent demands of hydroprocessing high-boiling and nondistillable coal liquids or similar feedstocks. Their principal deficiency is their susceptibility to deactivation by reactions which cause the deposition of carbon and metals. There are two broad areas of liquefaction research which could contribute to resolving this problem. The first entails the control of primary coal dissolution by dispersed catalysts in order to generate products which can be upgraded by conventional supported catalysts . The second approach , which is of our current interest, concerns the development of improved or novel supported catalysts for hydroprocessing the coal liquids.

Improvements to the performance of the existing family of hydroprocessing supported catalysts can be made by changes in the metals loading, in the physical structure of the support and by the use of additives. The range of catalyst metals which are investigated needs to be extended well beyond the combinations of Co, Ni, Mo and W. Novel support materials should be examined to introduce different surface chemistry. In this way, it will be possible to alter the role of the support and the activity and selectivity of the supported phases by changing in nature of the catalyst-support interaction. Exploratory research has already begun to reveal the potential of some non-conventional support materials: mixed oxides; ion-exchange supports; carbons; carbon-coated alumina [1].

Catalyst performance is strongly affected by the pore structure of the support. The pore size distribution must be adapted to the type of feed being processed to ensure ready

access of the reactant molecules and minimize processes which cause deactivation. Small pore catalysts provide high surface and activity but are most susceptible to pore-mouth blockage. Larger pore catalysts generally possess surface areas which are too low for high activity. However, their wider pore mouths allow the more slowly diffusing metal-precursor compounds to penetrate into the catalyst before metals are deposited. This provides increased capacity for deposited metals and a slower rate of pore-mouth blockage. The shape and size of the catalyst particles can also influence catalyst life. Increasing the catalyst pore size and reducing the particle size can improve coal and asphaltene conversion. The large pores are required to suppress pore-mouth blockage and sustain catalyst activity.

Because of their special characteristics like high crystallinity with uniform pore size, controlled acidity, high thermal stability, good surface area, etc., zeolite molecular sieves are widely used in petroleum and petrochemical industry. But their use is limited by small molecules conversion as they are restricted to maximum of 1.4 nm pore size. Recently, Mobil workers have reported a new series of mesoporous molecular sieves [2,3], MCM-41 is one of the members of this extensive family of mesoporous series possesses a hexagonal array of uniform mesopores. The pore dimensions of which can be tailored, in the range of 1.5-10 nm, through the choice of surfactant and auxiliary chemicals as templates and synthesis conditions. The BET surface area of these materials is more than 1000 m^2/g with high sorption capacities of 0.7 cc/g and greater. These materials can be synthesized in a large range of framework Si/Al ratios, and therefore can develop variable acidity. Considering these special features of novel mesoporous molecular sieves, MCM-41, they may be a good support to formulate a new type of supported catalysts to overcome the problems facing with conventional supported catalysts in upgrading the coal liquids.

As part of our ongoing project on coal liquefaction and upgrading, in this particular task we intend to explore the possibility of using these mesoporous molecular sieves to upgrade the coal-derived oils to produce stable jet fuels. This task can be devided into to three parts: 1) synthesis of mesoporous molecular sieves, 2) characterization and 3) their catalytic evaluation for the conversion of polycyclic aromatic compounds (as model compounds) and then coal-derived oils.

In this report we present some of our preliminary studies on synthesis of mesoporous molecular sieves, MCM-41.

Experimental:

Synthesis of mesoporous aluminosilicate molecular sieves, Al-MCM-41, was done hydrothermally in about 100 ml Teflon lined autoclaves. Three series of samples with

varying Si/Al ratios and using three different aluminum sources were synthesized using two different procedures. Procedures are shown in Scheme I and II, the main difference in both these methods was the sequence of aluminum source addition. Synthesis gel compositions and crystallization conditions are shown in Table 23.

In a typical synthesis, 4 g of fumed silica (Cab-O-Sil, Cabot Corporation, IL, USA) was dissolved in 25.7 g of water while stirring for 15 min. Then the mixture of 11.6 g Tetramethyl ammonium silicate and 5.47 g of sodium silicate was added and stirred for another 15 min. The resulting solution was combined with a mixture of 12.9 g cetyltrimethyl ammonium bromide and 87 g of water and stirred for 20 min. Finally the required amount and type of aluminum sources, for an example 0.45 g of aluminum isopropoxide to have Si/Al of 100, was added and stirred for 15 min. before loading into Teflon lined stainless-steel autoclaves. Then the crystallization was done keeping the autoclaves in an oven at 373 K for 24 hours. After crystallization, the product was filtered, washed with deionized water, dried at 373 K in a vacuum oven for 6 hours and calcined. The calcination was done in tubular furnace by increasing the temperature at the rate of 5 K/min. until 813 K in nitrogen flow and continued for an hour, then 6 hours in air flow at the same temperature. Pure-silica polymorph of MCM-41 was synthesized using the same procedure, except that no aluminum source was added.

X-Ray Diffraction (XRD) patterns of both calcined and non-calcined samples were obtained using CuK_{α} radiation on a Phillips diffractometer (APD1700) equipped with a graphite monochromator.

Results and Discussion:

Three series of samples using three different alumnium sources, aluminum isopropoxide, alumina (Catapal B) and aluminum sulfate, with Si/Al ratios 50, 25, 12.5 and 0 were synthesized using two procedures. Details are tabulated in Table 23. XRD patterns of all the samples were obtained and shown in Figures 64 through 66. The major XRD peak intensities, two theta and *d* spacing values are tabulated in Table 24 XRD patterns show that almost all the samples are well crystallized and phase pure with a very strong peak and three weak peaks . However, non-calcined samples show some extra peaks which disappeared upon calcination (Figure 67). This could be due to the presence of large amounts surfactants, about 50 wt% within in channels. It is also observed that XRD patterns of calcined samples exhibit peaks with increased intensity and a shift to lower two theta (Figure 67). Same results were observed by earlier workers and it was predicted that calcination leads to a contraction of unit cell accompanied by a loss in silanol density via condensation of Si-OH groups .

Figure 68 depicts the influence of Si/Al ratio on crystallinity (major XRD peak intensities) of three series of Al-MCM-41 samples prepared using different aluminum sources. Results show that within each series of samples, a decrease in Si/Al ratio hinders crystallization process. It is a known phenomena observed in all high silica molecular sieves that the more aluminum in the gel more difficult to crystallize because of some stability reasons. However, the level of crystallinity decreases upon increasing the aluminum content varied with type of aluminum source. This could probably explain the reactivity of alumnium source by hydrolysis to react with silica source and form a gel of certain nature. The nature of the resulting gel influences the crystallinity and amount of aluminum incorporation in the framework. It seems that aluminum sulfate is easily hydrolyzed, reacted with silica and formed a gel of low pH. This may be the reason why the crystallinity is lower for the samples prepared with aluminum sulfate. Samples prepared with Catapal B show high crystallinity almost same as the sample prepared without aluminum, which seems to indicate that all the alumina is not reacting to form gel instead staying remained as alumina. This may be confirmed from no change in pH of the resulting gel upon increasing the aluminum content.

XRD characteristics show that there is not much difference attributable to change in the synthesis procedures (Table 24) for samples prepared using Catapal B. However, the samples prepared with aluminum sulfate and aluminum isopropoxide have shown the difference for different procedures. Our preliminary data is not enough to conclude the reasons.

Figure 69 shows a plot of Si/Al ratio versus d spacing for all three series of samples. In this case of mesoporous molecular sieves, MCM-41, crystal structure was indexed to hexagonalunit cell with $a = 2d_{100}/\sqrt{3}$. Results show that d spacing is increased with decreasing Si/Al ratio for all the samples, which indicates that increase in aluminum content in the gel increases the unit cell parameter. This is a common observation for all aluminosilicates molecular sieves, which is due to the incorporation of large aluminum ions as compared to silicon in the framework leads to an expansion of unit cell. It is also observed that an expansion is linearly proportional to the aluminum incorporation in the framework. Our results indicate that the order of expansion of unit cell with increasing aluminum content using three different sources is aluminum sulfate > aluminum isopropoxide > Catapal B alumina. This should be due to the incorporation of aluminum in the same order. This can be again explained from the nature of gel obtained with different aluminum sources.

From these preliminary studies, it is possible to synthesize phase pure mesoporous aluminosilicate molecular sieves, Al-MCM-41, with varying Si/Al ratios and using different

aluminum sources. It seems that aluminum sulfate is a better source to incorporate more aluminum in the framework, however, crystallization is poor probably due to the lower pH of the gel. Hence aluminum isopropoxide could be a better source to prepare mesoporous aluminosilicate molecular sieves. However, these results have to be further confirmed by other characterization techniques like surface area, temperature programmed desorption of ammonia and solid state NMR before their catalytic evaluation.

References:

1. F. J. Derbyshire, in Catalysis in Coal Liquefaction, *IEA Coal Research Publication,* IEACR/08, 1988.

2. C. T. Kresge, M. E. Leonowicz, W. J. Roth, J. C. Vartuli and J. S. Beck, *Nature*, 1992, **359**, 710.

3. J. S. Beck, J. C. Vartuli, W. J. Roth, M. E. Leonowicz, C. T. Kresge, K. D. Schmitt, C. T. W. Chu, D. H. Olson, E. W. Sheppard, S. B. McCullen, J. B. Higgins and J. C. Schlenker, *J. Am. Chem. Soc.,* 1992, **114**, 10834.

4. Cong-Yan Chen, Hong-Xin Li, M. E. Davis, *Microporous Materials,* 1993, **2**, 17.

APPENDIX I

Tables

Table 1. Reaction mechanism for the straight–chain alkane decomposition.

Reaction	Arrhenius A–factor ($L\ mol^{-1}\ s^{-1}$ or s^{-1})	Activation energy ($kcal\ mol^{-1}$)
$RH + O_2 \Rightarrow R^{\bullet} + HO_2^{\bullet}$	1×10^{-1}	0.0
$R^{\bullet} + O \Rightarrow RO_2^{\bullet}$	3×10^{9}	0.0
$RO_2^{\bullet} + RH \Rightarrow RO_2H + H$	3×10^{9}	10.0
$RO_2^{\bullet} + RO_2^{\bullet} \Rightarrow$ termination	3×10^{9}	0.0
$RO_2^{\bullet} + AH \Rightarrow RO_2H + A^{\bullet}$	3×10^{9}	5.0
$A^{\bullet} + O \Rightarrow AO_2^{\bullet}$	3×10^{9}	0.0
$AO_2^{\bullet} + RH \Rightarrow AO_2H + R^{\bullet}$	3×10^{5}	10.0
$AO_2^{\bullet} + AH \Rightarrow AO_2H + A^{\bullet}$	3×10^{9}	5.0
$AO_2^{\bullet} + AO_2^{\bullet} \Rightarrow$ products	3×10^{9}	0.0
$R^{\bullet} + R^{\bullet} \Rightarrow R_2$	3×10^{9}	0.0
$RO_2H \Rightarrow RO^{\bullet} + {}^{\bullet}OH$	1×10^{15}	42.0
$RO^{\bullet} + RH \Rightarrow ROH + R^{\bullet}$	3×10^{9}	10.0
$RO^{\bullet} \Rightarrow R_{prime}^{\bullet} + CO$	1×10^{16}	15.0
${}^{\bullet}OH + RH \Rightarrow H_2O + R^{\bullet}$	3×10^{9}	10.0
$RO^{\bullet} + RO^{\bullet} \Rightarrow RO^{\bullet}$termination	3×10^{9}	0.0
$R_{prime}^{\bullet} + RH \Rightarrow$ alkane $+ R^{\bullet}$	3×10^{9}	10.0

Table 2. Molar Yields of Products from the Pyrolysis of Decalins at 450 °C under Initial 0.79-MPa N_2.

reactant name	*cis*-decalin					*trans*-decalin				almost equimolar decalin			
experimental no.	TS80	TS40	TS57	TS13	TS70	TS41	TS58	TS14	TS71	TS42	TS59	TS64	TS72
residence time[a]	0.5 h	1 h	2.5 h	4 h	8 h	1 h	2.5 h	4 h	8 h	1 h	2.5 h	4 h	8 h
total gas (C_1~C_4) yield[b] (wt %)	0.3	1.3	2.9	5.0	11.2	0.5	0.7	0.8	3.7	1.4	3.0	4.2	6.9
conversion[c] (mol %)	11.8	27.6	55.9	76.7	90.2	7.7	11.3	16.4	36.7	11.0	18.0	25.3	38.9
product yield[c] (mol %)													
hydrogen	1.33	4.38	4.43	8.83	15.23	2.01	1.66	3.21	8.08	4.21	7.76	6.11	11.65
methane	0.15	1.26	3.48	9.89	22.03	0.57	0.98	1.62	8.71	1.41	3.97	6.73	13.44
ethylene	0.00	0.11	0.25	0.18	0.31	0.12	0.03	0.05	0.19	0.06	0.22	0.27	0.16
ethane	0.22	1.12	2.48	5.75	12.30	0.38	0.68	0.89	4.09	1.23	2.83	4.12	7.32
propene	0.26	0.78	0.98	0.80	1.79	0.39	0.45	0.35	0.73	0.70	1.42	1.29	1.26
propane	0.35	1.66	3.95	6.93	13.34	0.43	0.50	0.71	3.45	1.89	3.66	5.19	7.60
1-butene	0.00	0.01	0.04	0.08	0.10	0.01	0.01	0.01	0.06	0.02	0.07	0.07	0.09
n-butane	0.01	0.03	0.15	0.37	0.97	0.01	0.02	0.03	0.29	0.05	0.14	0.29	0.66
n-pentane		0.06	0.06	0.10	0.35	0.02		0.02	0.37	0.10	0.07	0.08	0.34
n-hexane		0.05	0.11	0.38	0.65			0.06	0.16		0.06	0.22	0.53
benzene	0.04	0.16	0.53	0.99	1.31	0.02	0.07	0.09	1.43	0.18	0.32	0.51	0.90
toluene	0.26	0.69	2.24	4.18	5.95	0.12	0.37	0.53	3.16	0.49	1.22	2.06	4.23
C_2-benzene	0.03	0.06	0.38	1.02	1.81	0.01	0.04	0.17	0.69	0.14	0.25	0.49	1.30
C_3-benzene			0.04	0.12	0.31			0.01	0.09	0.01	0.02	0.03	0.19
C_4-benzene	0.10	0.04	0.52	0.86	0.61		0.20	0.37	0.63	0.04	0.40	0.52	0.85
C_1-cyclopentane		0.03	0.11	0.92	2.00			0.06	1.35		0.16	0.41	1.37
cyclohexane		0.07	0.30	1.80	3.01		0.02	0.06	0.16	0.12	0.16	0.75	2.12
C_2-cyclopentene	0.07	0.24	0.27	0.69	0.96	0.06	0.10	0.27	0.84	0.14	0.19	0.24	0.56
methylcyclohexenes	0.86	2.66	4.35	4.33	2.69	0.53	0.97	1.20	1.98	1.11	3.10	3.27	1.15
ethylcyclopentane			0.07	0.20	0.41			0.01	0.11			0.07	0.18
methylcyclohexane	0.03	0.29	0.99	2.68	4.26	0.01	0.07	0.14	2.24	0.18	0.48	1.01	2.56
C_2-cyclohexene	0.05	0.16	0.17	0.18	0.14	0.02	0.04	0.11	0.18	0.16	0.21	0.12	0.15
ethylcyclohexane		0.02	0.07	0.20	0.34		0.02	0.07	0.08	0.01	0.05	0.09	0.22
propylcyclohexane			0.02	0.07	0.10				0.03		0.01	0.02	0.07
C_4-cyclohexene	1.54	2.23	6.48	7.23	7.23	1.68	1.78	3.71	5.79	2.62	4.41	6.14	7.35
butylcyclohexane	0.05	0.16	0.32	0.08	0.13	0.04		0.04	0.17	0.09	0.16	0.25	0.17
trans-decalin	6.22	16.84	30.76	40.63	39.26	*92.27*	*88.68*	*83.55*	*63.34*	*52.67*	*54.89*	*56.42*	*51.65*
cis-decalin	*88.19*	*72.40*	*44.11*	*23.27*	*9.85*	2.33	3.25	4.66	6.44	*36.33*	*27.13*	*18.26*	*9.48*
C_1-decalin		0.78	1.63	1.40	0.99	0.21	0.48	0.67	0.96	0.79	1.08	1.20	1.03
C_2-decalin		0.02	0.07	0.29	0.34	0.02	0.06	0.11	0.39	0.02	0.09	0.17	0.38
C_3-decalin	0.03	0.27	0.49	0.73	0.71	0.08	0.18	0.48	0.79	0.31	0.37	0.66	0.84
tetralin	0.22	0.20	0.84	2.04	2.31	1.71	1.81	1.59	2.89	0.56	0.84	1.28	1.92
C_1-tetralin			0.13	0.08	0.10	0.01	0.04	0.07	0.09	0.01	0.05	0.12	0.14
indan			0.11	0.11	1.15			0.08	0.45		0.06	0.08	0.63
C_1-indan			0.15	0.80	1.84	0.05	0.31	0.32	1.13	0.04	0.19	0.53	1.36
C_2-indan			0.03	0.23	0.29				0.04			0.10	0.13
naphthalene	0.02	0.02	0.12	1.00	2.99	0.02	0.18	0.22	1.16	0.04	0.15	0.45	2.12
2-methylnaphthalene				0.11	0.35			0.01	0.12			0.04	0.20
1-methylnaphthalene			0.01	0.10	0.28			0.01	0.11				0.20
C_2-naphthalene				0.03	0.19				0.05			0.01	0.11
acenaphthene				0.04	0.07				0.02				0.04
fluorene				0.01	0.03				0.01				0.02
methylbiphenyl			0.02	0.11	0.20				0.12			0.04	0.15
anthracene or phenanthrene				0.03	0.05							0.02	0.04

a) Pyrolysis of 5-ml reactant in 28-ml reactors plunged into the sandbath preheated to 450 °C.
b) The yield based on initial weights of reactants (*cis*-decalin, *trans*-decalin, or almost equimolar decalin mixture).
c) The molar yield or conversion based on initial reactants (*cis*-decalin, *trans*-decalin, or almost equimolar decalin mixture).

Table 3 Catalyzed Isomerization of *cis*-Decalin (Staring Reactant is 1-g Commercial Decalin[a]) for 2 h with 0.79 MPa of UHP H_2 or N_2.

Catalyst	Temperature (℃)	Gas	Product[b] (wt %)				*trans/cis* DHN	*cis*-DHN conversion[b]	*trans*-DHN selectivity
			trans-DHN	*cis*-DHN	Tetralin	Others[c]			
PtM38	200	H_2	92.73	7.27	0	0	12.8	43.4	1.00
PdM38	200	H_2	92.75	7.25	0	0	12.8	43.4	1.00
PtM21	200	H_2	92.03	7.97	0	0	11.6	42.7	1.00
PtM38	200	N_2	62.73	33.65	2.27	1.35	1.9	17.1	0.83
PdM38	200	N_2	54.61	42.51	1.85	1.03	1.3	8.2	0.74
LaHY	200	N_2	48.50	50.80	0.70	0	0.96	0	-
HY	250	N_2	66.16	19.11	0.60	14.13	3.5	31.6	0.56
LaHY	250	N_2	65.37	18.88	0.61	15.13	3.5	31.8	0.53
LaHY	250	H_2	66.01	16.79	0.59	16.61	3.9	33.9	0.51
HM38	250	N_2	53.19	31.70	0.38	14.73	1.7	19.0	0.25

a) Composition of reactant (wt %): 48.5% trans-DHN, 50.8% cis-DHN, and 0.7% tetralin.
b) Based on the initial amount of decalin.
c) Products of ring-contraction isomerization and ring-opening cracking reactions.

Table 4. Calculated Equilibrium Constant and Composition for a Binary Mixture System of *cis*-DHN and *trans*-DHN.

Temperature (°C)	Equilibrium constant[a]	Composition (wt %)	
		cis-DHN	*trans*-DHN
200	20.5	4.65%	95.35%
235	16.3	5.79%	94.21%
250	14.9	6.30%	93.70%
265	13.7	6.82%	93.18%
275	12.9	7.17%	92.83%
300	11.4	8.06%	91.94%
350	9.1	9.87%	90.13%
400	7.6	11.69%	88.31%
450	6.4	13.48%	86.52%

(a) Equilibrium constant (K) for the reaction

cis-DHN $\leftrightarrow$ *trans*-DHN

$$K = \frac{[trans\text{-DHN}]}{[cis\text{-DHN}]}$$

Table 5. Catalyzed Isomerization of *cis*-Decalin (Staring Reactant is 1-g Pure *cis*-Decalin) under an Initial Pressure of 0.79 MPa UHP N_2.

	Catalyst: 0.2 g of LaHY										
temperature (°C)	235	235	235	235	250	250	265	265	265	275	275
residence time[a] (min)	60	120	240	480	120	120	9	18	60	9	18
reaction time[b] (min)	54	114	234	474	115	115	4	13	55	5	14
product yield[c] (wt %)											
trans-DHN	7.4	11.5	22.7	43.0	47.7	46.3	11.7	32.7	50.4	24.2	37.9
cis-DHN	90.6	85.2	70.8	42.8	29.4	32.5	83.5	51.4	10.2	61.2	31.2
trans-/cis-DHN ratio	0.08	0.13	0.32	1.00	1.62	1.42	0.14	0.64	4.94	0.40	1.21
cis-DHN conversion[c]	9.1	14.4	28.8	56.8	70.2	67.1	16.1	48.2	89.4	38.4	68.4
rate constant, k (h^{-1})	0.105	0.082	0.087	0.106	0.63	0.58	2.62	3.02	2.45	5.83	4.92
trans-DHN selectivity	0.80	0.79	0.79	0.76	0.68	0.69	0.72	0.67	0.56	0.63	0.55

	Catalyst: 0.2 g of HY									
temperature (°C)	235	235	235	250	250	265	265	265	275	275
residence time[a] (min)	120	240	480	30	60	9	18	30	9	18
reaction time[b] (min)	114	234	474	25	55	4	13	25	5	14
product yield[c] (wt %)										
trans-DHN	21.1	47.6	57.0	23.2	46.1	20.7	34.6	51.9	35.8	47.8
cis-DHN	74.1	37.8	23.0	69.6	36.8	71.6	51.1	19.4	45.9	23.1
trans-/cis-DHN ratio	0.29	1.26	2.48	0.33	1.25	0.29	0.68	2.67	0.78	2.07
cis-DHN conversion[c]	25.5	61.8	76.6	30.0	62.9	28.0	48.5	80.3	53.7	76.5
rate constant, k (h^{-1})	0.155	0.247	0.184	0.85	1.08	4.86	3.01	3.89	9.03	6.22
trans-DHN selectivity	0.82	0.77	0.74	0.77	0.73	0.73	0.71	0.64	0.67	0.62

a) Reactor residence time in sand bath preheated to reaction temperature.
b) Corrected reaction time (reactor residence time minus heat-up time).
c) Based on the initial amount of *cis*-DHN.

Table 6. The thermal stressing of 1-phenylhexane at 400°C

Thermal Stressing Time (Min)	% 1-Phenylhexane neat thermal stressing	% 1-Phenylhexane thermally stressed in the presence of JP-8C
0	100	100
60	83.3	99.1
120	66.7	98.4
240	50.6	97.2
360	35.1	96.6

Table 7. Deviations of Estimated Critical Temperatures from Measured Values for Nine Jet Fuels (Estimated T_c - Measured T_c, °F)

	Method[a]					
Fuel	I	II	III	IV	V	VI
JP-8P	-18	-17	-19	-21	-24	-29
JP-8P2	-7	-9	-9	-12	-13	-20
Jet A	-3	-4	-4	-7	-9	-15
Jet A-1	-1	0	-2	-4	-7	-12
JP-7	-10	-12	-12	-15	-15	-23
JPTS	-9	-7	-10	-12	-15	-19
JP-8C	-23	-23	-22	-26	-31	-33
JP-8CA	-28	-27	-26	-30	-36	-37
JP-8CB	-21	-23	-21	-25	-30	-33

[a] I = Roess (API Technical Data Book, 1987); II = Brule et al. (1982); III = Twu (1984); IV = Riazi and Daubert (1980); V = Cavett (1962); VI = Kesler and Lee (1976).

Table 7. Deviations of Estimated Critical Temperatures from Measured Values for Nine Jet Fuels (Estimated T_c - Measured T_c, °F)

	Method[a]					
Fuel	I	II	III	IV	V	VI
JP-8P	-18	-17	-19	-21	-24	-29
JP-8P2	-7	-9	-9	-12	-13	-20
Jet A	-3	-4	-4	-7	-9	-15
Jet A-1	-1	0	-2	-4	-7	-12
JP-7	-10	-12	-12	-15	-15	-23
JPTS	-9	-7	-10	-12	-15	-19
JP-8C	-23	-23	-22	-26	-31	-33
JP-8CA	-28	-27	-26	-30	-36	-37
JP-8CB	-21	-23	-21	-25	-30	-33

[a] I = Roess (API Technical Data Book, 1987); II = Brule et al. (1982); III = Twu (1984); IV = Riazi and Daubert (1980); V = Cavett (1962); VI = Kesler and Lee (1976).

Table 8. Deviations of Estimated Critical Temperatures from Literature Values for Selected Hydrocarbons (Estimated T_c - Literature T_c, °F)[a]

	Method[b]					
Compound Name	I	II	III	IV	V	VI
cyclohexane	-22	-8	-9	-3	-24	-18
methylcyclohexane	-21	-6	-11	-7	-23	-19
ethylcyclohexane	-24	-13	-17	-16	-28	-26
n-propylcyclohexane	-32	-24	-28	-29	-37	-37
n-butylcyclohexane	-38	-35	-37	-39	-45	-47
cis-decalin	-26	-35	-27	-30	-40	-37
trans-decalin	-27	-31	-26	-29	-38	-36
n-nonane	0	14	2	3	-2	-2
n-decane	3	10	3	3	-1	-3
n-undecane	4	5	2	1	0	-5
n-dodecane	5	0	2	0	1	-7
n-tridecane	7	-3	2	1	3	-8
n-tetradecane	4	-11	-1	-2	1	-12
n-pentadecane	7	-12	1	0	5	-11
benzene	-2	-6	5	24	-13	2
methylbenzene	3	1	9	19	-7	4
ethylbenzene	7	4	11	15	-4	4
n-propylbenzene	8	6	11	11	-2	2
n-butylbenzene	9	6	11	8	-1	0
n-pentylbenzene	10	6	10	5	0	-2
n-hexylbenzene	10	4	9	3	0	-4

[a] Literature T_c's as well as boiling points and specific gravities, which are needed for T_c calculations, are from API Technical Data Book (1987). [b] I = Roess (API Technical Data Book, 1987); II = Brule et al. (1982); III = Twu (1984); IV = Riazi and Daubert (1980); V = Cavett (1962); VI = Kesler and Lee (1976).

Table 9. Model Compounds and Related Properties for Correlation Development for Coal-Derived Jet Fuels

Compound Name	SG, 60/60 °F[a]	Normal T_b, °F[a]	T_c, °F[a]
cyclohexane	0.7835	177.33	536.70
methylcyclohexane	0.7748	213.68	570.27
ethylcyclohexane	0.7921	269.21	636.80
cis-1,2-dimethylcyclohexane	0.8006	265.51	631.40
trans-1,2-dimethylcyclohexane	0.7803	256.01	613.40
cis-1,3-dimethylcyclohexane	0.7704	248.16	604.40
trans-1,3-dimethylcyclohexane	0.7892	256.01	617.00
cis-1,4-dimethylcyclohexane	0.7873	255.78	617.00
trans-1,4-dimethylcyclohexane	0.7670	246.83	602.60
n-propylcyclohexane	0.7981	314.10	690.80
isopropylcyclohexane	0.8064	310.57	684.90
n-butylcyclohexane	0.8034	357.70	740.93
isobutylcyclohexane	0.8161	340.32	729.05
sec-butylcyclohexane	0.8172	354.70	710.17
tert-butylcyclohexane	0.8168	340.83	702.39
bicyclohexyl	0.8900	462.27	848.93
cis-decalin	0.9018	384.47	804.38
trans-decalin	0.8755	369.16	777.02
1-methyl-cis-decalin	1.0146	469.40	899.53
9-ethyl-cis-decalin	0.8900	451.00	837.77
9-ethyl-trans-decalin	0.8648	437.00	817.27
tetralin	0.9748	405.77	836.60
1-methyl-tetralin	0.9623	429.06	835.25
1-ethyl-tetralin	0.9569	463.23	860.00
1-n-propyl-tetralin	0.9480	493.52	880.36

[a] All data are from API Technical Data Book (1987).

Table 10. Some results obtained after stressing of Dodecane+5% Decalin +50 mg PX-21 at 425°C.

Liquid sample	Liquid color				Deposit on the reactor walls, mg				Pressure (cold reactor), psi				Liquid yield, ml				Increase of weight of solid, mg			
Time	0.5h	1h	3h	5h	0.5h	1h	3h	5h	0.5h	1h	3h	5h	0.5h	1h	3h	5h	0.5h	1h	3h	5h
Dodecane+ 5%Decalin	yellow	yellow	yellow	light brown	n.m*	20	35	42	730	900	1300	1700	8.0	7.5	5.5	4.7	-	-	-	-
Dodecane+ 5% Decalin +PX-21	colorless	colorless	light yellow	yellow	-	-	-	-	700	850	1000	1600	7.2	6.6	5.0	4.0	19	25	28	40
Dodecane+ 5% Decalin +PX-21, 900°C, N_2	colorless	colorless	yellowish	light yellow	-	-	-	-	700	700	950	1300	7.5	7.0	4.6	4.4	18	20	28	32

Table 11. Major Compounds identified in the liquids obtained after stressing of Dodecane+ 5%Decalin + 50 mg PX-21 at 425°C for different times.

Compounds identified	Dodecane+5% Decalin, wt%				Dodecane+ 5% Decalin+PX-21, wt%				Dodecane+5%Decalin+ PX-21, 900°C, N_2, wt%			
Time	0.5h	1h	3h	5h	0.5h	1h	3h	5h	0.5h	1h	3h	5h
n pentane+ 1 pentene	2.07	4.92	2.60	5.77	3.36	4.78	4.14	3.96	2.52	4.74	2.62	3.70
n hexane+ 1 hexene	5.70	8.33	6.34	8.24	3.71	7.02	4.88	22.5	3.97	7.80	3.19	5.24
methyl cyclopentane	0.24	0.91	0.68	0.68	0.33	0.71	0.33	3.11	0.23	0.66	0.19	0.41
n heptane	2.80	6.38	4.50	7.15	3.57	6.59	4.83	4.98	2.79	4.83	3.33	5.13
methyl cyclohexane	0.32	1.17	0.49	1.05	0.37	0.93	0.47	0.66	0.26	0.75	0.28	0.62
n octane	2.69	5.77	4.33	6.33	3.44	6.01	4.60	4.65	2.64	4.39	3.28	4.78
ethyl cyclohexane +br. alkane	0.40	0.68	0.40	0.91	0.34	0.69	0.34	0.45	0.21	0.41	0.21	0.37
toluene	0.13	0.61	0.18	0.52	0.16	0.60	0.19	0.28	0.10	0.38	0.11	0.26
n nonane	2.84	5.21	4.30	5.89	3.41	5.52	4.52	4.49	2.74	4.13	3.34	4.77
C_3 cyclohexane	0.07	0.39	0.23	0.37	0.09	0.35	0.17	0.19	0.07	0.24	0.11	0.20
n decane	0.93	1.99	1.49	2.13	1.35	2.30	2.01	1.91	1.03	1.66	1.42	2.08
C_3 benzene	0.04	0.21	0.14	0.25	0.06	0.24	0.14	0.15	0.07	0.14	0.08	0.15
n undecane	0.58	1.18	0.97	1.28	0.76	1.25	0.94	0.95	0.55	0.90	0.68	1.04
trans decalin	5.37	4.21	4.54	3.73	3.55	3.33	3.94	2.26	4.05	3.76	3.98	3.48
cis decalin	3.22	1.57	2.15	1.27	2.03	1.21	1.66	0.72	2.70	1.87	2.23	1.59
n dodecane	59.2	36.2	51.1	34.0	58.3	39.6	51.1	32.0	63.3	45.4	61.9	50.4
naphthalene	0.36	0.6	0.52	0.60	0.87	1.29	1.42	1.20	0.53	0.85	0.8	1.22

Table 12. BET N_2 surface area of activated carbon PX-21 before and after stressing with dodecane+5% decalin

Thermal stressing of Dodecane+5% Decalin at 425°C	BET N_2 surface area before thermal stressing, m^2/g	BET N_2 surface area after thermal stressing, m^2/g
PX-21	2830	180
PX-21 outgassed at 900°C in N_2	2670	440

Table 13. The antioxidants screened at 425°C.

antioxidant	source
phenol	Aldrich
2,6-di-*tert* -butyl-4-methylphenol	Aldrich
1,1,1,3,3-Hexafluoro-2-phenyl-2-propanol	Aldrich
pentaerythrytol	Aldrich
aminodiphenylmethane	Aldrich
benzylamine	Aldrich
tritylamine	Aldrich
2-mercaptoimidazole	Aldrich
2-mercaptobenzothiazole	Aldrich
2-naphthalenethiol	Aldrich
triphenylmethylmercaptan	Aldrich
dibutyltin dilaurate	Aldrich
Mark 1900 (organotin)	Witco
Mark 1901 (alkyltin mercaptide)	Witco
Mark 1925 (organotin)	Witco
Mark 1044 (alkyltin maleate)	Witco
Mark 2255 (butyltin mercapto carboxylate)	Witco

Table 14. Equilibrium Decalin Isomer Distribution from Nap Hydrogenation Over Pd/ HM21 Catalyst in 200°C Runs

time (h)	run no.	%Nap conv.	Product Distribution (mole percent)				trans/cis DeHN
			TeHN	trans-DeHN	cis-DeHN	total DeHN's	
1	174	100.00	0.00	76.50	23.50	100.00	3.26
6	175	99.95	0.00	93.08	6.92	100.00	13.46
10	176	100.00	0.00	93.22	6.78	100.00	13.74
24	177	100.00	0.00	93.15	6.85	100.00	13.59

Table 15. Nap Hydrogenation Over Pd/HY Catalyst in 200°C Runs

time (min)	run no.	%Nap conv.	Product Distribution (mole percent)				trans/cis DeHN
			TeHN	trans-DeHN	cis-DeHN	total DeHN's	
6	188	100.00	0.00	62.94	37.06	100.00	1.70
15	189	99.97	0.05	64.70	35.25	99.95	1.84
30	190	100.00	0.00	68.94	31.06	100.00	2.22
60	171	100.00	0.00	72.94	27.06	100.00	2.69

Table 16. Nap Hydrogenation Over PtHY Catalyst in 200°C Runs

time (min)	run no.	%Nap conv.	Product Distribution (mole percent)				trans/cis DeHN
			TeHN	trans-DeHN	cis-DeHN	total DeHN's	
6	184	99.89	48.42	9.97	41.61	51.58	0.24
15	185	100.00	0.29	20.35	79.36	99.71	0.26
15	186	100.00	2.29	19.10	78.62	97.71	0.24
30	187	100.00	0.04	20.51	79.46	99.96	0.26
60	166	99.94	2.58	15.12	82.30	97.42	0.18

Table 17. Nap Hydrogenation Over Pd/HM38 Catalysts in 200°C Runs

time (min)	run no.	%Nap conv.	Product Distribution (mole percent) TeHN	trans-DeHN	cis-DeHN	total DeHN's	trans/cis DeHN
Pd/HM38(AS) prpared by A. Schmitz							
6	195	100.00	0.00	78.86	21.14	100.00	3.73
15	196	100.00	0.00	88.92	11.08	100.00	8.03
30	197	100.00	0.00	92.46	7.54	100.00	12.27
60	198	100.00	0.00	93.08	6.92	100.00	13.46
Pd/HM38 prpared by G. Bowers							
15	161	100.00	0.00	65.36	34.64	100.00	1.89
30	162	100.00	0.00	72.19	27.81	100.00	2.60
60	163	100.00	0.00	81.56	18.44	100.00	4.42

Table 18. Nap Hydrogenation Over Pt/HM38 Catalysts in 200°C runs

time (min)	run no.	%Nap conv.	Product Distribution (mole percent) TeHN	trans-DeHN	cis-DeHN	total DeHN's	trans/cis DeHN
Pt/HM38(AS) prpared by A. Schmitz							
6	191	100.00	0.00	53.86	46.14	100.00	1.17
15	192	100.00	0.00	71.15	28.85	100.00	2.47
30	193	100.00	0.00	84.75	15.25	100.00	5.56
60	194	100.00	0.00	92.50	7.50	100.00	12.33
Pt/HM38 prpared by G. Bowers							
15	158	99.65	0.08	46.18	53.74	99.92	0.86
30	159	99.98	0.02	55.69	44.29	99.98	1.26
60	160	100.00	0.00	70.10	29.90	100.00	2.34

Table 19 Nap Hydrogenation Over (Pt or Pd) HM17 Catalysts in 12 h Runs at 25°C

catalyst	run no.	%Nap conv.	Product Distribution (mole percent) TeHN	trans-DeHN	cis-DeHN	total DeHN's	trans/cis DeHN
Pt/HM21	182	87.60	92.60	1.56	5.85	7.40	0.27
Pd/HM21	183	26.01	99.67	0.09	0.24	0.33	0.39

Table 20. Thermal Gravimetric Analysis of Desiccated and Re-Calcined Samples

catalyst	description of treatment	tga sample mass, mg	absolute weight loss, mg	% weight loss	% corrected weight loss[1]
Pt/HM21	G. Bowers sample stored 1 year in desiccator	4.345	0.46	10.59 %	8.51 %
Pt/HM21	Stored sample calcined 4 h at 500 °C	4.479	0.24	5.36 %	3.34 %
Pd/HM21	G. Bowers sample stored 1 year in desiccator	4.534	0.5	11.03 %	9.03 %
Pd/HM21	Stored sample calcined 4 h at 500 °C	3.815	0.25	6.55 %	4.18 %

[1] Empty sample crucible weight loss under same conditions is 0.0904 mg. Crucible pre-cleaned in base, then acid, then calcined at 500 °C for 12 h, and equilibrated in ambient for 4 h before TGA run.

Table 21. Naphthalene Hydrogenation Over Pd/HM21 in 200°C Runs
Effect of Ageing, Calcination and Moisture

description	time (h)	run no.	%Nap conv.	Product Distribution (mole %)				
				TeHN	trans-DeHN	cis-DeHN	total DeHN's	trans/cis DeHN
original GB data	2	G11	99.90	0.20	64.70	34.60	99.30	1.87
original GB data	4	G12	99.50	0.00	65.00	34.50	99.50	1.88
stored sample	1	174	100.00	0.00	76.50	23.50	100.00	3.26
stored sample re-calcined 4 h at 500 °C	1	178	100.00	0.04	76.80	23.20	99.96	3.32
re-calcined sample with 40 mg added water[1]	1	179	100.00	0.01	70.50	29.50	99.99	2.39

[1] Total moisture: (250 mg catalyst x 4.18%) + 40 mg added water = 50.45 mg; water/dry-catalyst mass = 0.21.

Table 22. Naphthalene Hydrogenation Over Pt/HM21 in 200°C Runs
Effects of Ageing, Calcination and Moisture

description	time (h)	run no.	%Nap conv.	Product Distribution (mole %)				
				TeHN	trans-DeHN	cis-DeHN	total DeHN's	trans/cis DeHN
original GB data	2	G3	75.00	79.80	7.60	12.40	20.00	0.61
original GB data	4	G4	98.70	39.90	21.60	38.20	59.80	0.57
stored sample	1	167	100.00	0.00	45.50	54.50	100.00	0.83
stored sample re-calcined 4 h at 500 °C	1	180	100.00	0.00	48.30	51.70	100.00	0.93
re-calcined sample with 60 mg added water[1]	1	181	100.00	0.00	35.30	64.70	100.00	0.55

[1] Total moisture: (400 mg catalyst x 3.34%) + 60 mg added water = 73.36 mg; water/dry-catalyst mass = 0.19.

Table 23

Synthesis of mesoporous aluminosilicate, Al-MCM-41 samples

Molar Compn: $50SiO_2$ xAl_2O_3 $2.19(TMA)_2O$ $7.81(CTMA)_2O$ $3165\ H_2O$
Temp.: 100°C; Time: 24 hours

S.No.	Sample ID	Al source	x	procedure
1	MRK9A	Al Isopropoxide	0.50	I
2	MRK9B	Al Isopropoxide	1.00	I
3	MRK9C	Al Isopropoxide	2.00	I
4	MRK9D	Al Isopropoxide	0.50	II
5	MRK10A	Catapal B	0.50	I
6	MRK10B	Catapal B	1.00	I
7	MRK10C	Catapal B	2.00	I
8	MRK10D	Catapal B	0.50	II
9	MRK11A	Al Sulfate	0.50	I
10	MRK11B	Al Sulfate	1.00	I
11	MRK11C	Al Sulfate	2.00	I
12	MRK11D	Al Sulfate	0.50	II
13	MRK12	No Al source	0.00	I

Table 24

XRD characteristics of mesoporous aluminosilicate, Al-MCM-41 samples

Sample	Two Theta (deg)	Peak Intensity (cps)	D spacing (A)
MRK9AC	2.36	2967	37.4
MRK9BC	2.28	2906	38.7
MRK9CC	2.33	2272	37.9
MRK9DC	2.66	491	33.1
MRK10AC	2.68	3642	32.9
MRK10BC	2.58	3216	34.2
MRK10CC	2.54	2722	34.7
MRK10DC	2.64	2095	33.4
MRK11AC	2.48	2511	35.6
MRK11BC	2.34	2204	37.7
MRK11CC	2.32	583	38.1
MRK11DC	2.46	3032	35.8
MRK12C	2.6	2829	33.9

APPENDIX II

Figures

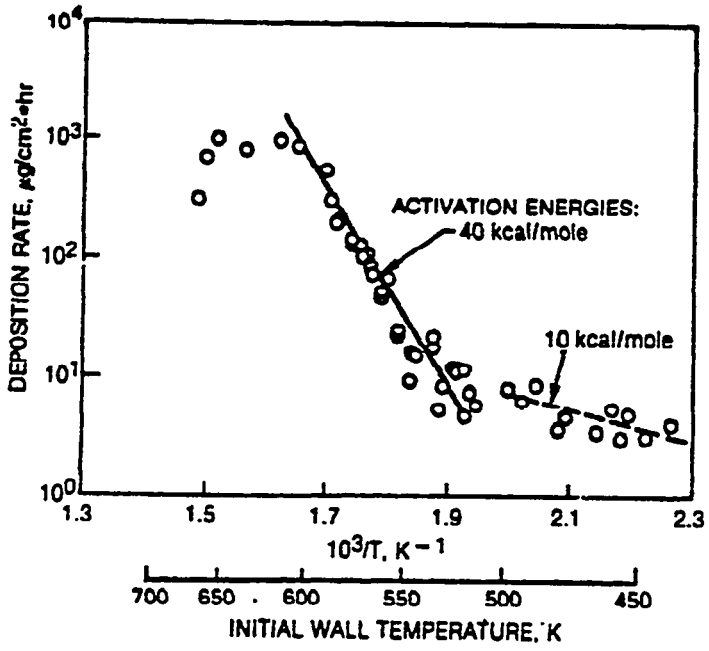

Figure 1. Arrhenius plot of deposition rates in jet fuel JP–5.

a)

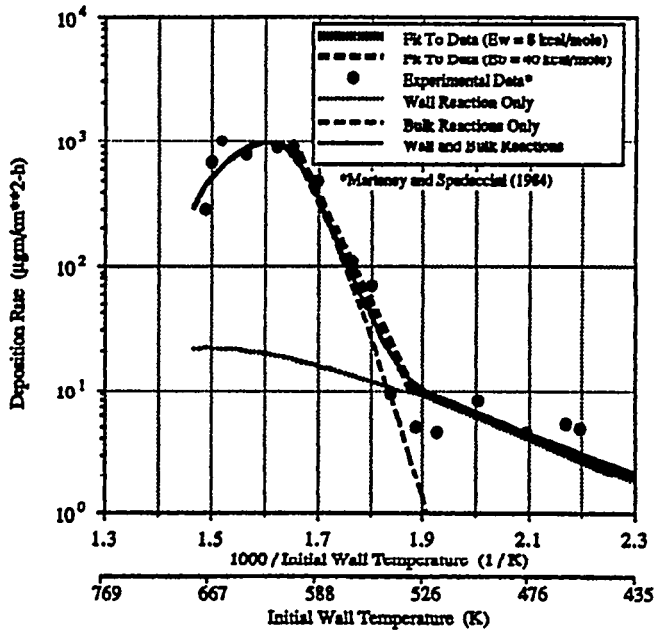

(b)

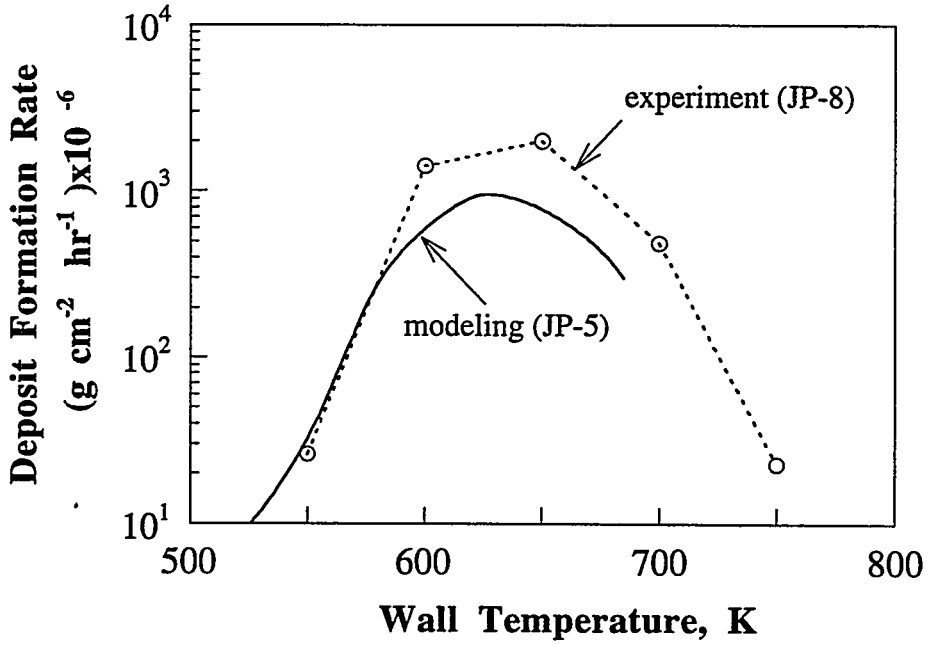

Figure 2. (a) Effect of wall and bulk reactions on deposition rates in jet fuel JP–5; (b) The comparison of the results obtained from the CFDC model and the JP–8 decomposition experiment.

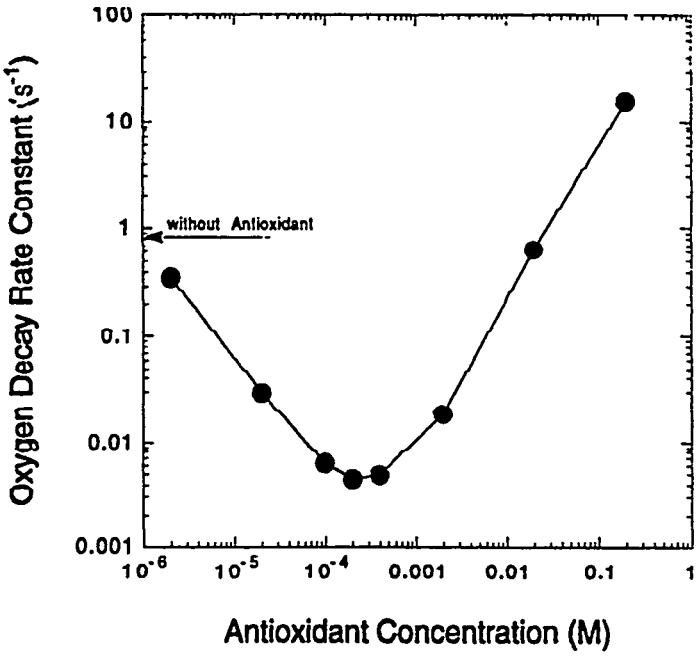

Figure 3. Log–log plot of oxygen decay rate constant vs. antioxidant concentration at 473 K.

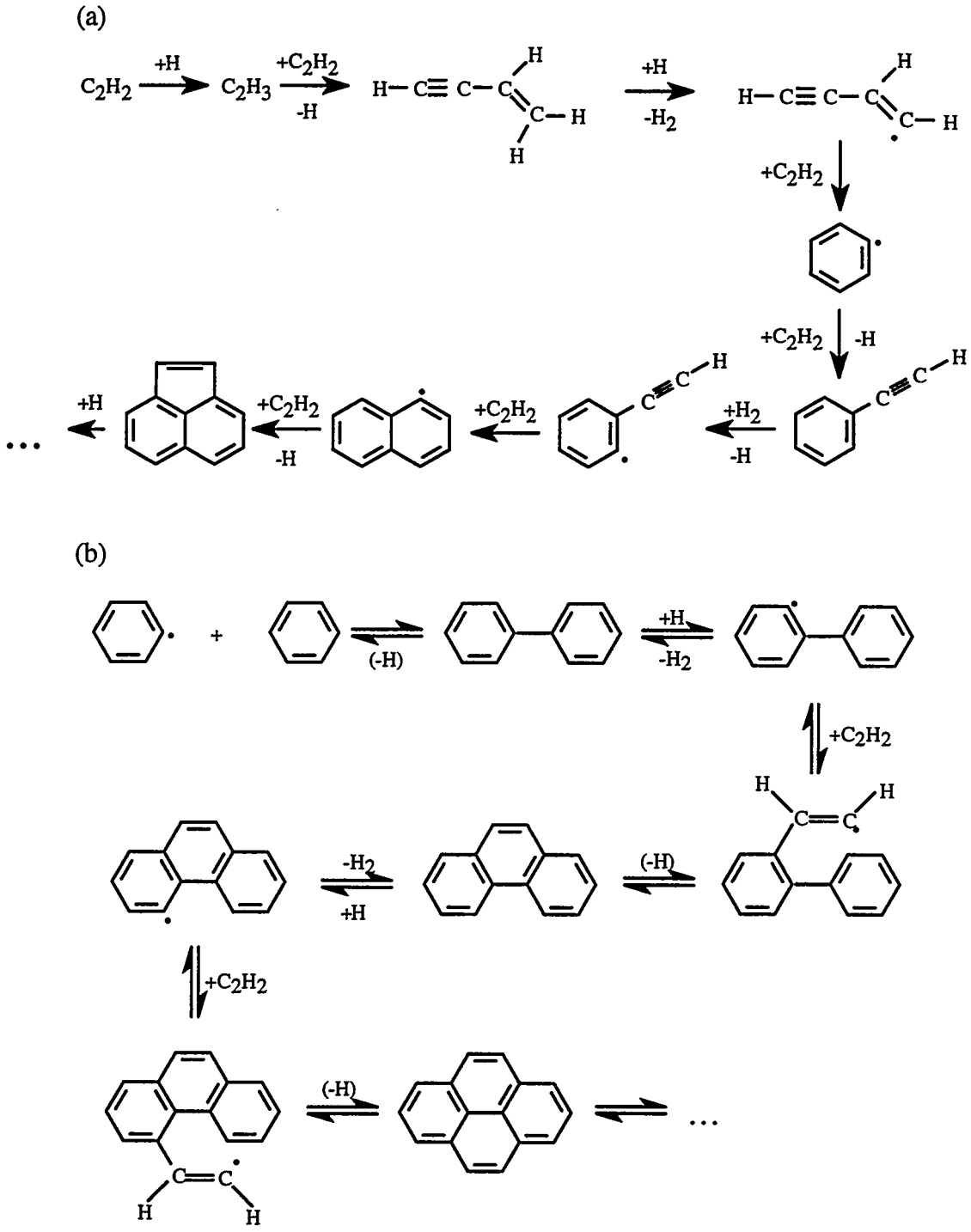

Figure 4. (a) Principal reaction pathway for formation of polyaromatics through acetylene; (b) reaction pathway for formation of small polycyclic aromatics in pyrolysis of benzene.

(a)

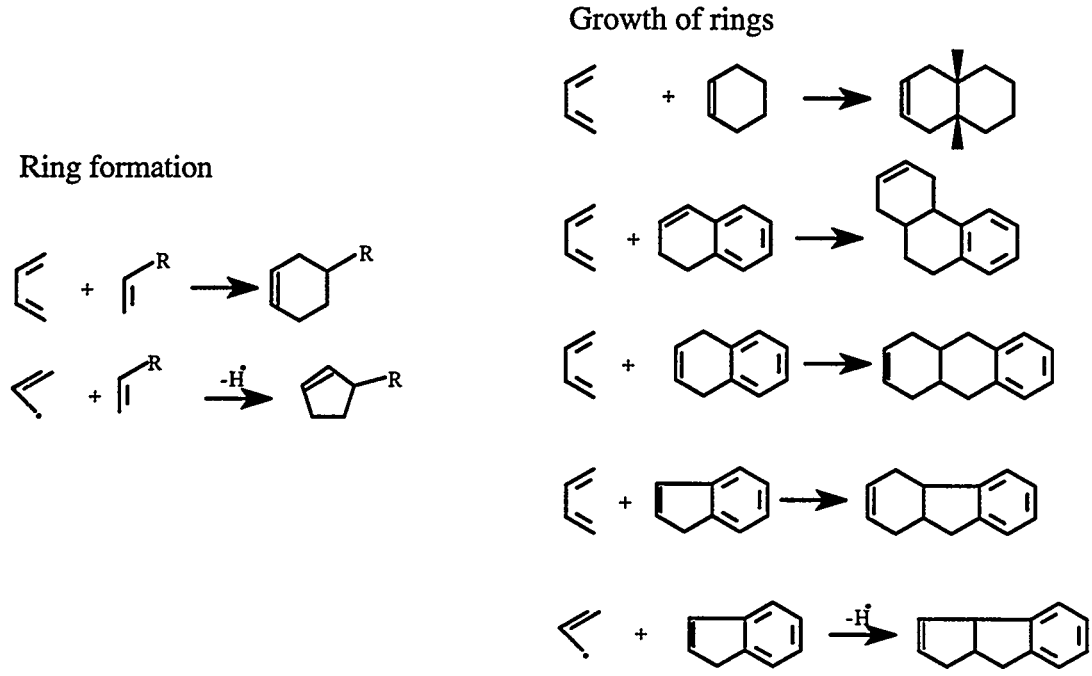

(b)

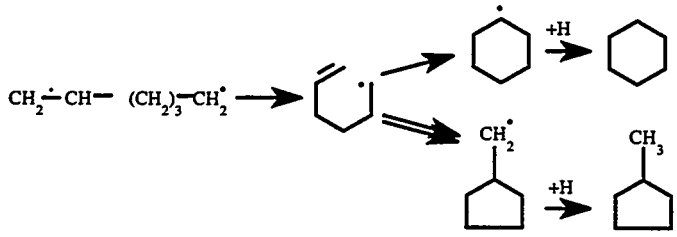

Figure 5. (a) Diels–Alder reaction type pathway for first ring formation and ring growth; (b) ring–closure reaction of 5–hexenyl radical as a possible pathway for cyclic compound production;

(c)

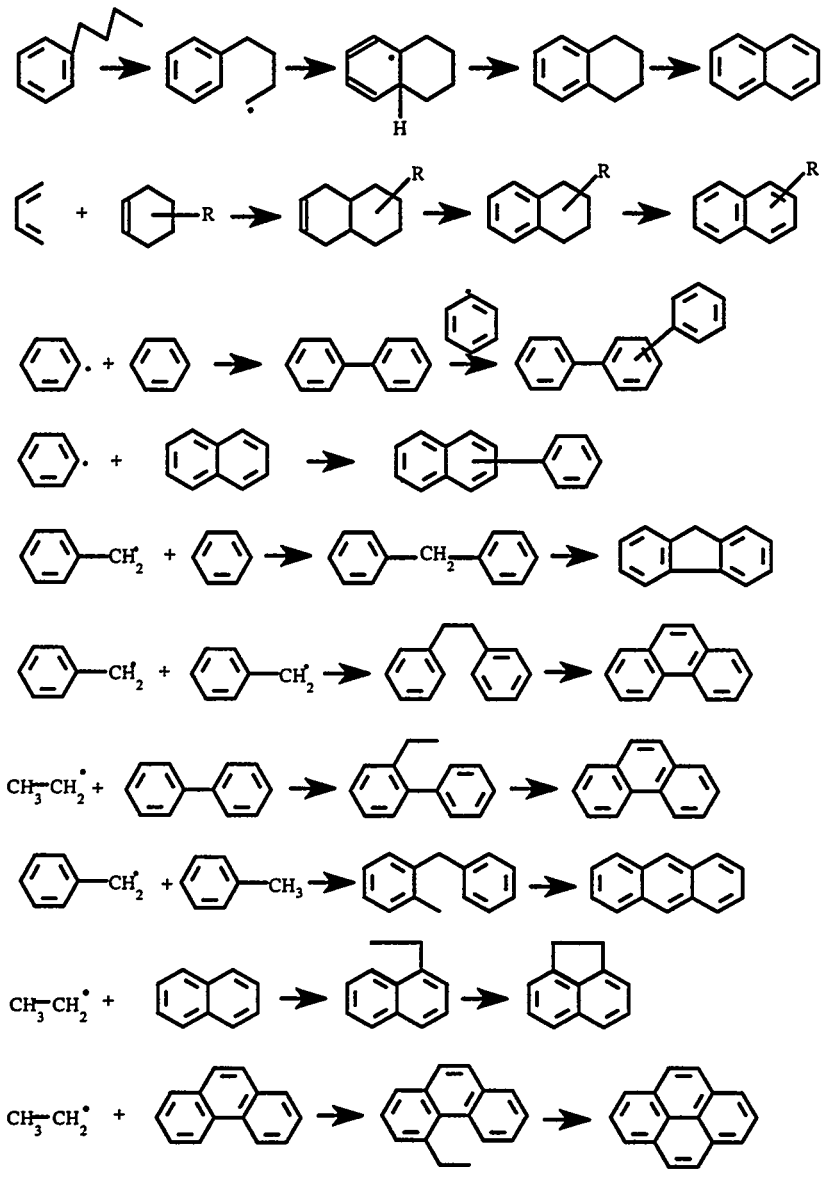

Figure 5. (c) Possible mechanism for the formation of PAHs.

phenyl radical + acetylene

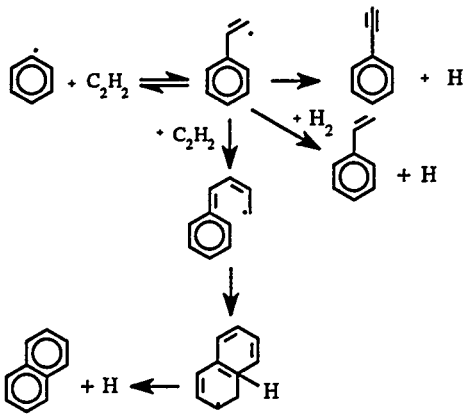

phenyl radical + vinylacetylene

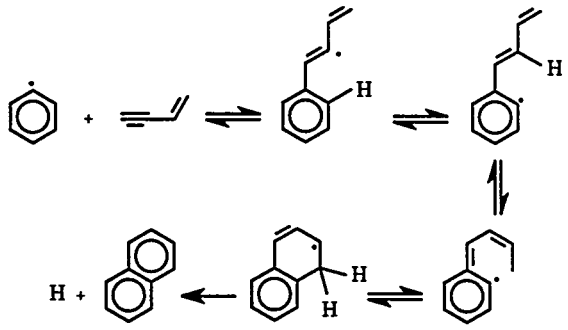

benzyl radical + acetylene

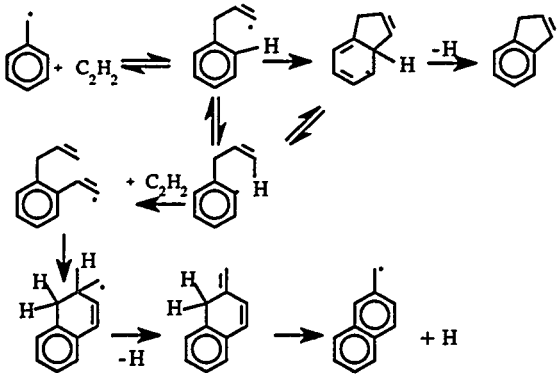

benzyl radical + vinylacetylene

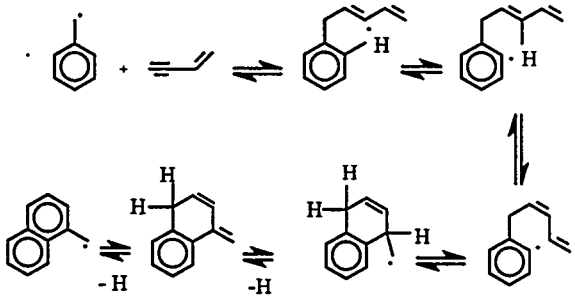

Figure 6. Possible free radical addition schemes for PAH formation.

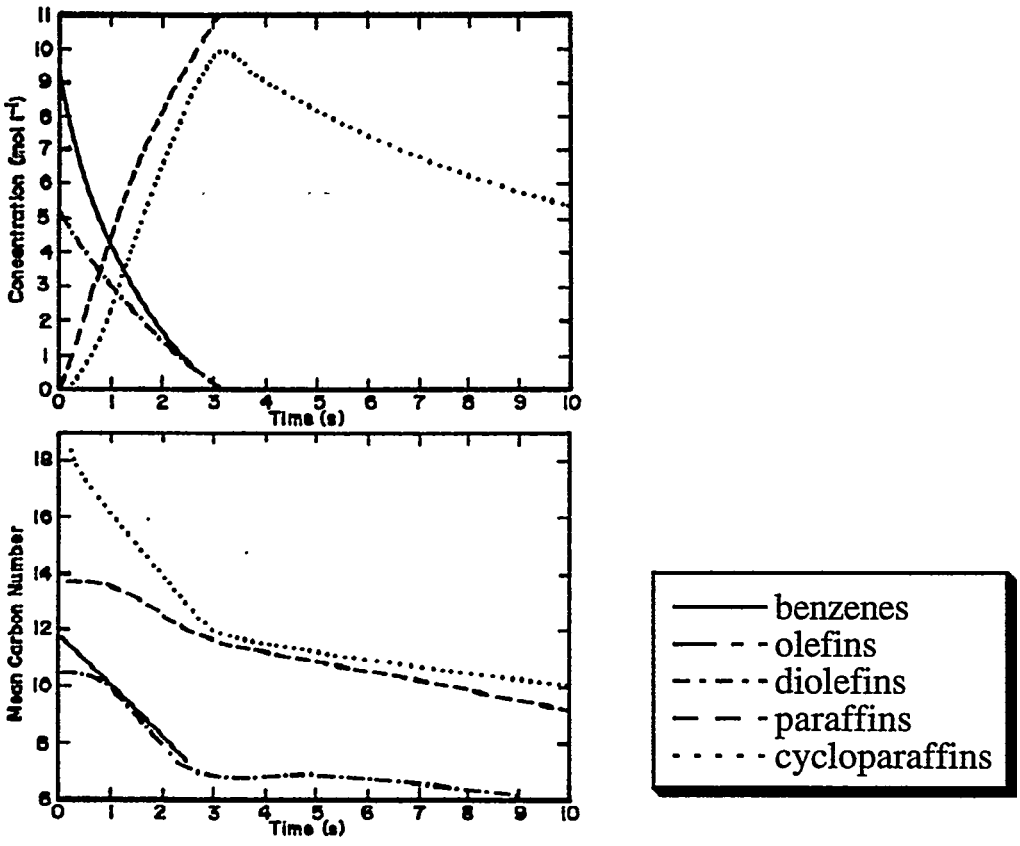

Figure 7. Evolution of the compound class concentration (above) and mean carbon number (below) during the decomposition of benzene–olefin initial mixture, with hydrogen concentration 10 mol/L at 870 K.

a.)

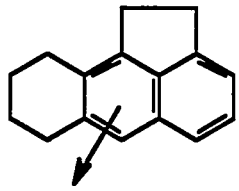

A6-a six carbon aromatic ring

b.)

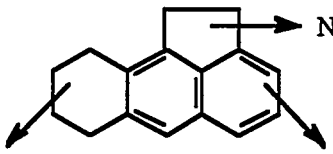

N2-a two carbon naphtenic ring increment

N4-a four carbon naphtenic ring increment

A4-a four carbon aromatic ring increment

c.)

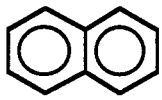

A6	A4	A2	N6	N5	N4	N3	N2	N1	R	br	me	IH	AA	NS	RS	AN	NN	RN	NO	RO	KO
1	1	0	0	0	0	0	0	0	0	0	0	0	0	0	0	0	0	0	0	0	0

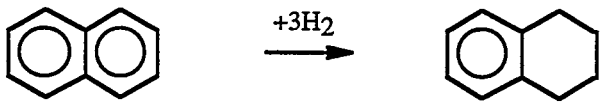

reactant selection rule **A4 not equal zero** and **A2=0**

(reactant)

A6	A4	A2	N6	N5	N4	N3	N2	N1	R	br	me	IH	AA	NS	RS	AN	NN	RN	NO	RO	KO
1	1	0	0	0	0	0	0	0	0	0	0	0	0	0	0	0	0	0	0	0	0

-1 **+1** product generation rule **A4 → A4-1** **N4 → N4+1**

A6	A4	A2	N6	N5	N4	N3	N2	N1	R	br	me	IH	AA	NS	RS	AN	NN	RN	NO	RO	KO
1	0	0	0	0	1	0	0	0	0	0	0	0	0	0	0	0	0	0	0	0	0

(product)

Figure 8. Examples of structural subsystems and their vector representation: (a) A6 as a group that can exist by etself when all other incremental structures are absent; (b) A4, N4, N1 as example of incremental structures that must be attached to some other object; (c) vector representation of naphthalene and its hydrogenation.

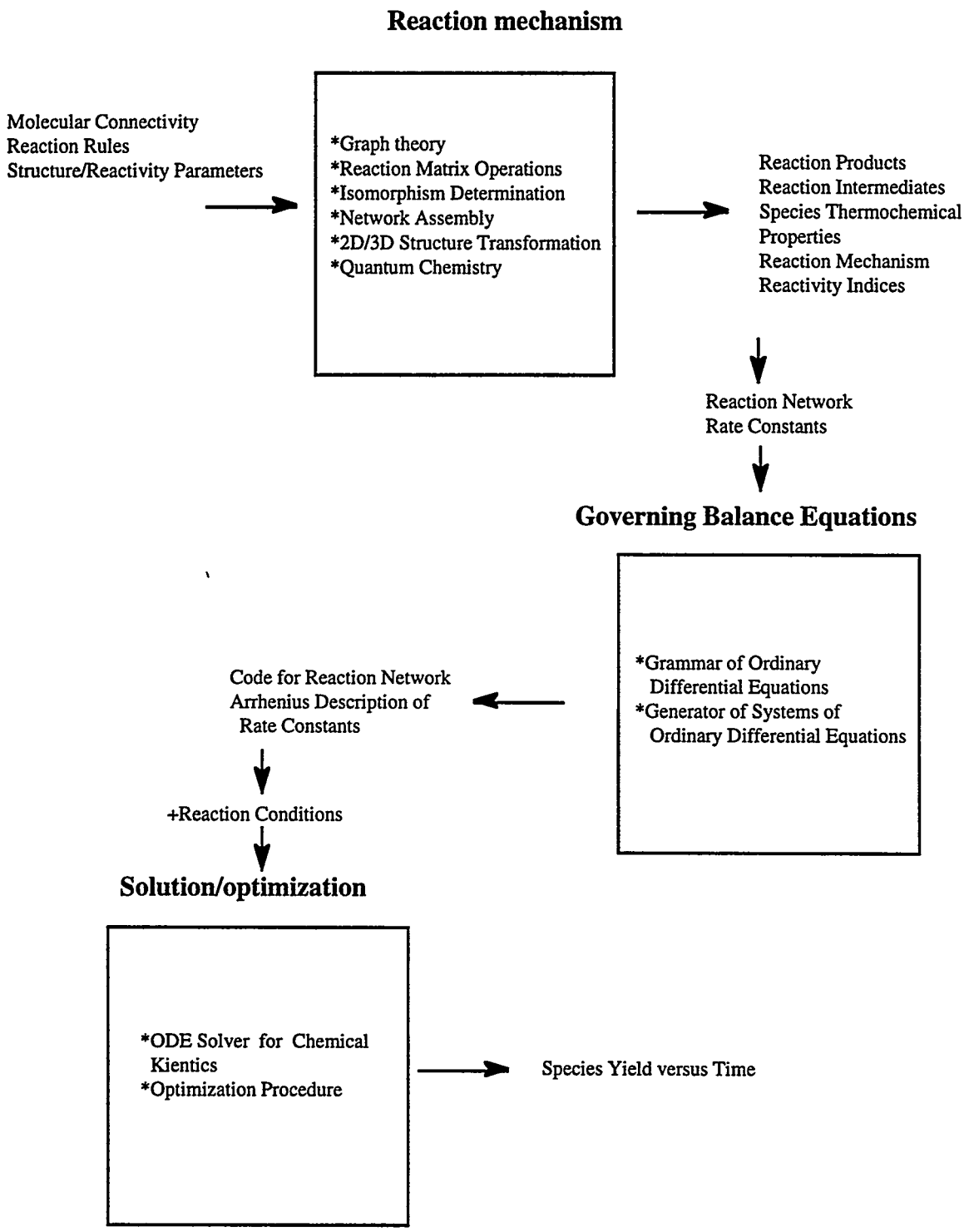

Figure 9. Vision of integrated computer-generated modeling through the development of module models.

(a)

$H^{\bullet}[1]$

and

$$\begin{array}{c} C \\ H \\ H \\ H \\ H \end{array}\begin{bmatrix} 0 & 1 & 1 & 1 & 1 \\ 1 & 0 & 0 & 0 & 0 \\ 1 & 0 & 0 & 0 & 0 \\ 1 & 0 & 0 & 0 & 0 \\ 1 & 0 & 0 & 0 & 0 \end{bmatrix} \rightarrow \begin{array}{c} C \\ H \\ H \\ H \\ H \\ H^{\bullet} \end{array}\begin{bmatrix} 0 & 1 & 1 & 1 & 1 & 0 \\ 1 & 0 & 0 & 0 & 0 & 0 \\ 1 & 0 & 0 & 0 & 0 & 0 \\ 1 & 0 & 0 & 0 & 0 & 0 \\ 1 & 0 & 0 & 0 & 0 & 0 \\ 0 & 0 & 0 & 0 & 0 & 1 \end{bmatrix} \rightarrow \begin{array}{c} H \\ C \\ H^{\bullet} \\ H \\ H \\ H \end{array}\begin{bmatrix} 0 & 1 & 0 & 0 & 0 & 0 \\ 1 & 0 & 0 & 1 & 1 & 1 \\ 0 & 0 & 1 & 0 & 0 & 0 \\ 0 & 1 & 0 & 0 & 0 & 0 \\ 0 & 1 & 0 & 0 & 0 & 0 \\ 0 & 1 & 0 & 0 & 0 & 0 \end{bmatrix}$$

(b)

$$\begin{array}{c} H \\ C \\ H^{\bullet} \end{array}\begin{bmatrix} 0 & 1 & 0 \\ 1 & 0 & 0 \\ 0 & 0 & 1 \end{bmatrix} + \begin{bmatrix} 0 & -1 & 1 \\ -1 & 1 & 0 \\ 1 & 0 & -1 \end{bmatrix} = \begin{array}{c} H \\ C \\ H^{\bullet} \end{array}\begin{bmatrix} 0 & 0 & 1 \\ 0 & 1 & 0 \\ 1 & 0 & 0 \end{bmatrix}$$

(c)

$$\begin{array}{c} H \\ C \\ H^{\bullet} \\ H \\ H \\ H \end{array}\begin{bmatrix} \mathbf{0} & \mathbf{0} & \mathbf{1} & 0 & 0 & 0 \\ \boldsymbol{0} & \boldsymbol{1} & \mathbf{0} & 1 & 1 & 1 \\ \boldsymbol{1} & \boldsymbol{0} & \mathbf{0} & 0 & 0 & 0 \\ 0 & 1 & 0 & 0 & 0 & 0 \\ 0 & 1 & 0 & 0 & 0 & 0 \\ 0 & 1 & 0 & 0 & 0 & 0 \end{bmatrix} \Rightarrow \begin{array}{c} H \\ H \end{array}\begin{bmatrix} 0 & 1 \\ 1 & 0 \end{bmatrix} \textit{and} \begin{array}{c} C^{\bullet} \\ H \\ H \\ H \end{array}\begin{bmatrix} 1 & 1 & 1 & 1 \\ 1 & 0 & 0 & 0 \\ 1 & 0 & 0 & 0 \\ 1 & 0 & 0 & 0 \end{bmatrix}$$

Figure 10. (a) Methane BE matrix and hydrogen atom BE matrix being transferred to reactant matrix for hydrogen abstraction. (b) Application of the hydrogen abstraction matrix to a minimal BE representation of reactant matrix (a). (c) Product matrix and its separation to molecular hydrogen matrix and methyl radical matrix.

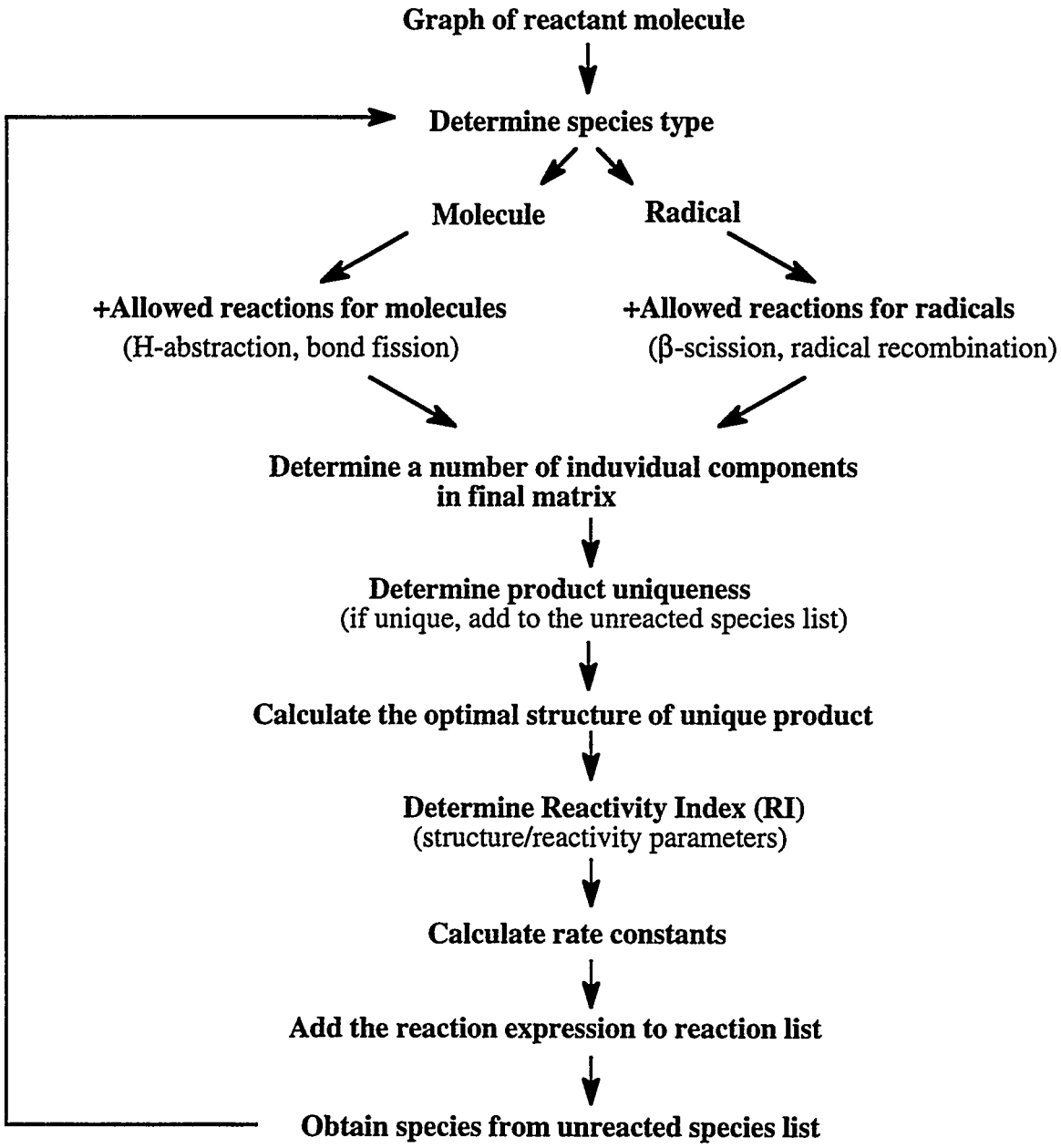

Figure 11. Logic of the algorithm for the generation of specie array and the assembly of the reaction mechanism in graph notation.

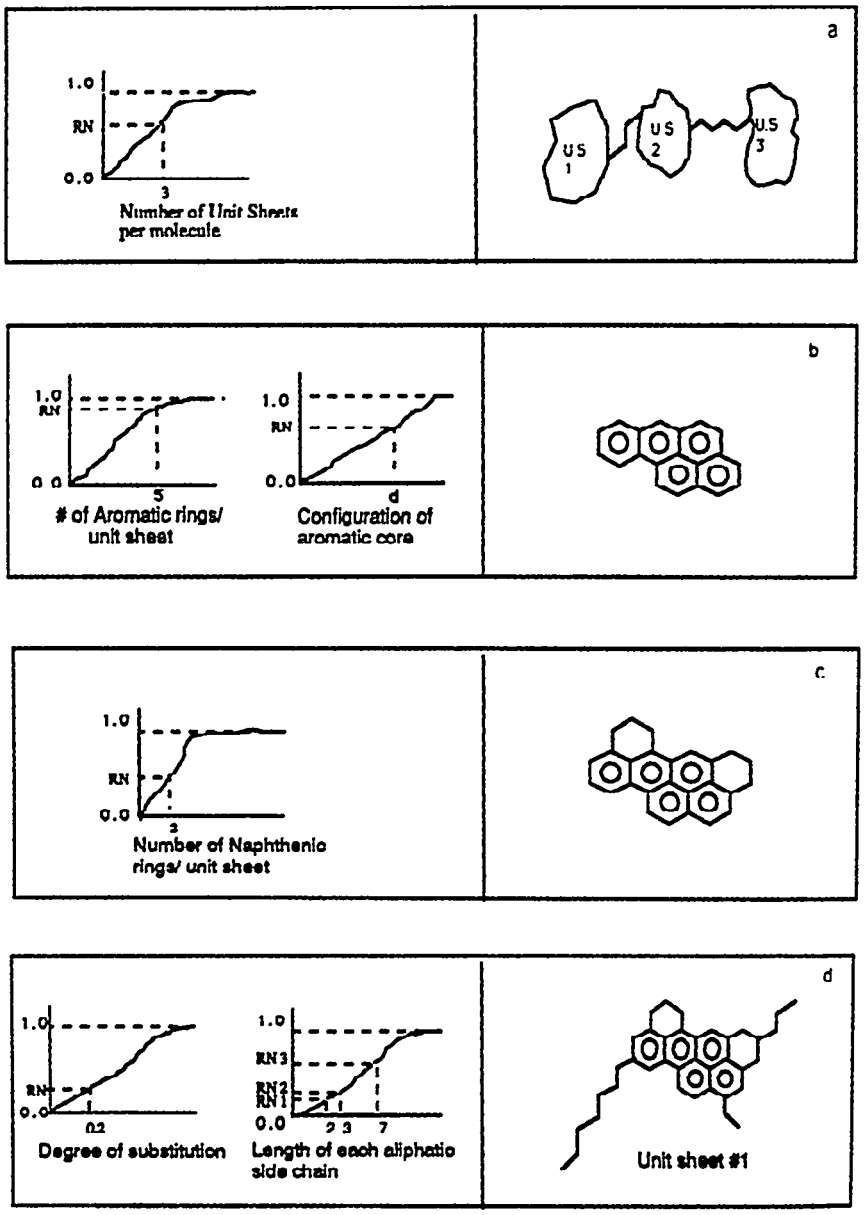

Figure 12. Initial structural distribution for a generic asphaltene feed.
(a) Number of unit sheets per molecule; (b) number of rings per sheet and arrangement of the aromatic core;
(c) number of naphtenic rings;
(d) number and length of asphaltic substituents.

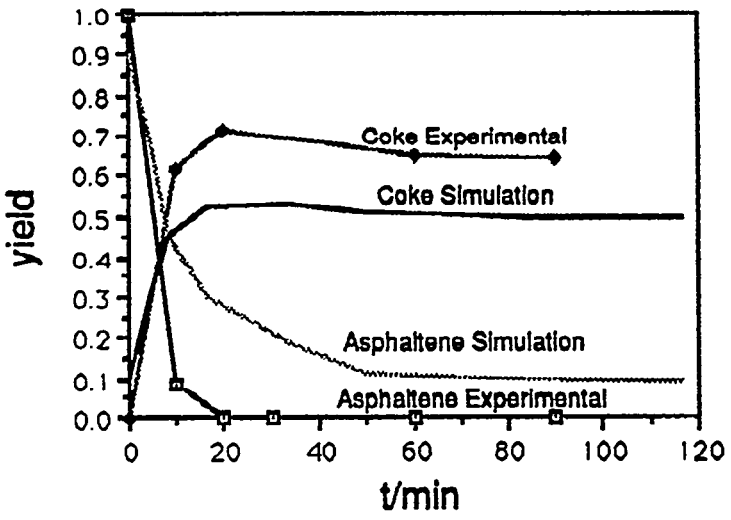

Figure 13. Simulation and experimental results for asphaltene pyrolysis at 720 K.

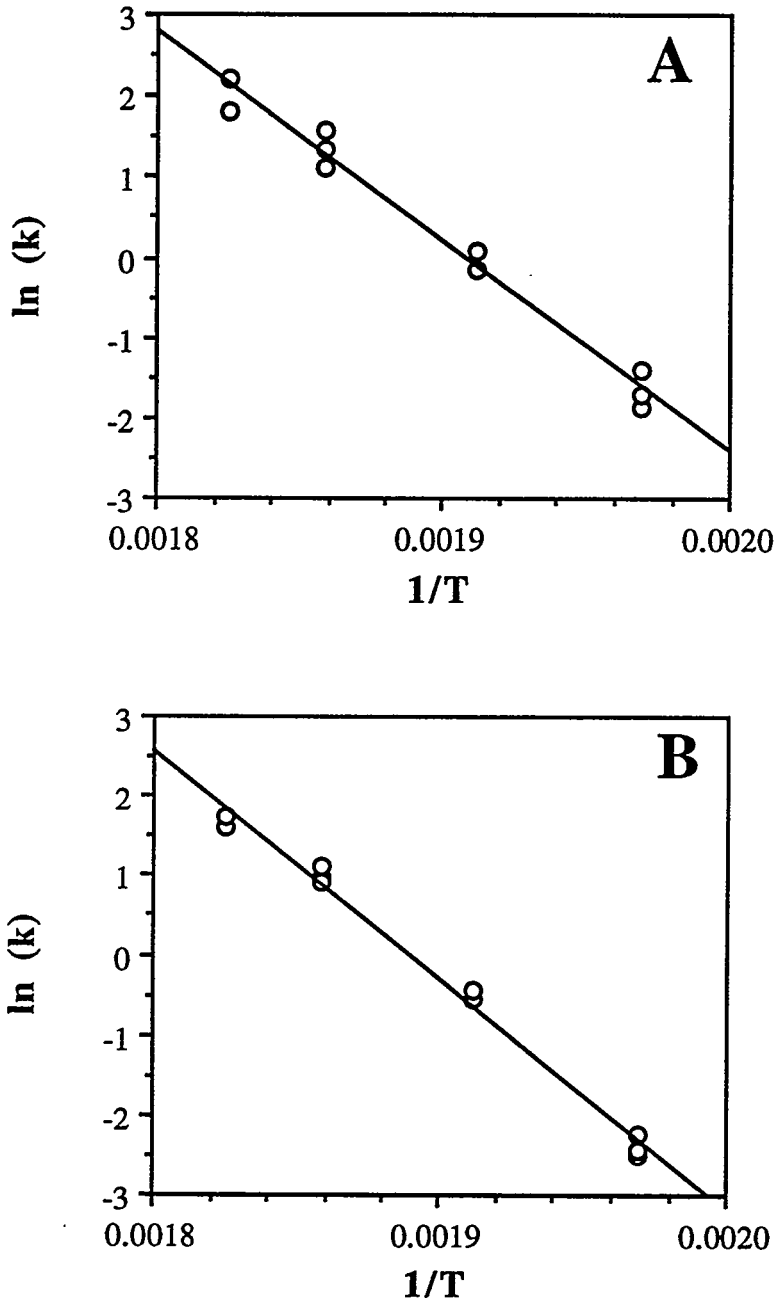

Figure 14. Arrhenius Plots for Catalyzed Isomerization of *cis*-Decalin under an Initial Pressure of 0.79 MPa UHP N_2 using 0.2-g catalyst HY (A) and LaHY (B).

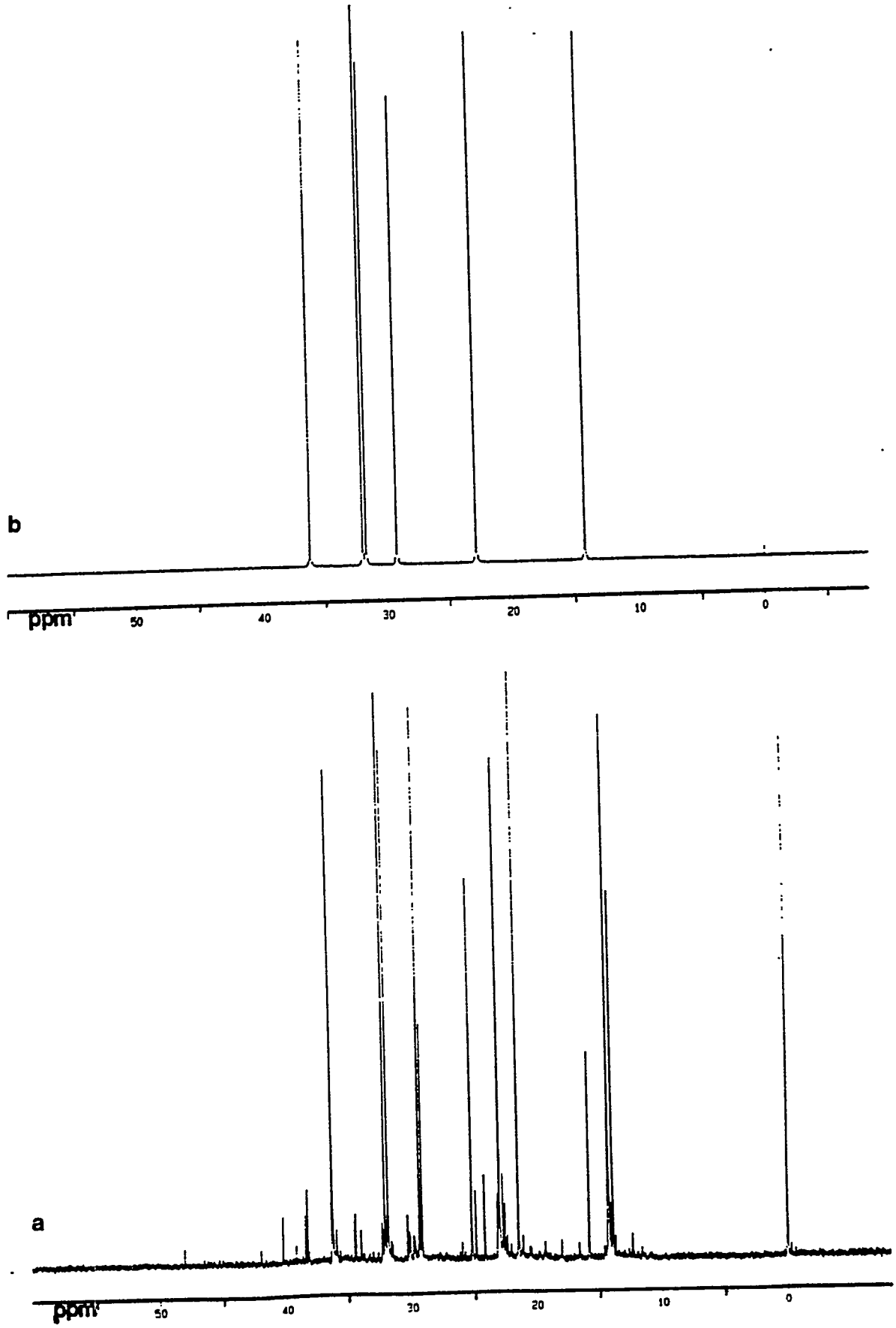

Figure 15. The ^{13}C NMR spectra of 1-phenylhexane (a) after 6 hours of thermal stressing.at 400° C (b) unstressed.

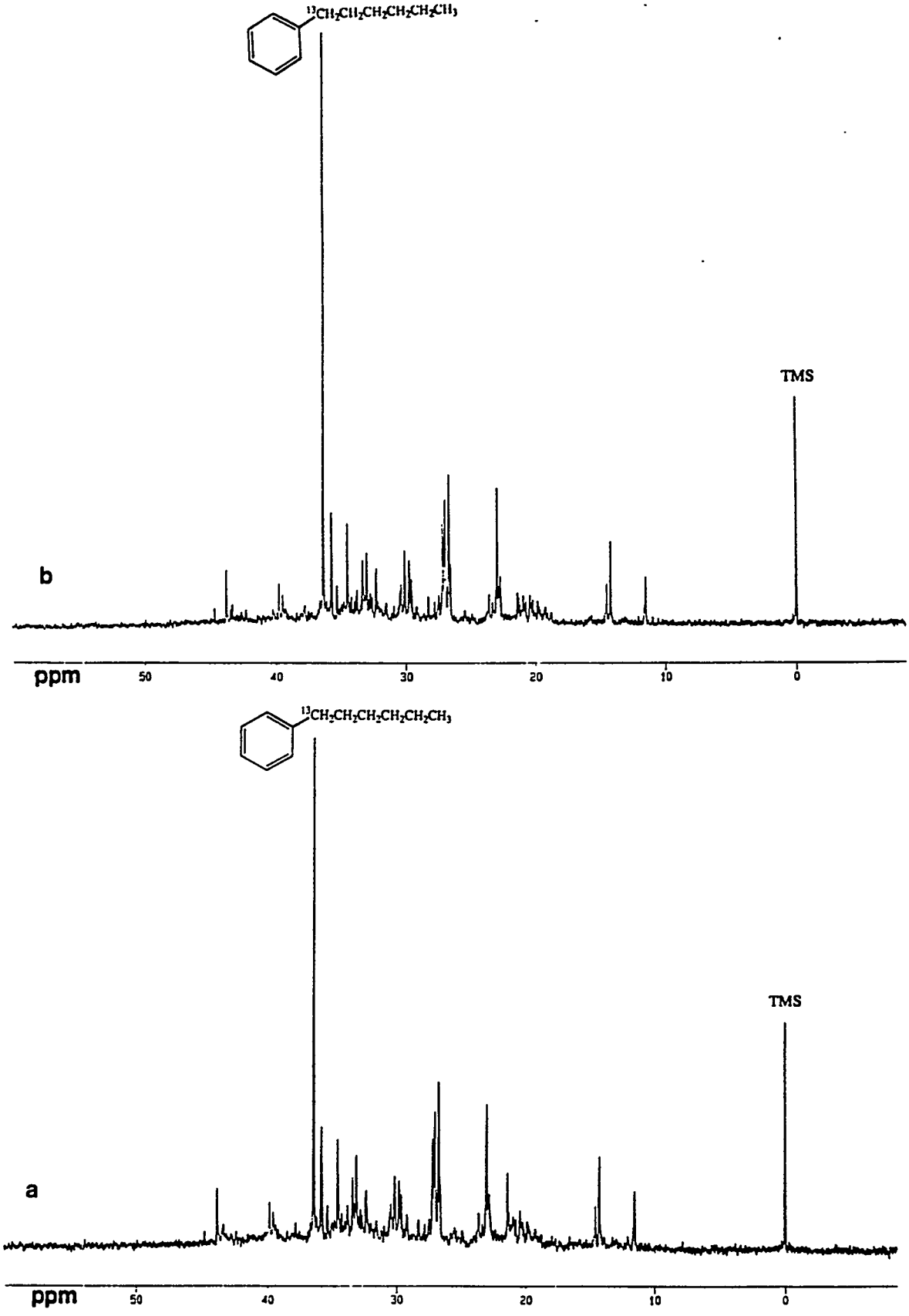

Figure 16. The ^{13}C NMR spectra of 1-phenyl-1-^{13}C-hexane (a) after 6 hours of thermal stressing at 400° C (b) unstressed.

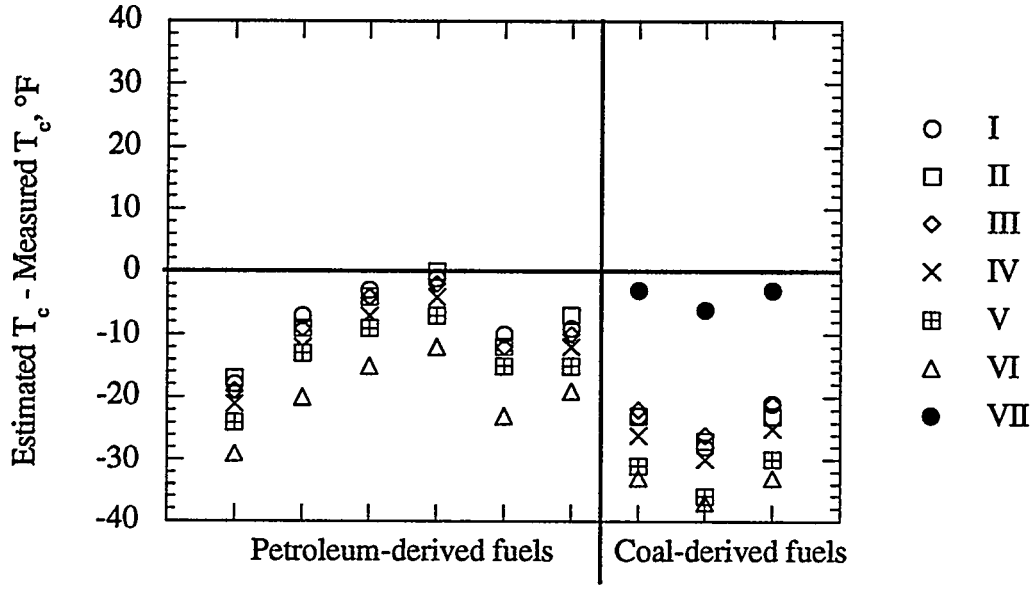

Figure 18. Comparison of Seven T_c Estimation Methods for Nine Jet Fuels.

I = Roess (API Technical Data Book, 1987); II = Brule et al. (1982); III = Twu (1984); IV = Riazi and Daubert (1980); V = Cavett (1962); VI = Kesler and Lee (1976); VII = New correlation for coal-derived jet fuels.

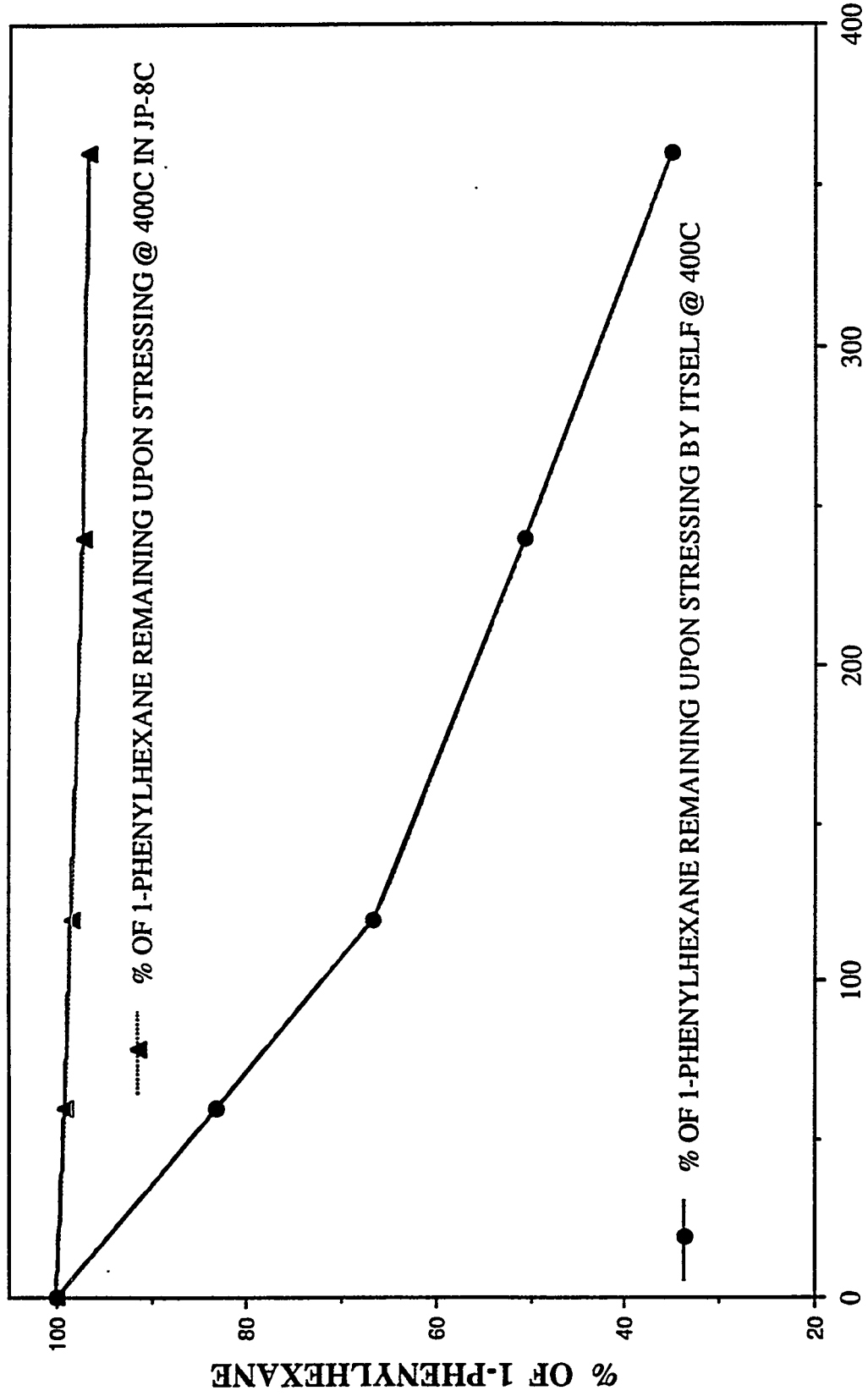

Figure 17. A graph of the % 1-phenylhexane remaining after thermal stressing in the presence and absence of JP-8C at 400° C.

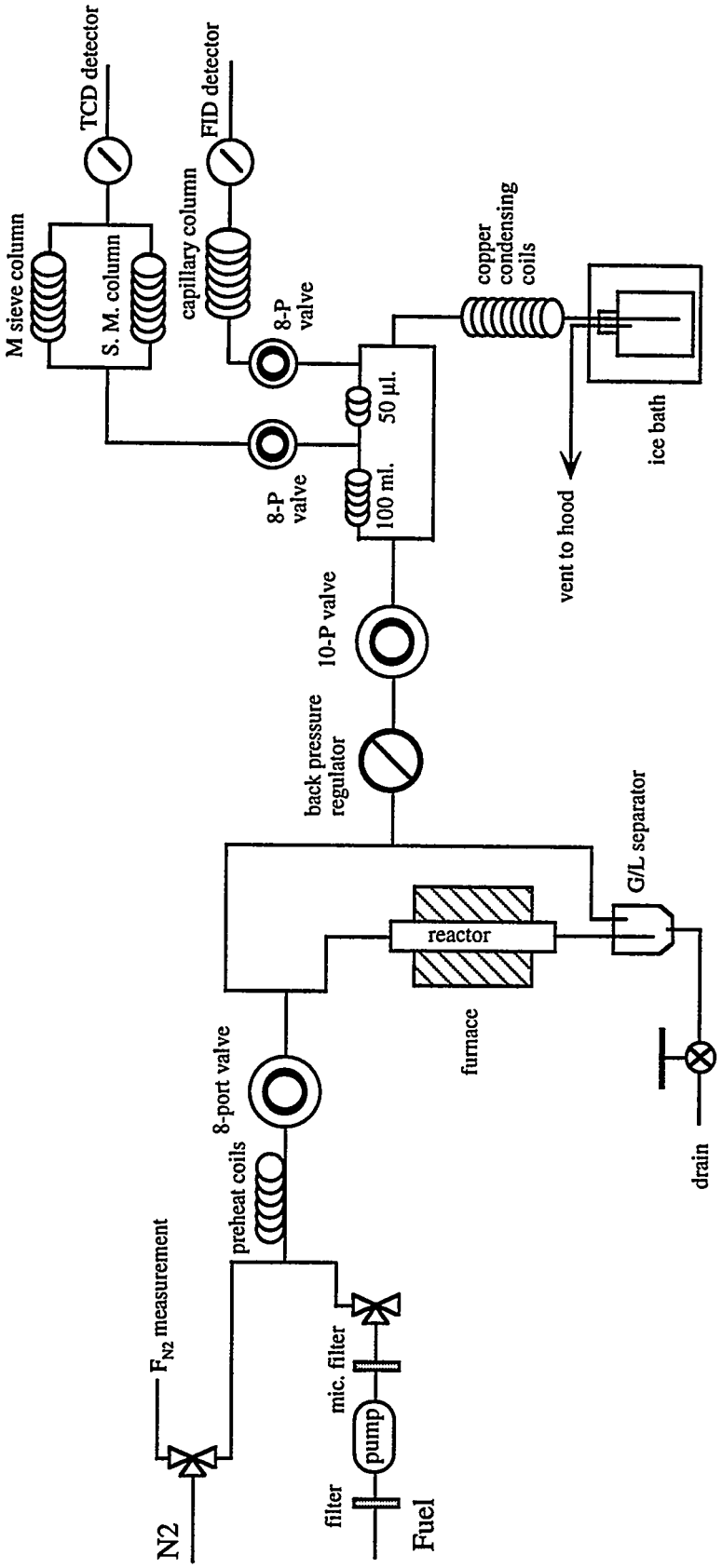

Figure 19. Schematic diagram of the CDS Bench Scale Flow Reactor.

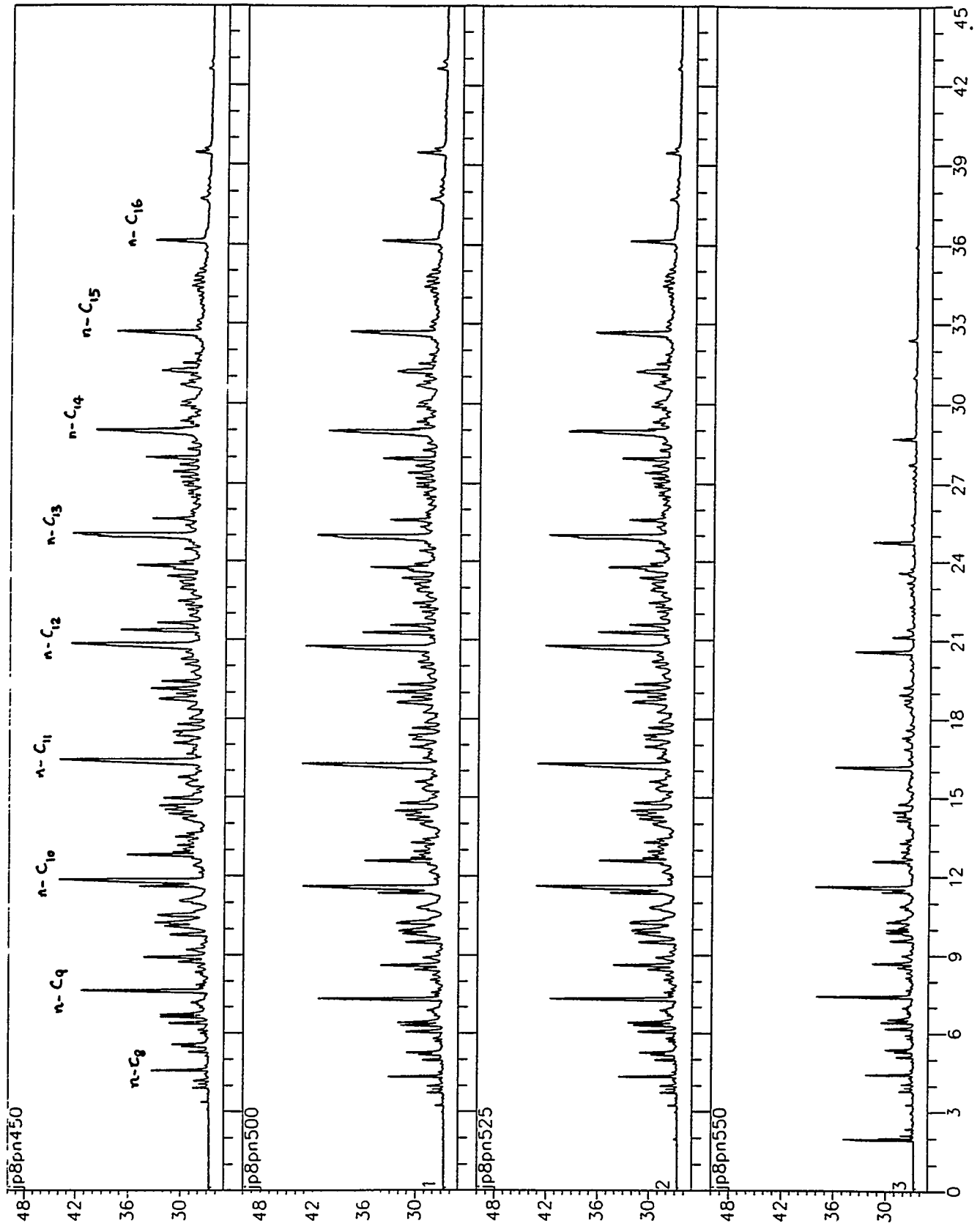

Figure 20a. GC Chromatogram of Jet Fuel JP-8P after Thermal Reaction at 450, 500, 525, and 550 °C in the Flow Reactor.

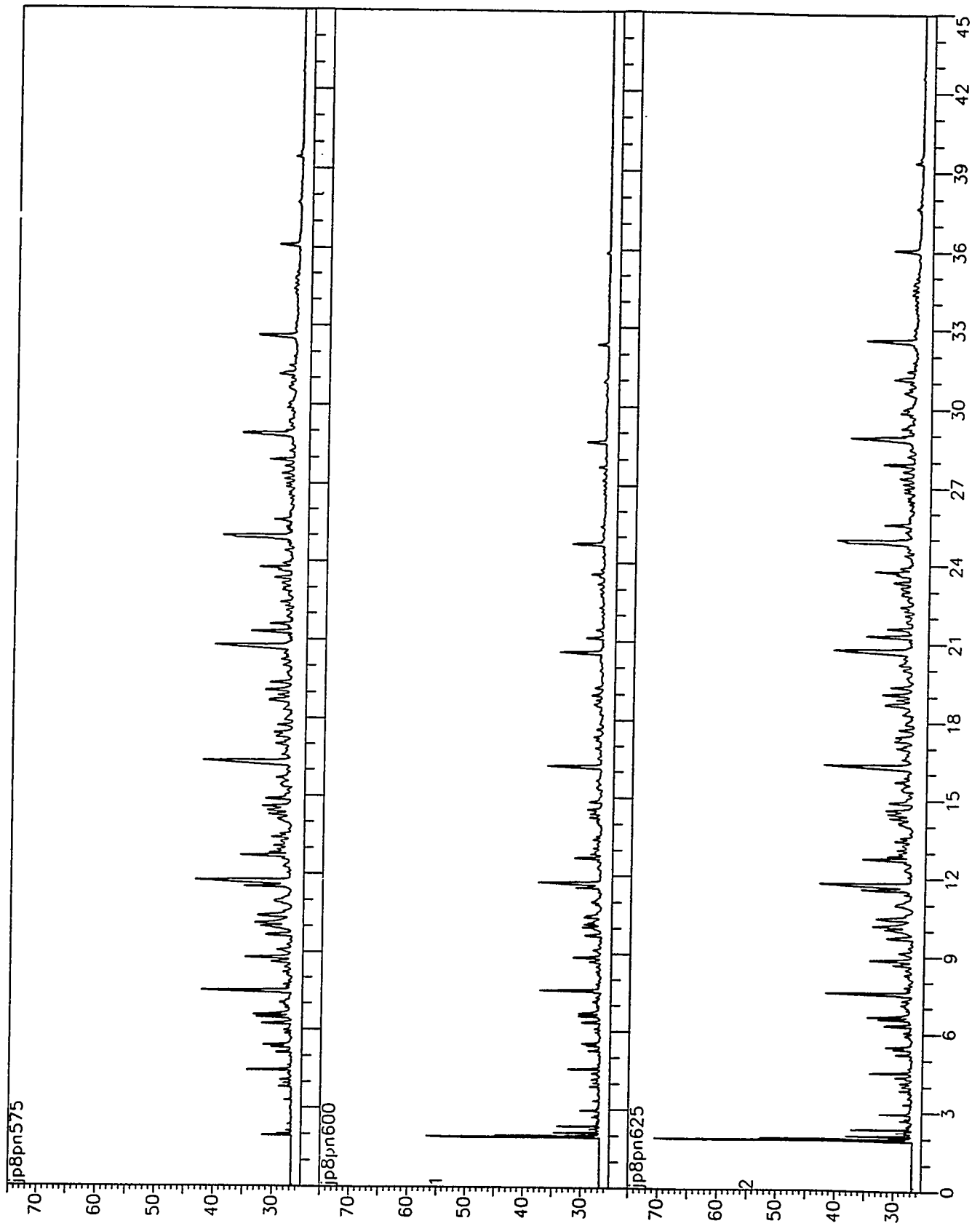

Figure 20b. GC Chromatogram of Jet Fuel JP-8P after Thermal Reaction at 575, 600, and 625 °C in the Flow Reactor.

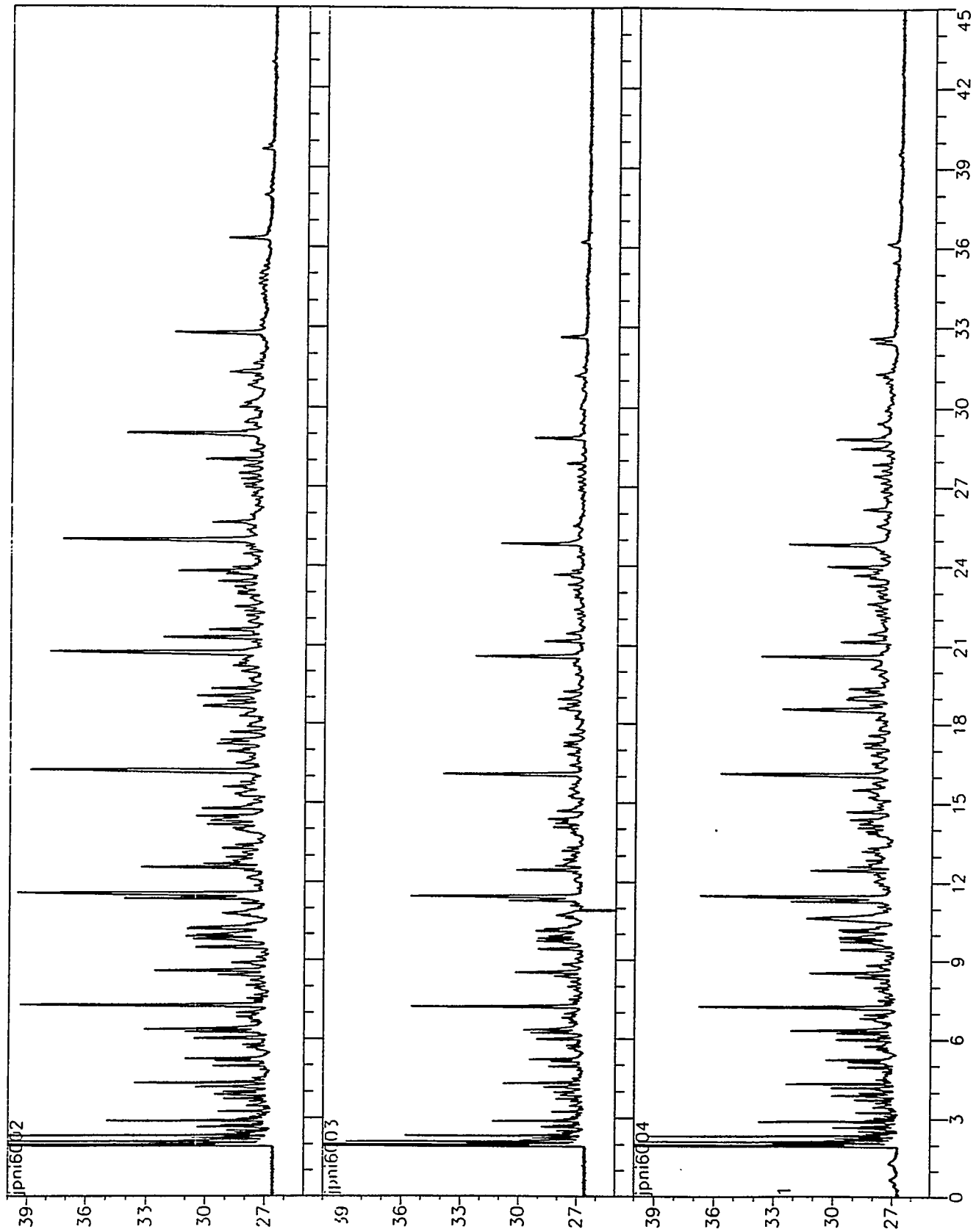

Figure 21a. GC Chromatogram of JP-8P after Thermal Reaction with the Insertion of Nickel Coupons at 100, 195, and 295 minutes at 600 °C in the Flow Reactor.

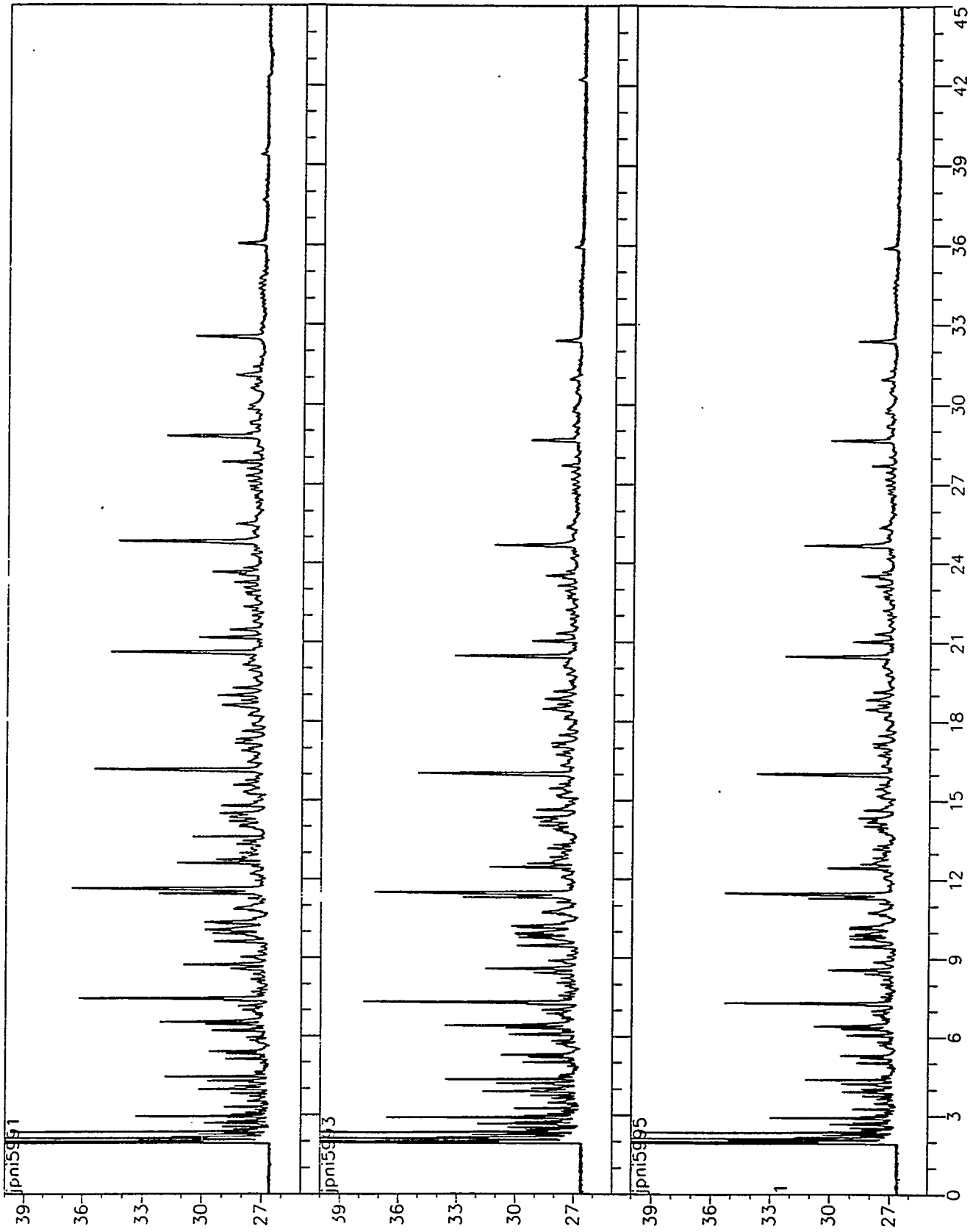

Figure 21b. GC Chromatogram of JP-8P after Thermal Reaction with the Insertion of Nickel Coupons at 35, 370, and 570 minutes at 600 °C in the Flow Reactor.

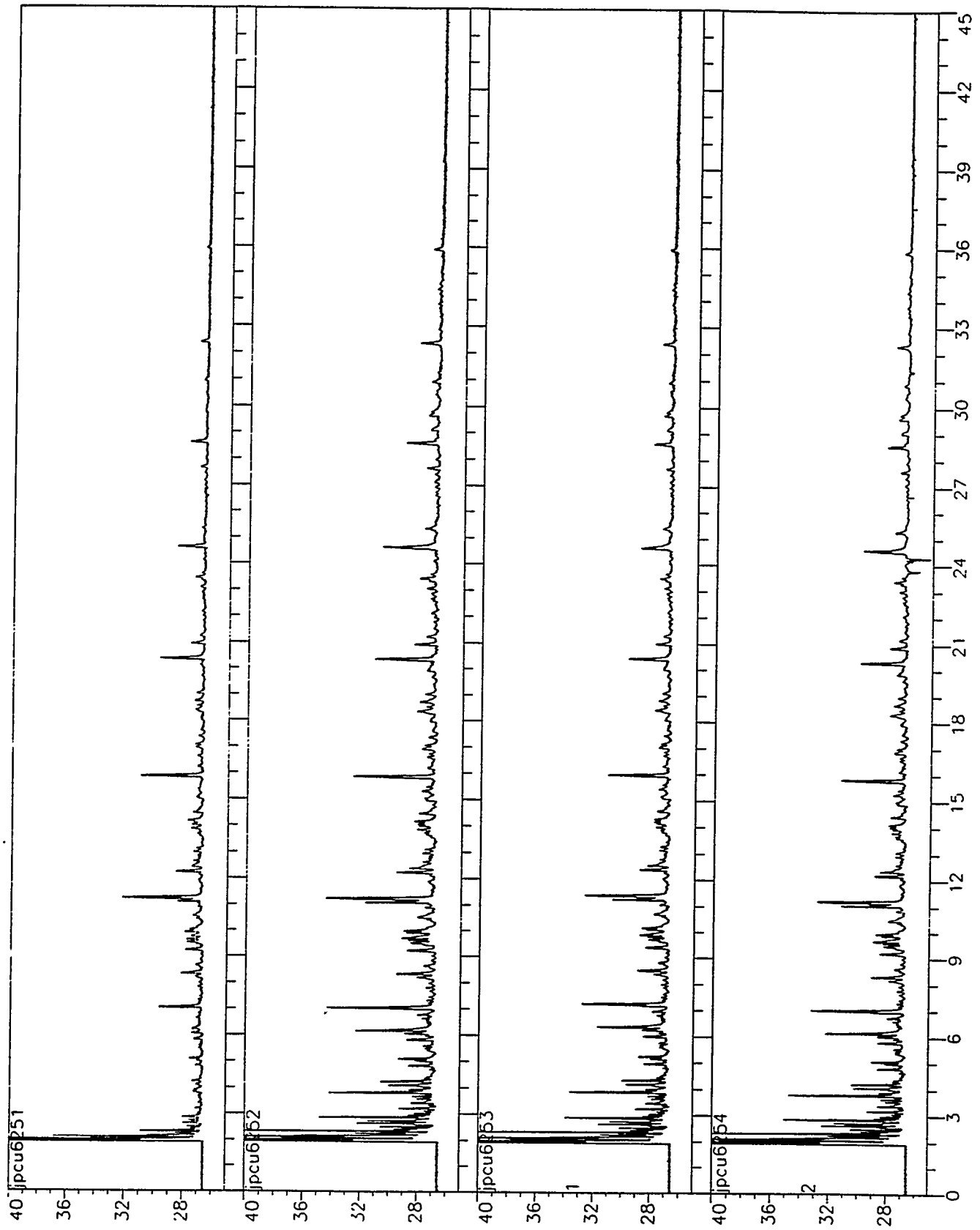

Figure 22. GC Chromatogram of JP-8P after Thermal Reaction with Coppper Coupons at 5 (jpcu6251), 90, 190, and 270 minutes at 625 °C in the Flow Reactor.

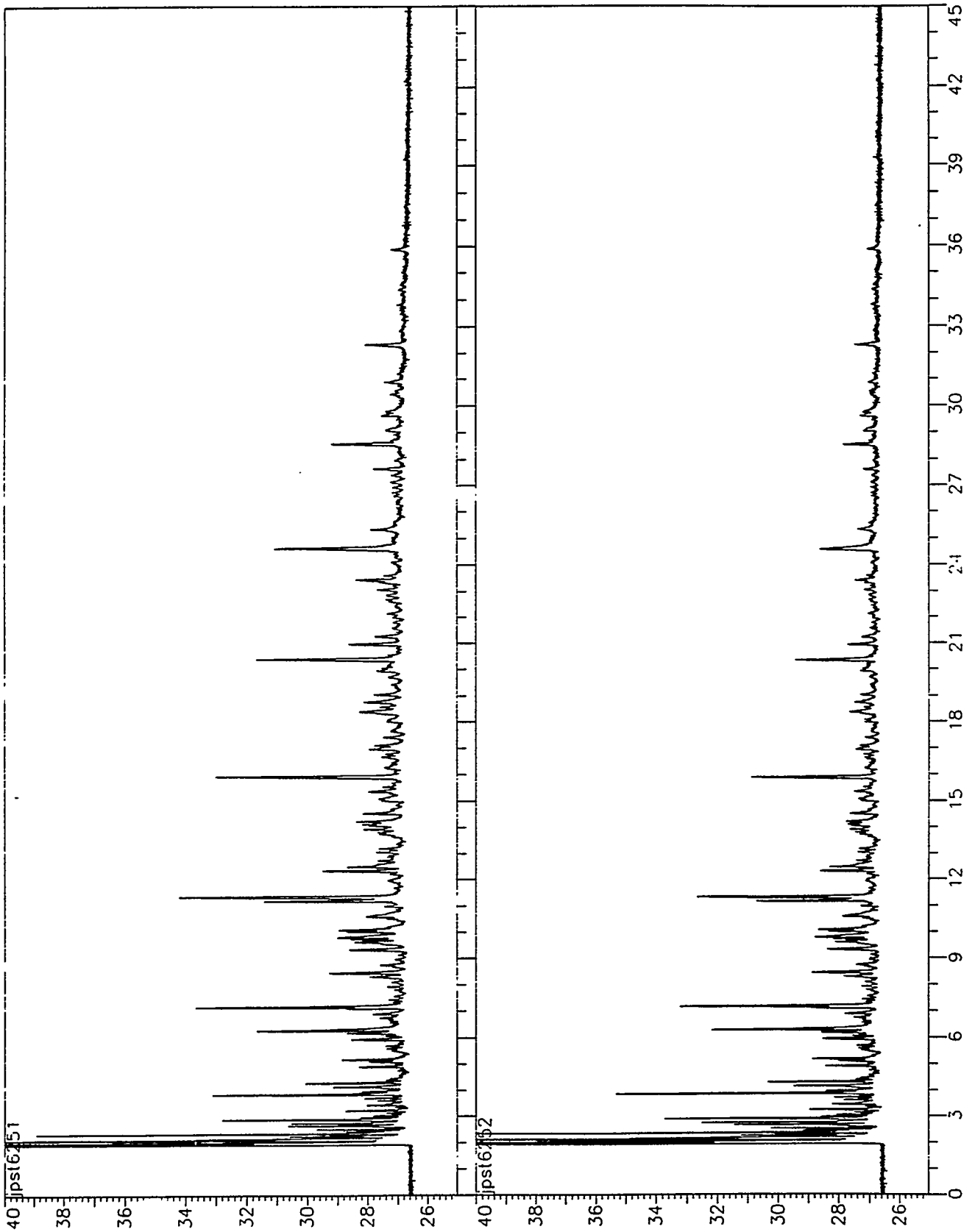

Figure 23. GC Chromatogram of JP-8P after Thermal Reaction with Stainless Steel 304 Coupons at 10 (jpst6251), and 100 minutes at 625 °C in the Flow Reactor.

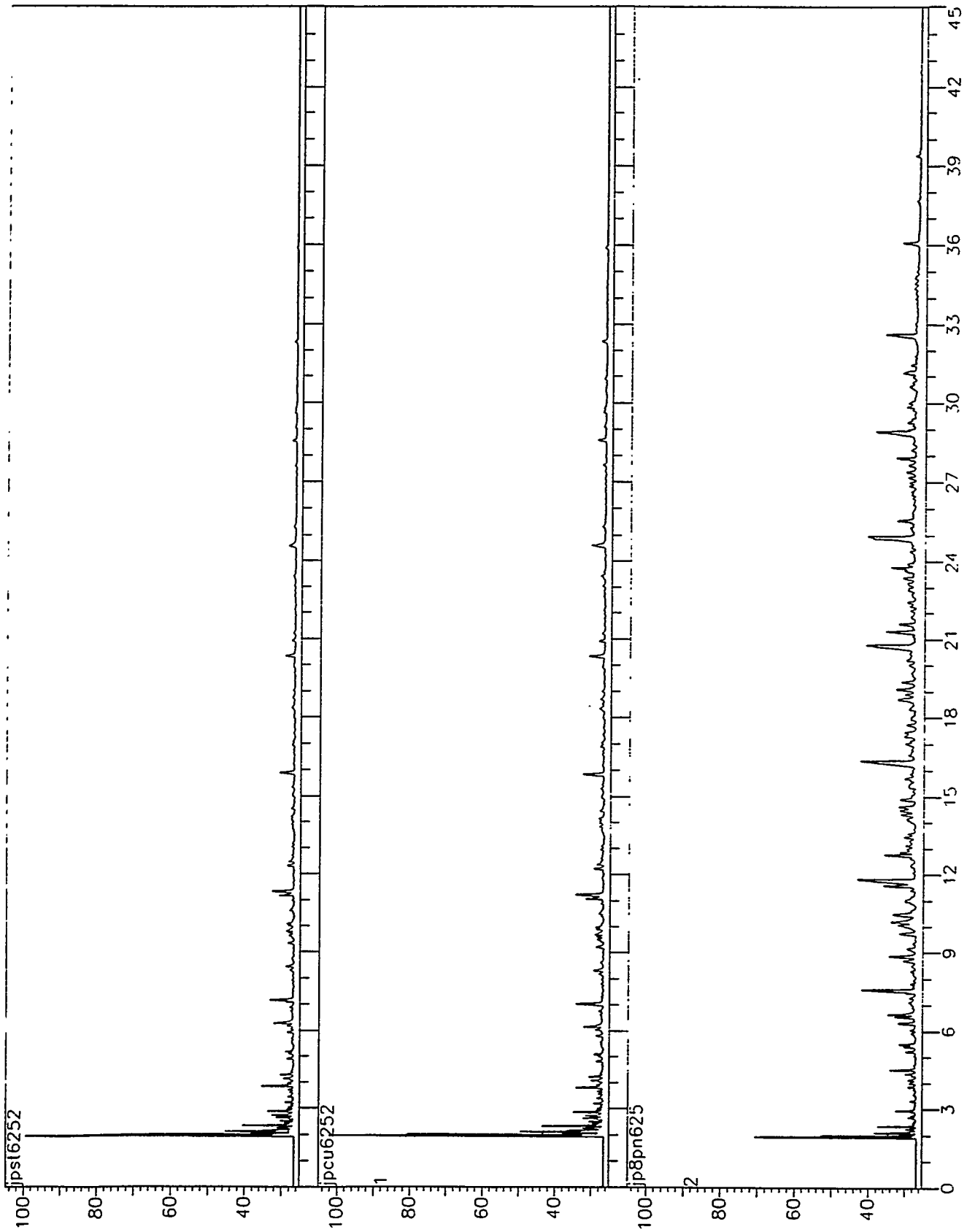

Figure 24a. Comparison of Conversion and Products Distribution of JP-8P after Thermal Reaction without Metal Coupons (jp8pn625), and with Nickel (jpni6003), Copper (jpcu6253), and Stainless Steel (jpst6252) in the Flow Reactor.

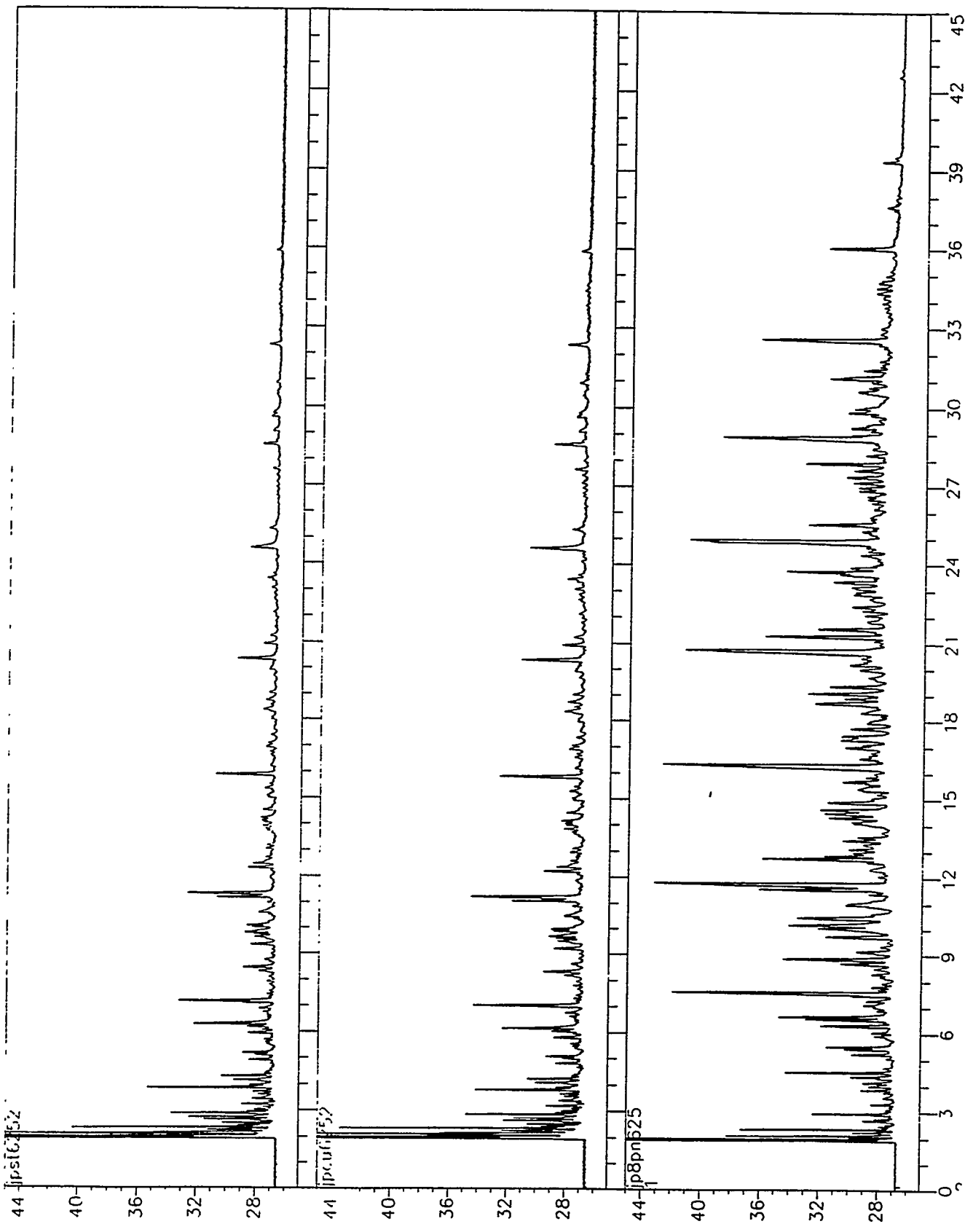

Figure 24b. Zoom in of Figure 24a.

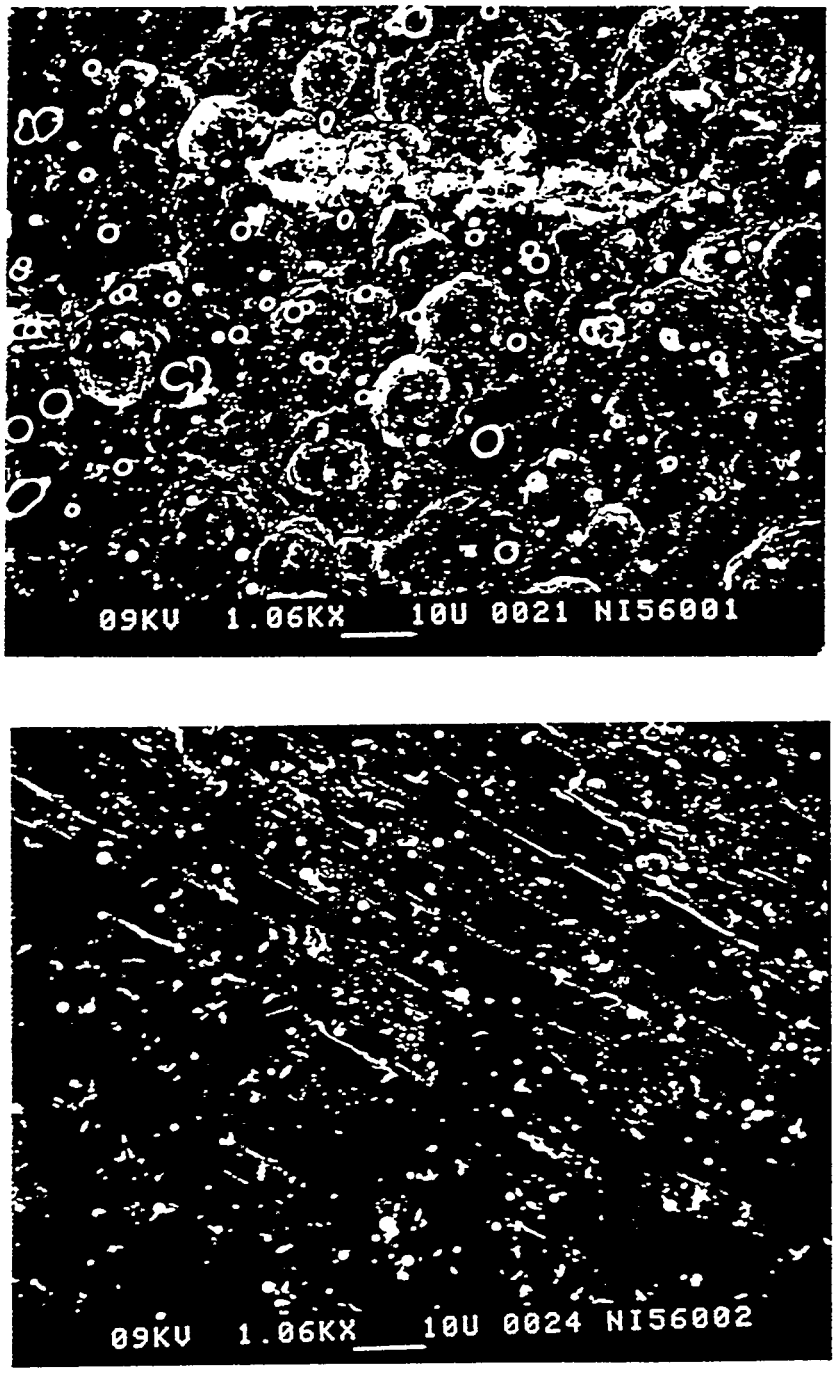

Figure 25. SEM Micrograph of Deposit on Nickel Surface after 5 Hour Reaction with JP-8P at 600 °C in the Flow Reactor. (a) Rough (above), (b) Polished (below).

Figure 26. SEM Micrograph of Deposit on Nickel Surface after 10 Hour Reaction with JP-8P at 600 °C. (a) Deposit Aggregates (above), (b) Close-up of (a) (below).

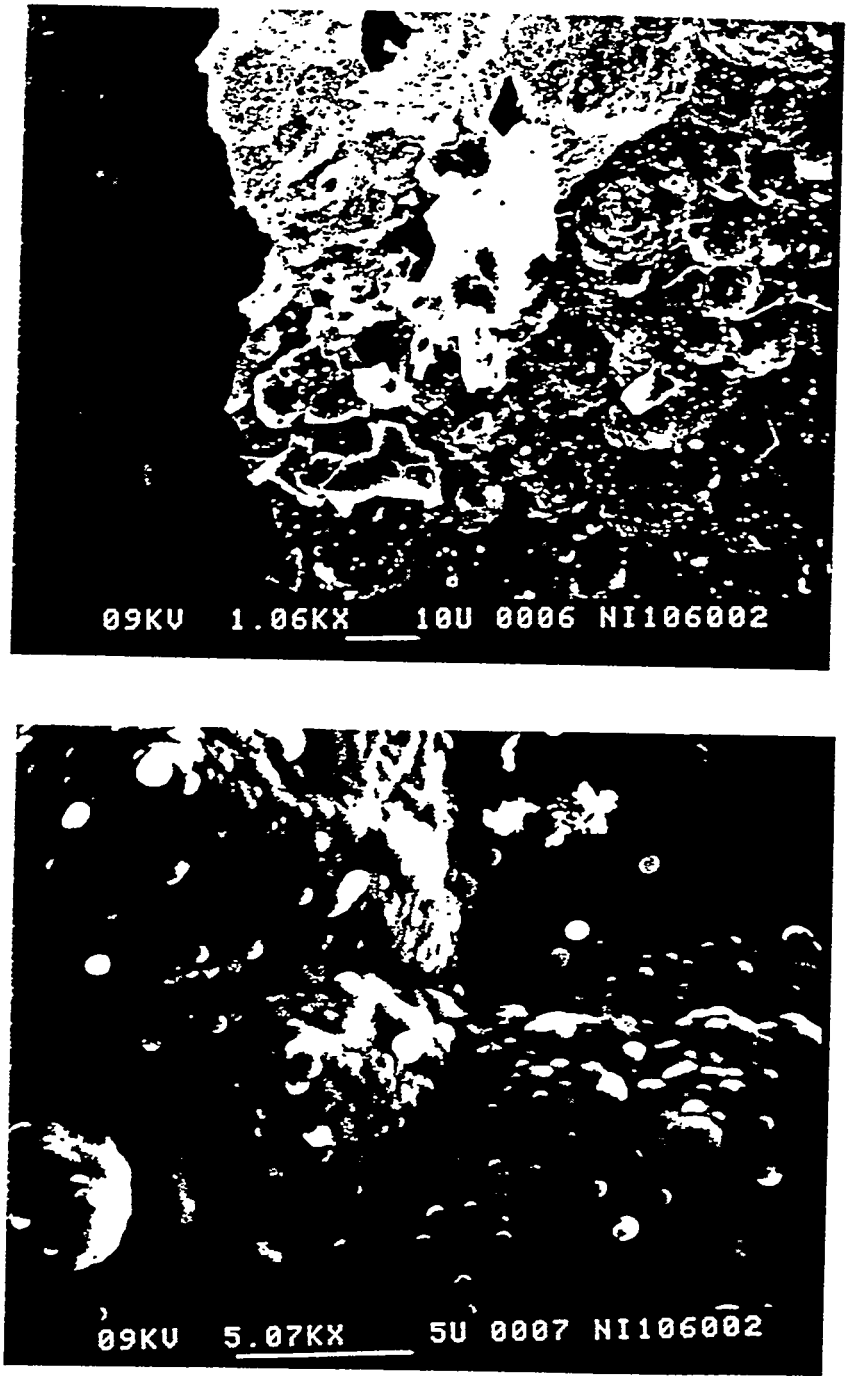

Figure 27. SEM Micrograph of Deposit on Nickel Surface after 10 Hour Reaction with JP-8P at 600 °C. (a) Grown Aggregates (above), (b) Close-up of (a) (below).

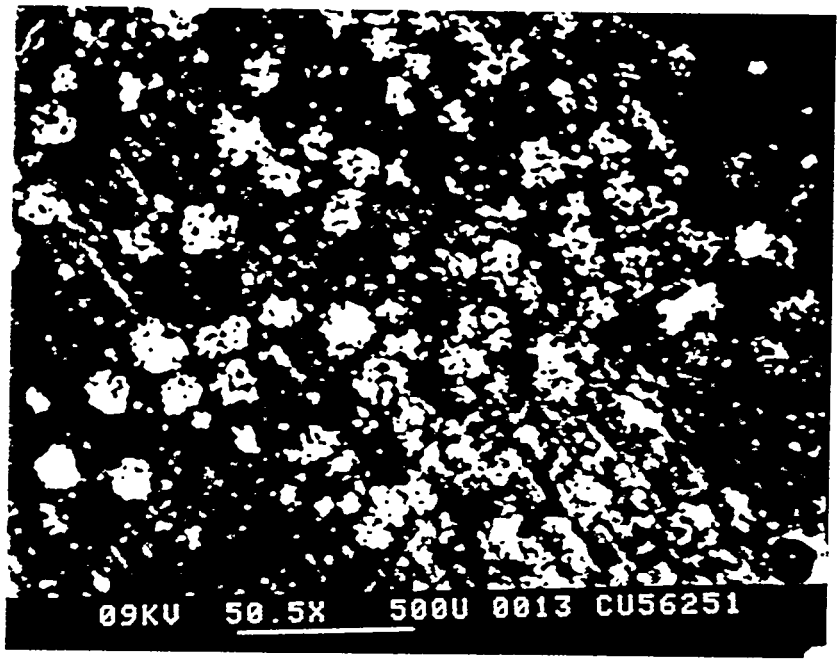

Figure 28. SEM Micrograph of Deposit on Copper Surface after 5 Hour Reaction with JP-8P at 625 °C. Deposit Colonies.

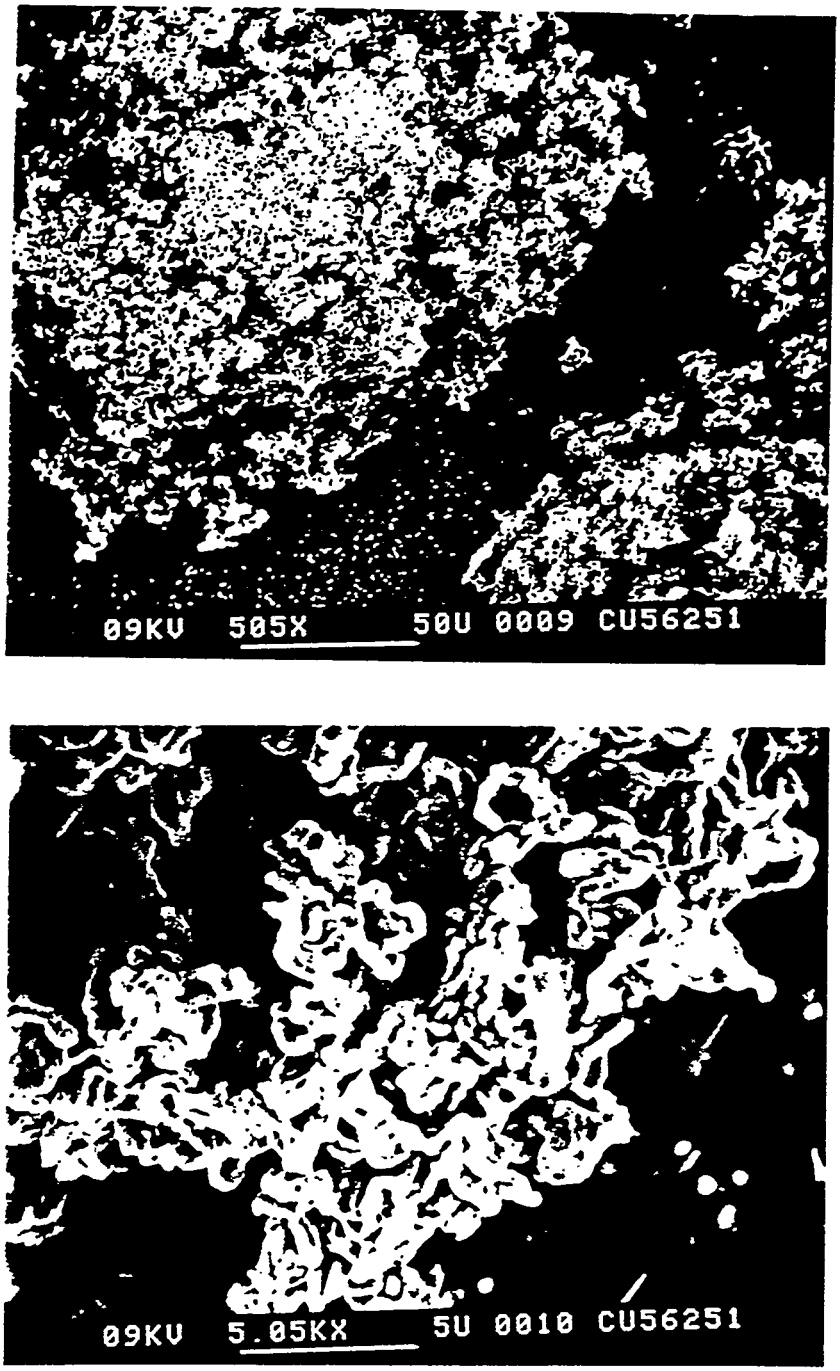

Figure 29. SEM Micrograph of Deposit on Copper Surface after 5 Hour Reaction with JP-8P at 625 °C. (a) Grown Aggregates (above), (b) Close-up of (a) (below).

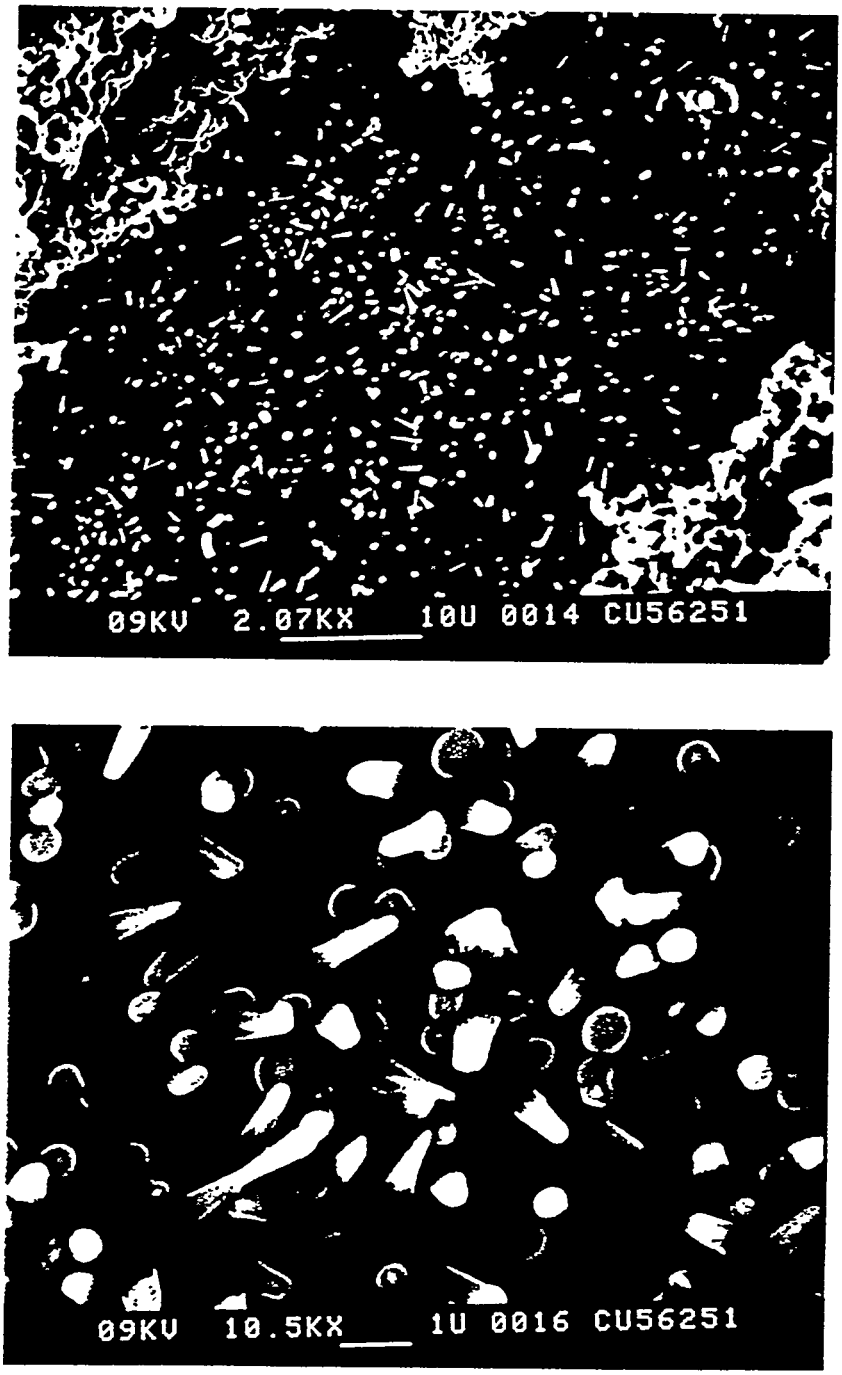

Figure 30. SEM Micrograph of Deposit on Copper Surface after 5 Hour Reaction with JP-8P at 625 °C. (a) Initial Arrow Head Deposit, (b) Close-up of (a) (below).

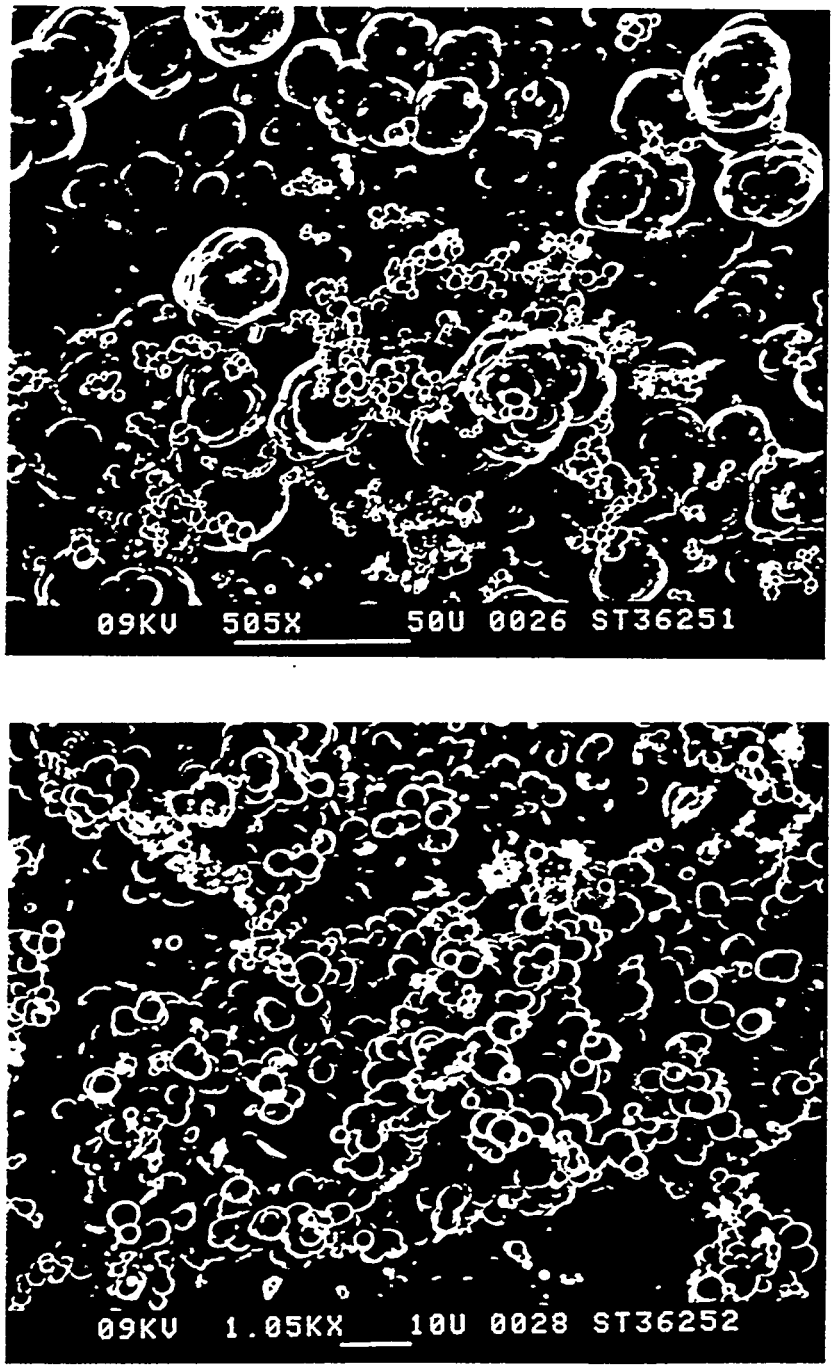

Figure 31. SEM Micrograph of Deposit on Stainless Steel Surface after 3 Hour Reaction with JP-8P at 625 °C. (a) Spherical Deposit Grown by Chain (above), (b) Similar Aggregates on Another Piece of Coupons (below).

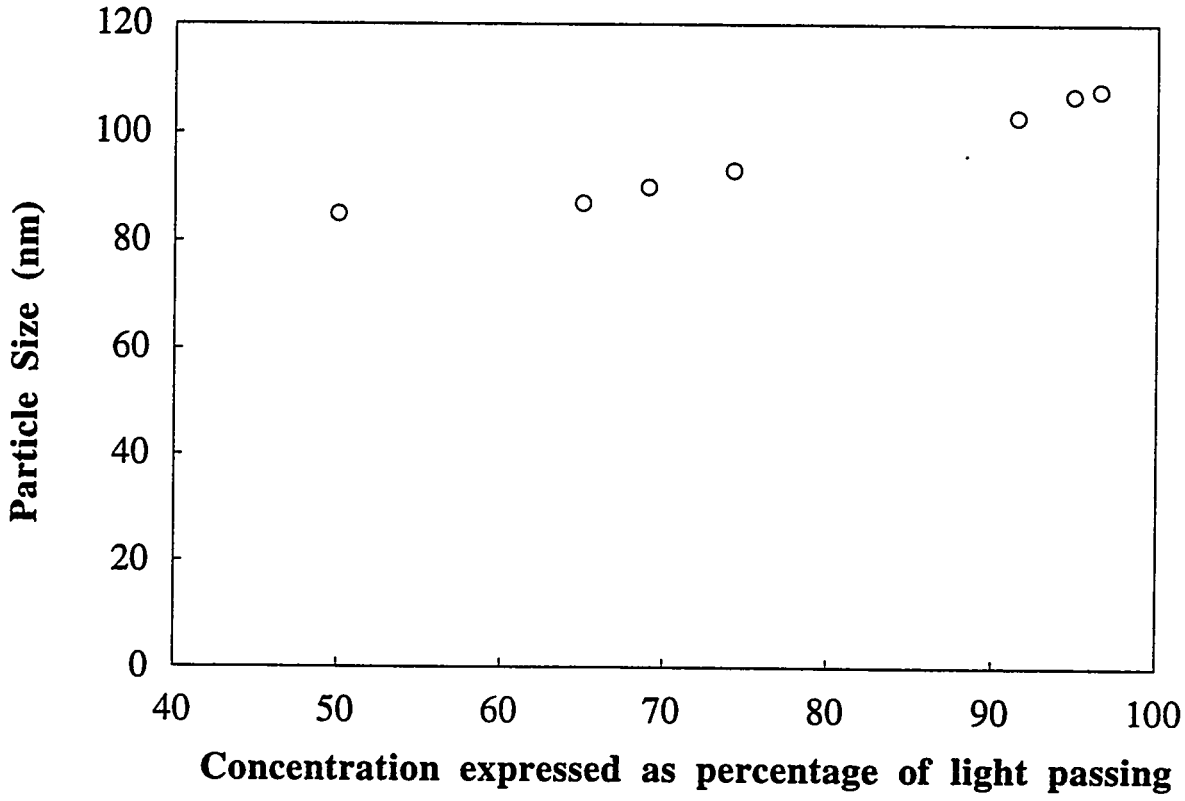

Figure 32. Variation in particle size with concentration for 100nm standard.

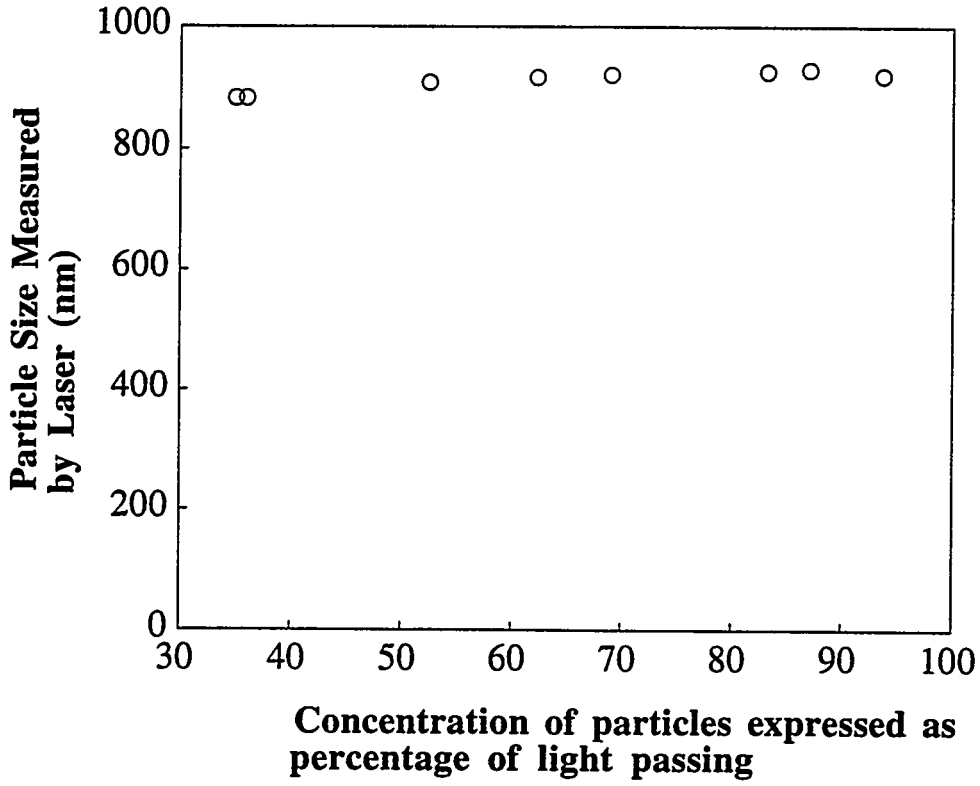

Figure 33. Variation in particle size with concentration for 900nm standard.

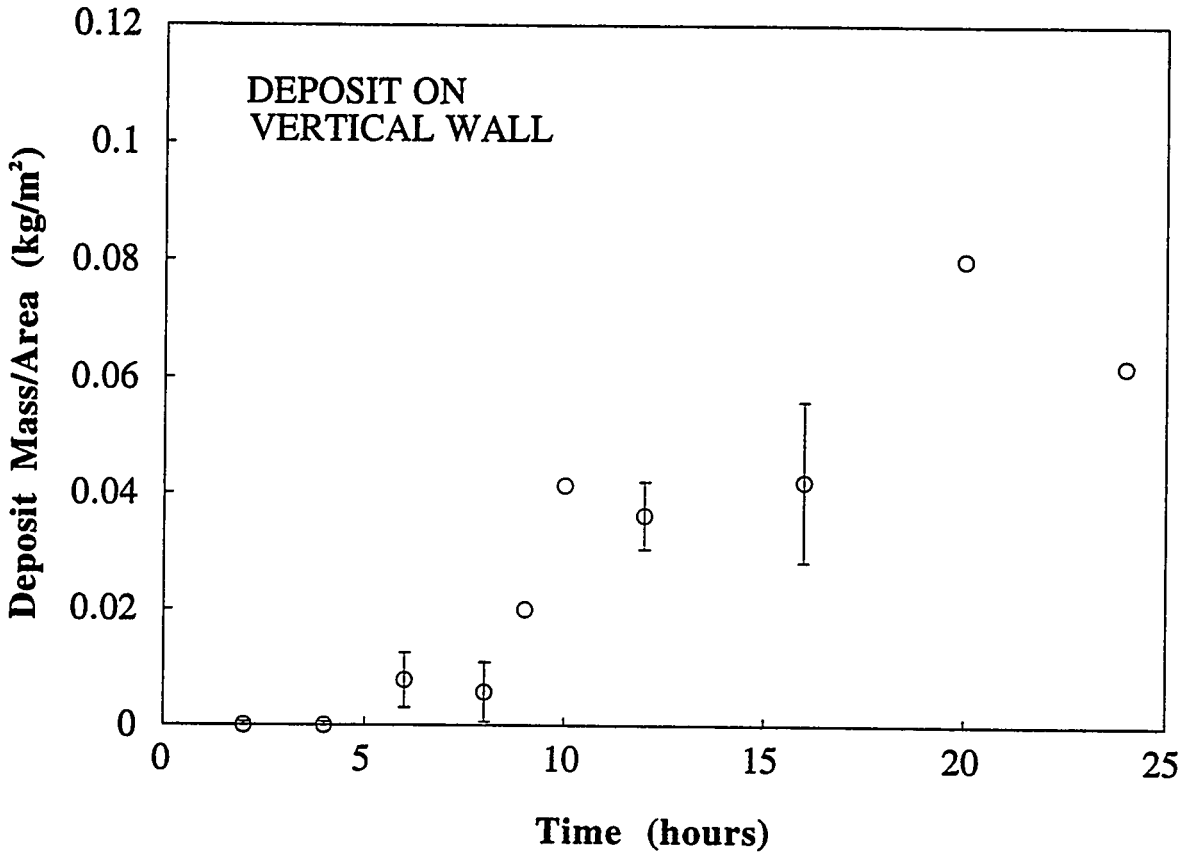

18.5 wt% tetradecane in JP8C at 450°C under nitrogen

Figure 34. Errors involved in calculation of deposit formation on the wall at 6, 8, 12, and 16 hours.

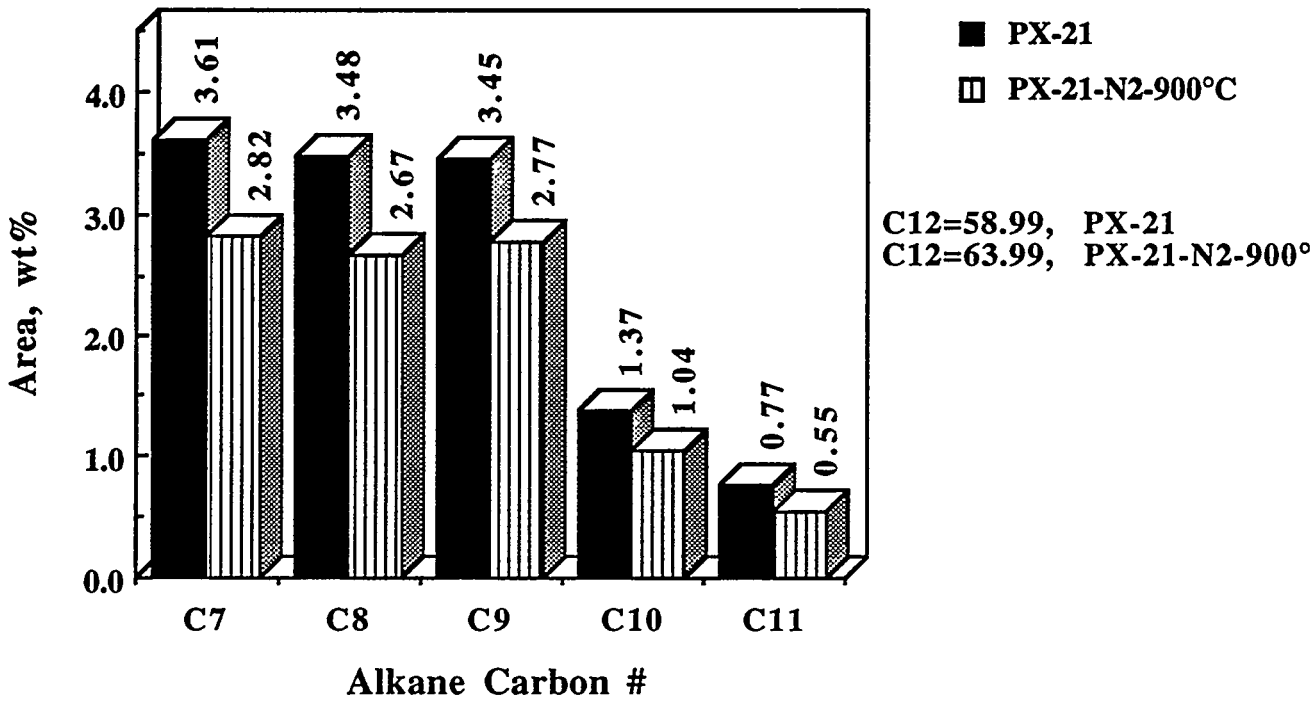

Figure 35. Variations of area percent of n-alkanes in the liquids obtained after thermal stressing of dodecane+5%decalin+50 mg PX-21 at 425°C for 0.5h

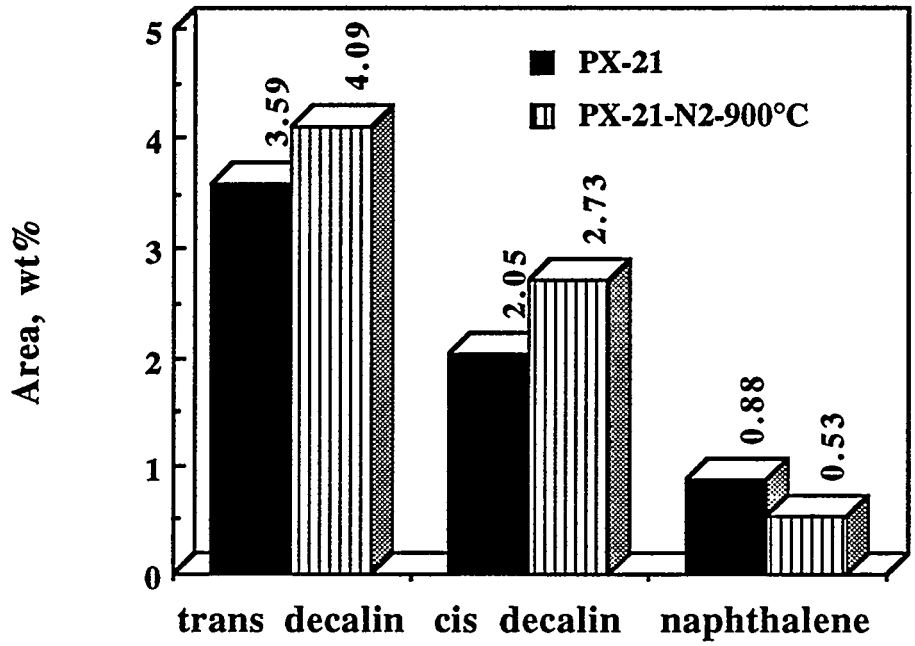

Figure 36. Variation of the area percent of decalin and naphthalene in the liquids obtained after thermal stressing of dodecane+5% decalin + 50 mg PX-21 at 425°C for 5h

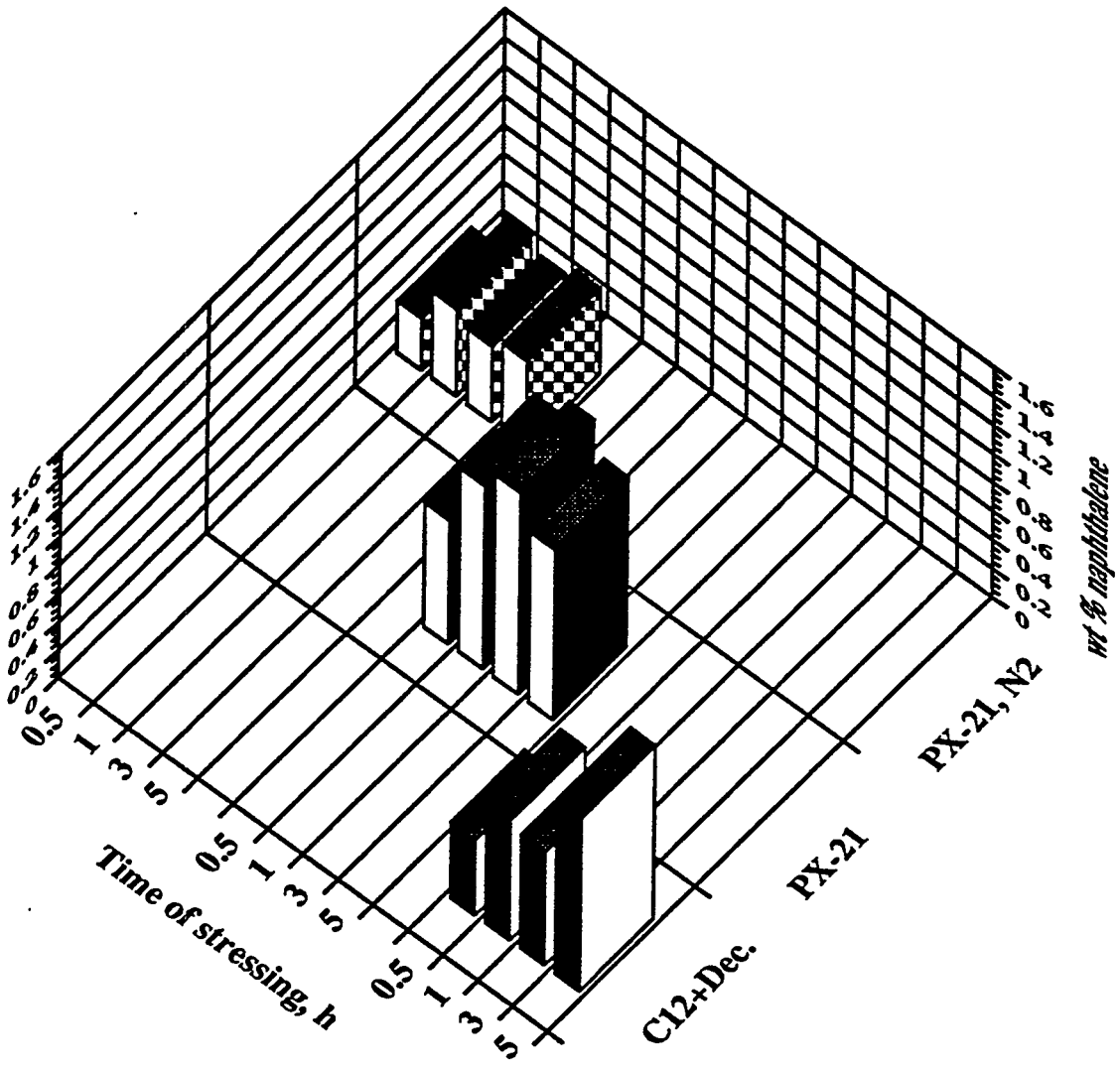

Figure 37. Variation of area percent of naphthalene in the liquids obtained after thermal stressing of dodecane+5% decalin+50 mg PX-21 at 425°C for different time of stressing

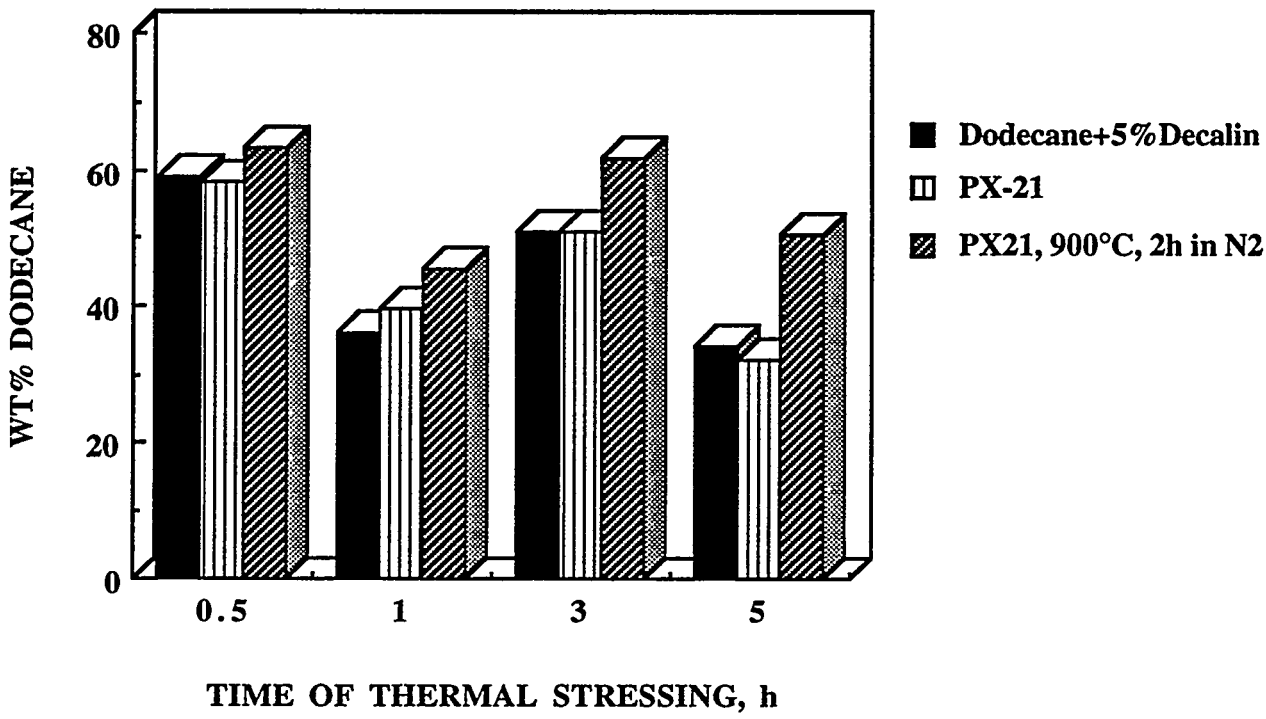

Figure 38. Variation of area percent of dodecane obtained after thermal stressing of dodecane+5% decalin+50 mg PX-21 at 425°C for different time of stressing

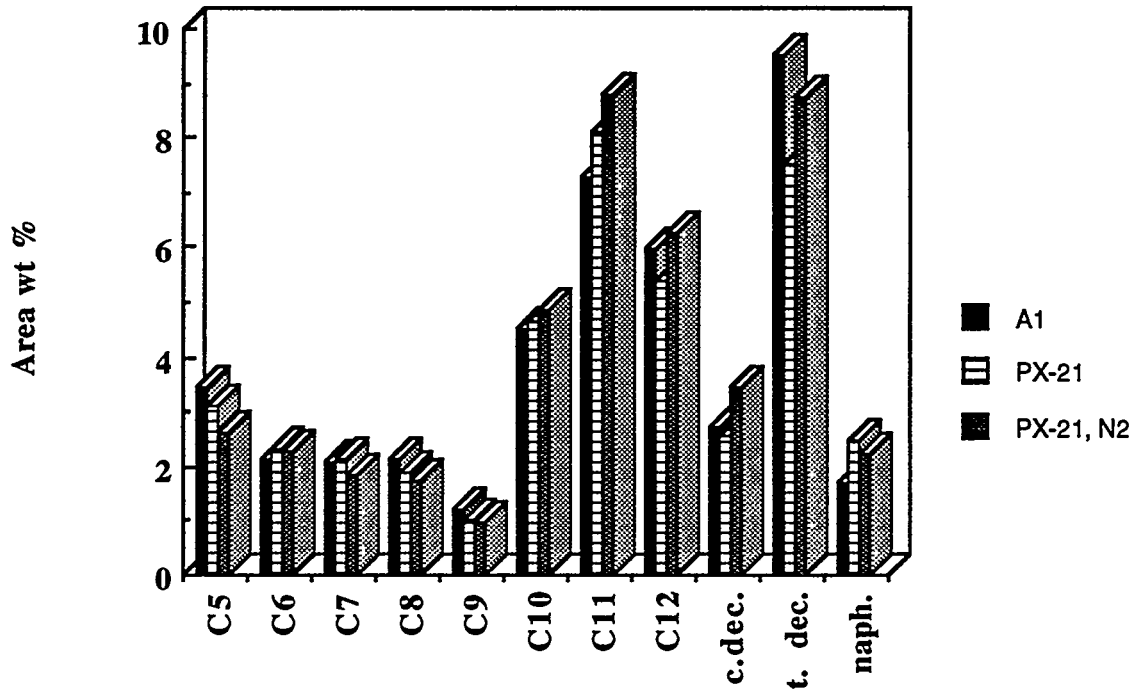

Figure 39. Weight percent of selected compounds identified in the liquid obtained after thermal stressing of A-1 jet fuel+5% decalin+ 50 mg PX-21 at 425°C for 5h

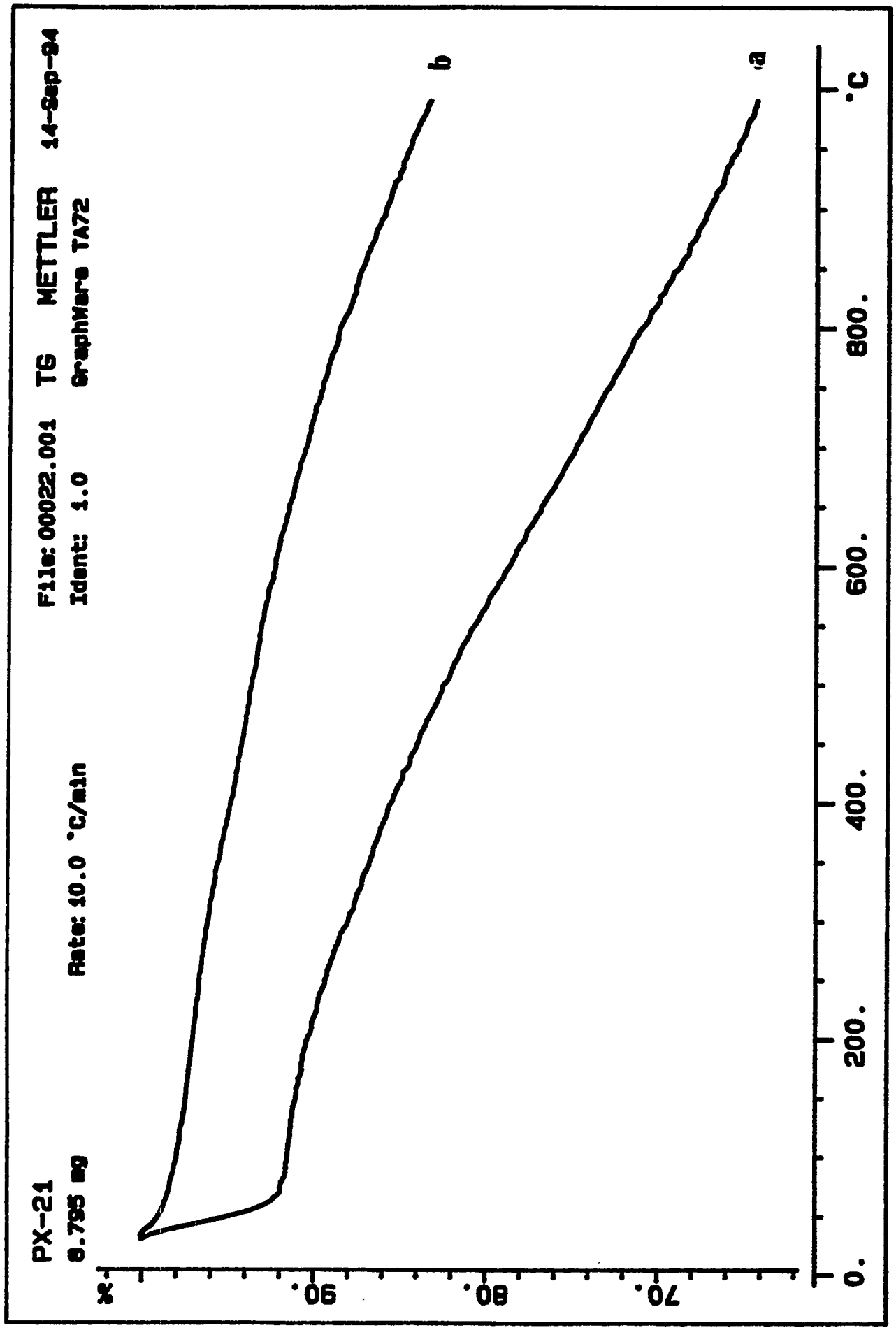

Figure 40. Thermogravimetric analyses of (a) PX-21 (b) PX-21 outgassed in N_2 at 900°C

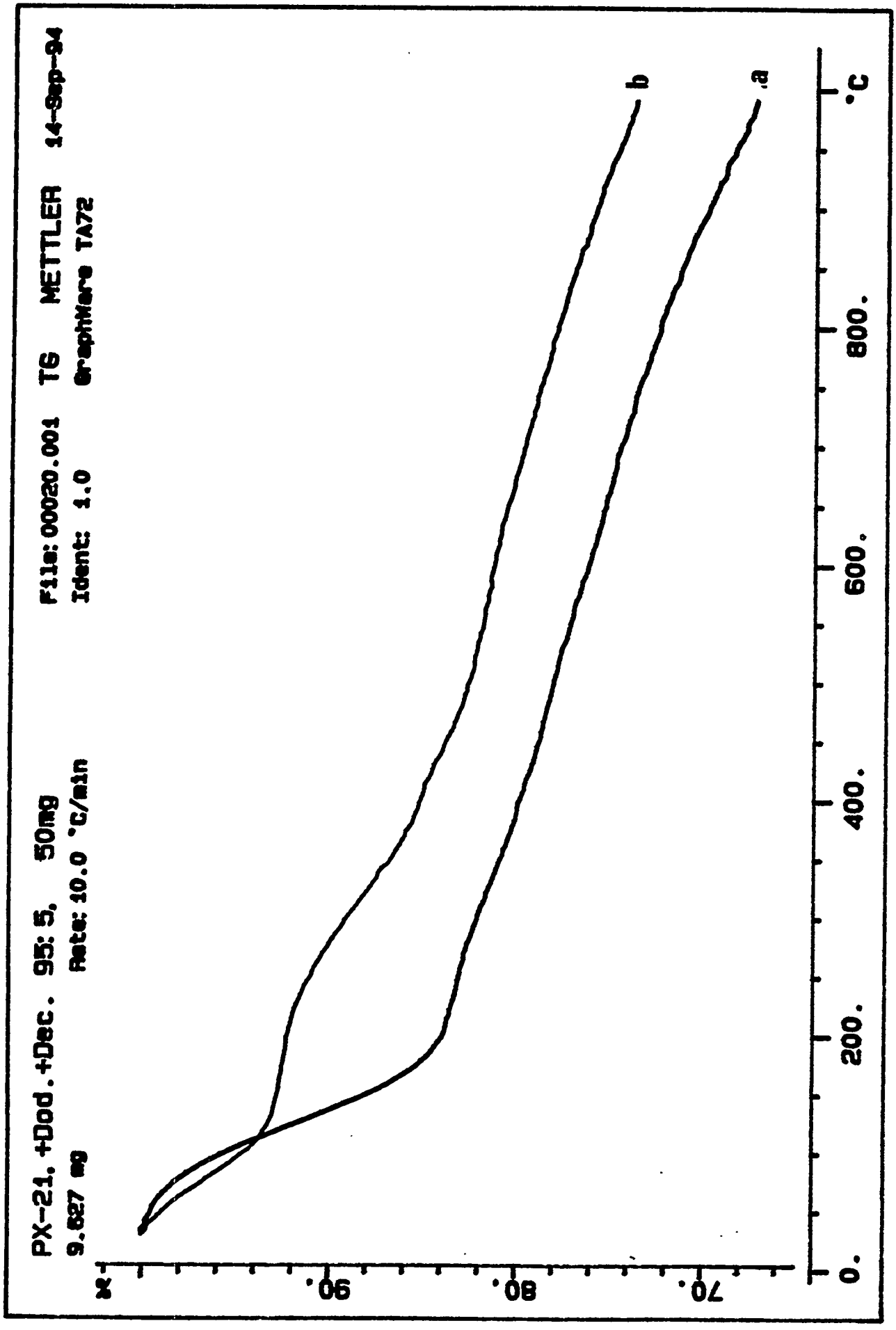

Figure 41. Thermogravimetric analysis of (a) PX-21 stressed with dodecane+decalin at 425°C for 5h, (b) PX-21 outgassed in N_2 at 900C and stressed with dodecane+decalin at 425°C for 5h

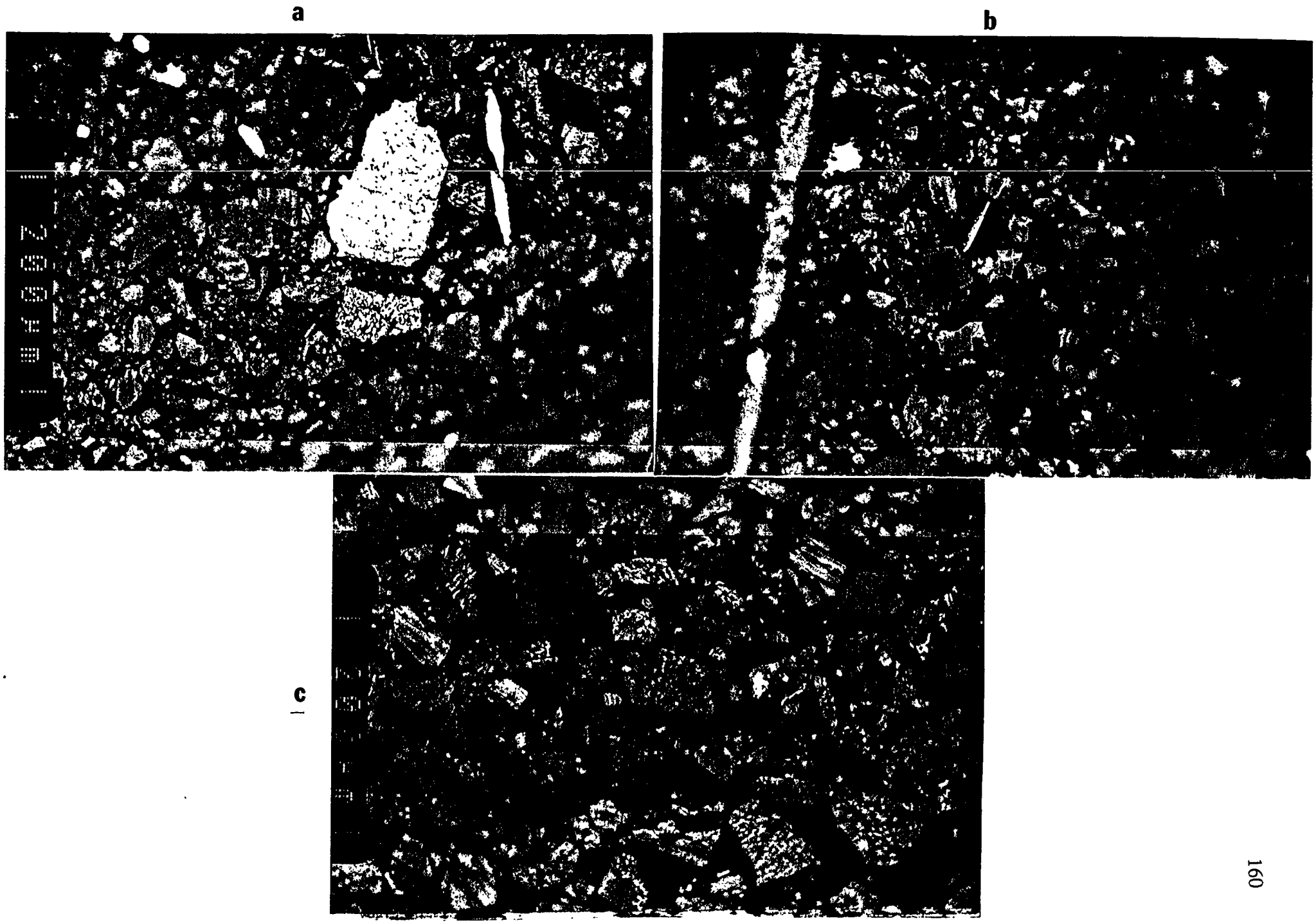

Figure 42. Polarized-light micrographs of (a), (b) PX-21 stressed with dodecane+decalin at 425°C for 5h (c) PX-21 outgassed in N_2 at 900°C and stressed with dodecane+decalin at 425°C for 5h

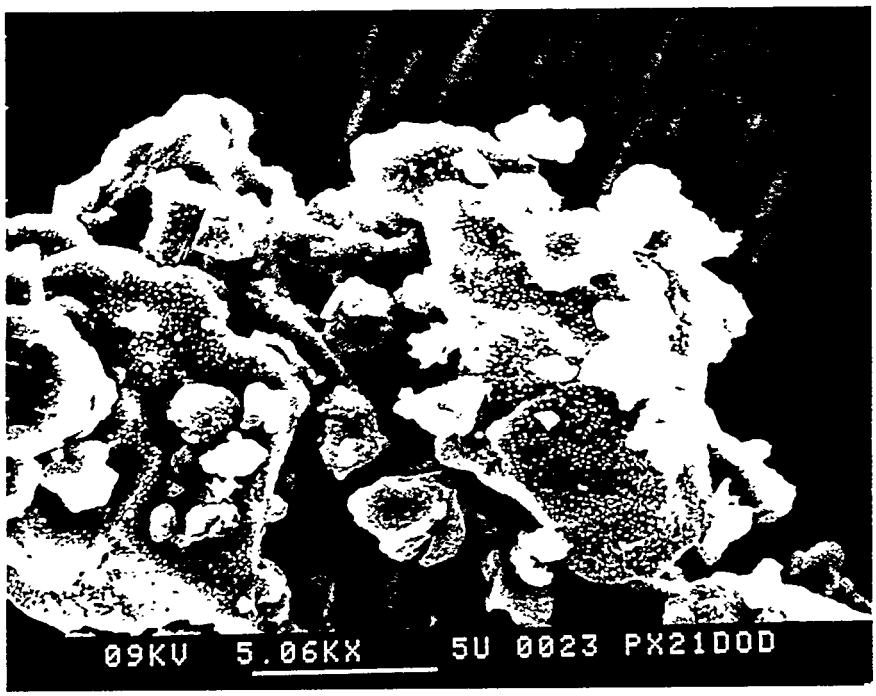

a

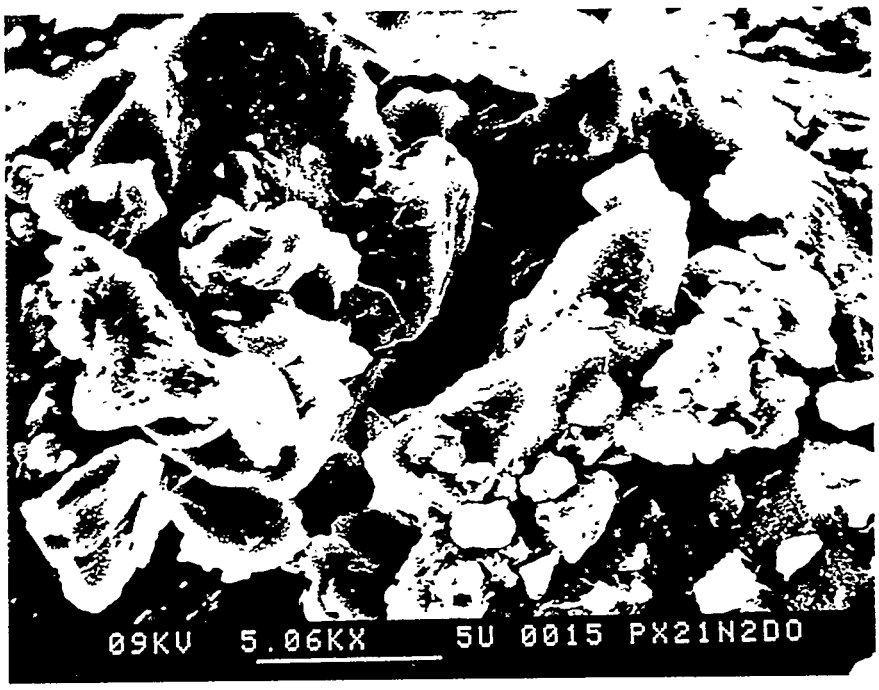

b

Figure 43. Scanning electron micrographs of (a) PX-21 stressed with dodecane+decalin at 425°C for 5h (b) PX-21 outgassed in N_2 at 900°C and stressed with dodecane+decalin at 425°C for 5h.

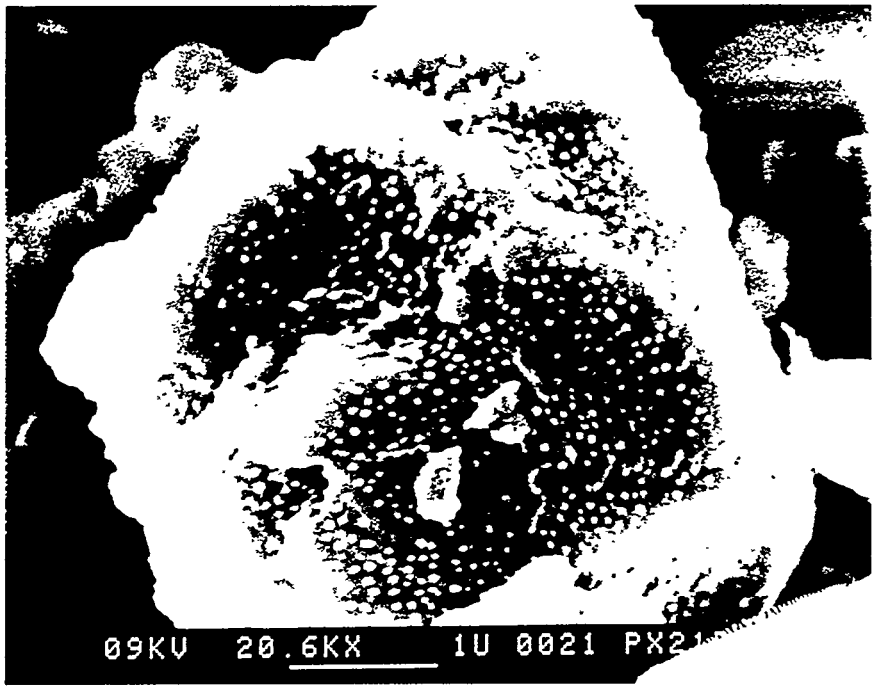

a

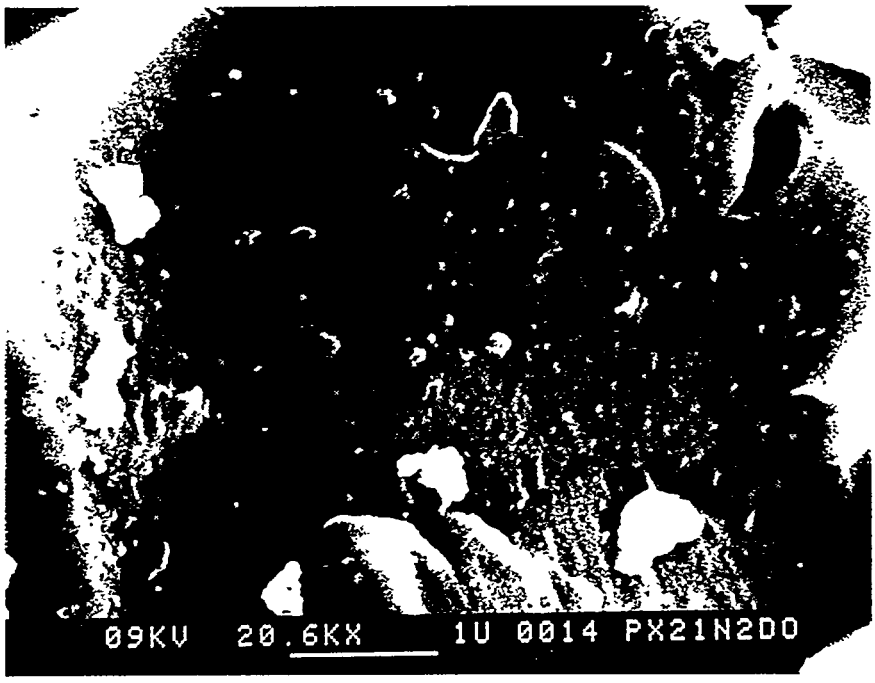

b

Figure 44. Scanning electron micrographs of (a) PX-21 Stressed with dodecane+decalin at 425°C for 5h (b) PX-21 outgassed in N_2at 900°C and stressed with dodecane+decalin at 425°C for 5h

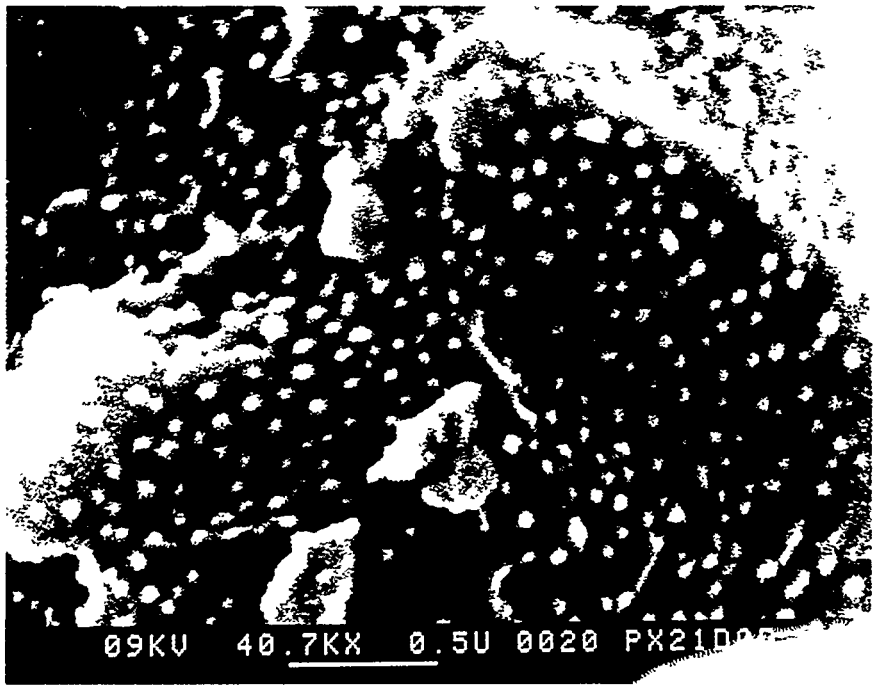

a

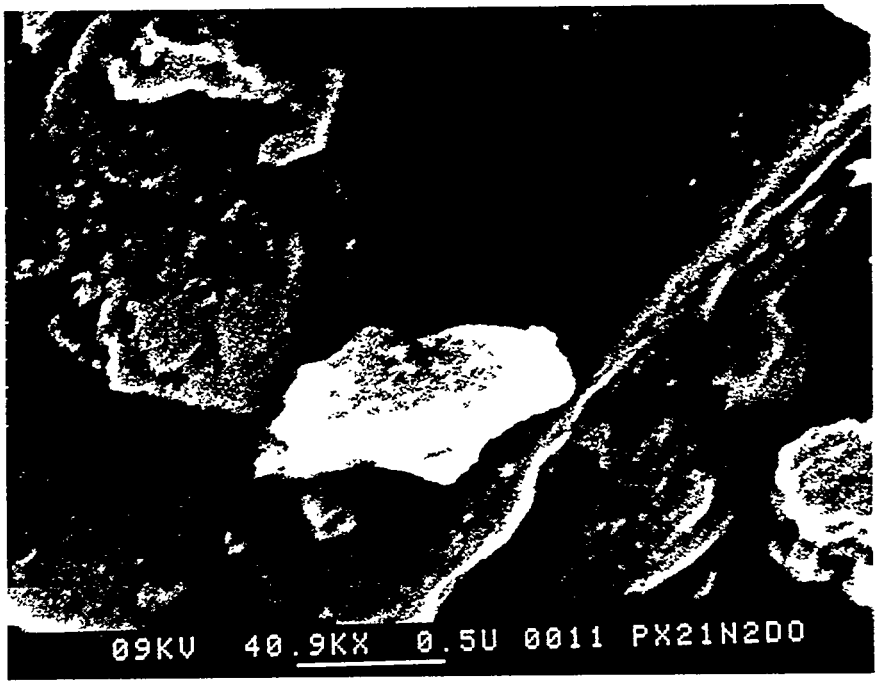

b

Figure 45. Scanning electron micrographs of (a) PX-21 stressed with dodecane+decalin at 425°C for 5h (b) PX-21 outgassed in N_2 at 900°C and stressed with dodecane+decalin at 425°C for 5h

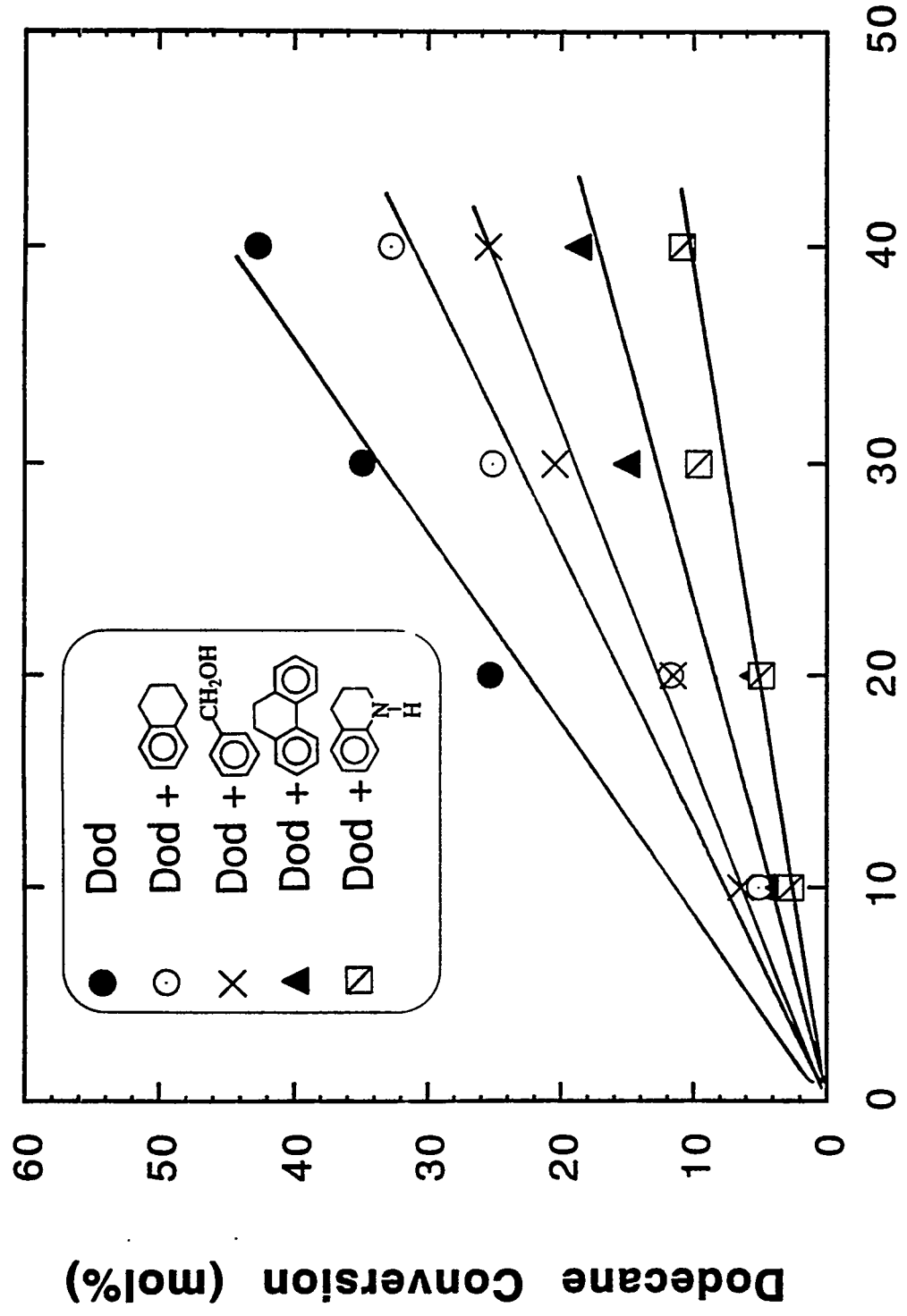

Figure 46. Effects of hydrogen donor additives on molar% conversion of dodecane at 450°C under initial N_2 pressure of 1.0 MPa. (Lines drawn are for visual aid only)

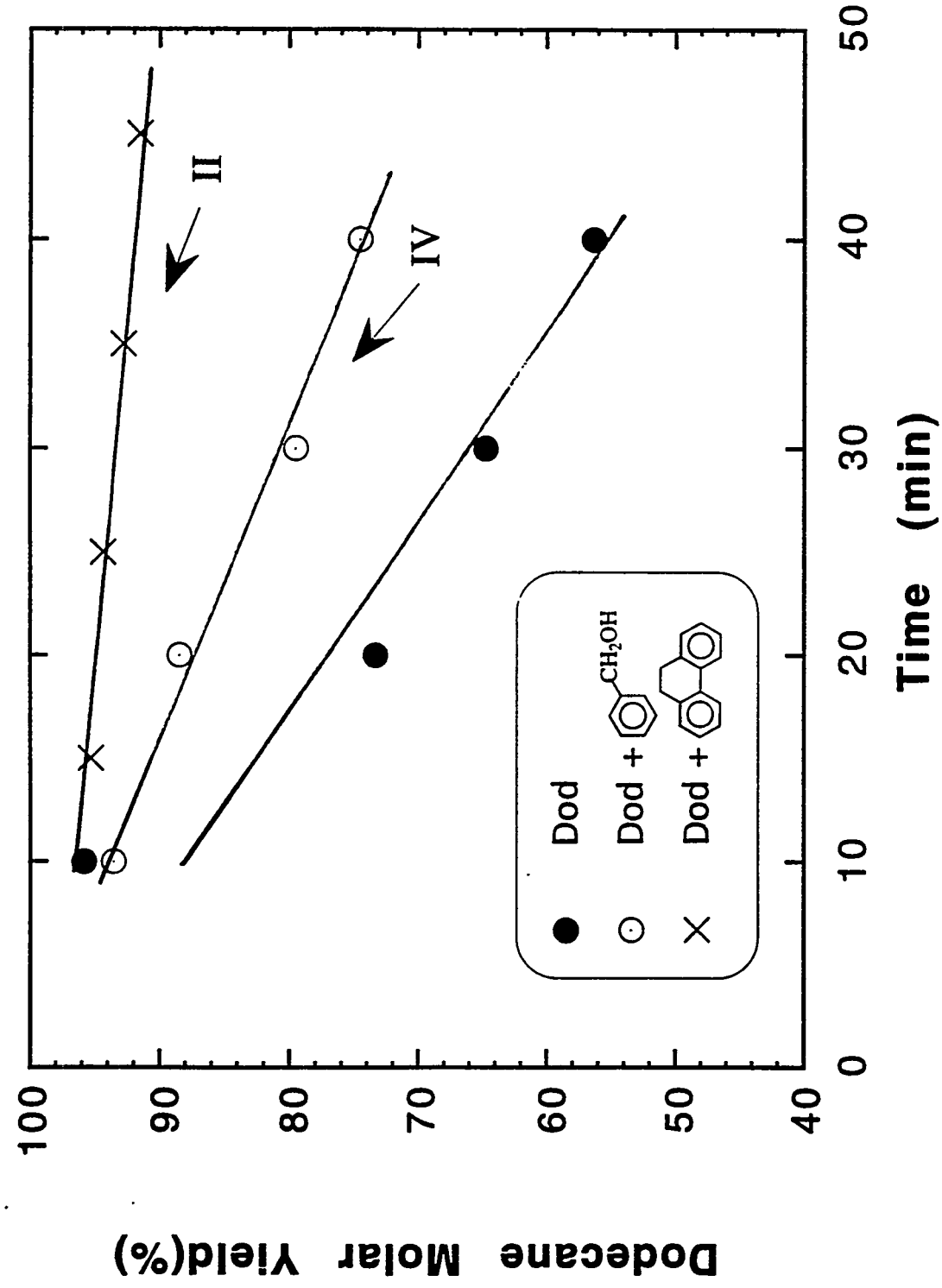

Figure 47. Effects of hydrogen donor additives (10 mol% II and IV on the molar yields of dodecane at 450°C under initial N_2 pressure of 0.69 MPa. (Lines are drawn for visual aid only)

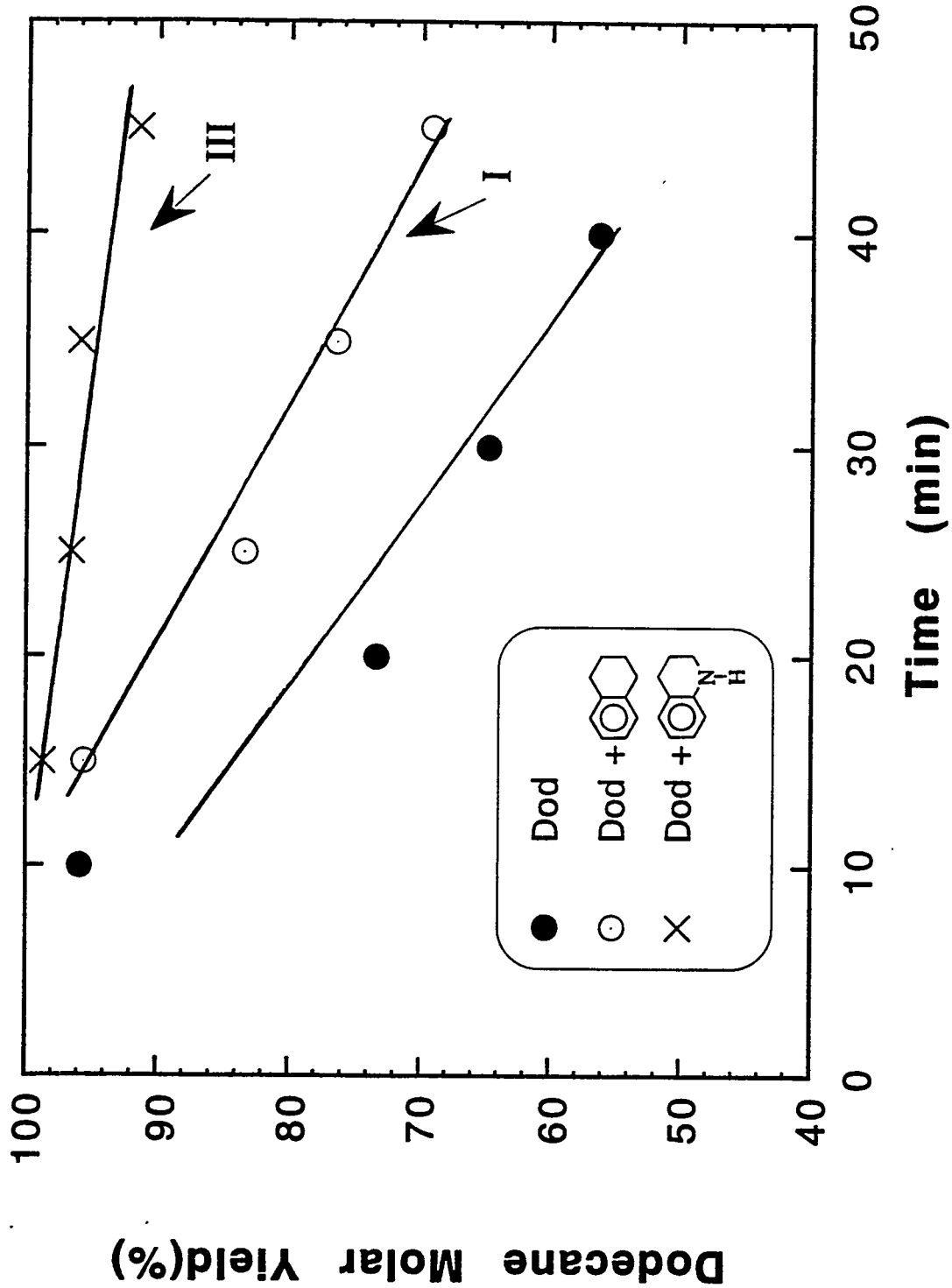

Figure 48. Effects of hydrogen donor additives (10mol%) I and III on the molar yields of dodecane at 450°C under initial N_2 pressure of 0.69 MPa. (Lines are drawn for visual aid only)

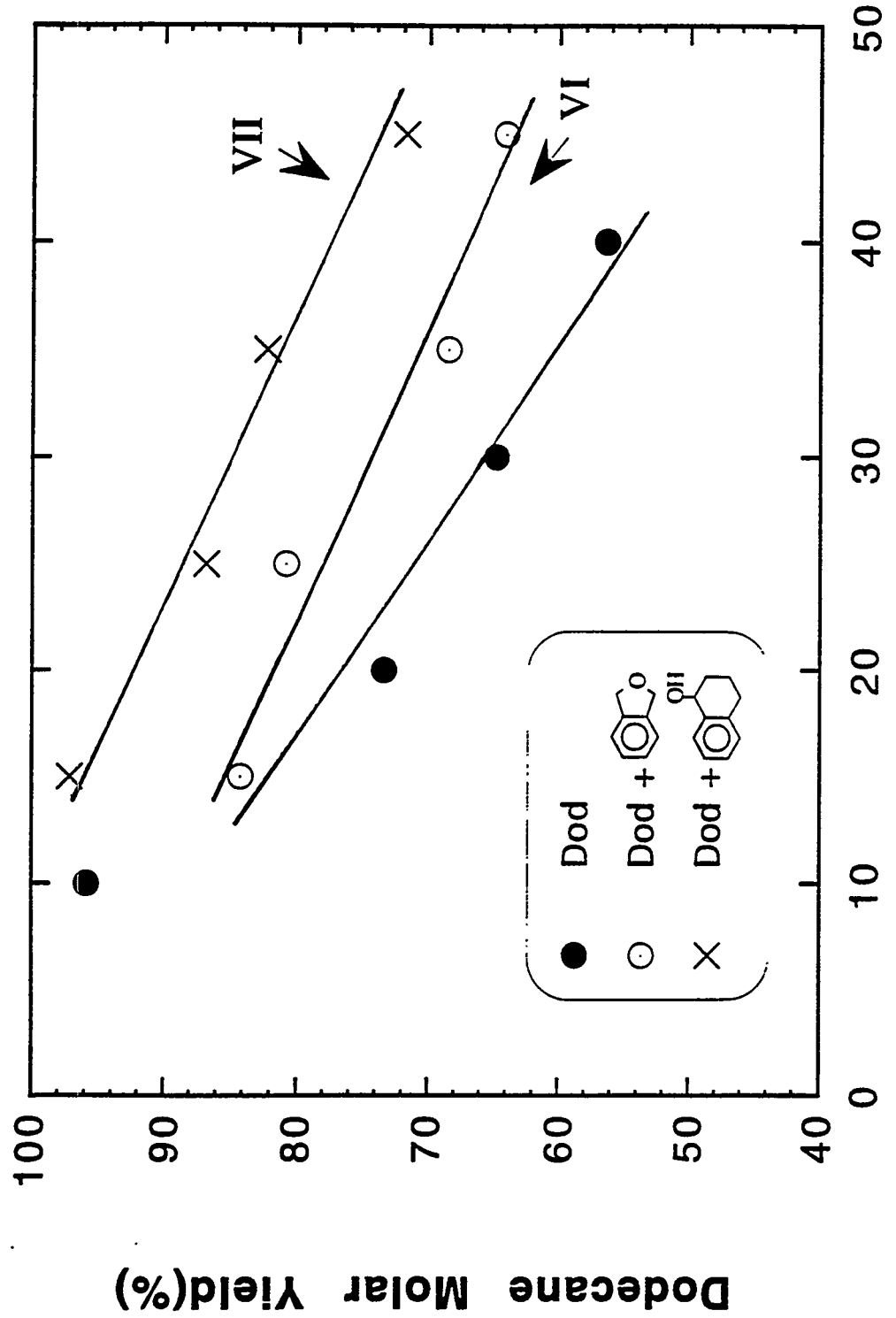

Figure 49. Effects of hydrogen donor additives (10mol%) VI and VII on the molar yields of dodecane at 450°C under initial N_2 pressure of 0.69 MPa. (Lines are drawn for visual aid only)

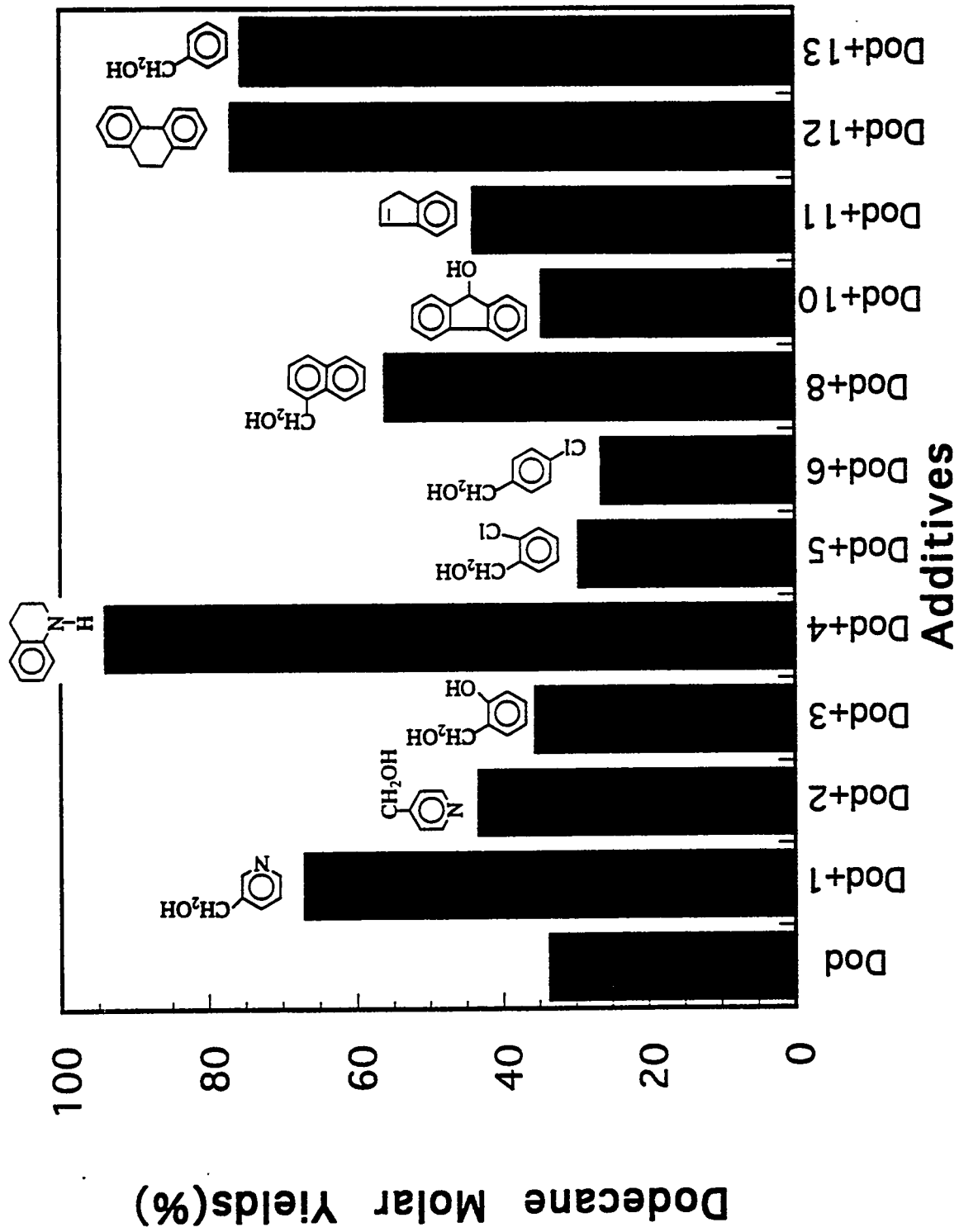

Figure 50. Effects of hydrogen donor additives 1 thru 13 on the molar yields of dodecane at 425°C for 6 hours under initial N_2 pressure of 0.69 MPa.

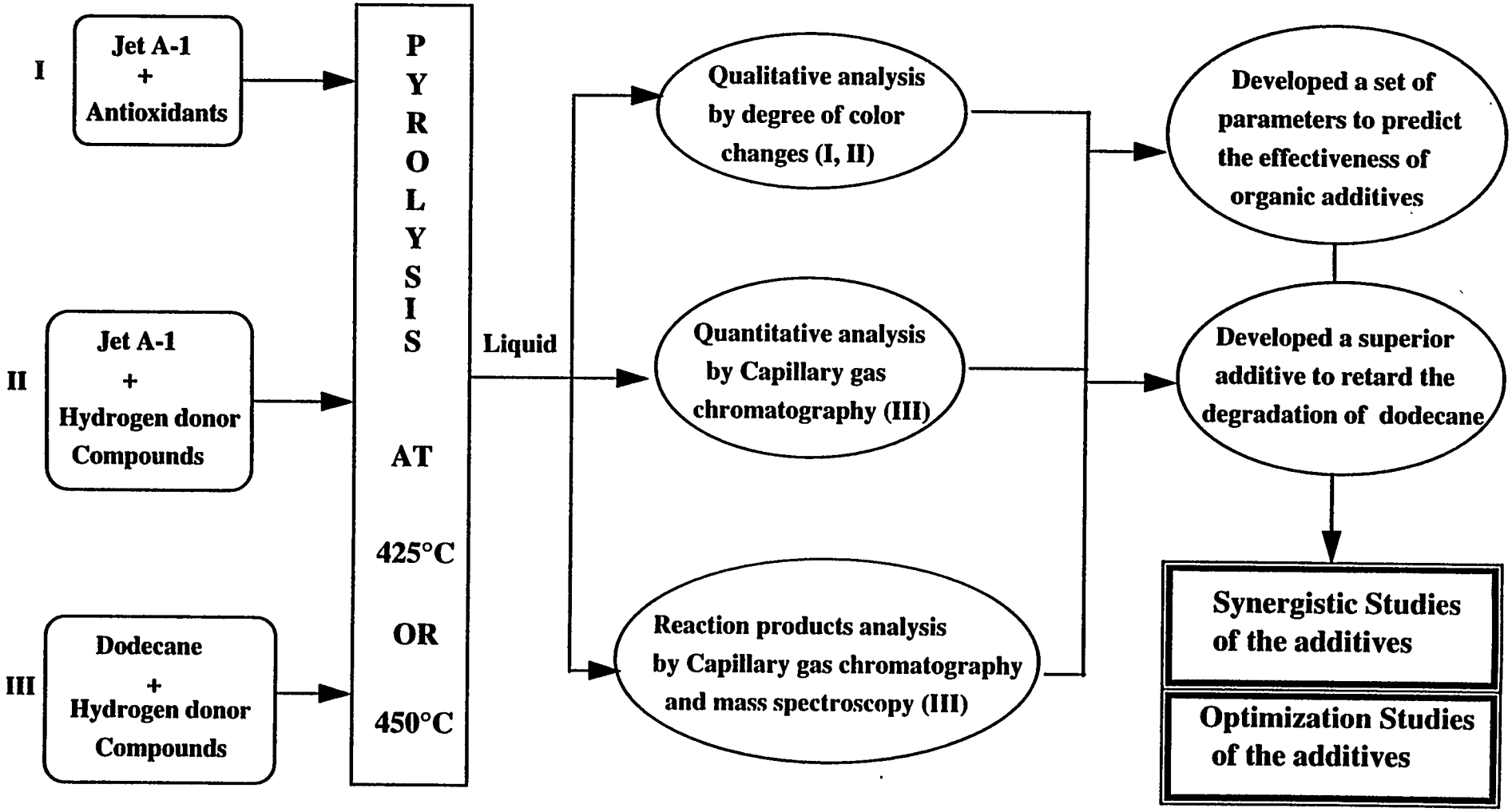

Figure 51. A Schematic diagram of the Research Approach

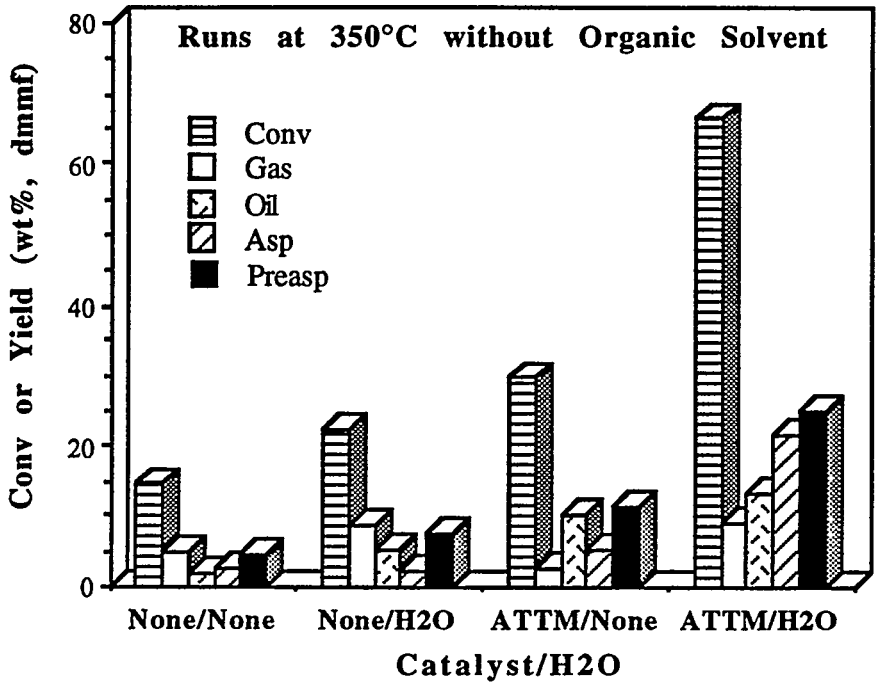

Figure 52. Effect of water on catalytic liquefaction of Wyodak coal at 350°C for 30 min.

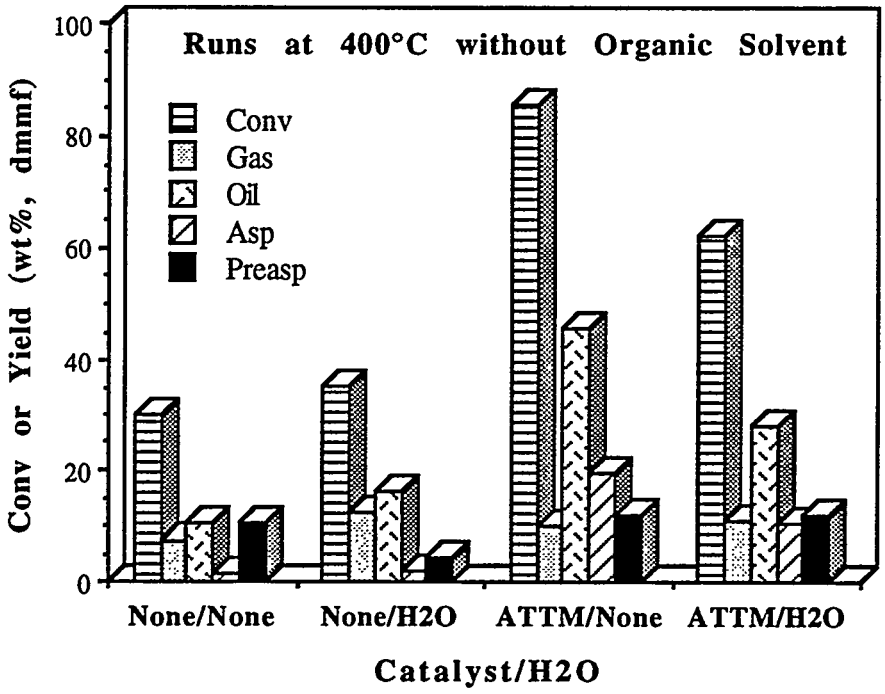

Figure 53 Effect of water on catalytic liquefaction of Wyodak coal at 400°C for 30 min.

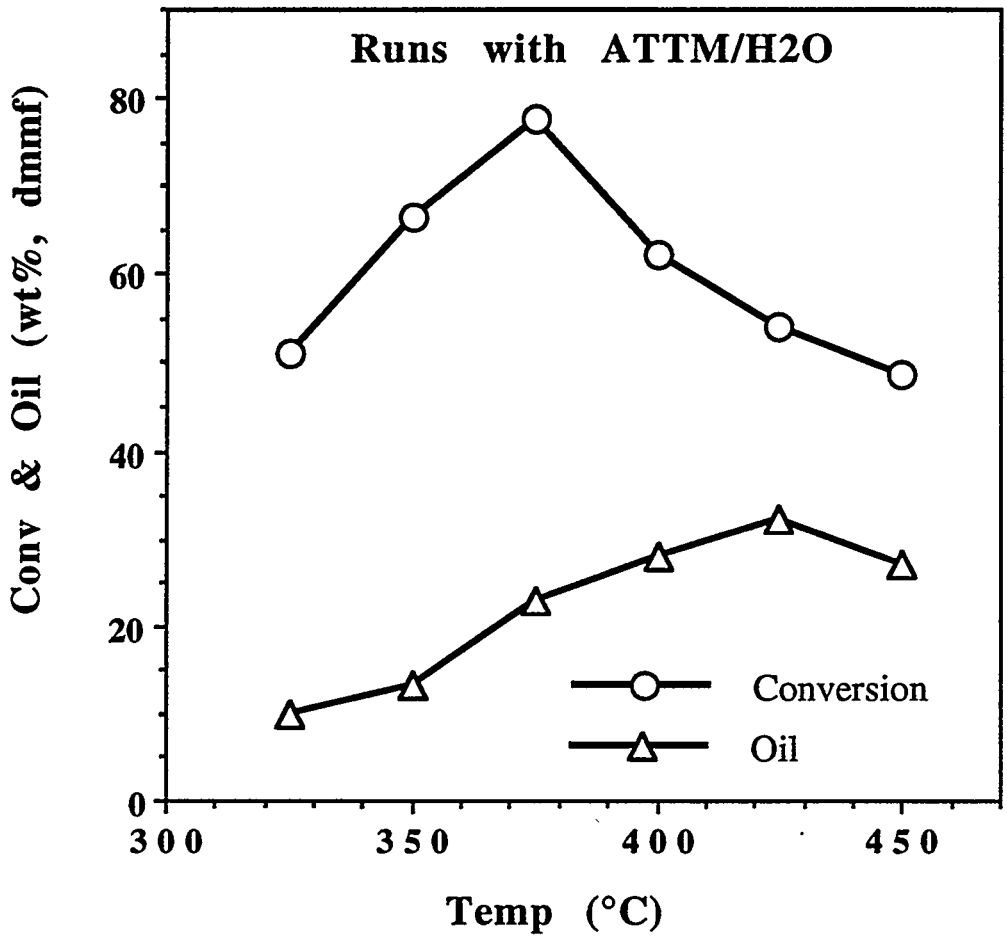

Figure 54. Effect of temperature on liquefaction of Wyodak coal with dispersed Mo catalyst and water.

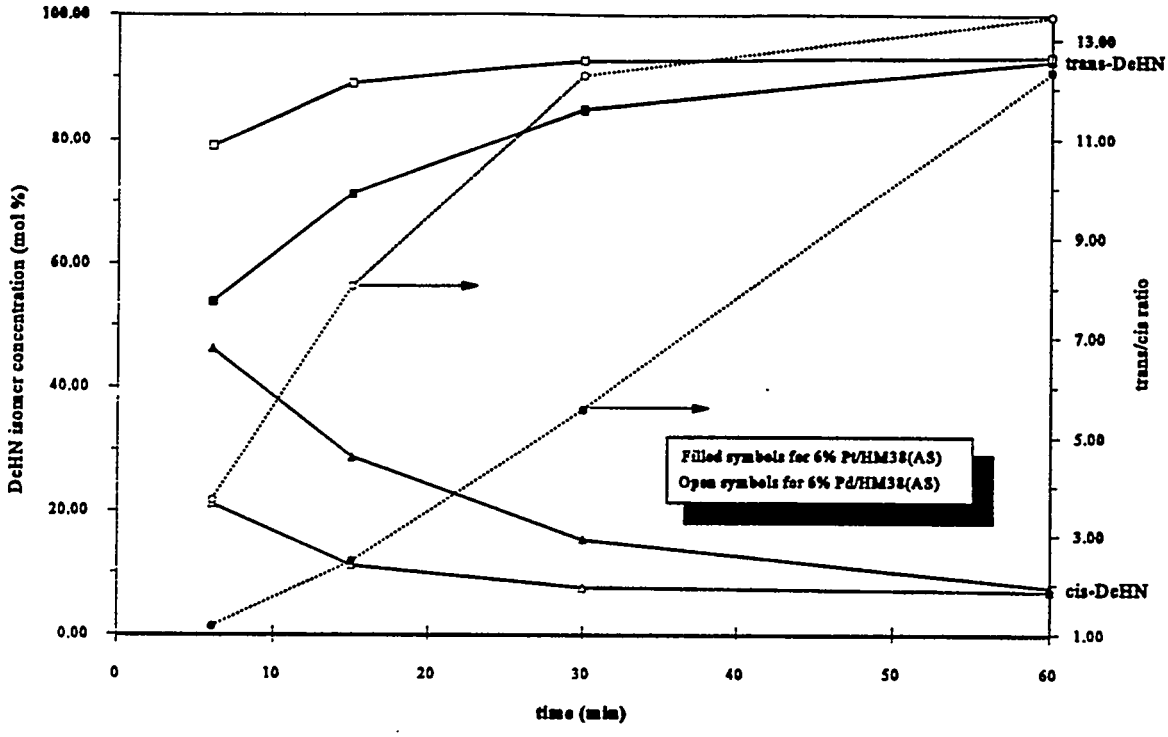

Figure 55. Comparison of decalin isomer distributions for Pd/HM38(AS) and Pt/HM38(AS).

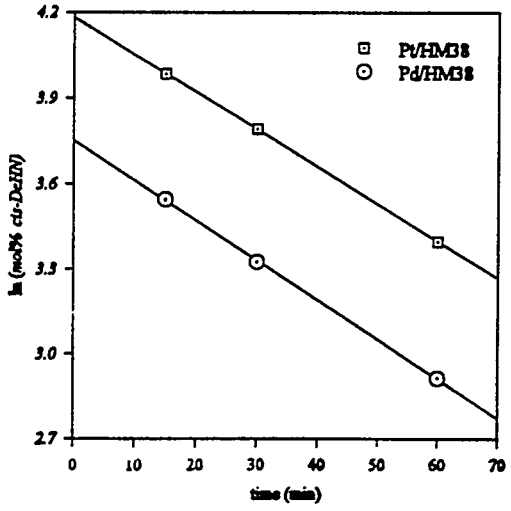

Figure 56. First-Order Plot for c-DeHN Isomerization over G. Bowers Catalysts

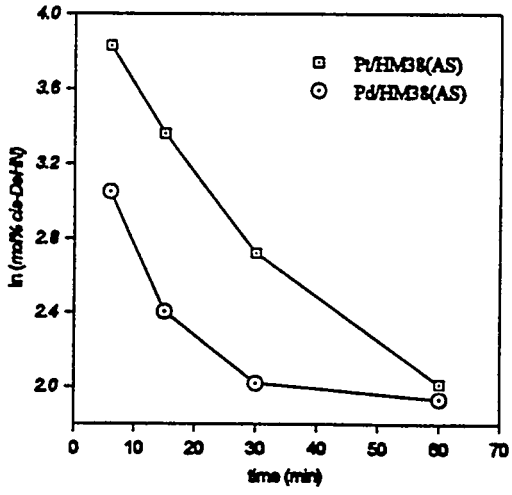

Figure 57 First-Order Plot for c-DeHN Isomerization over A. Schmitz Catalysts

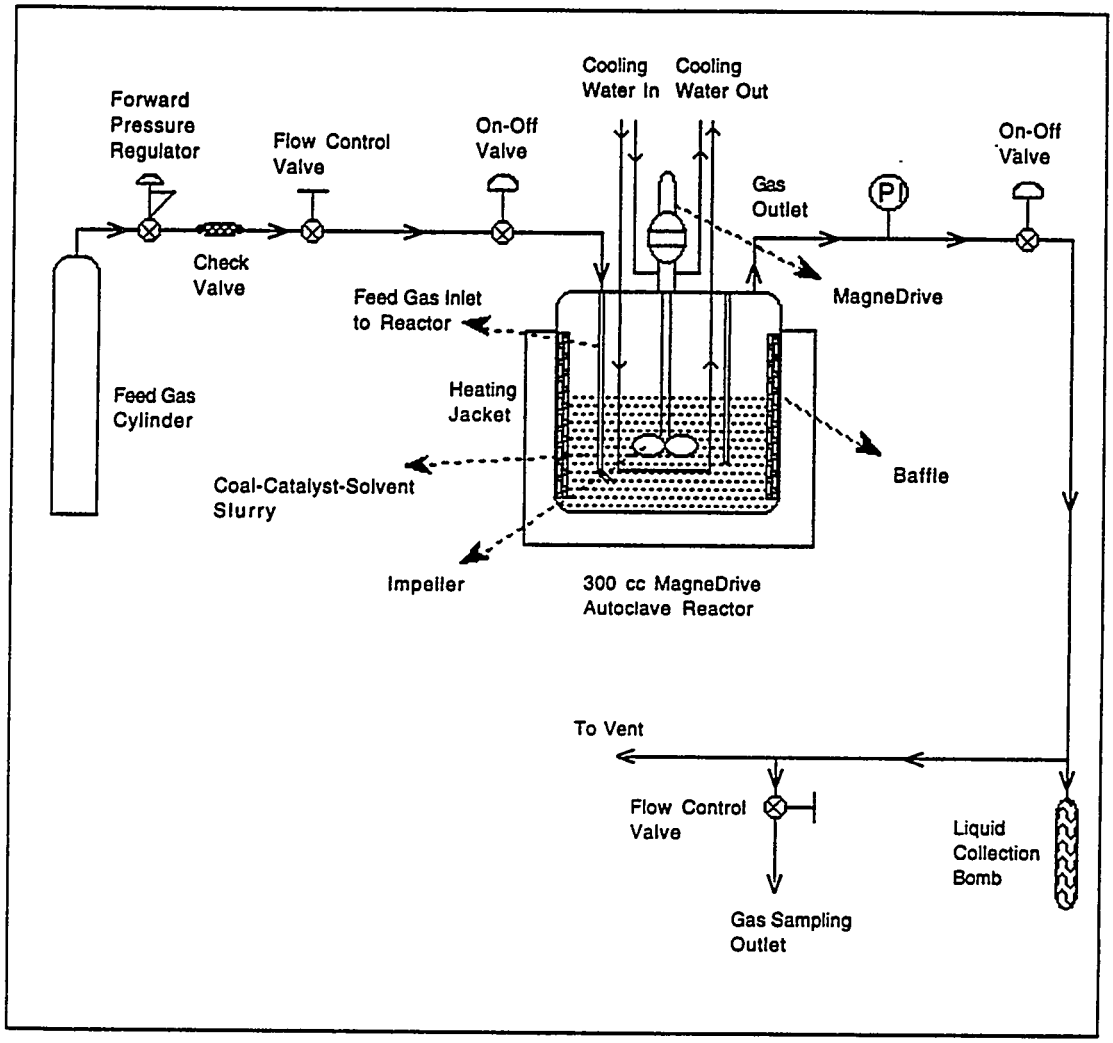

Figure 58. Schematic of the Batch Reactor System for Coal Liquefaction Process

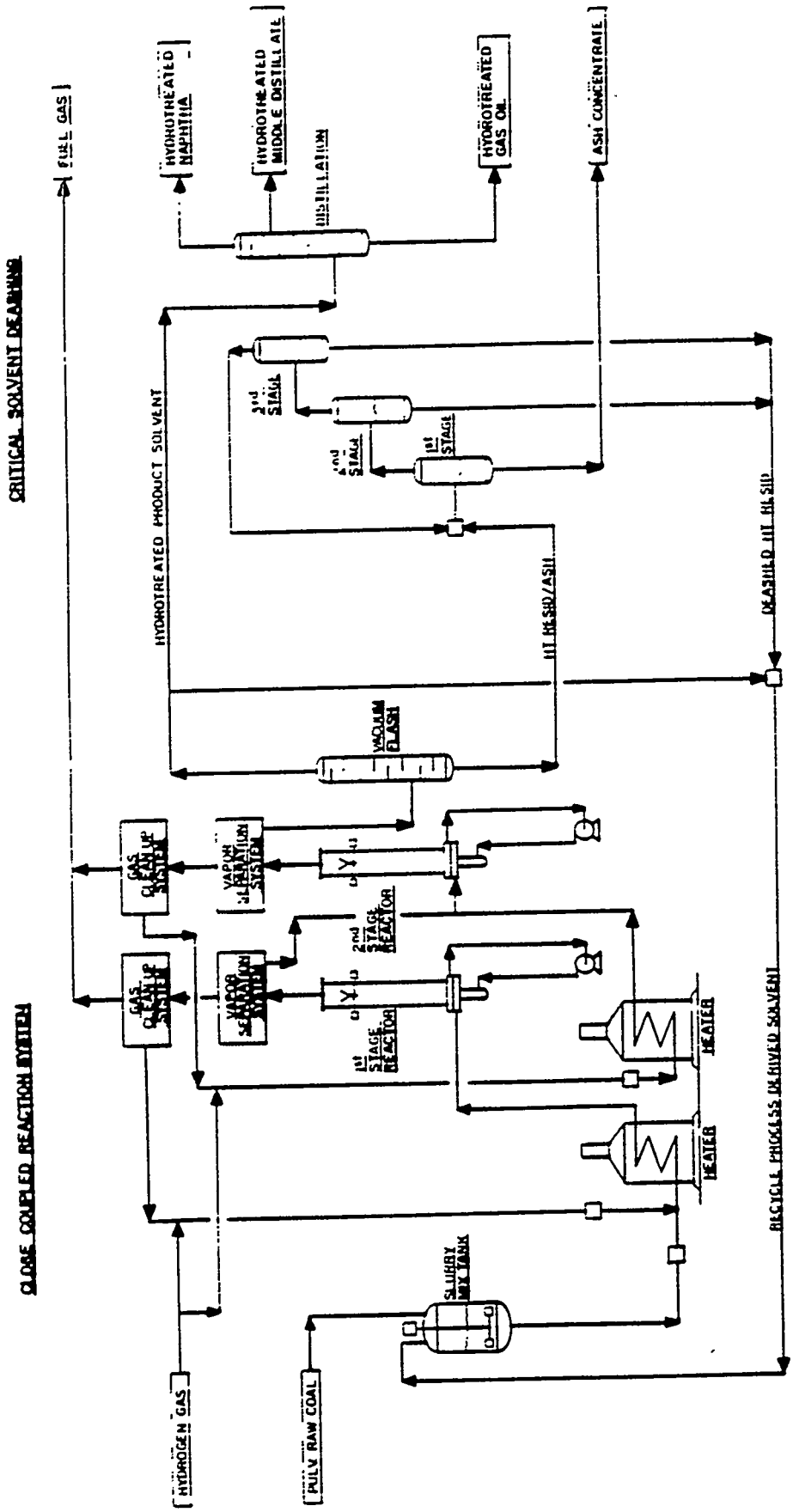

Figure 59. Wilsonville Facility - Close Coupled - Integrated Two Stage Liquefaction Unit

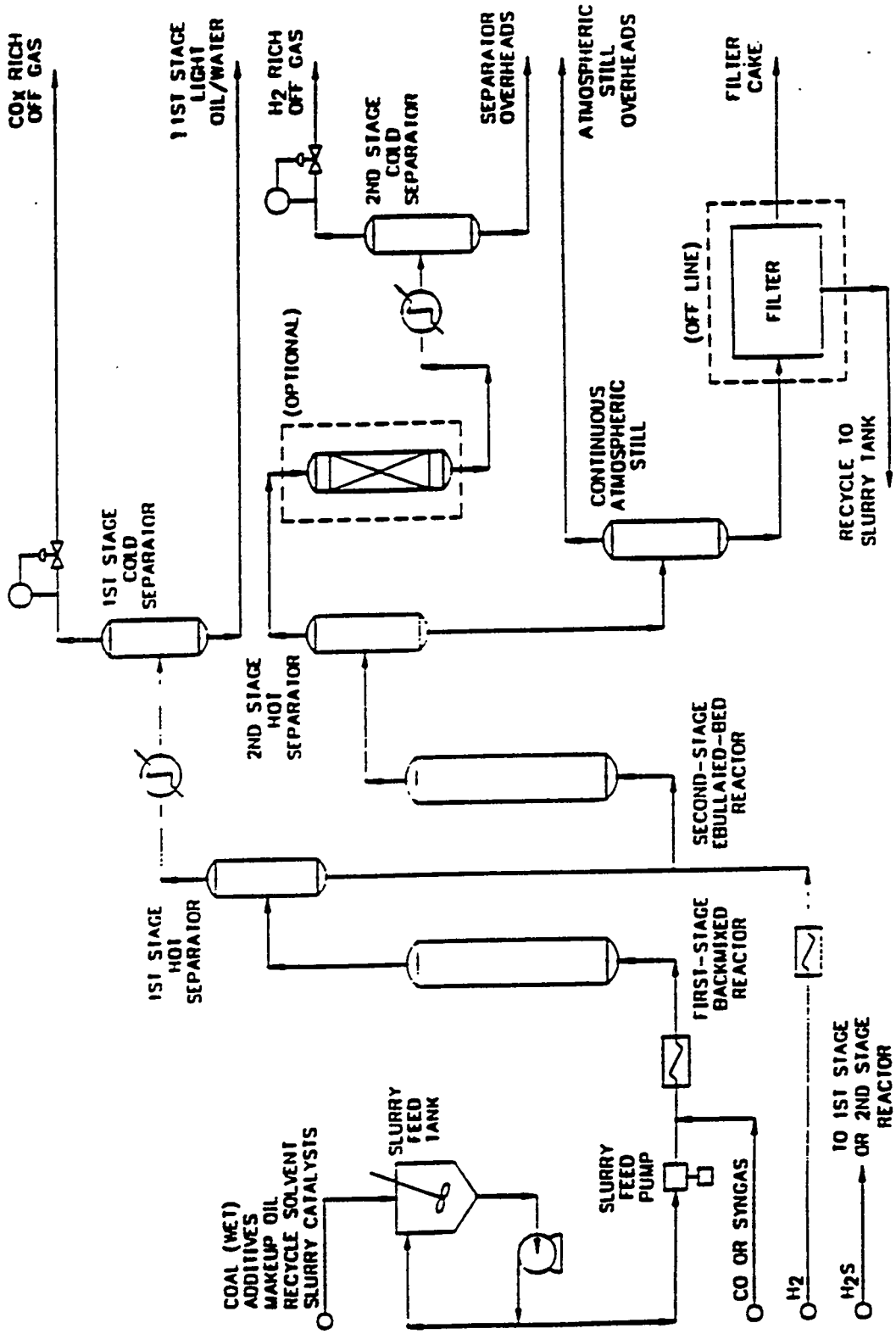

Figure 60. HRI Inc. Unit - Two Stage Coal Liquefaction Process Scheme

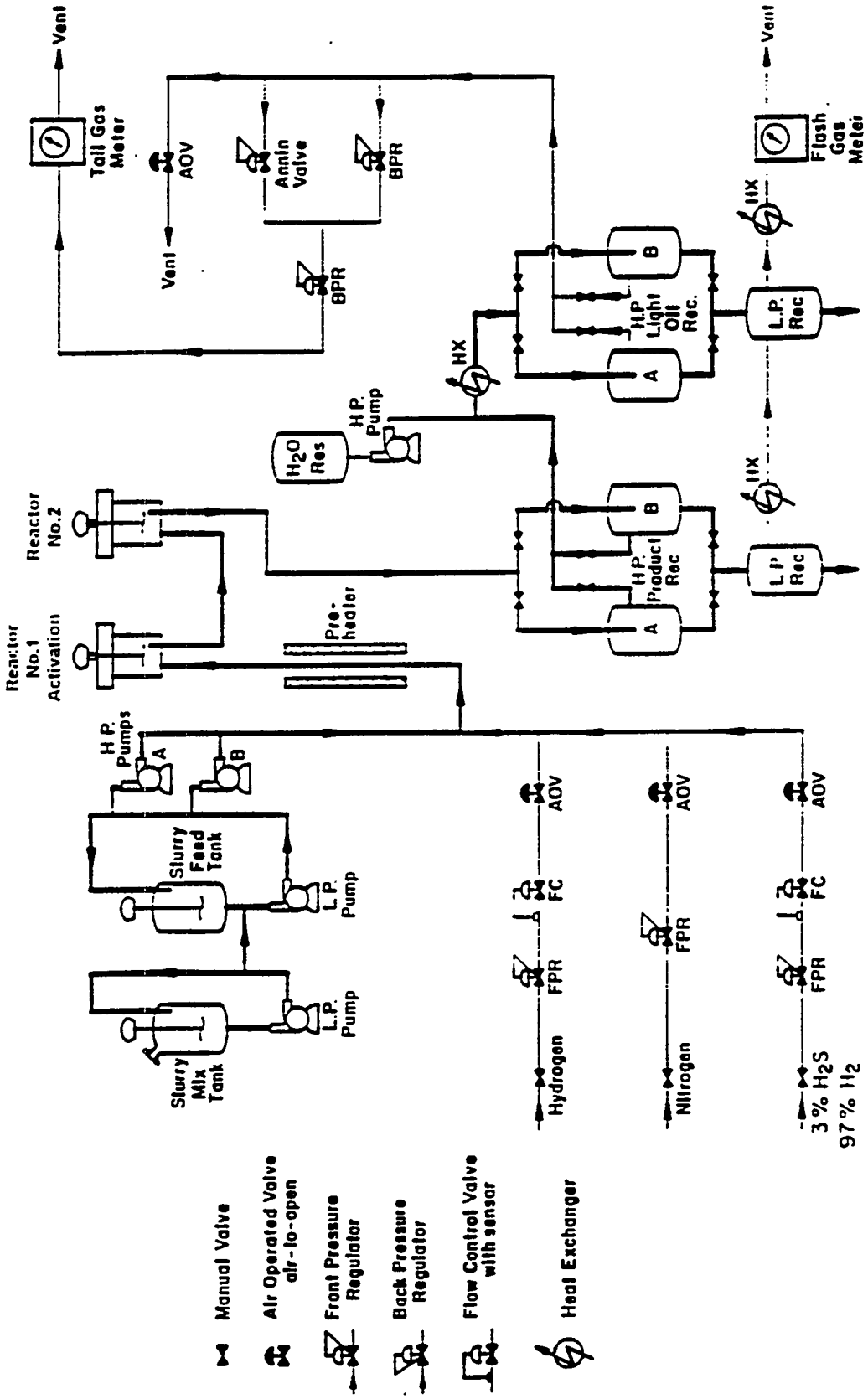

Figure 61. PETC - Bench-Scale Continuous Unit Configuration

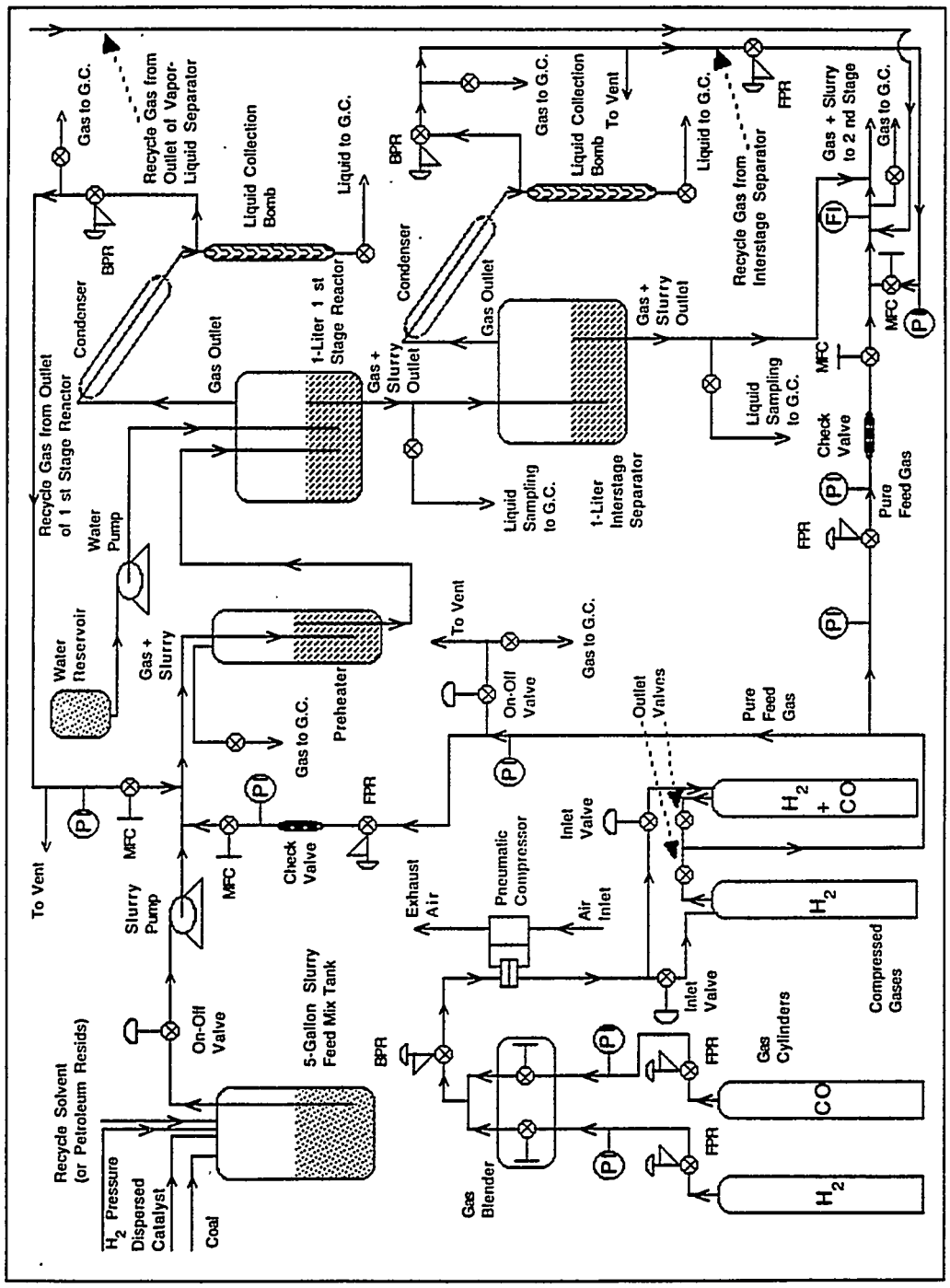

Figure 62. Conceptual Process Flow Diagram of the Proposed Mini-Pilot Plant for Coal Liquefaction Process in a Continuous Mode

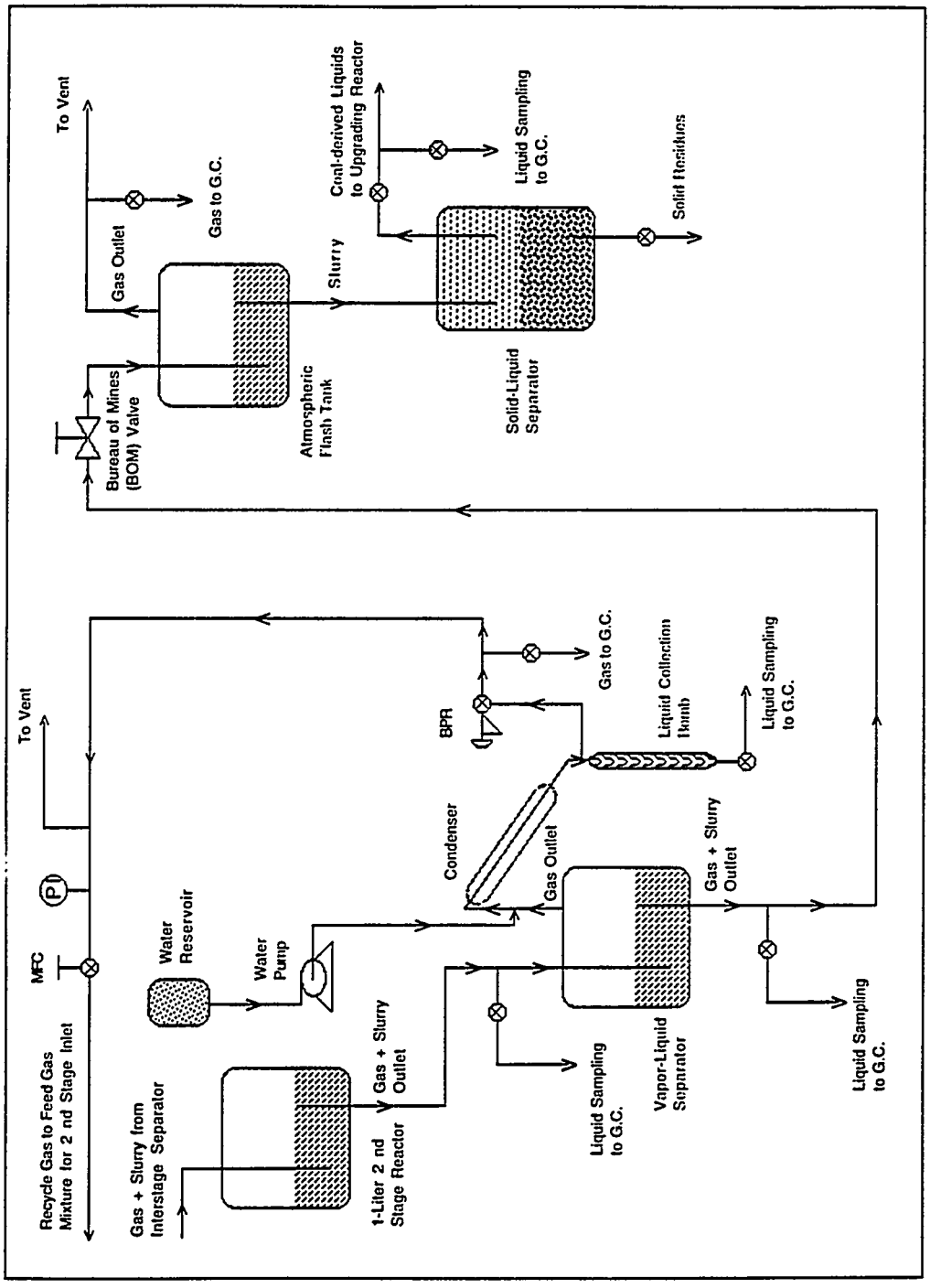

Figure 62. (Contd.). Conceptual Process Flow Diagram of the Proposed Mini-Pilot Plant for Coal Liquefaction Process in a Continuous Mode

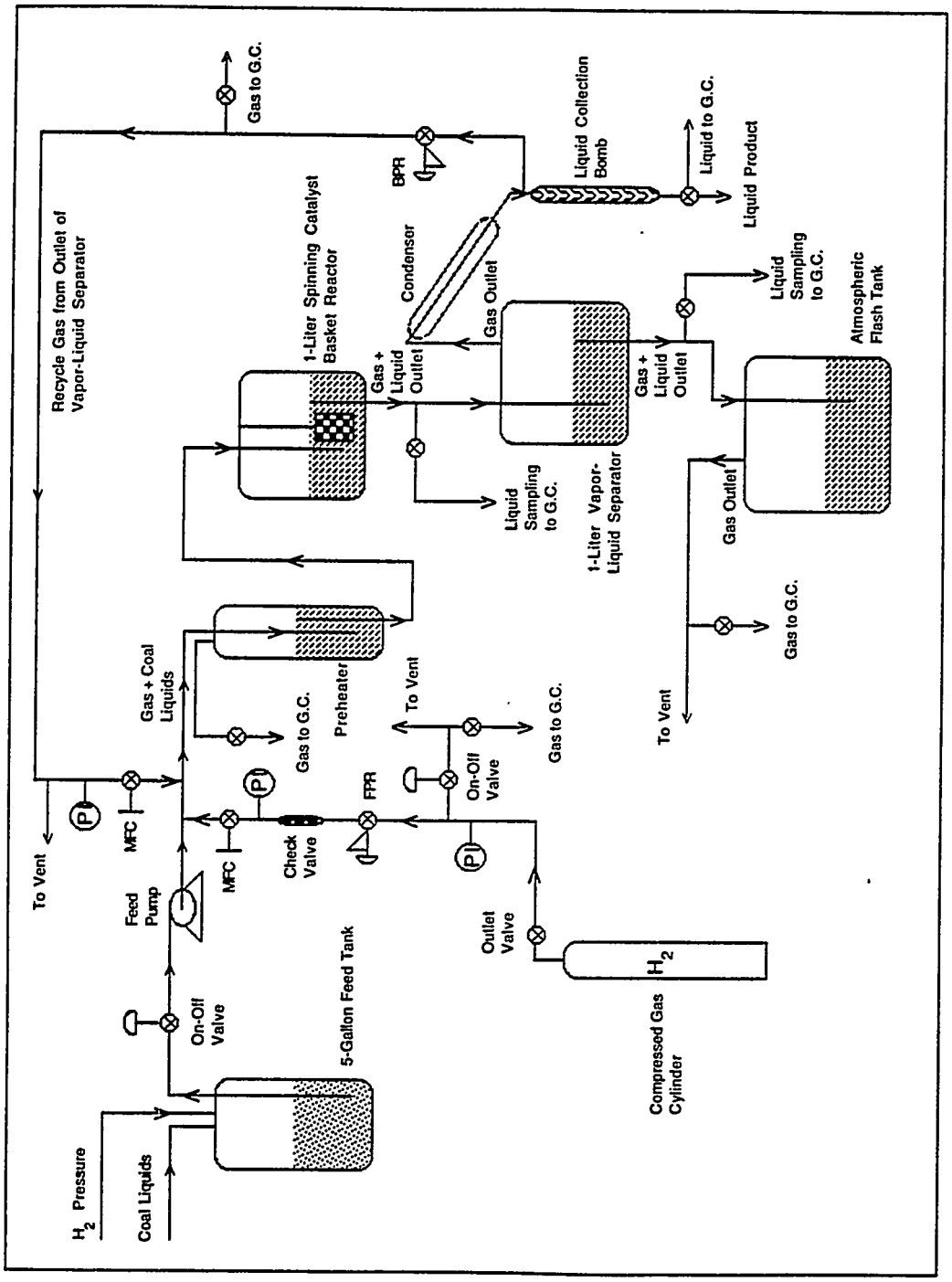

Figuire 63. Conceptual Process Flow Diagram of the Proposed Mni-Pilot Plant for Coal Liquids Upgrading Process in a Continuous Mode

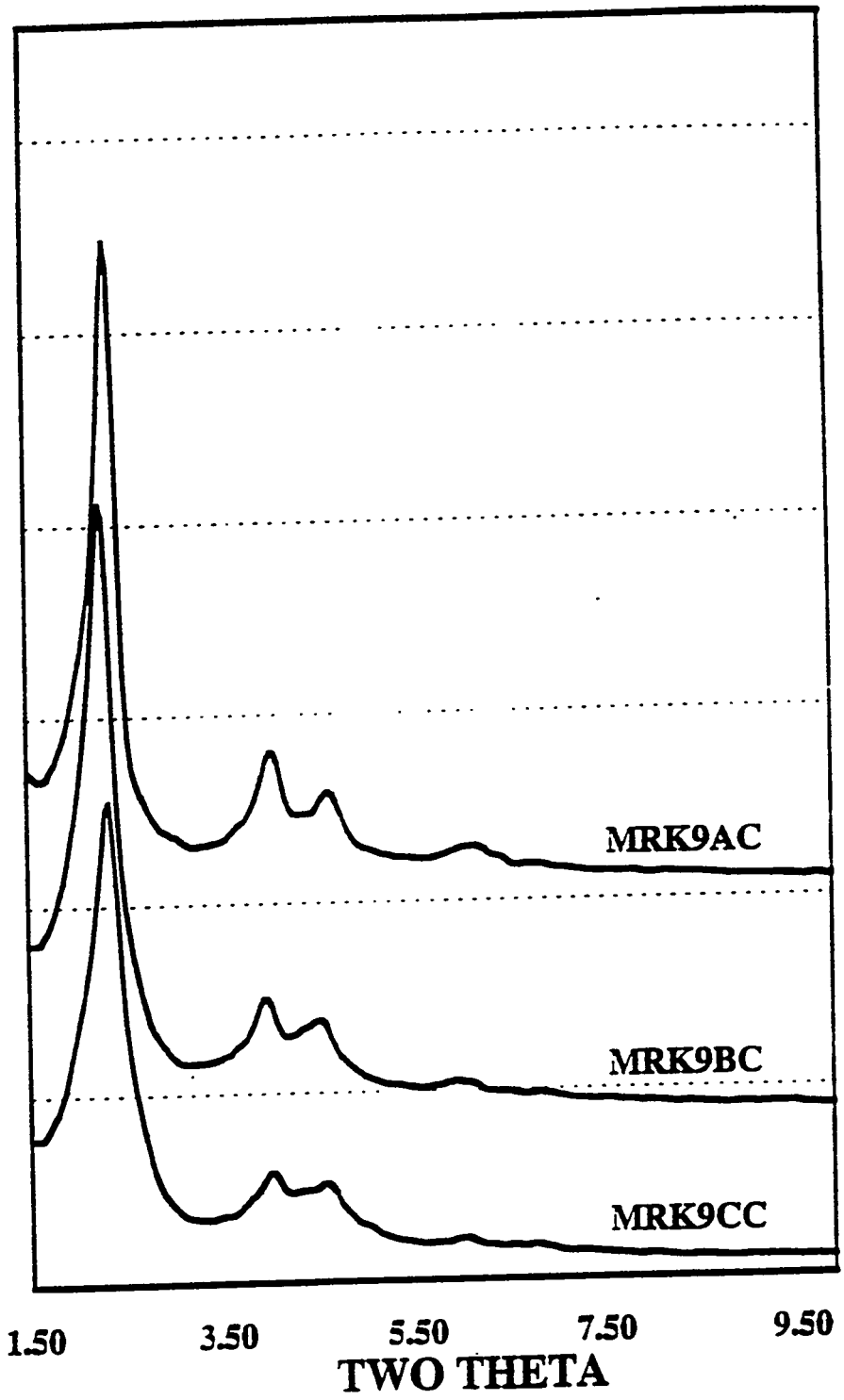

Figure 64. XRD Patterns of Calcined Al-MCM-41 samples of Si/Al -=50 (MRK9AC), 25 (MRK9BC) and 12.5 (MRK9CC), prepared using procedure I Molar Compn: $50SIO_2xAl_20_3$ 2.19$(TMS)_20$ 7.81(CTRMA) $_20$ 3165H_2H0
Source of Al: Aluminum isoproroxide

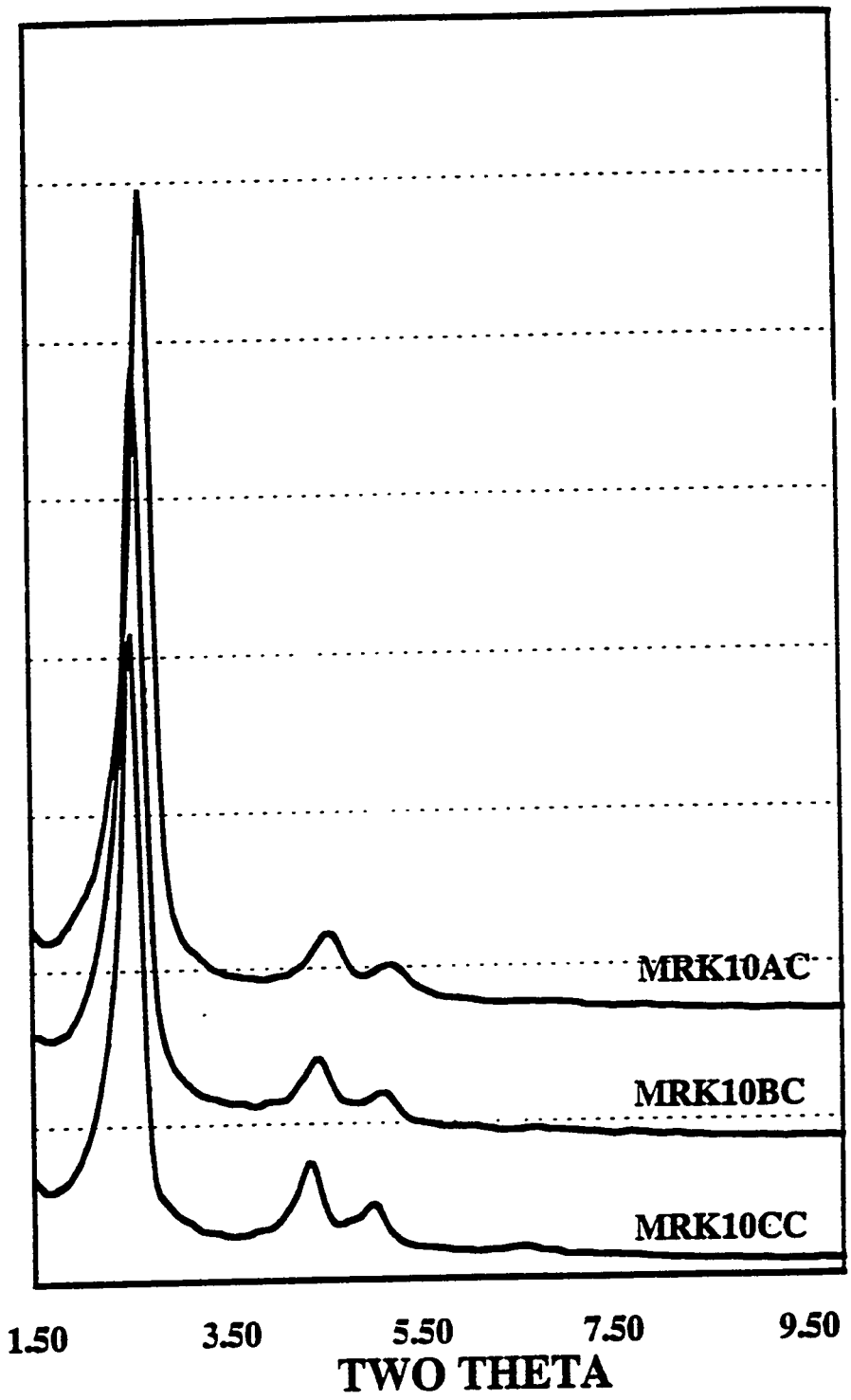

Figure 65. XRD Patterns of Calcined Al-MCM-41 samples of Si/Al -=50 (MRK10AC), 25 (MRK10BC) and 12.5 (MRK10CC), prepared using procedure I Molar Compn: $50SIO_2xAl_20_3$ $2.19(TMS)_20$ $7.81(CTRMA)_20$ $3165H_2H0$
Source of Al: Alumina (Catapal B)

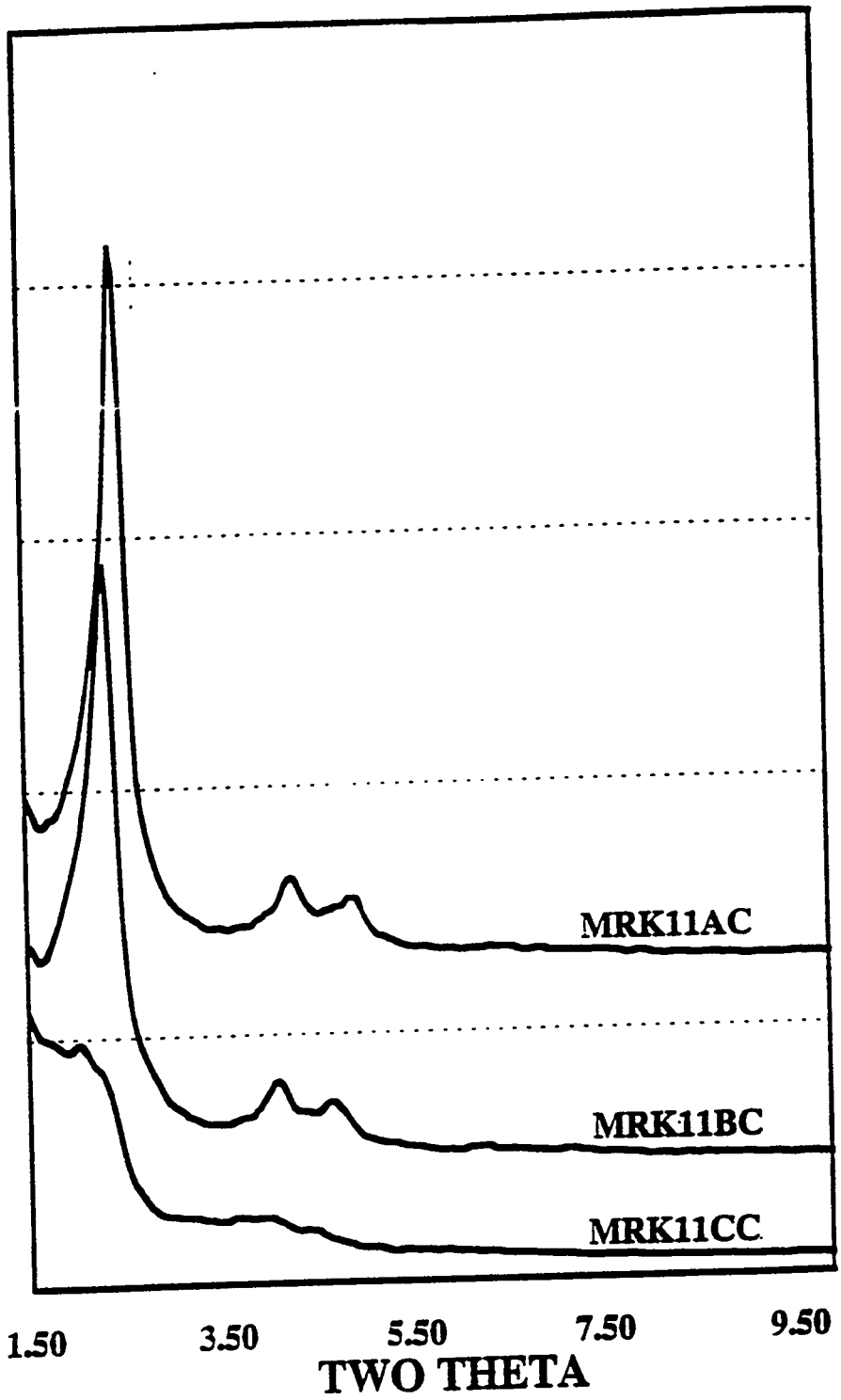

Figure 66. XRD Patterns of Calcined Al-MCM-41 samples of Si/Al -=50 (MRK11AC), 25 (MRK11BC) and 12.5 (MRK11CC), prepared using procedure I Molar Compn: $50SIO_2xAl_20_3$ 2.19$(TMS)_20$ 7.81(CTRMA) $_20$ 3165H_2H0
Source of Al: Aluminum sulfate

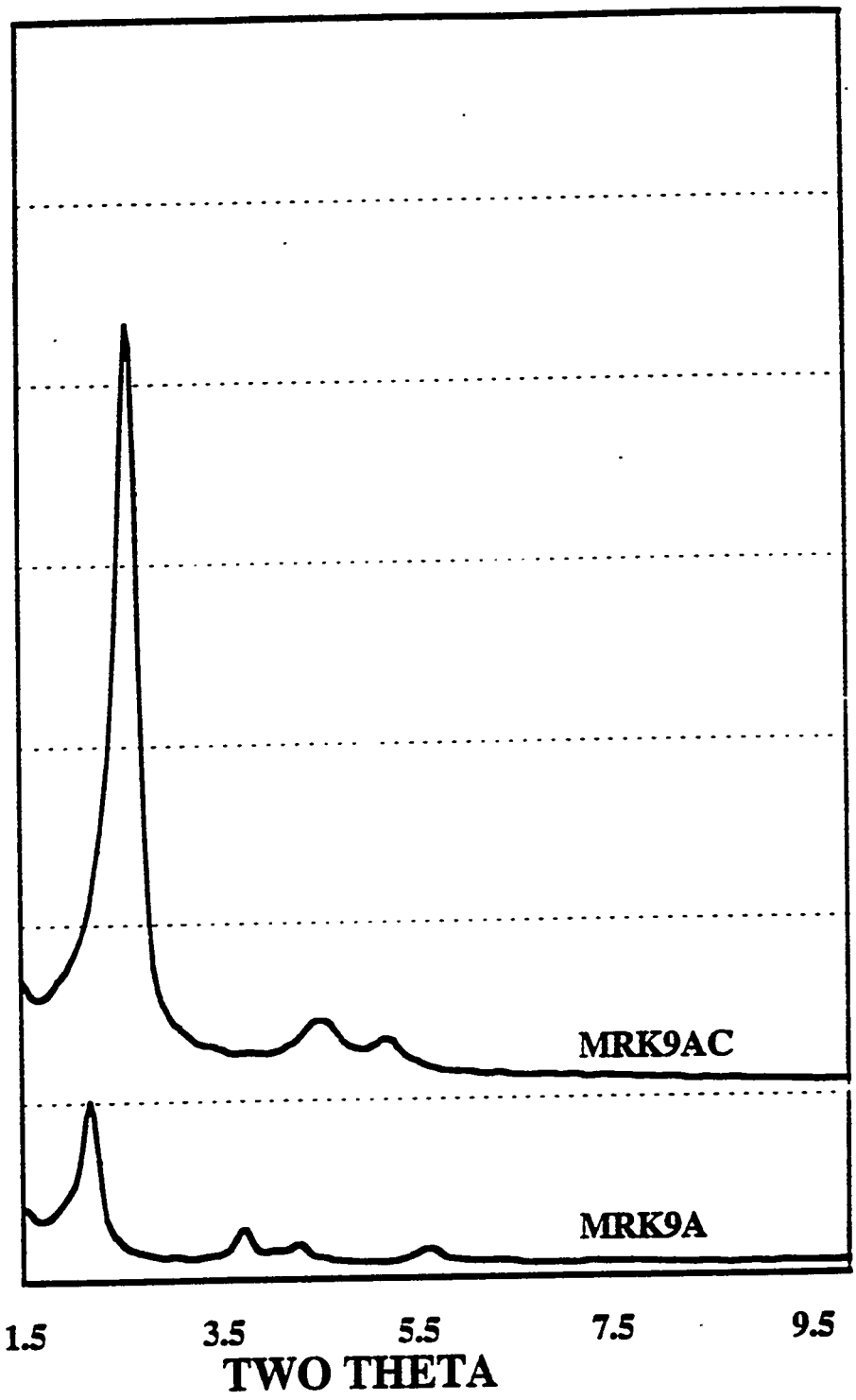

Figure 67. XRD Patterns of Al-MCM-41 samples MRK9A (non calcined) and MRK9AC (calcined)Molar compn: $50SiO_2$ $0.5Al_2O_3$ $2.19(TMS)_2O$ $7.81(CTMA)_2Br$ $3165H_2O$

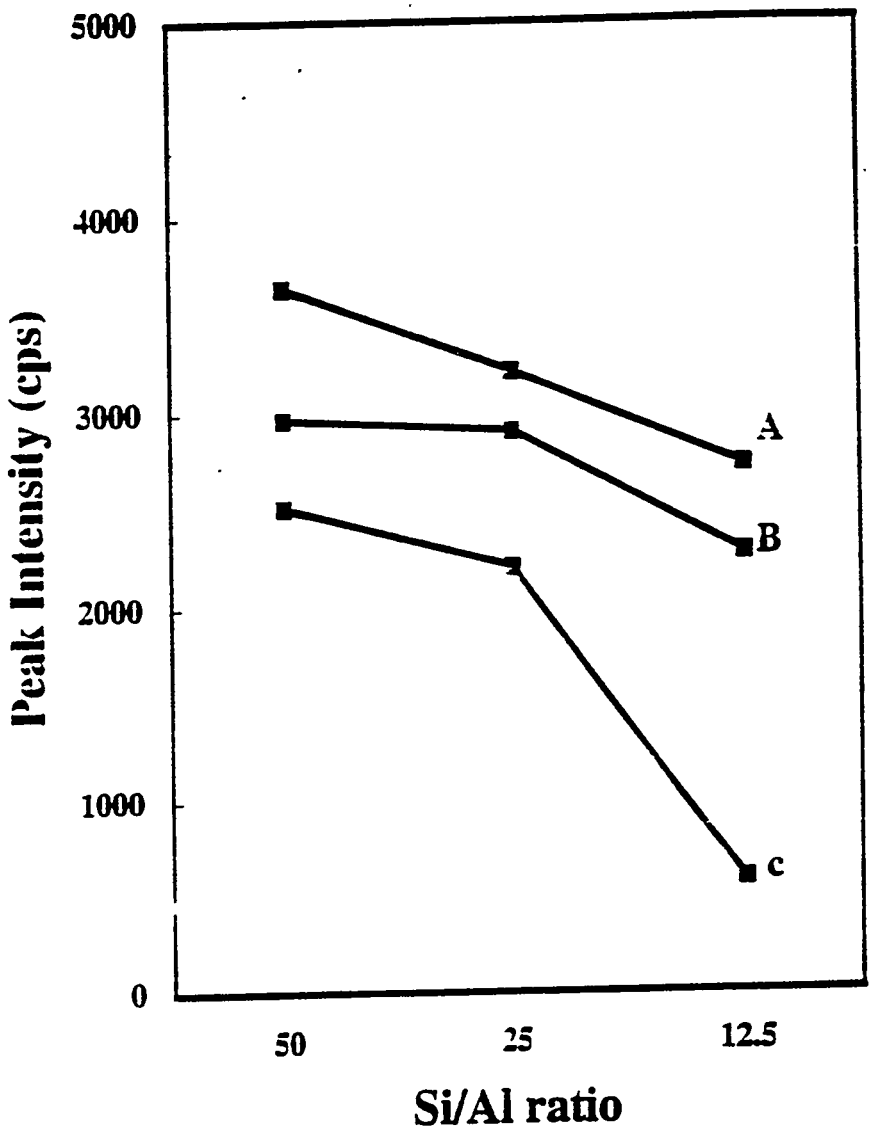

Figure 68. XRD Peak intensities versus Si/Al ratioi of Al-MCM-41 samples prepared using procedure I and Al source for A) Alumina (Catapal B), B) Aluminium Isopropoxide and C) Aluminum sulfate

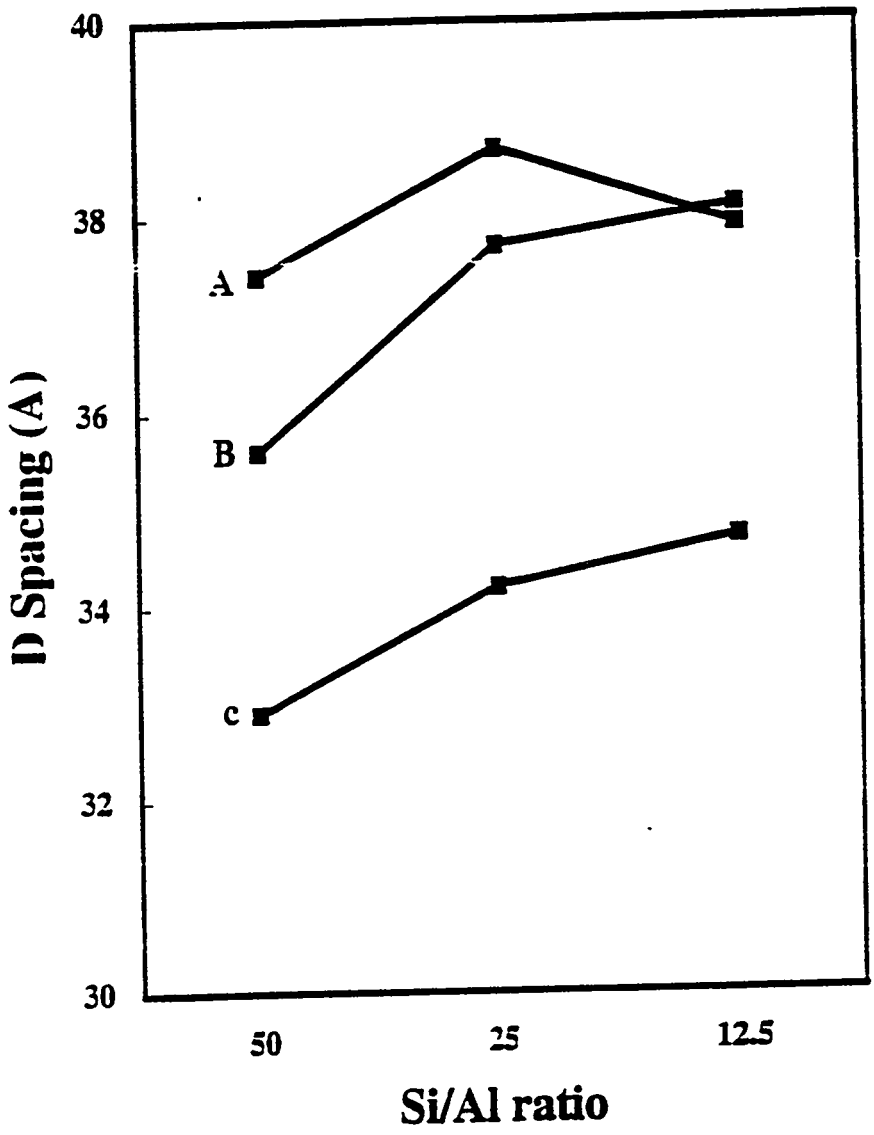

Figure 69. XRD D spacing versus Si/Al ratio of Al-MCM-41 samples prepared using procedure I and Al source for A) Aluminum sulfate, B) Aluminium Isopropoxide and C) Alumina (Catapal B)

APPENDIX III

Schemes

SYNTHESIS OF Al-MCM-41

PROCEDURE I:

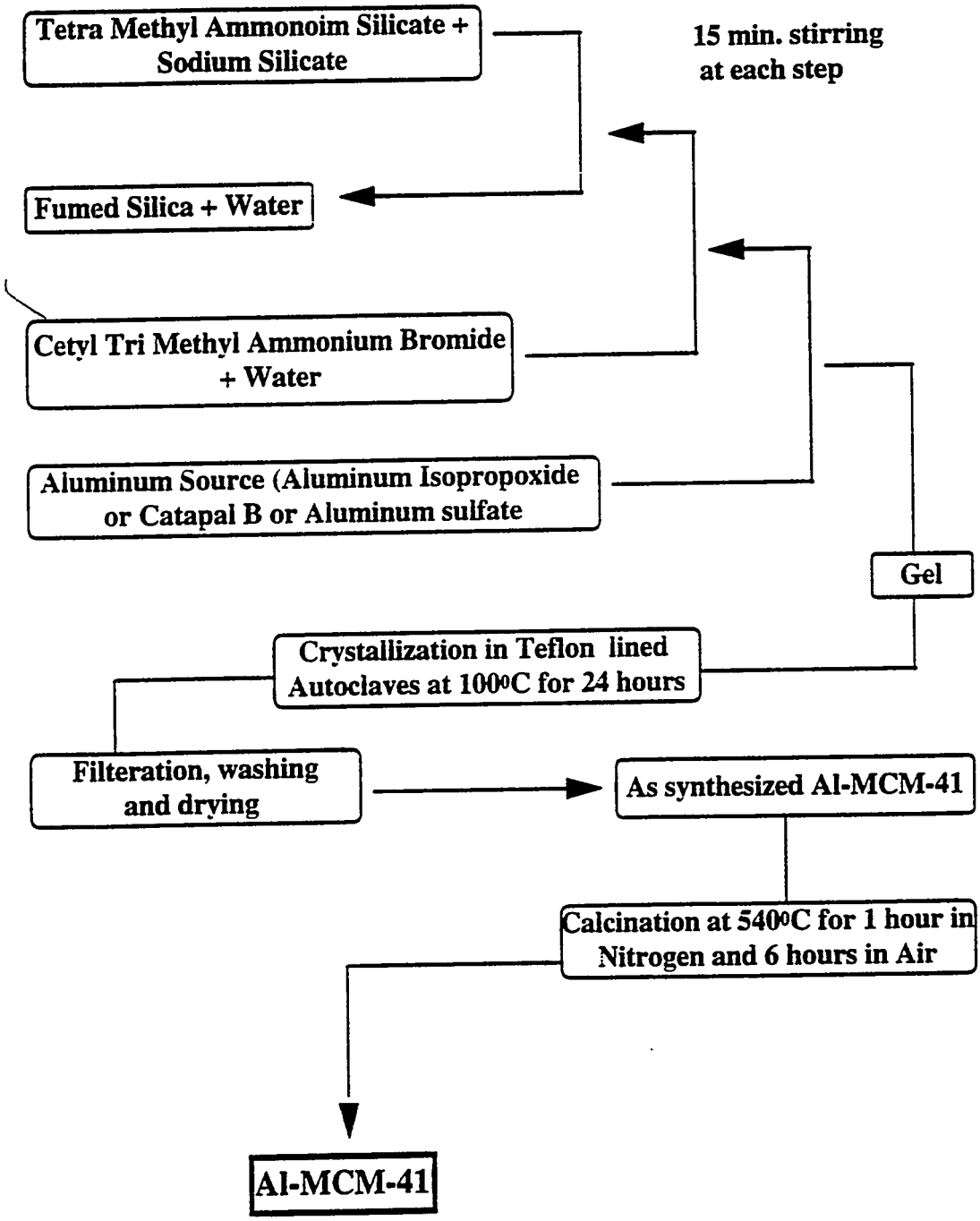

SYNTHESIS OF Al-MCM-41

PROCEDURE II: